19 February 2010 $10

Science

2009 Visualization Challenge

AAAS

cell sciences®

ultra pure cytokines

Produced in barley, these proteins are animal, bacterial, and viral free, and are ultra pure, with extremely low endotoxin.

www.cellsciences.com

Cell Sciences offers innovative, unique growth factors and hard-to-produce recombinant proteins, bypassing the use of bacterial or animal cell systems. These ultra pure proteins contain no contamination from other growth factors and negligible amounts of endotoxin.

Background: barley endosperm

The host organism, barley, with its specialized endosperm storage tissue, provides many unique features including proficient protein machinery, with eukaryotic folding, and a distinct route for long-term protein protection and storage. A biochemically inert environment, void of endotoxins, low protease activity and secondary metabolite content, and a simple protein profile, aid in downstream processing. Barley has also a G.R.A.S. (generally recognized as safe) status from the FDA.

Cell Sciences ultra pure growth factors and cytokines are produced for use in basic and applied medical scientific research, cell culture media and diagnostics.

- serum free
- animal, bacterial & viral free
- extremely low endotoxin (<0.005 ng/ug)
- highly biologically active
- easier regulatory clearance
- perfect for cell culture, drug development, stem cell research, animal research
- for use in all *in vitro* cellular studies
- for use in all *in vivo* animal studies

Ultra pure cytokines & growth factors

FGF1, human
FGF2, human
FLT3 ligand, human
GCSF, human
IFNA2, human
IFN gamma, human
IGF1, human
IL1-alpha, human
IL2, human
IL3, human
IL4, human
IL5, human
IL6, human
IL7, human
IL9, human
IL16, human
IL22, human
KGF, human
M-CSF, human
NRG1/HRG beta 2, human
SCF, mouse
SF20/IL25, human
TNF-alpha, human
TNF-beta, human
VEGF121, human
VEGF165, human

CELL SCIENCES INC • 480 NEPONSET STREET, BUILDING 12A, CANTON, MA 02021 • INFO@CELLSCIENCES.COM

TOLL FREE: (888) 769-1246 • TEL: (781) 828-0610 • FAX: (781) 828-0542 • WEB WWW.CELLSCIENCES.COM

R&D SYSTEMS 2010 CATALOG AVAILABLE NOW!

R&D Systems is a leading supplier of cell biology reagents with over 20 years of experience serving the research community. More than 97% of the products supplied by R&D Systems are developed and manufactured at our own facilities. This enables us to maintain strict manufacturing and quality control standards, ensuring that our reagents meet the high levels of performance and consistency expected by our customers.

OVER 1,600 NEW PRODUCTS!

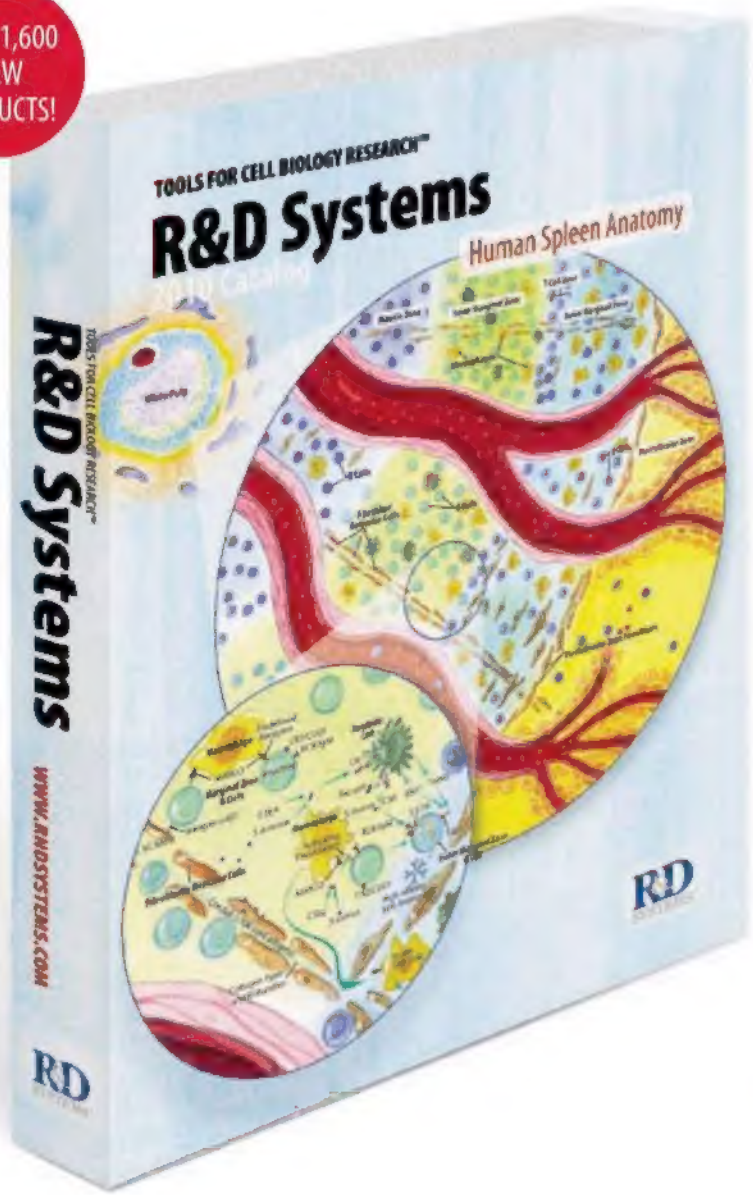

OFFERING MORE THAN 15,000 QUALITY PRODUCTS including:

Proteins

Antibodies

ELISAs

Multiplex Immunoassays

Stem Cell Products

& More!

Request a catalog online:
www.RnDSystems.com/go/Catalog

R&D Systems Tools for Cell Biology Research™

USA & Canada **R&D Systems, Inc.** Tel: (800) 343-7475 info@RnDSystems.com

Europe **R&D Systems Europe, Ltd.** Tel: +44 (0)1235 529449 info@RnDSystems.co.uk

China **R&D Systems China Co., Ltd.** Tel: +86 (21) 52380373 info@RnDSystemsChina.com.cn

Selection expanding weekly—visit **www.RnDSystems.com/go/request** to sign up for weekly new product updates.

R&D SYSTEMS®

GE Healthcare
Life Sciences

Inspired Ägain

Who better to draw inspiration for the new ÄKTA™ avant system than from customers using the 30,000 ÄKTA systems already in use around the world? Well, you spoke and we listened. The new ÄKTA avant system for process development is faster — enabling quicker insights. It minimizes the chance of error, even while working at higher speeds. And it allows for direct, reliable scalability. At GE Healthcare, our focus is on helping scientists achieve even more, faster. It's a commitment we have in our genes. And all this is backed by the service, support, and investment in the future that being part of GE can bring.

Want to know more? Why not talk with us today. Visit **www.gelifesciences.com/aktaavant**

I **ÄKTA** I Amersham I Biacore I IN Cell Analyzer I Whatman I GE Service I

The New ÄKTA avant

imagination at work

EDITORIAL

NEWS OF THE WEEK

NEWS FOCUS

SPECIAL FEATURE

LETTERS

BOOKS *ET AL.*

POLICY FORUM

PERSPECTIVES

CONTENTS continued >>

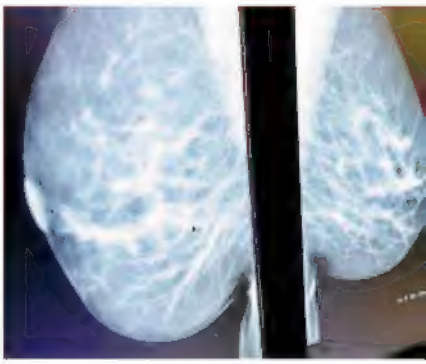

page 936

page 962

COVER

"Branching Morphogenesis," an installation made from more than 75,000 interconnected cable zip ties, illustrates the predicted forces generated by human lung endothelial cells as they form networks within an extracellular matrix over time. Winners of the 2009 *Science*/NSF International Science & Engineering Visualization Challenge are featured in a special section starting on page 945.

Image: Jenny E. Sabin; installation: Peter Lloyd Jones, Jenny E. Sabin, Andrew Lucia, Annette Fierro/Sabin+Jones LabStudio, University of Pennsylvania

DEPARTMENTS

Choose QIAGEN for detection

Detection platforms, assays, and analysis software by QIAGEN

Use QIAGEN® solutions from sample to result, and benefit from sensitive and reliable detection systems:

- **Quantitative, real-time PCR detection**
- **Automated analysis of DNA fragments and RNA**
- **Pyrosequencing® sequence-based DNA detection and quantification**
- **Optimized, ready-to-use assays and reagents**

Making improvements in life possible — www.qiagen.com

QIAGEN®

Sample & Assay Technologies

CONTENTS continued >>

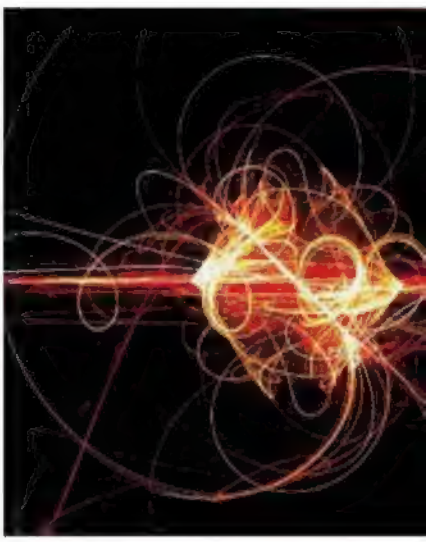

page 960

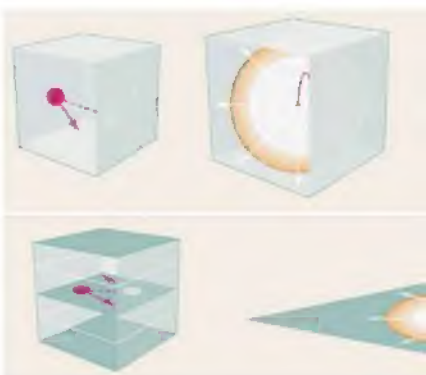

pages 969 & 980

page 1014

Call for Papers

Science Signaling

Science Signaling, from the publisher of ***Science***, AAAS, features top-notch, peer-reviewed, original research weekly. Submit your manuscripts in the following areas of cellular regulation:

- Biochemistry
- Bioinformatics
- Cell Biology
- Development
- Immunology
- Microbiology
- Molecular Biology
- Neuroscience
- Pharmacology
- Physiology and Medicine
- Systems Biology

Science Signaling is indexed in CrossRef and MEDLINE.

Chief Scientific Editor
Michael B. Yaffe, M.D., Ph.D.
Associate Professor, Department of Biology
Massachusetts Institute of Technology

Editor
Nancy R. Gough, Ph.D.
AAAS

Submit your research at:
www.sciencesignaling.org/about/help/research.dtl

Subscribing to the weekly ***Science Signaling*** ensures that you and your lab have the latest cell signaling resources. For more information visit **www.ScienceSignaling.org**

Science Signaling
AAAS

SCIENCEONLINE

SCIENCEXPRESS
www.sciencexpress.org

Design of Polymethine Dyes with Large Third-Order Optical Nonlinearities and Loss Figures of Merit
J. M. Hales et al.

Nonlinear optical materials are designed and characterized for potential applications in all-optical switching.
10.1126/science.1185117

SCIENCENOW
www.sciencenow.org
Highlights From Our Daily News Coverage

Is That Elephant Running? Don't Bet on It

New study argues that, regardless of their speed, elephants don't actually run.

What Doesn't Kill Microbes, Makes Them Stronger

Low levels of antibiotics trigger mutations that cause resistance.

Ancient Human Sequenced for First Time

Strands of hair paint detailed picture of 4000-year-old Greenlander.

SCIENCESIGNALING
www.sciencesignaling.org
The Signal Transduction Knowledge Environment

RESEARCH ARTICLE: Microbial Hijacking of Complement–Toll-Like Receptor Crosstalk
M. Wang et al.,

Pathogen-instigated crosstalk between the complement C5a receptor and Toll-like receptor 2 disables innate immune function

RESEARCH ARTICLE: Deciphering Protein Kinase Specificity Through Large-Scale Analysis of Yeast Phosphorylation Site Motifs
J. Mok et al.

A high-throughput peptide array approach reveals insight into kinase substrates and specificity.

CONNECTIONS MAP: Jasmonate Biochemical Pathway
A. Gfeller et al.

Jasmonates are potent physiological and developmental regulators synthesized from fatty acid precursors.

CONNECTIONS MAP: *Arabidopsis* Jasmonate Signaling Pathway
A. Gfeller et al.

Jasmonates regulate various aspects of physiology and development in *Arabidopsis thaliana*

PODCAST
G. Hajishengallis and A. M. VanHook

The pathogen *Porphyromonas gingivalis* evades the innate immune system by initiating signaling cross talk

SCIENCECAREERS
www.sciencecareers.org/career_magazine
Free Career Resources for Scientists

Tooling Up: The Applications Scientist Career Track
D. Jensen

An "applications scientist" job can link the bench to other industry careers.

Protecting Poland's Rapeseed Crop
A. Curry

Malgorzata Jedryczka's system for detecting crop pathogens has become a national industry-sponsored program

Perspective: Audacity Is Overrated
E. Diamandis

The audacious approach to science is not the best approach, especially for scientists in training

SCIENCETRANSLATIONALMEDICINE
www.sciencetranslationalmedicine.org
Integrating Medicine and Science

COMMENTARY: Ten Years of the Immune Tolerance Network—An Integrated Clinical Research Organization
J. A. Bluestone et al.

New insights from old programs yield the equation for a successful research program.

COMMENTARY: Medical Education Research as Translational Science
W. C. McGaghie

Early incorporation of translational science in physician education will improve patient care.

RESEARCH ARTICLE: Long-Term Thermostabilization of Live Poxviral and Adenoviral Vaccine Vectors at Supraphysiological Temperatures in Carbohydrate Glass
R. Alcock et al.

A sucrose-trehelose glass film dried onto a filter can preserve the activity of vaccine viral vectors.

RESEARCH ARTICLE: S-Nitrosylation from GSNOR Deficiency Impairs DNA Repair and Promotes Hepatocarcinogenesis
W. Wei et al.

An enzyme that removes harmful marks from cellular proteins guards against liver cancer.

SCIENCESIGNALING
Insight into an oral pathogen

SCIENCEPODCAST
www.sciencemag.org/multimedia/podcast
Free Weekly Show

Download the 19 February *Science* Podcast to hear about predicting human mobility patterns, a possible mechanism of prebiotic sugar formation, the winners of the 2009 *Science*/NSF Visualizaton Challenge, and more.

SCIENCEINSIDER
blogs.sciencemag.org/scienceinsider
Science Policy News and Analysis

SCIENCE (ISSN 0036-8075) **is published weekly on Friday, except the last week in December, by the American Association for the Advancement of Science, 1200 New York Avenue, NW, Washington, DC 20005.** Periodicals Mail postage (publication No. 484460) paid at Washington, DC, and additional mailing offices. Copyright © 2009 by the American Association for the Advancement of Science. The title SCIENCE is a registered trademark of the AAAS. Domestic individual membership and subscription (51 issues): $146 ($74 allocated to subscription). Domestic institutional subscription (51 issues): $855, Foreign postage extra: Mexico, Caribbean (surface mail) $55; other countries (air assist delivery) $85. First class, airmail, student, and emeritus rates on request. Canadian rates with GST available upon request, GST #1254 88122. Publications Mail Agreement Number 1069624. **Printed in the U.S.A.**

Change of address: Allow 4 weeks, giving old and new addresses and 8-digit account number. **Postmaster:** Send change of address to AAAS, P.O. Box 96178, Washington, DC 20090–6178. **Single-copy sales:** $10.00 current issue, $15.00 back issue prepaid includes surface postage; bulk rates on request. **Authorization to photocopy** material for internal or personal use under circumstances not falling within the fair use provisions of the Copyright Act is granted by AAAS to libraries and other users registered with the Copyright Clearance Center (CCC) Transactional Reporting Service, provided that $20.00 per article is paid directly to CCC, 222 Rosewood Drive, Danvers, MA 01923. The identification code for *Science* is 0036-8075. *Science* is indexed in the *Reader's Guide to Periodical Literature* and in several specialized indexes.

AAAS
ADVANCING SCIENCE, SERVING SOCIETY

CREDIT: PHOTOS.COM

"The fastest separations and the gold standard method.

That's electroforward thinking."

Next-generation precast gels. No special buffers required.

Introducing long shelf life Mini-PROTEAN™ TGX (**T**ris-**G**lyc ne e**X**tended) Gels from Bio-Rad. The nnovative TGX formulation delivers consistent, inear separat on without the need for expensive, spec alized buffers.

Get resu ts faster with:

- Run times as short as 15 minutes
- Transfer in as ittle as 15 minutes
- New bottom-opening cassette design for faster setup and less handling for downstream applications

Ge with us at **www.miniprotean.com.**

Research. Together.

To find your local sales office, visit **www.bio-rad.com/contact/**
In the U S call toll free at 1-800-4BIORAD (1-800-424 6723)

Visit us at www.bio-rad.com

BIO-RAD

<< From Big Fish to Big Whales

evolution of whales

To Degrade or Not to Degrade

Regulating the turnover of proteins within the cell is of fundamental importance to almost every physiological process. **Hwang *et al.*** (p. 973, published online 28 January; see the Perspective by **Mogk and Bukau**) now find that acetylated N-terminal methionine (Met) is a degradation signal. This degron is recognized by *Saccharomyces cerevisiae* Doa10, a transmembrane E3 ubiquitin ligase that resides in the endoplasmic reticulum and inner nuclear membrane. The removal of N-terminal Met by Met aminopeptidases generates N-terminal residues that are often N-terminally acetylated. Doa10 selectively binds to the resulting N-degrons, which may represent the most prevalent class of cellular protein degradation signals.

2D Quantum Critical Transitions

Quantum critical transitions occur at near-zero temperatures when the properties of quantum matter are tuned by an external parameter such as the magnetic field or pressure. Heavy fermion materials, which have effective charge carrier masses hundreds of times heavier than the bare electron mass, have emerged as a prototypical system for studying these transitions. Now, **Shishido *et al.*** (p. 980; see the Perspective by **Coleman**) use a heavy fermion compound to experimentally realize a new type of quantum phase transition where the tuning parameter is the dimensionality of the system. They engineer a family of superlattices made up of a fixed number of layers of the conventional metal $LaIn_3$ and varying numbers of layers of the heavy fermion material $CeIn_3$. As the number of layers of $CeIn_3$ is decreased, the system gradually changes character from three- to two-dimensional, with corresponding changes in its transport properties.

Detecting Distant Planets

More than 400 planets have been detected outside the solar system, most of which have masses similar to that of the gas giant planet, Jupiter. **Borucki *et al.*** (p. 977, published online 7 January) summarize the planetary findings derived from the first six weeks of observations with the Kepler mission whose objective is to search for and determine the frequency of Earth-like planets in the habitable zones of other stars. The results include the detection of five new exoplanets, which confirm the existence of planets with densities substantially lower than those predicted for gas giant planets.

Silicate in the Primordial Soup

Direct evidence for how prebiotic synthesis of complex organic molecules paved the way for the origin of life is extremely scarce. Thus, studies are mainly limited to controlled simulations of likely reactions in early Earth conditions. Similarly, chemical reactions in the laboratory may generate the products necessary for biosynthesis, but may nevertheless be geochemically irrelevant. **Lambert *et al.*** (p. 984) show that silicate ions, present in Earth's surface waters at relatively high concentrations, catalyze the formation of four- and six-carbon sugars from simple sugars via the formose reaction. The resulting complexes stabilize the sugar molecules, allowing sugars to accumulate in greater abundance. Silicate stabilization also circumvents the need for the formose reaction to proceed at high temperatures, thus extending the range of possible environments in which life could have originated.

Acid Assistance

Protons are quite versatile catalysts of organic reactions, but because they are achiral, they cannot induce stereoselectivity on their own. One productive way around this problem has been to use chiral conjugate bases and perform reactions in media where the bases remain tightly attracted to protonated substrates. **Xu *et al.*** (p. 986; see the Perspective by **Schreiner**) thoroughly explored the mechanism of an alternative approach, in which an achiral acid was used in conjunction with a second, chiral molecule (a urea derivative) for catalysis. High selectivity was attained with this method in the coupling of aryl imines with olefins. Extensive kinetic and computational studies showed that the acid and its chiral partner acted cooperatively in binding the substrates, optimizing the tradeoff between speed and selectivity.

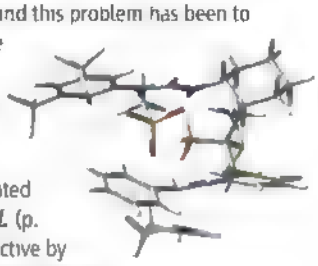

Metabolic Regulation Through Acetylation

Covalent modification of lysine residues in various proteins in the nucleus is a recognized mechanism for control of transcription. Now two papers suggest that acetylation may represent an

Continued on page 919

CREDITS (TOP TO BOTTOM): © ROBERT NICHOLLS, PALAEOCREATIONS; XU ET AL.

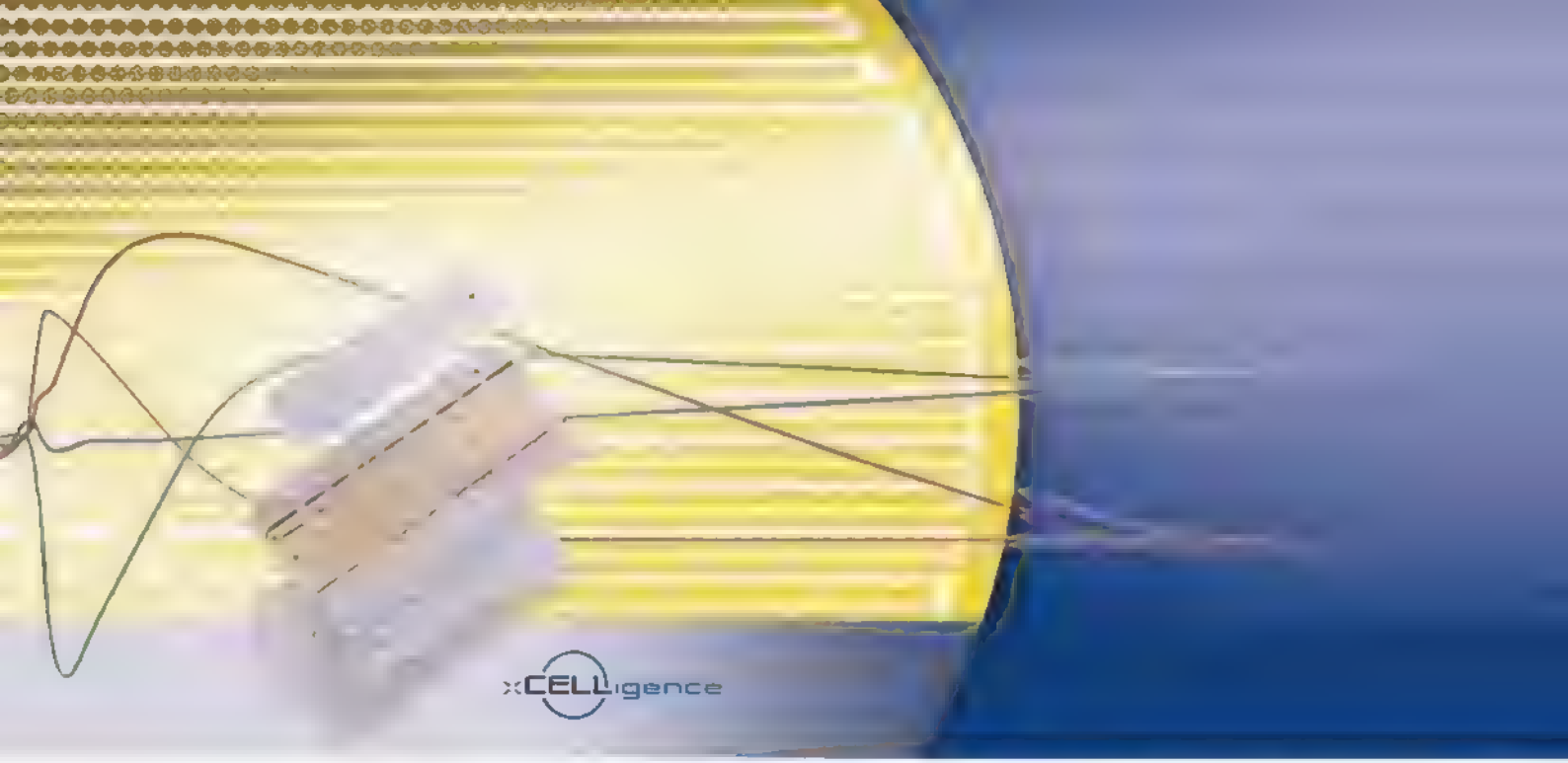

xCELLigence System: CIM-Plate 16

Monitor Cell Migration in Real-Time

Exceed the Limits of Cellular Analysis

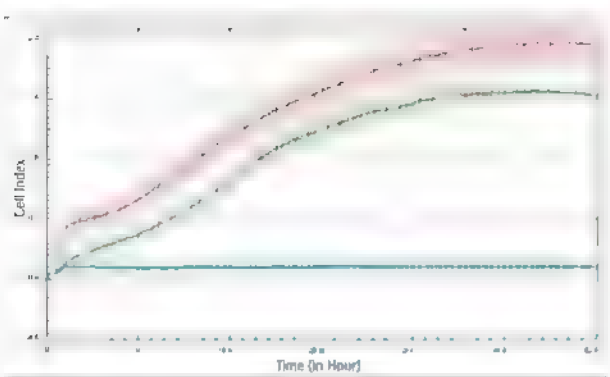

Continuous monitoring of HT1080 cell migration using a fibronectin-coated CIM-Plate 16 with 10% serum serving as the chemoattractant in the lower chamber.
Cells in fibronectin-coated wells (**red** trace) show enhanced migration compared to cells grown without fibronectin-coating (**green** trace). Cells maintained in serum-free media served as a control (**blue** trace).

Take a step forward in cancer research with the new CIM-Plate 16 for the xCELLigence System, featuring electronic sensing to directly study cell migration and invasion. Replace exogenous labeling with impedance-based technology.

- **Monitor cell invasion and migration continuously in real-time** over the entire time course of the experiment
- **Obtain unbiased data using label-free measurements** that do not perturb cells
- **Experience the full flexibility of the RTCA DP Instrument:** Combine E-Plate 16 to measure cell proliferation and CIM-Plate 16 to quantify cell migration and invasion

Go beyond techniques requiring cell labeling. Focus on physiologically relevant cell responses using the xCELLigence System – now with cell invasion and migration electronic sensing.

For more information, visit: **www.xcelligence.roche.com**

ACEA BIOSCIENCES, INC.

Roche Diagnostics GmbH
Roche Applied Science
Werk Penzberg
82372 Penzberg, Germany

Roche

Continued from page 917

important regulatory mechanism controlling the function of metabolic enzymes (see the Perspective by **Norvell and McMahon**). **Zhao *et al.*** (p. 1000) found that a large proportion of enzymes in various metabolic pathways were acetylated in human liver cells. Acetylation regulated various enzymes by distinct mechanisms, directly activating some, inhibiting one, and controlling the stability of another. Control of metabolism by acetylation appears to be evolutionarily conserved: **Wang *et al.*** (p. 1004) found that the ability of the bacterium *Salmonella enterica* to optimize growth on distinct carbon sources required differential acetylation of key metabolic enzymes, thus controlling flux through metabolic pathways.

Cropland Acidification in China

China is experiencing increasing problems with acid rain, groundwater pollution, and nitrous oxide emissions. Rapid development of industry and transportation has accelerated nitrate (N) emissions to the atmosphere. Consequently, soil degradation, water shortage, and pollution, in addition to atmospheric quality decline are becoming major public concerns across China. Since the 1990s, China has become both the largest consumer of chemical N fertilizers and the highest cereal producer in the world, which has consequences for arable soil acidification. **Guo *et al.*** (p. 1008, published online 11 February) present a meta-analysis of a regional acidification phenomenon in Chinese arable soils that is largely associated with higher N fertilization and higher crop production. Such large-scale soil acidification is likely to threaten the sustainability of agriculture and affect the biogeochemical cycles of nutrients and also toxic elements in soils.

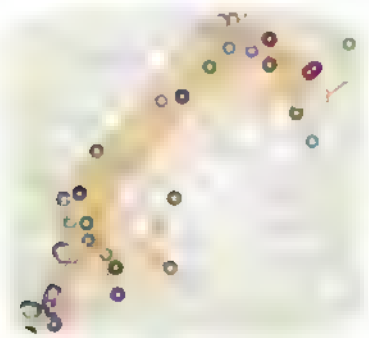

Predictable Travel Routines

While people rarely perceive their actions to be random, current models of human activity are fundamentally stochastic. Processes that rely on human mobility patterns, like the prediction of new epidemics, traffic engineering, or city planning, could benefit from highly accurate predictive models. To investigate the predictability of human dynamics, **Song *et al.*** (p. 1018) used the recorded trajectories of millions of mobile phone users, collected by mobile phone companies and anonymized for research purposes. They hypothesized that given the wide range of travel patterns that different users follow, there would be significant differences between their predictability as well: Users who travel less should be easier to predict than those who are constantly on the road. Surprisingly, there was 93% predictability across the whole user base, and individuals' predictability did not in general fall significantly below 80%.

Killing *Pseudomonas*

Gram-negative *Pseudomonas* bacteria are opportunistic pathogens, and drug-resistant strains present a serious health problem. **Srinivas *et al.*** (p. 1010) synthesized a family of peptidomimetic antibiotics that is active only against *Pseudomonas*. These antibiotics do not lyse the cell membrane, but instead target an essential outer membrane protein, LptD, which plays a role in the assembly of lipopolysaccharide in the outer cell membrane. Activity in a mouse infection model suggests that the antibiotics might have therapeutic potential. In addition, LptD is widely distributed in gram-negative bacteria and so its validation as a target has the potential to drive development of antibiotics with a broader spectrum of activity against gram-negative pathogens.

Examining the Backbone

Determination of tertiary protein structures by nuclear magnetic resonance (NMR) currently relies heavily on side-chain NMR data. The assignment of side-chain atoms is challenging. In addition, proteins larger than 15 kilodaltons (kD) must be deuterated to improve resolution and this eliminates the possibility of measuring long-range interproton distance constraints. Now **Raman *et al.*** (p. 1014, published online 4 February) use backbone-only NMR data—chemical shifts, residual dipolar coupling, and backbone amide proton distances—available from highly deuterated proteins to guide conformational searching in the Rosetta structure prediction protocol. Using this new protocol, they were able to generate accurate structures for proteins of up to 25 kD.

CREDIT: SONG ET AL.

Rare Mutation Matters!

Find it by deep sequencing of whole exome or candidate genes

BGI'S GENOMICS BAR

华大基因 BGI
tech@genomics.cn
www genomics cn
86-755-25273395

Would 128 Illumina HiSeq 2000 Sequencing Systems, 500 bioinformaticians and the use of cutting-edge software programs developed by BGI satisfy your taste?

One of the world's biggest genome centers is looking for collaborators!

Peter Agre is the president of AAAS and director of the Malaria Research Institute at Johns Hopkins University.

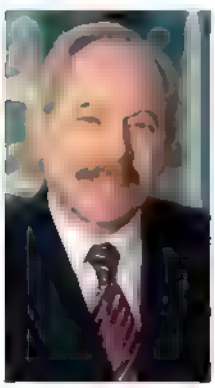

Alan I. Leshner is the chief executive officer of AAAS and executive publisher of *Science*.

Bridging Science and Society

THE THEME OF THIS YEAR'S ANNUAL MEETING OF THE AMERICAN ASSOCIATION FOR THE ADVANCEMENT of Science (AAAS) seems especially timely: Bridging Science and Society. Virtually every major issue now confronting society has a science and technology component, and this means that "the need for general scientific understanding by the public has never been larger, and the penalty for scientific illiteracy never harsher."* Today, science and technology are receiving unprecedented financial and policy support worldwide, as more countries invest in science and science education with the belief that these investments will enhance economic strength and improve the lives of their citizens. In the United States, the current national leadership frequently focuses on science, science education, and science-based policy-making. As well, the U.S. National Science Board just reported in *Science Indicators 2010* that the general citizenry continues to hold scientists in high regard, second only to firefighters in prestige. But this confidence and prestige depend on a belief in the integrity and credibility of science, as well as in the scientific community's ability to help solve global problems. A spate of recent incidents has threatened the public's trust and argues that greater attention is essential to maintaining a strong bridge between science and the rest of society.

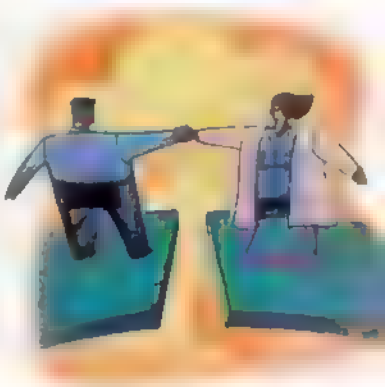

The ability of science to deliver on its promise of practical and timely solutions to the world's problems does not depend solely on research accomplishments but also on the receptivity of society to the implications of scientific discoveries. That receptivity depends on the public's attitude about what science is finding and on how it perceives the behavior of scientists themselves. The past decade saw substantial tension in the science/society relationship emerge when scientific advances and theories conflicted with certain cultural values or religious beliefs. Much of the turmoil surrounding the teaching of evolution in public schools, for example, derives from conflict between a modern understanding of evolution and religious beliefs in creation. Likewise, objections to embryonic stem cell research arise from the belief of some religions that life begins at the moment of conception. These kinds of tensions are best addressed by engaging with the public on the issues and seeking common ground whenever possible. This approach requires scientists to listen and respond to the public's concerns and to educate their fellow citizens about scientific advances. Public engagement is increasingly being facilitated by governmental and nongovernmental institutions, and it has become a high priority for many individual scientists around the world. A focus on creating a genuine dialogue has consistently been more productive than unidirectional attempts at "public education" about science.

Inappropriate behavior by scientists also weakens the bridge between science and society, at times to a degree out of proportion to the incidents. Widely publicized examples of scientific misconduct, or even mere accusations of misconduct, can tarnish the image and diminish the credibility of the entire scientific enterprise. Likewise, undisclosed conflicts of interest, whether real or apparent, can call into question the integrity of the whole scientific community. Scientists also jeopardize the credibility of science by overinterpreting or misstating scientific facts. Recent examples include misinformation on the prospects of Himalayan glaciers and the effects of climate change there, and newly discovered problems with a 1998 report linking vaccines to autism. These types of revelations are highly problematic for policy-makers, the public, and the scientific community. Every such case should be investigated, with a follow-up public explanation. Scientists should not tolerate threats to the integrity of science, whether they come from outside the scientific community or from within it.

The scientific community can strengthen the bridge between science and society by ensuring vigorous enforcement of scientific behavioral norms and standards, aggressively focusing on problems of global importance, and actively engaging with the public. As scientists and policy-makers convene in San Diego this week at the AAAS meeting, we all should commit to pursuing these goals.

– Peter Agre and Alan I. Leshner

10.1126/science.1188231

*P. Agre, Nobel Banquet Speech, 2003, http://nobelprize.org/nobel_prizes/chemistry/laureates/2003/agre-speech.html.

CREDITS: (TOP LEFT) JOHNS HOPKINS MALARIA RESEARCH INSTITUTE; (BOTTOM LEFT) MICHAEL J. COLELLA/COLELLA PHOTOGRAPHY; (RIGHT) DAVID TILLINGHAST/GETTY IMAGES

Only days left until bio begins

www.wherebiobegins.com

ASTRONOMY

View from the Ground

Over the past few years, space telescopes have enabled scientists to study the atmospheres of planets outside our solar system. Two studies now show that ground-based telescopes can also be put to this use. Swain *et al.* used NASA's Infrared Telescope Facility in Hawaii to collect spectra of HD 189733b, a hot Jupiter-like planet 63 light-years away from Earth. Water, carbon dioxide, and methane had been detected already in its atmosphere. The new ground-based observations suggest fluorescent emission from methane, similar to that detected from Jupiter, Saturn, and Titan; thus the atmosphere of this planet is more complex than previously thought. In a separate study, Janson *et al.* used the Very Large Telescope in Chile to acquire a spectrum of one of the three known giant planets orbiting around the star HR 8799. This planetary system, located 130 light-years from Earth, had been directly detected in images taken with the Keck and Gemini telescopes in 2008. Likewise, the spectrum of HR 8799c, a planet 10 times more massive than Jupiter, was obtained directly, without the need to rely on a transit to separate the light of the planet from that of the star. Current theoretical models cannot reproduce the spectrum of this planet, underscoring the limitations of our current understanding of exoplanetary atmospheres. — MJC

Nature **463**, 637 (2010); *Astrophys. J.* **710**, L35 (2010).

ECONOMICS

Increasing Turnover

Used car salesmen and yard sale bargain hunters depend on secondary markets, in which the seller of a good is not the first to have sold the good. These markets are crucial for the efficient reallocation of resources to meet changing demands. Yet regulations on the use and trade of some goods can influence the efficiency with which a secondary market functions. Such is the case with the U.S. wireless spectrum market. Much has been written about the Federal Communications Commission's (FCC's) use of auctions to make initial allocations of bandwidth, less is known about how licenses are later bought and sold. Mayo and Wallsten analyzed FCC records on license transfer since 1994 to assess how regulatory control and approval processes influenced the emergence and function of a secondary spectrum market. Their findings suggest that steps taken by the FCC in the early 2000s to improve secondary markets have had a positive impact. The volume of trading has become comparable to the volume of initial allocations. Also, the average time needed to approve trades has diminished from 150 days for a personal communications service license in 1998 to less than 50 days in 2005. — BW

CREDITS (TOP TO BOTTOM): VINETTE COOK/GEMINI OBSERVATORY/ISTOCKPHOTO.COM

Inf. Econ. Policy **22**, 10.1016/j.infoecopol.2009.12.005 (2010)

CHEMISTRY

Make or Break

In the past several years, increasingly selective chemical methods have emerged to append different groups to specific sites along the periphery of aromatic rings. Two recent studies focus instead on manipulating the ring framework itself. Donohoe and Bower show that a widely used olefin metathesis catalyst can direct the formation of furan rings by stitching together an enone and an allylic alcohol. An advantage of this process is the ease with which diverse functional groups can be introduced through substitution of the precursors. The immediate product of metathesis is pushed along to the final aromatic cycle by either a separate acid catalyst or a Heck protocol that appends an additional aryl substituent.

Sattler and Parkin work from the other end of the spectrum, showing that an intact quinoxaline falls rather dramatically apart on contacting a tungsten complex. Aromatic carbon bonds are among the strongest in organic molecular skeletons, yet in this product—formed at 90°C and characterized crystallographically—two carbon atoms previously bounding an edge of the ring are separated and linked independently to the tungsten center. Their hydrogen substituents are also lost in the process. Though the mechanism remains uncertain, the authors postulate that insertion of the tungsten into the C-H bonds precedes C-C scission. — JSY

Proc. Natl. Acad. Sci. U.S.A. **107**, 10.1073/pnas.0913466107 (2010); *Nature* **463**, 523 (2010)

APPLIED PHYSICS

Remember, Repeat After Me

Quantum information processors in which information is encoded in single photons require the development of multiple components, to generate the single photons, store them, and then reliably read them from mem-

Continued on page 925

ESOF2010 EUROSCIENCE OPEN FORUM

On July 2-7, 2010, Torino, Italy, will host the fourth edition of ESOF

ESOF - Euroscience Open Forum - is an international meeting held every two years dedicated to scientific research and innovation. It was designed by Euroscience as a unique opportunity to present and discuss the frontiers of scientific and technological advancement, the relationship between science and society and the policies supporting research.

Close encounters with top scientists

Conferences, workshops and keynote lectures (part of the **Scientific Programme**) will be held at the impressive Lingotto venue, where the **Exhibition** will also be set up. There will also be plenty of activities specifically dedicated to young researchers (**Career Programme**) and potential entrepreneurs and investors in highly innovative businesses (**Science to Business Programme**). In addition, Torino will showcase many original events aimed at the general public (**Science in the City Programme**), held in historical palaces, squares and streets of the city.

The Scientific Programme: main features at Torino

We have chosen **ten main themes** as a focus for debate:

- Sustainable living and moving
- Evolution, development and adaptation of organisms
- Moving into and up from our quantum world
- Responding to global needs
- Frontiers in energy research
- Science, knowledge, and belief
- Memory and learning in organisms, social and artificial systems
- Languages, cultures, and variability
- Integrating science with health care
- Policies - what follows?

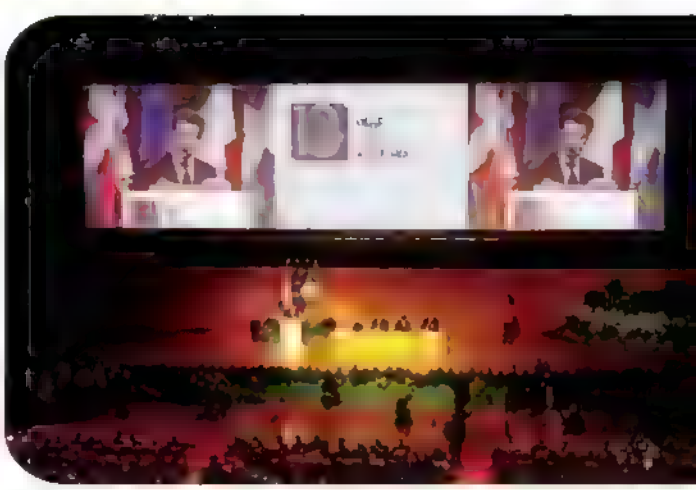

The Scientific Programme at a glance

105 sessions, 454 speakers from 39 countries, 7 Nobel laureates among the speakers: 1 Opening Lecture by **Julia Fischer**, 4 Plenary Lectures by **Peter Agre**, **Kurt Wüthrich**, **Ada Yonath** and **Anton Zeilinger**, 18 Keynote Lectures by prominent scientists.

ESOF2010 is organized by TopESOF - Torino per ESOF2010, an association set up by

COMPAGNIA di San Paolo · Agorà Scienza · Città della Scienza

Continued from page 923

ory and pass them on. Light, however, is always on the move, usually quickly, and so solid-state quantum memories represent a crucial component, as they would allow the bits of information to be stored while other bits can be manipulated. Afzelius *et al.* present a solid-state quantum memory in which an absorbed photon is stored as an electronic excitation within a rare earth ion–doped crystal. The energy levels and optical transitions of the crystal can be controlled and manipulated by a series of laser pulses, so that the absorbed photon can be stored for several tens of microseconds. The process can then be reversed to retrieve the photon from the stored electronic state. Such a robust on-demand quantum memory and repeater should prove invaluable for long-distance quantum communication networks. — ISO

Phys. Rev. Lett. **104**, 40503 (2010).

DEVELOPMENT

The Fantastic Fourth No Longer

The number of exogenously expressed factors that can reprogram somatic cells into what are called induced pluripotent stem cells (iPSCs) has grown over the past 3 years. The original quartet of transcription factors—Oct4, Sox2, Klf4, and c-Myc—heads a list that includes familial relatives of the last three and other proteins such as the transcription factor Nanog and the RNA-binding protein Lin28. Oct4 had appeared to be indispensable and thus had been considered an essential part of the reprogramming code.

However, Heng *et al.* report that Oct4 can be replaced. They screened 19 nuclear receptors and found that exogenous expression of the nuclear receptor Nr5a2 in mouse embryonic fibroblasts could enhance reprogramming efficiency by a factor of 4 as compared to the famous four factors alone. Moreover, Nr5a2 could in fact replace Oct4 and act with Sox2, Klf4, and c-Myc to reprogram somatic cells. The gene expression and chromatin modification profiles of these iPSCs (like the iPSCs generated by expression of the original four factors) were more similar to those of embryonic stem cells than those of mouse embryonic fibroblasts. Furthermore, the target genes of Nr5a2 overlap with targets of Sox2 and Klf4 that are important in embryonic stem cell identity, such as Nanog. — LDC

Cell Stem Cell **6**, 167 (2010)

CELL BIOLOGY

One-Way Ticket

Within the nucleus, chromatin is spatially organized, and the intranuclear locations of genes can be correlated with their transcriptional activity. Ahmed *et al.* have identified two DNA sequences in chromatin that target genomic loci to the nuclear envelope in yeast. Peripheral targeting of genes, particularly those activated by stresses such as heat shock or nutrient deprivation, such as *INO1*, is linked to active transcription. Using deletion analyses and engineered plasmids, the authors identified an eight-base sequence in the promoter of *INO1*, that when mutated, inhibited targeting of ectopic *INO1* to the nuclear periphery, as well as its transcriptional activation. They also identified several protein components of the nuclear pore complex (the exit channels from the nucleus to the cytoplasm) that were required for this localization. For peripheral targeting of the endogenous *INO1* gene, a second sequence in an upstream gene was also required. Searching through the genome, the authors identified 94 promoters that contained the eight-base targeting sequence, many of which were activated by heat shock, suggesting a common mechanism of activation and peripheral localization. — HP

Nat. Cell Biol. **12**, 111 (2010).

MOLECULAR BIOLOGY

An RNA Mimic of DNA

RNAs—of the types known in the classical world as ribosomal, transfer, and messenger—are critical for the readout of DNA sequence into protein. On the other hand, numerous regulatory processes are governed by the modern upstarts known collectively as noncoding RNAs. Kino *et al.* have used a yeast two-hybrid screen to search for genes encoding binding partners for the DNA binding domain of the human glucocorticoid receptor and come upon a noncoding RNA known as growth arrest–specific (Gas) 5, so-called because this single-stranded RNA accumulates in cells exposed to conditions that prevent growth. The glucocorticoid receptor is a ligand-activated transcription factor, and Gas5 binds to the receptor, inhibiting its ability to activate its target genes. The authors propose that a portion of the Gas5 RNA may mimic the glucocorticoid receptor binding site in DNA, establishing another means of modulating the transcriptional activities of nuclear receptors. — LBR

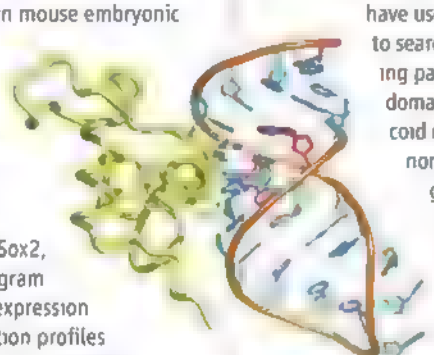

CREDIT: KINO ET AL., SCI. SIG. 3, RA8 (2010)

Sci. Sig. **3**, ra8 (2010)

www.sciencemag.org

Science

1200 New York Avenue, NW
Washington, DC 20005
Editorial: 202-326-6550, FAX 202-289-7562
News: 202-326-6581, FAX 202-371-9227

Bateman House, 82-88 Hills Road
Cambridge, UK CB2 1LQ
+44 (0) 1223 326500, FAX +44 (0) 1223 326501

Subscription Services For change of address, missing issues, new orders and renewals, and payment questions: 866-434-AAAS (2227) or 202-326-6417, FAX 202-842-1065. Mailing addresses: AAAS, P.O. Box 96178, Washington, DC 20090-6178 or AAAS Member Services, 1200 New York Avenue, NW, Washington, DC 20005

Institutional Site Licenses please call 202-326-6755 for any questions or information.

Reprints: Author Inquiries 800-635-7181
Commercial Inquiries 803-359-4578

Permissions 202-326-7074, FAX 202-682-0816

Member Benefits AAAS/Barnes&Noble.com bookstore www.aaas.org/bn; AAAS Online Store www.apisource.com/aaas/ code MKB6; AAAS Travel: Betchart Expeditions 800-252-4910, Apple Store www.wapple/eppstore/aaas; Bank of America MasterCard 1-800-833-6262 priority code FAA3YU, Cold Spring Harbor Laboratory Press Publications www.cshlpress.com/affiliates/aaas.htm, GEICO Auto Insurance www.geico.com/landingpage/go51.htm?logo=17624, Hertz 800-654-2200 CDP#343457, Office Depot https://bsd.officedepot.com/portal_login.do; Seabury & Smith Life Insurance 800-424-9883, Subaru VIP Program 202-326-6417; VIP Moving Services www.vipmayflower.com/domestic/index.html, Other Benefits: AAAS Member Services 202-326-6417 or www.aaasmember.org.

science_editors@aaas.org	(for general editorial queries)
science_letters@aaas.org	(for queries about letters)
science_reviews@aaas.org	(for returning manuscript reviews)
science_bookrevs@aaas.org	(for book review queries)

Published by the American Association for the Advancement of Science (AAAS). *Science* serves its readers as a forum for the presentation and discussion of important issues related to the advancement of science, including the presentation of minority or conflicting points of view, rather than by publishing only material on which a consensus has been reached. Accordingly, all articles published in *Science*—including editorials, news and comment, and book reviews—are signed and reflect the individual views of the authors and not official points of view adopted by AAAS or the institutions with which the authors are affiliated.

AAAS was founded in 1848 and incorporated in 1874. Its mission is to advance science, engineering, and innovation throughout the world for the benefit of all people. The goals of the association are to: enhance communication among scientists, engineers, and the public; promote and defend the integrity of science and its use; strengthen support for the science and technology enterprise; provide a voice for science on societal issues; promote the responsible use of science in public policy; strengthen and diversify the science and technology workforce; foster education in science and technology for everyone; increase public engagement with science and technology; and advance international cooperation in science.

Information for Authors
See pages 352 and 353 of the 15 January 2010 issue or access www.sciencemag.org/about/authors

EDITOR-IN-CHIEF **Bruce Alberts**
EXECUTIVE EDITOR **Monica M. Bradford** NEWS EDITOR **Colin Norman**
MANAGING EDITOR, RESEARCH JOURNALS **Katrina L. Kelner**
DEPUTY EDITORS **R. Brooks Hanson, Barbara R. Jasny, Andrew M. Sugden**

Editorial SENIOR EDITOR/PERSPECTIVES Lisa D. Chong; SENIOR EDITORS Gilbert J. Chin, Pamela J. Hines, Paula A. Kiberstis (Boston), Marc S. Lavine (Toronto), Beverly A. Purnell, L. Bryan Ray, Guy Riddihough, H. Jesse Smith, Phillip D. Szuromi (Tennessee), Valda Vinson. ASSOCIATE EDITORS Kristen L. Mueller, Jake S. Yeston, Laura M. Zahn; ONLINE EDITOR Stewart Wills, ASSOCIATE ONLINE EDITORS Robert Frederick, Tara S. Marathe; WEB CONTENT DEVELOPER Marlyn Green; BOOK REVIEW EDITOR Sherman J. Suter; ASSOCIATE LETTERS EDITOR Jennifer Sills; EDITORIAL MANAGER Cara Tate; SENIOR COPY EDITORS Jeffrey E. Cook, Cynthia Howe, Harry Jach, Barbara P. Ordway, Trista Wagoner; COPY EDITORS Chris Filsaime, Lauren Kmec; EDITORIAL COORDINATORS Carolyn Kyle, Beverly Shields; PUBLICATIONS ASSISTANTS Ramatoulaye Diop, Carlos L. Durham, Joi S. Granger, Jeffrey Hearn, Lisa Johnson, Scott Miller, Jerry Richardson, Jennifer A. Seibert, Brian White, Anita Wynn; EDITORIAL ASSISTANTS Emily Guise, Michael Hicks, Patricia M. Moore; EXECUTIVE ASSISTANT Sylvia S. Kihara; ADMINISTRATIVE SUPPORT Maryrose Madrid

News DEPUTY NEWS EDITORS Robert Coontz, Eliot Marshall, Jeffrey Mervis, Leslie Roberts; Contributing Editors Elizabeth Culotta, Polly Shulman; NEWS WRITERS Yudhijit Bhattacharjee, Adrian Cho, Jennifer Couzin, David Grimm, Constance Holden, Jocelyn Kaiser, Richard A. Kerr, Eli Kintisch, Andrew Lawler (New England), Greg Miller, Elizabeth Pennisi, Robert F. Service (Pacific NW), Erik Stokstad; INTERN Jackie D. Grom; CONTRIBUTING CORRESPONDENTS Dan Charles, Jon Cohen (San Diego, CA), Daniel Ferber, Ann Gibbons, Robert Koenig, Mitch Leslie, Charles C. Mann, Virginia Morell, Evelyn Strauss, Gary Taubes; COPY EDITORS Linda B. Felaco, Melvin Gatling, Melissa Raimondi; ADMINISTRATIVE SUPPORT Scherraine Mack, Fannie Groom; BUREAUS New England: 207-549-7755, San Diego, CA: 760-942-3252, FAX 760-942-4979, Pacific Northwest: 503-963-1940

Production DIRECTOR James Landry; SENIOR MANAGER Wendy K. Shank; ASSISTANT MANAGER Rebecca Doshi; SENIOR SPECIALISTS Steve Forrester, Chris Redwood; SPECIALIST Anthony Rosen, PREFLIGHT DIRECTOR David M. Tompkins, MANAGER Marcus Spiegler; SPECIALIST Jason Hillman

Art DIRECTOR Yael Kats, ASSOCIATE ART DIRECTOR Laura Creveling; ILLUSTRATORS Chris Bickel, Katharine Sutliff; SENIOR ART ASSOCIATES Holly Bishop, Preston Huey, Nayomi Kevitiyagala; ART ASSOCIATE Jessica Newfield, PHOTO EDITOR Leslie Shizard

Science International
Europe (science@science-int.co.uk) EDITORIAL: INTERNATIONAL MANAGING EDITOR Andrew M. Sugden; SENIOR EDITOR/PERSPECTIVES Julia Fahrenkamp-Uppenbrink; SENIOR EDITORS Caroline Ash, Stella M. Hurtley, Ian S. Osborne, Peter Stern, ASSOCIATE EDITOR Maria Cruz; LOCUM EDITOR Helen Packer-sgill; EDITORIAL SUPPORT Deborah Dennison, Rachel Roberts, Alice Whaley; ADMINISTRATIVE SUPPORT John Cannell, Janet Clements; NEWS: EUROPE NEWS EDITOR John Travis; DEPUTY NEWS EDITOR Daniel Clery; CONTRIBUTING CORRESPONDENTS Michael Balter (Paris), John Bohannon (Vienna), Martin Enserink (Amsterdam and Paris), Gretchen Vogel (Berlin); INTERN Claire Thomas

Asia Japan Office: Asca Corporation, Eiko Ishioka, Fusako Tamura, 1-8-13, Hirano-cho, Chuo-ku, Osaka-shi, Osaka, 541-0046 Japan; +81 (0) 6 6202 6272, FAX +81 (0) 6 6202 6271, asca@os.gulf.or.jp; ASIA NEWS EDITOR Richard Stone (Beijing: rstone@aaas.org); CONTRIBUTING CORRESPONDENTS Dennis Normile (Japan: +81 (0) 3 3391 0630, FAX +81 (0) 3 5936 3531, dnormile@gol.com); Hao Xin (China: +86 (0) 10 6307 4439 or 6307 3676, FAX +86 (0) 10 6307 4358, cindyhao@gmail.com); Pallava Bagla (South Asia: +91 (0) 11 2271 2896, pbagla@vsnl.com)

EXECUTIVE PUBLISHER **Alan I. Leshner**
Publisher **Beth Rosner**

Fulfillment Systems and Operations (membership@aaas.org); DIRECTOR Waylon Butler; SENIOR SYSTEMS ANALYST Jonny Blaker; CUSTOMER SERVICE SUPERVISOR Pat Butler; SPECIALISTS Latoya Casteel, LaVonda Crawford, Vicki Linton, April Marshall; DATA ENTRY SUPERVISOR Cynthia Johnson; SPECIALISTS Emtou Bowden, Tarrika Hill, William Jones

Business Operations and Administration DIRECTOR Deborah Rivera-Wienhold; ASSISTANT DIRECTOR, BUSINESS OPERATIONS Randy Yi; MANAGER, BUSINESS ANALYSIS Michael LoBue; MANAGER, BUSINESS OPERATIONS Jessica Tierney; FINANCIAL ANALYSTS Priti Parmar, Celeste Troxler; RIGHTS AND PERMISSIONS: ADMINISTRATOR Emilie David; ASSOCIATE Elizabeth Sandler; MARKETING DIRECTOR Ian King; MARKETING MANAGER Allison Pritchard; MARKETING ASSOCIATES Aimee Aponte, Alyson Chandler, Mary Ellen Crowley, Julianne Wielga, Wendy Wise; MARKETING EXECUTIVE Jennifer Reeves; MARKETING/MEMBER SERVICES EXECUTIVE Linda Rusk; DIRECTOR, SITE LICENSING Tom Ryan; DIRECTOR, CORPORATE RELATIONS Eileen Bernadette Moran; PUBLISHER RELATIONS, E-RESOURCES SPECIALIST Kiki Forsythe; SENIOR PUBLISHER RELATIONS SPECIALIST Catherine Holland; PUBLISHER RELATIONS, EAST COAST Phillip Smith; PUBLISHER RELATIONS, WEST COAST Philip Tsolakidis; FULFILLMENT SUPERVISOR Iquo Edim; FULFILLMENT COORDINATOR Laura Clemens; ELECTRONIC MEDIA: MANAGER Lizabeth Harman; PROJECT MANAGER Trista Snyder; ASSISTANT MANAGER Lisa Stanford; SENIOR PRODUCTION SPECIALISTS Christopher Coleman, Walter Jones; PRODUCTION SPECIALISTS Nichele Johnston, Kimberly Oster

Advertising DIRECTOR, WORLDWIDE AD SALES Bill Moran

Product (science_advertising@aaas.org); MIDWEST/WEST COAST/W. CANADA Rick Bongiovanni: 330-405-7080, FAX 330-405-7081; EAST COAST/E. CANADA Laurie Faraday: 508-747-9395, FAX 617-507-8189; UK/EUROPE/ASIA Roger Goncalves: TEL/FAX +41 43 243 1358; JAPAN Mashy Yoshikawa: +81 (0) 3 3235 5961, FAX +81 (0) 3 3235 5852; SENIOR TRAFFIC ASSOCIATE Delandra Simms

Commercial Editor Sean Sanders, 202-326-6430

Project Director, Outreach Brianna Blaser

Classified (advertise@sciencecareers.org) U.S.: SALES MANAGER Daryl Anderson: 202-326-6543; SENIOR SALES REPRESENTATIVE Tina Burks: 202-326-6577, KEY ACCOUNT MANAGER/MIDWEST Jonbah Abte: EAST COAST Alexis Fleming: 202-326-6578; WEST/SOUTH CENTRAL Nicholas Hintibidze: 202-326-6533; SALES COORDINATORS Rohan Edmonson, Shirley Young; INTERNATIONAL: SALES MANAGER Tracy Holmes, +44 (0) 1223 326525, FAX +44 (0) 1223 326532; SALES Susanne Kharraz, Dan Pennington, Alex Palmer; SALES ASSISTANT Louise Moore; JAPAN Mashy Yoshikawa +81 (0) 3 3235 5961, FAX +81 (0) 3 3235 5852; ADVERTISING SUPPORT MANAGER Karen Foote: 202-326-6740; ADVERTISING PRODUCTION OPERATIONS MANAGER Deborah Tompkins; SENIOR PRODUCTION SPECIALIST/GRAPHIC DESIGNER Amy Hardcastle; SENIOR PRODUCTION SPECIALIST Robert Buck; SENIOR TRAFFIC ASSOCIATE Christine Hall; PUBLICATIONS ASSISTANT Mary Lagnaoui

AAAS Board of Directors RETIRING PRESIDENT, CHAIR James J. McCarthy; PRESIDENT Peter C. Agre; PRESIDENT-ELECT Alice Huang; TREASURER David E. Shaw; CHIEF EXECUTIVE OFFICER Alan I. Leshner; BOARD Alice Gast, Linda P. B. Katehi, Nancy Knowlton, Cherry A. Murray, Julia M. Phillips, Thomas D. Pollard, David S. Sabatini, Thomas A. Woolsey

AAAS
ADVANCING SCIENCE, SERVING SOCIETY

EDITED BY JOCELYN KAISER

Food and Flying

German scientists have figured out why tomato juice tastes better aboard an airplane than on the ground (and coffee tastes worse). Low atmospheric pressure dampens the experience of sweet and salty tastes whereas sour comes through unchanged and bitter is slightly intensified, says flavor chemist Andrea Burdack-Freitag of the Frauenhofer Institute for Building Physics in Holzkirchen.

She and her colleagues asked 30 taste testers to rate their perceptions of different foods and wine while sitting in a partial Airbus A310 in a chamber with adjustable pressure. At ground pressures, tasters perceived tomato juice as musty, but at a low pressure typical in flight they found it fruitier, with cool notes. The complex aromas picked up by the nose that give coffee its flavor were barely perceived at low pressure, unmasking caffeine's bitterness, Burdack-Freitag says. Lufthansa's catering arm, which sponsored the study, wants to use the data to improve its menus.

Elephant Gears

How does an elephant shift up to 5 tons of bulk with each step? To find out, researchers in Thailand had trainers ride 34 elephants down 8 meters of force-sensing plates at different speeds. Combining the data with video, the researchers mapped out the force the elephants exerted on the ground at each point in their stride.

An elephant hits the ground with at most 1.4 times its body weight, the team reports in the current *Journal of Experimental Biology*. By comparison, a human runner exerts peak forces of three times his or her body weight. And even at top speed, an elephant's center of mass moves up and down a centimeter. " 'Glide'? No, that's not the right word," says lead author Norman Heglund, a biomechanics expert at the Catholic University of Louvain in Belgium. But it's close.

"The fact that they were able to set up force plates with elephants and get data this good is really mind-boggling," says Daniel Schmitt, an expert in primate and animal locomotion at Duke University in Durham, North Carolina.

The table manners of false killer whales put ours to shame. Once they've caught a fish, each whale politely takes a bite and passes it on to another. If there's a human nearby, he or she will be offered some, too. Dan McSweeney once had half a large tuna handed to him by a 5-meter-long false killer whale. "I pushed it back. He took it and started chewing on it and then left. It was one of those magical moments," says McSweeney of the Wild Whale Research Foundation in Hawaii.

Their compulsive food sharing is one trait that has endeared Hawaii's false killer whales, which are actually dolphins, to whale watchers and divers. But over the past 2 decades, the state's genetically distinct population has plummeted from more than 500 to 123 animals. The first-ever study based on satellite tagging the species, published last week in *Endangered Species Research* by McSweeney and others, found that at least once a month they venture far enough offshore to get caught on the hooks of longline fishers, who are barred from near-shore waters.

This week, a federally appointed "take reduction team" is expected to consider extending the no-fishing zone. Fishing gear is a leading cause of the decline, along with pollutants and the overfishing of the tuna they depend on, says lead author Robin Baird of the Cascadia Research Collective in Olympia, who's a member of the panel.

Mega-Noise Over Nanotech

A 4-month national debate in France over the pros and cons of nanotechnology has ended prematurely after heckling by antinanotech protesters in five cities made public meetings impossible. Two weeks ago, the committee organizing the series of 17 debates threw in the towel, replacing the final two meetings with "Internet workshops" and making the wrap-up event in Paris on 23 February by invitation only.

The main agitator appears to be a Grenoble-based group called Pièces et Main d'Oeuvre (French for "Parts and Labor"). PMO, a self-described "Luddite" group whose members remain anonymous, calls the events a "pseudo-debate" masking a fait accompli. In an e-mail to *Science*, the group said it is fighting a "totalitarian nanoworld" in which "cyborgs and bionic humans" are enslaved through technology.

"Shutting up a public debate this way is completely unacceptable," says University of Rennes 1 physicist Ronan Lefort, a panelist at a 7 January debate that hecklers disrupted. The committee still plans to issue a report, but many worry about future public debates on environmental issues, which are required by a 1995 law.

CREDITS (TOP TO BOTTOM): DAN J. MCSWEENEY (INSET); DERON VERBECK/IAMAQUATIC.COM; COURTESY OF NORMAN HEGLUND; PATRICK SAGNES/SCAPE EVÉNEMENTS

The battle against invasive carp
932

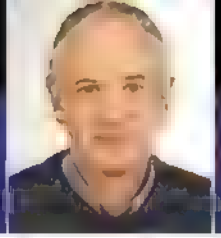

Newsmaker interview: Phil Jones
934

BRAZIL

Race for Cellulosic Fuels Spurs Brazilian Research Program

CAMPINAS, BRAZIL—The ambition of plant biologist Marcos Buckeridge is echoed in the works he listens to during his commute to a new research laboratory here in Brazil's sugar-cane country. Right now, he's into *American Prometheus*, a biography of J. Robert Oppenheimer, father of the Manhattan Project; next, a history of the U.S. space program.

Buckeridge is hoping to keep Brazil in another international technology race. He is the scientific director of Brazil's Bioethanol Science and Technology Center (CTBE), a $40 million facility inaugurated on 22 January. His task: to organize a world-class research program. "The Americans are spending more money," says Buckeridge, "but if we succeed, we will be regarded like Pelé, and scientific discovery will be treated as an act of heroism in Brazil." At stake is Brazil's position as the world's most efficient producer of ethanol.

Brazil got its start running cars on ethanol during a 1970s oil-independence push. These days, nearly every new car sold in Brazil can run on it. The country's sugar-cane mills make ethanol for half of what it costs in the United States, where ethanol is made from corn. Exports have surpassed 3 billion liters per year.

Keeping that lead won't be easy. Although Brazilian sugar cane is the most competitive ethanol feedstock today, the United States and Europe are investing heavily in next-generation approaches. In 2009, the U.S. Department of Energy alone budgeted more than $325 million for biofuel science and demonstration plants. Much of that effort is aimed at "cellulosic ethanol," or how to obtain fermentable sugars cheaply from straw, wood chips, and other plant material normally considered waste (*Science*, 16 March 2007, p. 1488).

CTBE represents Brazil's big bet to keep pace in cellulosic technology. Construction has started on a $12 million pilot plant, where scientists from across Brazil will study how to use enzymes to break down and access sugars that normally remain trapped in sugar-cane straw and processed stalks, known as bagasse. "Not investing would be a very big risk," says Marco Aurélio Pinheiro Lima, a theoretical physicist who is CTBE's director. "Brazil would end up having to purchase technology in areas it has always led. The government is very aware of that."

Raising cane. President Luiz Inácio Lula da Silva and plant biologist Marcos Buckeridge at the inauguration of Brazil's national Bioethanol Science and Technology Center last month

Until now, Brazil's biofuel research has had a strongly practical bent. Industry agronomists developed new cane varieties, and steam-power experts taught sugar mills how to burn cane waste and make electricity. Engineers in Brazil also led the development and launch of flex-fuel vehicles that burn both ethanol and gasoline. Since 1975, the amount of ethanol squeezed from each acre of sugar cane has more than doubled.

Given that track record, not everyone in Brazil is convinced by the new cellulosic push. "The view I defend is that the first-generation technology still has space to improve," says José Goldemberg, a professor at the University of São Paulo and former education minister. Goldemberg thinks that ethanol production can be vastly increased by expanding sugar-cane agriculture and introducing genetically modified crops, all well before cellulosic ethanol reaches economic viability. And because many Brazilian mills already burn cane waste to make electricity (producing about 3% of the country's electricity), there's competition for cheap cellulose. Suani Teixeira Coelho, director of the Brazilian Reference Center on Biomass at the University of São Paulo, thinks the new national lab represents "a kind of megalomania. They are thinking if we don't dominate the technology, someone else will."

Buckeridge says it's critical that Brazil play a role in developing next-generation technology. He notes that about two-thirds of sugar cane's sugars remain trapped in straw and bagasse in forms that ethanol-producing yeast can't digest. Using conservative estimates, he calculates that cellulosic technology could increase per-acre ethanol production by 40%. "I don't think you're going to get that with the first-generation technology," he says.

CTBE grew out of a study commissioned by Brazil's Ministry of Science and Technology in 2005 that concluded that the country needed an internationally competitive national lab to coordinate its growing research efforts. Although precise figures are not available, public-sector funding for biofuel research has grown in Brazil by some 500% during the past decade and now totals about $90 million per year, says Carlos Henrique de Brito Cruz, scientific director of the State of São Paulo Research Foundation. "The main change in Brazil's

CREDIT: GUSTAVO TILIO/CTBE

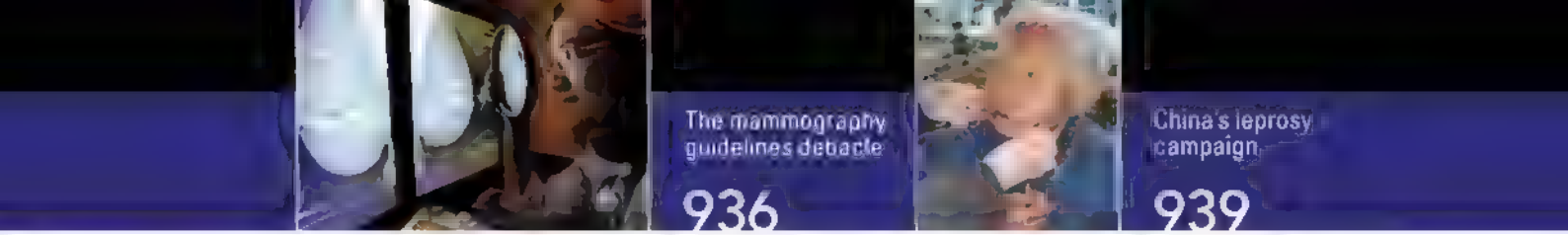

The mammography guidelines debacle 936

China's leprosy campaign 939

strategy in bioethanol is making it much more science-based," says Brito Cruz. That's a recognition that the competition comes from "countries that use a lot of science to improve their technology."

Brazil's government has been anxious about losing ground. In 2008, science minister Sérgio Rezende publicly complained when Monsanto paid $290 million to acquire two homegrown biotech start-ups, Alellyx and Canavialis, then developing new sugar-cane varieties. Rezende lamented the loss of two domestic technology "jewels" to "foreigners." Yet Monsanto turned out to be only among the first in a wave of multinationals looking for footholds in Brazil. This month, Royal Dutch Shell agreed to a $12 billion joint venture with Brazil's largest ethanol producer, Cosan. As part of the deal, Shell contributed its stake in two cellulosic ethanol start-ups, indicating that it planned to apply the technology first in Brazil.

"Everyone wants to play in Brazil because of the cheap sugar. The technology is going to come whether Brazil develops it or not," says Carl E. Pray, an economist at Rutgers University, New Brunswick, who has been studying international aspects of biofuel R&D. Pray thinks Brazil stands to reap the benefits first no matter where cellulosic technology is developed: "Stuff that is developed in a lab in the U.S. is moving to Brazil that night by e-mail."

BIOFUELS PAPERS

Rank	Nation	Citations	Papers	Citations per paper
1	U.S.A.	5143	498	10 33
2	Turkey	864	158	5.47
3	China	442	145	3.05
4	India	1076	139	7 74
5	Sweden	608	135	4.5
6	Germany	501	118	4 25
7	Japan	879	117	7 51
8	England	502	92	5 46
9	Spain	552	90	6.13
10	Canada	622	87	7 15
11	Brazil	345	80	4.31
12	Greece	245	55	4 45
13	Taiwan	247	55	4 49
14	Finland	215	52	4.13
15	Italy	306	52	5.88
16	Netherlands	317	47	6.74
17	France	150	46	3 26
18	Poland	25	38	0 66
19	South Korea	167	35	4.77
20	Belgium	314	33	9 52

For Brazilian academics, the growing interest in sugar cane is a chance to forge new international relationships. Last year, Brazil's federal science agency issued a joint call for proposals to develop cellulosic ethanol with the European Union. For its part, CTBE signed a cooperation deal with the U.S. National Renewable Energy Laboratory. "We each work on our own feedstock but then trade notes," says Pinheiro Lima.

So far, CTBE's offices and laboratories are mostly empty. But equipment has begun arriving, and the center plans to have 170 scientific and technical staff by 2013. The laboratory will focus on some immediate problems, such as developing farm machinery that uses GPS to run along trails and avoids compacting soil. But cellulosic technology remains the top goal. Starting next year, the lab will carry out what it terms "mega-experiments" to test ideas from researchers across Brazil in the pilot plant's fermentation tanks and enzyme chambers. "For Brazil to have a role in this technology, we will have to work together," says Pinheiro Lima.

–ANTONIO REGALADO

U.S. CONGRESS

Ehlers's Retirement Called 'Big Loss' for Science

Vernon Ehlers, a staunch supporter of science and one of three physicists in the U.S. House of Representatives, is retiring after 17 years in Congress.

His announcement last week, which came as Washington, D.C., grappled with a historic blizzard, was characteristic of the soft-spoken, self-effacing former college professor. The 76-year-old Republican from central Michigan has been a quiet but insistent force on the House science committee, working with both Democratic and Republican chairs on legislation to improve U.S. science and math education and bolster federal investments in research. His retirement at the end of the year will strip the science committee of arguably its two most influential members following a similar decision by its chair, Representative Bart Gordon (D–TN), not to seek reelection after 26 years in the House.

"It's a big, big loss," says Sherwood Boehlert, a former chair and a moderate Republican who retired in 2006. "He was Mr. Science in Congress, and he was my go-to guy whenever I had a question about research or science education."

"Mr. Science." Ehlers hopes to stay involved in science policy.

Although Ehlers told *Science* that he felt "it was time to move on," his retirement won't quench his lifelong passions. "I hope to stay involved," Ehlers said. "I've spoken to some of the powers-that-be in Washington, and I think I can still play a role." Ehlers said he couldn't talk yet about his new gig, noting only that "I won't be doing it for the money." He also wants to become "an elder statesman" on behalf of continued federal support for research.

Not one to toot his own horn, Ehlers nevertheless says he's concerned about the continued vitality of the science committee with his and Gordon's departure. "That was actually the biggest factor in my mind against retiring," he explains, noting that he considered retiring 2 years ago but changed his mind. "I recognize the role I've played on the committee over the years. But there are still some good people there who care a lot about science."

David Goldston, a longtime aide to Boehlert and former committee staff director, describes Ehlers as "thoughtful and independent, ... willing to work with anybody who takes these issues seriously." Now head of government affairs for the Natural Resources Defense Council, Goldston says Ehlers "is the kind of member that Congress needs more than ever these days."

–JEFFREY MERVIS

CREDITS (TOP TO BOTTOM): (SOURCE) THOMSON REUTERS; SCIENCE WATCH; U.S. CONGRESS

Eppendorf & *Science* Prize for Neurobiology

Get recognized!

US$ 25,000 Prize

2009 Winner
Richard Benton, Ph.D.
Assistant Professor
University of Lausanne
Switzerland

Kurstin Roe Photography

eppendorf & Science PRIZE FOR NEUROBIOLOGY

Deadline for entries
June 15, 2010

It's easy to apply! Learn more at
www.eppendorf.com/prize

Congratulations to Dr. Richard Benton on winning the 2009 Eppendorf & *Science* Prize for his studies on odor detection in the fruit fly, *Drosophila*. His findings have revealed unexpected evolutionary parallels between insect chemosensation, immune recognition and synaptic transmission.

The annual international Eppendorf & *Science* Prize for Neurobiology honors young scientists for their outstanding contributions to neurobiology research based on methods of molecular and cell biology. The winner and finalists are selected by a committee of independent scientists, chaired by *Science*'s Senior Editor, Dr. Peter Stern.

To be eligible, you must be 35 years of age or younger. If you're selected as this year's winner, you will receive US$ 25,000, have your work published in the prestigious journal *Science* and be invited to visit Eppendorf in Hamburg, Germany.

eppendorf
In touch with life

Science
AAAS

CHINA

Fear of MRI Scans Trips Up Brain Researchers

BEIJING—Neuroscientist Zang Yu-Feng and his colleagues at Beijing Normal University plan to use functional magnetic resonance imaging (fMRI) to probe differences in brain activity between healthy children and those with attention deficit hyperactivity disorder. Intending to enroll children in the study, university students last December handed out fliers at a primary school. But they came away empty-handed: Parents were worried that MRI scans might harm their children.

Although MRI is widely embraced in China as a diagnostic tool, parents are reluctant to expose children to strong magnetic fields. Such unease is not the only impediment. "It's getting harder to do MRI studies because public distrust of doctors is increasing," says Xie Sheng, a radiologist here at Peking University First Hospital. Reasons for distrust include heightened awareness of patients' rights and more debate in the media about the relative merits of different treatments, she says. The challenge of recruiting healthy children for studies has compelled Xie, for one, to resort to ill children—an approach that can backfire.

MRI marks the spot. Tan Li-hai's group found that dyslexic Chinese children, compared with controls, had less activity in a brain region important for Chinese reading and writing.

CREDITS (TOP TO BOTTOM): CDC; W. T. SIOK ET AL., PNAS 105, 14 (8 APRIL 2008); © NATIONAL ACADEMY OF SCIENCES, U.S.A.

After 3 decades in the clinic, MRI is considered safer than x-ray scans and proton emission tomography, says physicist Yihong Yang, chief of the MRI physics section at the National Institute on Drug Abuse in Baltimore, Maryland. The main danger is for people with a pacemaker or other metal in their bodies. "Millions of people have been examined with MRI so far; thus it seems now very unlikely that there would be a side effect," says Arno Villringer, director of cognitive neurology at the Max Planck Institute for Human Cognitive and Brain Sciences in Leipzig, Germany.

In China, that reassurance cuts little ice with many parents—and some scientists. "I would not dare to allow my children to be tested by MRI," says radiologist Han Hongbin of Peking University Third Hospital. "Nobody can ensure that there is no potential danger," such as during nonroutine MRI scans that use extremely powerful magnetic fields, he says.

In the face of such concerns, some researchers take shortcuts. For example, Xie recently submitted a report to *Epilepsy Research* on epilepsy in toddlers. Last month, however, the journal rejected her article because her control subjects were unhealthy. Xie acknowledges that's true: Most children she classified as controls had undergone MRI exams for other complaints. "It is too hard to recruit perfectly healthy children to take an MRI test," Xie says.

Some colleagues sympathize and suggest that exceptions to standard research practice should sometimes be allowed. Zang says that in Xie's case, children who are not afflicted with epilepsy and have no neurological complaints—but who may suffer from other ailments—are permissible controls. Not so, says Huang Ruiwang, a magnetic resonance physicist at Beijing Normal, who argues that it was correct to reject Xie's article.

Recruitment goes more smoothly in the United States, where "many parents will allow their children to take the test," says Damien Fair, a neuroscientist at Oregon Health and Science University in Portland. Even in China, some groups have had more success. Tan Li-hai, co-director of the State Key Laboratory of Brain and Cognitive Sciences at the University of Hong Kong, says he has never had trouble recruiting subjects for studies; his team recently identified brain regions crucial for reading and dyslexia in Chinese children.

Tan's success heartens Zang, who believes his group can get its study back on track. They will resume their recruitment drive after the Lunar New Year festival ends this week, although Zang says that this time around they will work harder to better inform parents about their research aims. —LI JIAO

Li Jiao is a writer in Beijing.

ScienceNOW.org

From *Science*'s Online Daily News Site

New Challenge to 'Chronic Fatigue Virus'
A theory linking chronic fatigue syndrome (CFS) to an infectious mouse virus known as XMRV has taken a second major hit. First proposed last October, the virus-CFS connection was quickly challenged by a British group. Now a second team of British virologists reports that, after examining tissue from 170 CFS patients, they have failed to find evidence of XMRV. http://bit.ly/virusfatigue

What Doesn't Kill Microbes Makes Them Stronger
If you are taking antibiotics, your doctor will admonish you not to skip any pills and to continue the treatment even after you start to feel better. That's because failure to kill the bugs making you sick can cause some of them to become resistant to the antibiotics. Now, a new study explains how nonlethal antibiotic concentrations can lead to resistance. The drugs trigger the release of so-called reactive oxygen species inside bacteria, which in turn cause mutations in the bugs' DNA—including some that happen to cause resistance. http://bit.ly/rosmicrobes

Holy Surgical Side Effect
People of many religious faiths share the belief that there is a reality that transcends their personal experience. Now, a study with brain cancer patients hints at brain regions that may regulate this aspect of spiritual thinking. The researchers found that some patients who had surgery to remove part of the parietal cortex became more prone to "self-transcendence." http://bit.ly/godspot

First Gene Mutations Linked to Stuttering
Researchers have pinpointed the first genetic mutations responsible for stuttering. The find links the condition, which afflicts about 5% of children and 1% of adults, to metabolic disorders and could lead to new treatments. http://bit.ly/stuttergene

Read the full postings, comments, and more on **sciencenow.sciencemag.org**.

INVASIVE SPECIES

Biologists Rush to Protect Great Lakes From Onslaught of Carp

With Asian carp poised to invade Lake Michigan, wildlife managers are urgently trying to figure out how many of the voracious 1.5-meter-long fish have already slipped past electric fish barriers in a waterway near Chicago and they are scrambling to shore up defenses. A new plan, released by federal agencies and other groups last week, aims to improve coordination among agencies dealing with the immediate threat and divvies up $78.5 million for control and research. Meanwhile, scientists and advocacy groups are pushing with renewed effort for what they say is the only long-term solution: severing the connection between the Great Lakes and the Mississippi River Basin, a proposal that doesn't sit well with the barge industry.

Pressing onward. DNA tests indicate silver and bighead carp (*left*) have passed electric barriers.

The two invasive species—bighead carp (*Hypophthalmichthys nobilis*) and silver carp (*H. molitrix*)—are native to China and were introduced for aquaculture in the southern United States in the 1970s. After escaping, the fast-growing, fecund fish moved up the Mississippi River and its tributaries. In some places, the carp have caused a 90% decline in crustacean zooplankton and are apparently outcompeting two native fish species, the gizzard shad and bigmouth buffalo. In addition, silver carp jump high out of the water when startled and have caused broken bones and concussions in boaters. Although eaten around the world, Asian carp have too many bones for the taste of most U.S. anglers.

Worried about the threat to the $7 billion recreational fishing industry in the Great Lakes from this and other invasive fish, Congress authorized the U.S. Army Corps of Engineers in 1996 to build a prototype electric fish barrier within a key choke point—the Chicago Sanitary and Ship Canal (*Science*, 11 July 2003, p. 157). After testing started in 2002, a second, full-scale barrier was added to help repel any fish that try to swim upstream through it. From monitoring the canal and the Illinois rivers, wildlife managers believed that the invasion front was still 25 to 30 kilometers south of the barriers.

But last year, they got a rude shock. David Lodge, an invasive species biologist at the University of Notre Dame in Indiana, began testing water samples for Asian carp DNA. Working with The Nature Conservancy, the team discovered DNA from silver and bighead carp several places above the barriers. Fish biologist Phil Moy of Wisconsin Sea Grant in Manitowoc believes the carp may have passed through the barriers a few years ago either during a power outage or when they were down for maintenance.

Most alarming, in December, Lodge's team found bighead and silver carp DNA in the mouth of the Calumet River—suggesting that some fish could already be in Lake Michigan. "That's what really lit a fire under everybody's seat," says Marc Gaden, legislative liaison of the Great Lakes Fishery Commission in Ann Arbor, Michigan. Soon, wildlife biologists netted a bighead and a silver carp where they found DNA.

The most immediate eradication measures are admittedly a stopgap. Over the next few weeks, the U.S. Fish and Wildlife Service and partners in Illinois will put more than 20 staff in up to nine boats for electrofishing and netting the carp, to the tune of $2.6 million. It won't be easy. "They are very difficult fish to catch at low density," cautions biologist Duane Chapman of the U.S. Geological Survey (USGS) in Columbia, Missouri. "The chances of getting all of them are close to nil." Still, he says, the more fish kept out of the Great Lakes, the better the chance of preventing an established population.

The strategic plan also includes $13 million for the corps to speed completion of a third electrical barrier, now expected by October. Another $13.2 million would accelerate construction of physical barriers on the Des Plaines River and a canal to prevent fish from moving through with floodwaters. Additional funds would go toward developing selective "bubble" barriers to keep fish from spawning areas in the Chicago-area waterways or, if necessary, in the Great Lakes. There's also $1.5 million for USGS to work on formulating fish poison that targets only Asian carp and $1 million to study pheromones that might help trap or deter carp.

The surest way to prevent carp from getting established, scientists say, is to achieve "ecological separation" by permanently closing the locks in Chicago and creating physical barriers to water flow in the other entry points to Lake Michigan. That might pose problems for the 50,000 or so recreational and commercial boats that pass through the Chicago River Lock each year. One option, say advocates, is to lift the boats over, but the American Waterways Operators opposes any substantial changes. In December, Michigan's attorney general sued the state of Illinois, demanding that the canal locks be closed, but the U.S. Supreme Court declined to hear the case.

Lodge and others says that an investment in separating the waterways would pay off by also preventing other invasive species, such as the northern snakehead fish, from reaching the Great Lakes—and reducing the odds that any of the more than 180 invaders in the lakes will travel inland via rivers. "It's far more expensive to always be reacting" to invasions, he says.

As part of the new plan, the Army Corps has moved up the deadline for its comprehensive study of how to prevent the movement of invasive species between the Great Lakes and the Mississippi River Basin to 2012. That's not fast enough for Gaden and others. "We don't have the time," he says. There will be quicker action, according the strategic plan: By 30 April, the corps could begin modifying Chicago River Lock operations—opening it for only a few days a week, for example—to reduce the chance of carp getting through.

–ERIK STOKSTAD

CREDITS (LEFT TO RIGHT): ASIAN CARP MANAGEMENT (SOURCE); THE NATURE CONSERVANCY AND UNIVERSITY OF NOTRE DAME; USACE

U.S. IMMIGRATION POLICY

Prominent Iranian Scientist Blocked From Attending Physics Meeting

Iranian physicist Farhad Ardalan has spent enough time in the United States to regard it as his second home. But a case of apparent mistaken identity may prevent him from ever visiting his adopted country again.

Last fall, Ardalan was named a fellow of the American Physical Society, in part because of his efforts to connect Iran to the global scientific community and strengthen bonds between Iran and the United States. The new class of fellows will be honored at the society's meeting next month in Portland, Oregon. But U.S. consular officials have derailed Ardalan's application for a visa after telling him that U.S. government records show he was arrested in the United States in 1983 for an unspecified offense. They also say that he may have been involved in deportation proceedings 20 years earlier.

Ardalan denies both charges, and his U.S. colleagues say that the State Department is making a big mistake. "He is precisely the kind of person who should be welcomed to the U.S.," says Stanford University physicist Herman Winick about Ardalan, a string theorist at the Institute for the Study of Fundamental Sciences in Tehran.

CREDIT: COURTESY OF FARHAD ARDALAN

Visa problems. Farhad Ardalan suspects a "doppelgänger" has tainted his application.

Ardalan first came to the United States in 1958 and attended Columbia University, where he received his bachelor's and master's degrees. After earning his Ph.D. in 1970, he returned to Iran to teach at Sharif University, where he helped create the first Iranian doctoral program in physics.

Ardalan spent sabbatical years at Yale and Stony Brook universities in 1974 and 1977 and made a short visit to the United States in 1986. He claims that, like most Iranians, he wasn't allowed to leave the country for several years after the 1979 Iranian Revolution. "I simply could not have been in the U.S. in 1983," he says about the government's charge, which he first learned about when he appeared for his visa interview on 29 January at the U.S. Embassy in Bern, Switzerland. (Iranians must go abroad for a U.S. visa.)

When Ardalan disputed the charge, he says, the official told him that his name and fingerprints matched the record of the arrest and that he would have to come back for another appointment to give officials time to look into the case. "I said, 'Forget it.' And I left," says Ardalan.

On 2 February, an e-mail from the U.S. Embassy leveled a new charge. "A check of U.S. records appears to suggest that you were involved in deportation proceedings before the New York office of the Immigration and Naturalization Service on July 5, 1962. Please confirm or dispute this information," the e-mail said.

"I don't know what they are talking about," says Ardalan. He says neither of these two charges were raised in 1993 when he and his wife received permanent residency in the United States. For the next decade, Ardalan spent several months every year as a visiting scientist at the University of Cincinnati in Ohio, working with his friend Freydoon Mansouri. Ardalan moved back to Iran after Mansouri died in 2003.

Ardalan guesses that the problem is a doppelgänger. "There was a person with the same name who was a leader of the Kurdish guerrilla movement; as a result, for years I was routinely stopped and interrogated at the Tehran airport," Ardalan says. It took a meeting with the head of airport security to clear his name. Ardalan says he deserves an apology for how he has been treated, and he refuses to go back to the embassy or reapply for a visa.

State Department officials did not return calls for comment. The department has been criticized for botching visa applications of prominent scientists, including Goverdhan Mehta, an Indian chemist whose visa application was denied in 2006 (*Science*, 17 February 2006, p. 933).

"We hope the issue can be resolved and Ardalan can come to the March meeting," says John Clark, a physicist at Washington University in St. Louis, Missouri, and former chair of APS's Forum on International Physics. The meeting runs from 15 to 19 March.

–YUDHIJIT BHATTACHARJEE

*Science*Insider

From the *Science* Policy Blog

The United Nations has formed a joint task force of experts from Haiti and around the world to provide **advice on recovering from last month's disaster.** The team hopes to generate a preliminary forecast of seismic activity and provide day-to-day advice to assist relief and recovery efforts. http://bit.ly/9USsek

The new chief of **Europe's top science policy office** says she's "passionate" about using research and innovation to spur economic development and push governments to invest 3% of their gross domestic product on science. Ireland's **Máire Geoghegan-Quinn** thinks that not being a scientist may actually help her to "break down the barriers" to gaining greater public support. http://bit.ly/98vfxh

First Lady Michelle Obama has launched a **major initiative on childhood obesity** that features a new nonprofit foundation. Let's Move embraces better school lunches, more exercise, and more accessible healthy food, including financial incentives to bring farmers' markets and full-service groceries to urban areas. http://bit.ly/agwuuA

A long-running battle among farmers, conservation groups, and U.K. science advisers took a new turn when a team from the U.K. Medical Research Council reported that **systematic culling of badgers does reduce outbreaks of bovine tuberculosis** in British cattle but not enough to justify the cost of the cull. The finding likely won't end the controversy. http://bit.ly/djH7MS

Foreigners living in one of the world's most polluted cities now have more information about the **quality of the air in Beijing.** The U.S. Embassy, which has been using Twitter to publish average hourly readings of fine particulate matter, has also begun tweeting hourly data on ground-level ozone, the prime component of smog. But local residents will have to use a proxy server to access the data because Twitter is blocked in China. http://bit.ly/cQXoPn

For the full postings and more, go to **blogs.sciencemag.org/scienceinsider.**

NEWSMAKER INTERVIEW

Embattled U.K. Scientist Defends Track Record of Climate Center

Phil Jones is at the center of a swirling controversy over e-mails stolen or leaked from the Climatic Research Unit (CRU) at the University of East Anglia in the United Kingdom, which he has directed since 2004. In the 3 months since those messages came to light, Jones has been battered by criticism that the e-mails reveal a failure to share climate data publicly and an effort to prevent certain papers from being cited in international climate change reports. He's stepped down temporarily from his job to allow for an independent inquiry, and he's been treated for depression.

But Jones hasn't walked away from the battlefield. "I've got no agenda here. I'm not a politician. I'm just a scientist," he told *Science* during an interview last week from the University of East Anglia. Jones declined to talk about allegations concerning the hacked e-mails, citing the ongoing investigation. But he forcefully defended the quality of the center's efforts to create a global temperature database, which points to an average 0.1°C warming of Earth's land areas per decade since 1900. That work earned him a 2002 medal from the European Geosciences Union, among other acclaim.

Here are some highlights from the interview, a longer version of which appears online.

–ELI KINTISCH

Q: If the CRU data set were set aside, are there other data that corroborate your findings about rising temperatures?

P.J.: There's the two other data sets produced in the U.S. [at NASA and the National Oceanic and Atmospheric Administration]. But there's also a lot of other evidence showing that the world's warming, by just looking outside and seeing glaciers retreating, the reduction of sea ice … overall, the reduction of snow areas in the Northern Hemisphere, the earlier [annual] breakup of sea ice and some land ice, and river ice around the world, and the fact that spring seems to be coming earlier in many parts of the world.

Q: Critics say that your producing the same trends as the NASA and NOAA data sets is insignificant given that you start with the same raw data.

P.J.: There are differences. The two American sets use a larger number of [temperature] stations than we do. They both use about 7200 stations, and we use about 5000 stations. But we look at that data in different ways and have different techniques for deciding whether the stations are used or not.

Q: One of the real challenges is going from the available raw data to the final temperature sets that you release. Do you feel that you have released enough information that someone could repeat that exercise?

P.J.: Yes, I feel they have. [Our papers] have been peer-reviewed; we've been doing this work for almost 30 years now. [NOAA] has something called the Global Historical Climatology Network, and people can download the station data it's essentially the same data, it may not be exactly the same they could go and take that data, make their own choices about what stations to use, … they could reproduce their own gridded temperature data. A lot of the people at the moment criticize what we do but [are not doing] anything constructive and new.

Online
sciencemag.org
An extended version of this interview can be found here

Q: A sticking point with some of your critics has been how much of the data *isn't* available.

P.J.: We've been putting up more of the data online on the U.K. Met Office site [covering] 80% of the stations we use. You can download the data and you can download the program we use to produce the data sets.

Q: One concern of your critics is whether there are adequate procedures in place to assure the quality of this data.

P.J.: That's the sort of work we've done in the past and published in the papers.

Q: You've emphasized that you have a small staff. Would more people checking these data be a useful thing?

P.J.: It could be useful, but then we've got to bring them up to speed in terms of what we're looking for. … The national meteorological services [which provide the raw numbers] are doing quality control on this data before it even reaches us.

Q: When during your career has pressure from outsiders to criticize or, as you would put it, "distort" your work become significant?

P.J.: In 2007, [as] the blog sites started then. I had responded to some of these people in years earlier but had given up. … I just didn't have the time to respond. They didn't seem to want to understand.

Q: One of the skeptics who wanted station data was Warwick Hughes. What did you mean when you wrote in an e-mail to him that "even if WMO [World Meteorological Organization] agrees, I will still not pass on the data. We have 25 or so years invested in the work."

P.J.: I'd rather not go there. It was an e-mail written in haste.

Q: When did the pressure become severe?

P.J.: In July 2009, we received 60 Freedom of Information requests in a few days—each request was for five countries' worth of data. We probably should've responded to these requests in a different way. We stand by the science that we were doing. Maybe we need to be more proactive and open about releasing data. But the 60 requests were just too much to deal with at that one time.

Q: Do you have any regrets about how you handled the chapter you've co-authored in the 2007 IPCC report?

P.J.: No regrets, but I don't really want to go talking about IPCC. I stand by that chapter.

Q: Why are you speaking out now?

P.J.: It just seems like the right time. It was too difficult back in November and December.

CREDIT: UEA

PSYCHIATRY

Behavioral Addictions Debut in Proposed *DSM-V*

In psychiatry, the only disorders that have been considered addictions are those involving alcohol or other drugs. Now, proposed revisions for the American Psychiatric Association's (APA's) *Diagnostic and Statistical Manual of Mental Disorders* (*DSM*) include for the first time "behavioral addictions"—a change some say is long overdue and others say is still premature (*Science*, 12 February, p. 770).

So far, only one behavior has made the cut gambling, which under the new proposal would join substance-use disorders as a full-fledged addiction. *DSM* has recognized pathological gambling for decades, but it has been consigned to a grab bag of "impulse control disorders not otherwise specified" along with kleptomania, hair-pulling, and fire-setting. Many scientists have long believed that compulsive gamblers closely resemble alcoholics, not only from the outside—destroying jobs, finances, and relationships in pursuit of their obsession—but, increasingly, on the inside as well. Brain imaging and neurochemical tests have made a "pretty strong case that [gambling] activates the reward system in much the same way that a drug does," says psychiatrist Charles O'Brien of the University of Pennsylvania and chair of the addictions work group for *DSM-V*. Gamblers report craving and highs in response to their stimulus of choice, gambling also runs along with other addictions in the same families.

Psychologist Gerhard Meyer of the University of Bremen in Germany says he's been arguing since 1982 that pathological gambling should be classified as a behavioral addiction. Research by his group has shown that problem casino gamblers show increases in heart rate and salivary stress hormones as well as blood levels of norepinephrine compared with non-problem gamblers. The former also show increases in dopamine, the key player in the brain's "reward circuit." Marc Potenza, a psychiatrist and gambling researcher at Yale University, says his group's brain-imaging studies show that when exposed to gambling videos, problem gamblers' brains show "important similarities" to changes in the brains of cocaine addicts when viewing a video about cocaine.

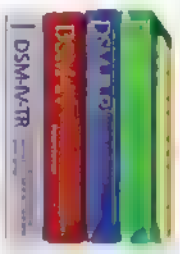

DSM-V
Second in a series

Other behaviors may eventually follow gambling into *DSM* as addictions, as more is revealed about their neurobiology and genetics. The top contender at present is "Internet addiction," which now has its foot in the *DSM* door; it will be listed in the appendix, a catch-all category for disorders that don't meet criteria for a full-fledged diagnosis. Some researchers have argued that people whose Internet use seems to be out of control show many hallmarks of addiction such as tolerance and withdrawal. But there is still no consensus on what constitutes so-called Internet addiction. Some argue that it is not the computer that's the issue but the content—mainly sex, gambling, and games—and that people hooked on the Internet suffer primarily from afflictions such as depression, personality disorders, and substance addictions.

Some researchers say a case could be made for classifying some eating disorders, bulimia in particular, as addictions. Family studies show that bulimia clusters with alcoholism and drug abuse. "Binge eating disorder," pulled out of the *DSM-IV* appendix and now proposed as a diagnosis in the eating disorders category, similarly has much in common with binge drinking. Columbia University physician Timothy Walsh, chair of the eating disorders work group, says he suspects "we'll discover underlying abnormalities in brain pathways" shared by addictions and some eating disorders. But as yet, diagnoses in his field are "still really descriptive" as opposed to biology-based.

"Sex addiction" has received a lot of press lately, but O'Brien says his work group found "no scientific evidence" that sex qualifies. APA psychiatrist Darrel Regier, co-chair of the *DSM* task force, says "it's not clear that reward circuitry is operative in the same way as in addictive areas." Nonetheless, a near equivalent may make it into the sexual disorders section of *DSM*: That work group is proposing a controversial new diagnosis of "hypersexual disorder."

The *DSM* teams have also tussled with the often-blurry line between addictions and compulsions. "I used to think [addictions] overlapped with OCD [obsessive-compulsive disorder]," says O'Brien. But new data from both brain-imaging and treatment studies suggest "more dissimilarities than similarities."

In another major change, O'Brien's group recommends dropping categories of "abuse" and "dependence" and labeling all problems major and minor as substance "use disorders" (or "disordered gambling"). Since the late 1980s, says O'Brien, "numerous large population studies" have shown there's no "breakpoint" where "abuse" becomes something more serious. He also says the term "dependence" only implies physiological dependence, which is not the same as the psychological obsession of addiction.

Some longtime addiction researchers, such as psychiatrist Victor Hesselbrock of the University of Connecticut, Farmington, have qualms about the direction *DSM* is moving. Hesselbrock believes behavioral addictions are dicey territory and prefers to limit the term "addiction" to substances, which are "pathogens we can identify." He also objects to fusing all drinking problems into "alcohol use disorder." Hesselbrock says he and others think there are proven subcategories of alcoholism that would aid both in treatment and discovering causes. "When you do a one-size-fits-all type of classification system," he says, "that will fit a lot of people but not so well."

–CONSTANCE HOLDEN

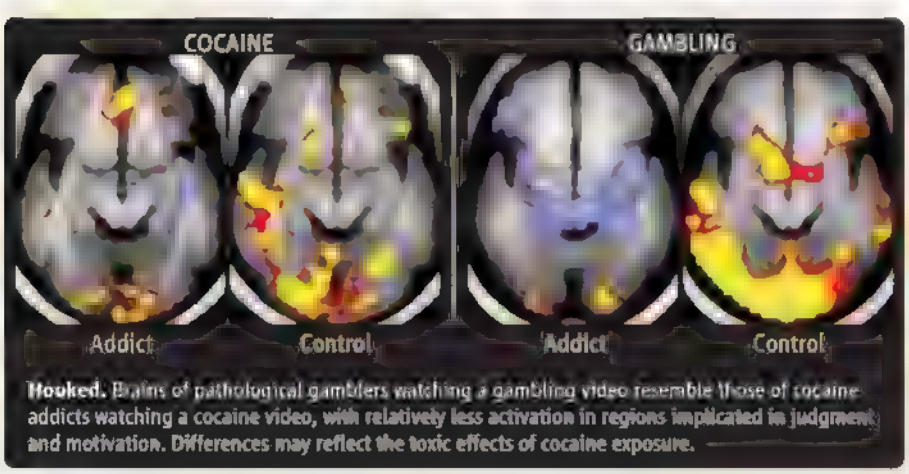

Hooked. Brains of pathological gamblers watching a gambling video resemble those of cocaine addicts watching a cocaine video, with relatively less activation in regions implicated in judgment and motivation. Differences may reflect the toxic effects of cocaine exposure.

CREDITS (BOTTOM): YALE

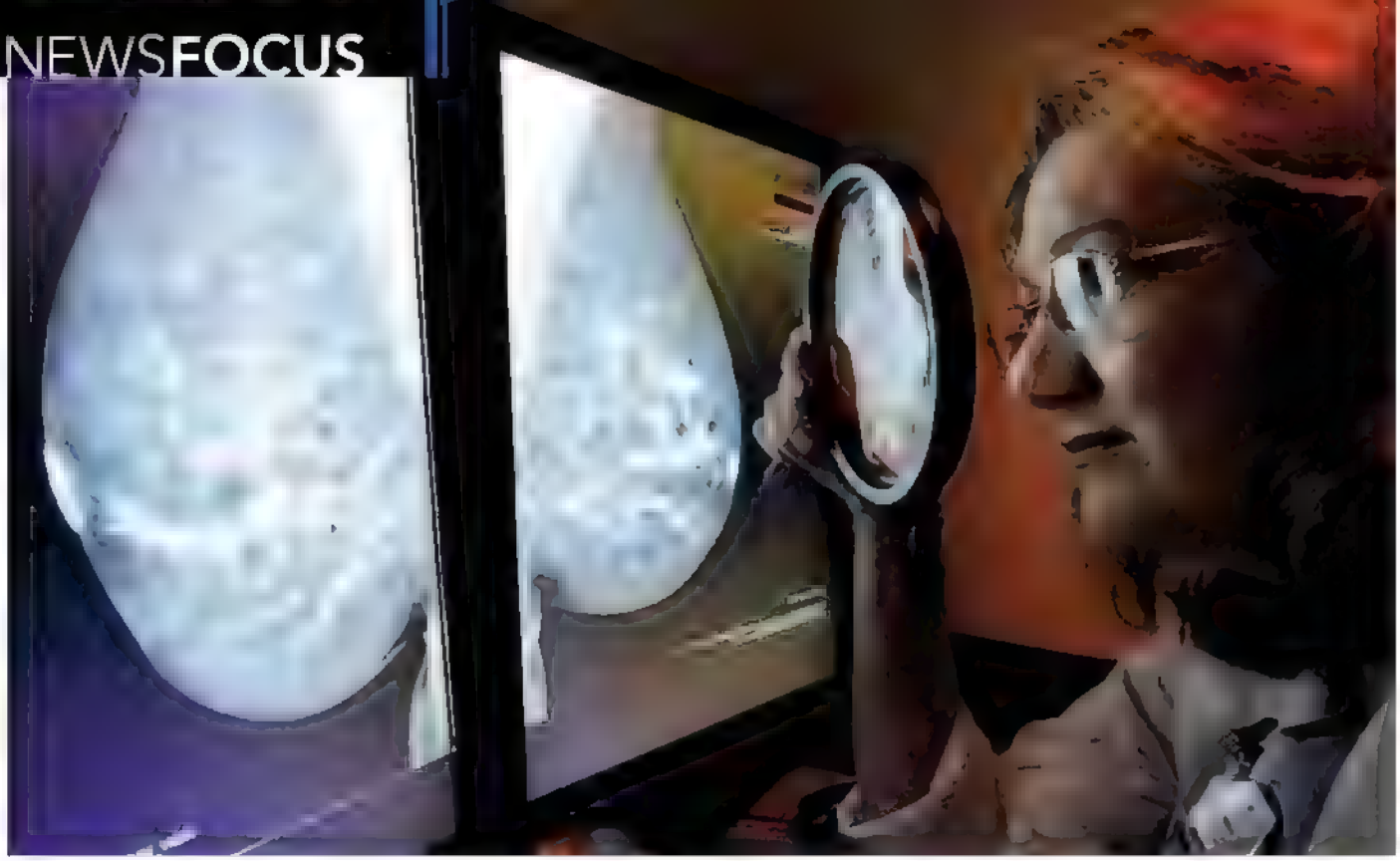

Brawling Over Mammography

A scientific study of the benefits and harms of screening women in their 40s got buried by politics

The Obama Administration is a self-described champion of science. But it was put on the spot last fall when it received a scientific report that questioned the value of screening women routinely for breast cancer before age 50. The timing was bad, coming just as Democrats were trying to push health reform through Congress. To opponents of the legislation, the report smacked of "medical rationing" by bureaucrats, the kind they claimed to see in the bills. It became a huge distraction, and in the end the Administration quietly distanced itself from the findings.

The flap continued, loud and angry, for days. Experts and nonexperts lobbed critiques and rebuttals, at times questioning one another's motives. Authors of the report rejected the "rationing" charge, saying they never took cost into account. The nonprofit American Cancer Society, which had endorsed early breast cancer screening (at age 40), announced it wasn't going to change its recommendation. But a leader of the American College of Radiology, Daniel Kopans of Massachusetts General Hospital in Boston, was less restrained. He circulated a critique saying that the sponsor of the new report—the U.S. Preventive Services Task Force (USPSTF)—"does not think it is worth saving women in their 40s; ... it thinks that women should be allowed to die from their breast cancers."

Secretary of Health and Human Services (HHS) Kathleen Sebelius weighed in on 18 November. Her agency is the official home of USPSTF, but she didn't defend its report. Instead, she ran for cover. She noted that USPSTF members are independent—not HHS staff—and were appointed in this case by George W. Bush. On CBS News, Sebelius advised women to "do what you've always done; ... talk to your doctor." Asked if she was "refuting" the task force, Sebelius said no, but added, "it is one panel of scientists and health officials who have waded into an area where the recommendations have gone back and forth for years."

Researchers who had worked on the USPSTF guidelines were disappointed that their analysis was being dismissed out of hand. "Politics got in the way of the science and the best public health practice," says Jeanne Mandelblatt, an M.D.-epidemiologist at Georgetown University in Washington, D.C., and first author of an analysis for USPSTF by six groups that compared models to find the best screening strategy. "It was very unfortunate," adds Heidi Nelson, an M.D.-epidemiologist at the Oregon Health & Science University in Portland, who led a separate team that gathered evidence for USPSTF.

Karla Kerlikowske, a breast cancer researcher at the University of California, San Francisco, was "amazed" that "people were reacting in 1 day" to studies that took her a long time to read. "I am a big believer in science and evidence. ... I thought people would really embrace the new science and say, 'Wow, this is really good.'" One lesson she learned is that it's hard to take away something that has been promoted in the past—and mammography at 40 has been widely promoted. Second, Kerlikowske says, "people just didn't like the answer—that's what it came down to, unfortunately."

Fury over the 40s

The argument over mammography was in many ways an echo of clashes over the same issues in 1996 and 2002, when USPSTF, an independent group whose advice is intended

CREDIT: JOE SONGER, BIRMINGHAM NEWS/LANDOV

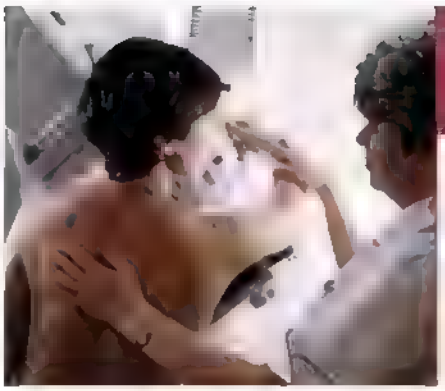

The closer you look. Experts are debating the false positives in mammograms of younger women.

CHANGING ADVICE ON MAMMOGRAPHY SCREENING, U.S. PREVENTIVE SERVICES TASK FORCE

1989	Screen ages 50–75 every 1–2 years
1996	Screen ages 50–69 every 1–2 years
2002	Screen ages 40–69 every 1–2 years
2009	Against routine screening ages 40–49 years, but screen ages 50–74 every 2 years

for primary care doctors and patients, issued its previous statements (*Science*, 21 February 1997, p. 1056; 1 March 2002, p. 1624). Indeed, many of the same protagonists came back to champion the same arguments. There was a difference, though. The 2002 USPSTF panel said that screening should begin at age 40; 7 years later, USPSTF said age 50 is when women with no known risk factors for breast cancer should begin screening.

Asked how the data changed in 2009, USPSTF task force co-chair Diana Petitti, an M D -biostatistician at Arizona State University, Tempe, said, "No change." She added: "The evidence has pretty much been the same all along; it's the packaging and the policy that goes with that packaging, and people's perceptions, ... which seem to continually cause the controversy"

The task force did alter the packaging: It took a closer look than did the earlier report at the potential "harms" of mammography These include downsides such as false positive x-ray results, extra doctor visits, biopsies, surgery, and the anxiety that goes with a result that indicates a possibility of cancer.

Many clinical trials have indicated that screening with mammography benefits women over 50, mainly because they have a fast-rising risk of developing breast cancer. Abnormalities picked up by x-rays are more likely to be dangerous; treating them as cancer is more likely to save lives, and the "price" in false alarms seems worth paying. The panel concluded, however, that for women in their 40s, the benefits of routine screening by mammography don't outweigh the harms

When to begin screening is complex. No one proposes that teenagers be screened, for example. Young women aren't good candidates because their tissue may be more opaque to x-rays and because abnormalities, if found, are not likely to be life-threatening (*Science*, 9 September 2005, p. 1664).

Common sense and individual experience—even a doctor's experience of treating cancer—isn't a guide, either. So says biostatistician Donald Berry of the M. D. Anderson Cancer Center in Houston, Texas. His warning applies especially to media reports like those aired last fall featuring young women who said that a mammogram had saved their life. Such testimony is powerful but not relevant, Berry says. "We are all duped by observations," Berry said in an e-mail, "and much of the medical community buys into screening. Some (exemplified by Dan Kopans) have their professional reputations on the line."

The paradox, explains epidemiologist Steven Goodman of Johns Hopkins University in Baltimore, Maryland, is that "every woman who has been diagnosed through mammography feels that she benefited, but we know that even without the screening her cancer would have had a very high chance of successful treatment." That is particularly true of a subcategory of small breast tumors known as ductal carcinoma in situ (DCIS), says Kerlikowske. Detection of DCIS has skyrocketed with mammography; incidence has increased 270% since 1987. Although nearly 100% of women survive DCIS, it's treated as cancer, often with surgery and chemotherapy, because it's not well understood, and who knows?—it might be dangerous. The diagnosis of cancers that won't progress, known as "overdiagnosis," is a "diabolical phenomenon," according to Goodman, because it can be seen only "through the prism of a population view."

Parallels. Karla Kerlikowske is developing markers to distinguish risky from benign DCIS tumors; since the 1980s, detection of DCIS exploded with the rise of mammography.

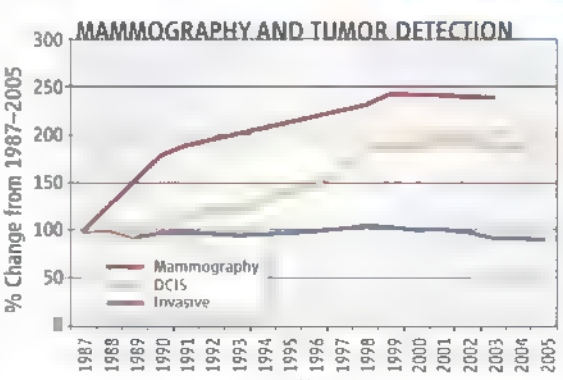

The best guide to the benefits of screening, statisticians say, is to look at deaths among women who sign up for screening in trials and compare this with deaths among those who don't sign up Nelson, who pulled together the data for the 2009 USPSTF review, conducted a meta-analysis combining the eight best randomized clinical trials since 1986. This review includes information not in the 2002 USPSTF study from older Swedish trials and from a new trial designed to look at women in their 40s, a U.K. study completed in 2006 known as the "Age" trial. (The Age study found a small benefit breast cancer deaths were down 17% in the screening group—but it wasn't significant.) Women in the screening group had about 15% less likelihood of dying from breast cancer. Nelson's group calculated that this corresponds to prevent one death from breast cancer for every 1904 women screened in their 40s. By the same index, screening 50-year-olds prevents one death per 1339 women screened a ratio the panel accepted.

That small benefit is no surprise to Peter Gøtzsche, an epidemiologist who heads the Nordic Cochrane Center in Copenhagen, Denmark. Gøtzsche and Ole Olsen co-authored analyses a decade ago that dismissed mammography-screening programs at any age as having no benefit for healthy women. Organized mammography is hyped, Gøtzsche has said—a "medical scandal" that has "seduced" thousands. Even Gøtzsche, however, recently adjusted his reading of mortality data. A 2009 review he co-authored acknowledges that trials have detected a slight decline—about 15%—in deaths among women of all ages

CREDITS: (TOP) SAMUEL ASHFIELD/GETTY IMAGES (DATA SOURCE) USPSTF (BOTTOM) KARLA KERLIKOWSKE (DATA SOURCE) AHRQ PUBLICATION, SEPTEMBER 2009

screened by mammography. But the review finds this is negated by false alarms and unneeded medical procedures.

At the opposite pole is Kopans. He sees a scandal, too, but for him it's a conspiracy to obscure the good news that mammography works. Kopans has basic objections to the way that USPSTF and others slice the data. He claims that the 2009 USPSTF analysis used "the lowest possible" number from trial data to represent the average benefit of mammography for women in their 40s. He insists that experts should have cited a range of results from the best trials from 15% to 44%. Or, he suggests, why not use the 44% benefit from the "Gothenburg" trial or the 35% benefit from the "Malmö" trial, both in Sweden. That's what he would do, and he credits mammography with reducing breast cancer deaths in the United States "by at least 30%" over 2 decades. And he insists that there is "no scientific support" for drawing a line at age 50. "The body doesn't know it's 50," he says. Nelson has a terse response: "Fishing around to find an answer you like is inappropriate."

There is "no scientific support" for limiting mammography screening to those over 50.

—DANIEL KOPANS, MASSACHUSETTS GENERAL HOSPITAL

"Much of the medical community buys into screening. ... We are all duped by [individual] observations."

—DONALD BERRY, M. D. ANDERSON CANCER CENTER

The dark side

Few dispute the USPSTF panel's estimate of the benefits of screening, but its reading of harms is more controversial. For the first time in 2009, USPSTF produced a detailed list of negative outcomes. The new data are from the U.S. Breast Cancer Surveillance Consortium, a collaboration of U.S. community groups: For every 1000 women screened in their 40s, the review found 97.8 false-positive mammograms per round of screening (up to 10 times a decade), 84.3 call-back doctor visits, and 9.3 biopsies. (Exposure to radiation isn't flagged as a major concern.) Expressed another way, for every case of invasive cancer detected, 556 women have mammograms and five have biopsies.

The false positives, the panel said, produce untold anxiety in addition to needless follow-up procedures. The report's attention to anxiety prompted snickers. In testimony for a House of Representatives panel in December, Petitti said, "The mention of anxiety and psychological distress as a harm of a false-positive test has ... been ridiculed." She added later that, "People are saying it's something we should ignore; I guess they've never been through a false-positive mammogram."

Goodman, who followed the debate closely, was also troubled by the gibes at the "harms" tally. He says he keeps a file of "cartoons that parody the reasoning of the task force, ... really terrible stuff." He thinks USPSTF was right; indeed, he urged the panel to be specific in a critique of its 2002 report. USPSTF authors, he wrote back then, were too "oblique" in adding up costs, and he called for hard data on the number of lumpectomies and mastectomies that follow false alarms.

Goodman thinks the adverse effects are still soft-pedaled in the 2009 report. He says that he's "totally shocked" that "the word 'mastectomy' doesn't appear" in the list of potential harms. The USPSTF evidence team considered getting into unnecessary surgery, according to Nelson, but she says a co-author at the Oregon Health & Science University, oncologist Arpana Naik, recommended against it. The reason, Nelson says: Naik argued that women opt for a mastectomy out of fear even when test results don't indicate it's needed, and Naik "talks people out of mastectomies every day." The team felt that the high surgery rate would reflect U.S. cultural norms, not medical norms.

RESULTS OF U.S. BREAST CANCER SCREENING

Per screening round, 1000 Women	Age 40–49	Age 50–59	Age 60–69	Age 70–79
False-negative mammograms	1.0	1.1	1.4	1.5
False-positive mammograms	97.8	86.6	79.0	68.8
Additional imaging	84.3	75.9	70.2	64.0
Biopsies	9.3	10.8	11.6	12.2
Screening detected invasive cancers	1.8	3.4	5.0	6.5
Screening detected ductal carcinoma in situ (DCIS)	0.8	1.3	1.5	1.4

Churning. For every 1000 women in their 40s screened with mammography, about 100 initially get a false positive result.

CREDIT: (DATA SOURCE) H. NELSON *ET AL.*, BREAST CANCER SURVEILLANCE CONSORTIUM

Mangled message

The 2009 review aimed for a "nuanced" view of the risks and benefits of screening, Petitti says, that would predict what might happen under different screening strategies. For this, USPSTF turned to "the best modelers from the top research institutions," says Mandelblatt. A group led by Berry, called the Cancer Intervention and Surveillance Modeling Network, drew on experience to estimate how different screening frequencies and starting points would affect the number of x-ray exams, deaths avoided, and false positives. The models plugged gaps in the trials. Among other things, Berry says, they confirmed the sketchy data on women in their 40s and "gave confidence" that screening recommendations would be solid particularly that having a mammogram every second year was fine for women over 50. They also confirmed that new treatments have not made older trial data obsolete.

The models led USPSTF to endorse the most efficient plan: Begin screening at age 50, screen every other year, and continue at least to age 74. Petitti later acknowledged that the technical language used in the message made it sound more negative than intended. When the furor erupted, USPSTF added a red-ink correction on the HHS Web site, making it clear that experts did not want women to avoid mammography and that women should "consult your doctor." She concedes, "We communicated what we really meant poorly."

Goodman agrees. USPSTF's presentation of findings was stiff and failed to consider how to communicate risks to a lay public. The task force, Goodman says, "was not prepared for what ensued" when it fell into the "tinderbox" of the congressional debate on health care.

Despite the intensity of the public disagreement that followed the release of the USPSTF recommendations, it's clear that people in all camps agree on at least one point: Research is needed to understand the biology of early-stage breast cancer better. Kerlikowske and others conclude that even the best analysis may not help the public understand risks if the disease is scary and the underlying biology is confused.

A better understanding of DCIS and other early changes in breast tissue might make it possible to differentiate risk better and earlier. It might even help reduce the number of explosive policy brawls on mammography. —ELIOT MARSHALL

CHINA

Leprosy's Last Stand—or Early Days of a War of Attrition?

China thought it had licked leprosy 10 years ago, but the disease is stubbornly hanging on

JIANGYAN, CHINA—Shunned by his home village, You Yu-Gan has lived in a moat-ringed compound here in eastern China's Jiangsu Province for 40 years. In 1970, the farmer was diagnosed with leprosy and bundled off to Jiangyan Leprosarium. Treatment with the antibiotic dapsone tamed his infection, but his hands and feet were irrevocably disfigured and You, like many leprosy victims, languished in quarantine until a drug cocktail in the 1980s brought a long-elusive cure. Free to leave the leprosarium, You opted to stay. The other 118 residents are "like family," explains You, 65, who earns a small income by helping in the clinic. Besides, he confesses, "I have nowhere else to go."

Some 20,000 disabled people still reside in 617 leprosaria or leprosy villages across China. After decades of neglect, the central government has launched a campaign to renovate decaying leprosy facilities. The overhaul is one prong of a reinvigorated strategy against an age-old malady that China nearly vanquished a decade ago but which persists mainly in remote parts of the southwest. To researchers' consternation, the number of new leprosy cases reported each year in China has held steady since the late 1990s. A fresh worry here is a possible uptick in resistance to rifampicin, the big gun in multidrug therapy.

Four years ago, conferees at a World Health Organization (WHO) forum concluded that leprosy was "on the verge of defeat." But the recalcitrant foe has not surrendered. "The transmission of leprosy is not totally interrupted yet," says Denis Daumerie, WHO's project manager for neglected tropical diseases. "Based on our current tools and knowledge, it is impossible to eradicate the disease," adds Wang Baoxi, director of the Chinese Center for Disease Control and Prevention's National Center for Leprosy Control (NCLC) in Nanjing.

Nations have made great strides in bringing the disease to heel. Since a cocktail of rifampicin, dapsone, and clofazimine became standard treatment 30 years ago, the global disease burden has declined from 5.2 million cases in 1985 to just over 213,000 last year. Leprosy continues to bedevil a few countries—for example, more than half of new cases in 2009 occurred in India. But by WHO's definition, the disease was eliminated as a public health threat a decade ago when prevalence fell under one case per 10,000 people worldwide.

Chinese officials have set a more ambitious target: They define elimination as a prevalence of less than one case per 100,000 people at the county level. A nationwide epidemiological survey in 1957 netted 300,000 cases, and by the early '70s, an army of village health workers called "barefoot doctors" was helping professionals ferret out patients and steer them to leprosaria. Prevalence fell from a peak of 23.5 cases per 100,000 people in 1966 to 0.5 cases per 100,000 in 2009, with the disease "eliminated" in 92% of China's 1464 counties—"a great achievement," says Zhang Guocheng, president of the China Leprosy Association.

Holding on. NCLC's Yan Liangbin and a Jiangyan patient he recently operated on. Leprosy is still a scourge in southwest China

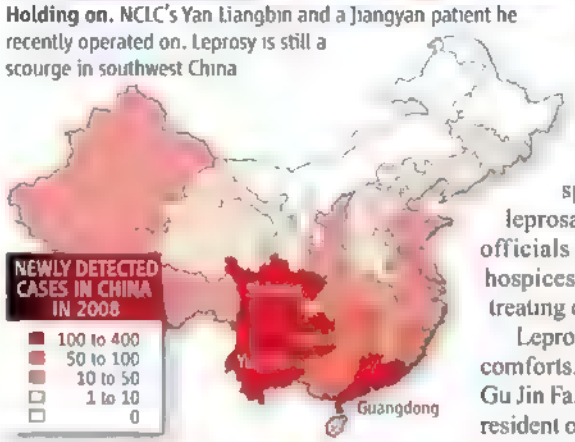

But the endgame is shaping up as a long march. Early infections of *Mycobacterium leprae* easily evade detection; it can take up to 20 years before symptoms from the slowly multiplying pathogen show. New cases in China have hovered at about 1600 a year for the past decade, with most occurring in poor, rural areas of three southwestern provinces, Guizhou, Sichuan, and Yunnan (see map). Elsewhere in China, the majority of cases last year was among the 180 million workers who migrated to the industrialized east and south in search of jobs. "Leprosy detection in this floating population is a severe challenge," Zhang says. An added complication is that in rural China, leprosy remains a social stigma. For that reason, Wang says, "many poor people refuse to be diagnosed."

Rifampicin resistance may pose a new threat. Whereas the other drugs in the cocktail hobble *M. leprae*, rifampicin slays it. Rifampicin-resistant strains emerged in the 1980s but may now be gaining traction in China. "We're seeing increasing numbers of cases with rifampicin resistance," says Chen Xiangsheng, a senior epidemiologist at NCLC. The center is now setting up a national surveillance system for monitoring resistant strains.

In the meantime, China is striving to make amends to the pariahs who have spent most of their adult lives in ramshackle wards. In December, Jiangyan Leprosarium completed a renovation of its 40-year-old facilities that included installing indoor plumbing, solar water heaters, and cable TV. The government is spending $32 million to refurbish leprosaria; after the leprosy victims die, officials say, the facilities will be used as hospices for AIDS patients or retreats for treating drug addicts.

Leprosy victims are relishing the creature comforts. "It's much better here now," says Gu Jin Fa, who at 54 years old is the youngest resident of Jiangyan Leprosarium. He smiles at NCLC's Yan Liangbin, who performed surgery on his feet a couple of years ago, enabling him to walk again after years in a wheelchair. Gu's affection seems genuine, but because the bacterium ravaged his facial nerves his expression is strained and his left eye is tearing. Like many with severe disabilities or who would be shunned if they returned to their villages, Gu has no interest in reintegrating into society. "This is my home," he says. **–RICHARD STONE**

CREDITS (TOP TO BOTTOM): R. STONE/SCIENCE; (SOURCE): NCLC

Bhutan biopharma brain trust. Entrepreneur Wangdi Jamyang (*left*) and mycologist Nigel Hywel-Jones.

BHUTAN

Improbable Partners Aim to Bring Biotechnology to a Himalayan Kingdom

A British mycologist and a local businessperson have launched a pharmaceutical venture grounded in a Buddhist reverence for the environment

THIMPU—In a quaint wooden house on a hill overlooking Bhutan's rustic capital, dozens of test tubes lie on a table bathed in the morning sun. "This is the worst way to store fungi," growls Nigel Hywel-Jones. The mycologist and a pair of young apprentices cooked up the growth medium themselves—potato dextrose agar—by chopping up and boiling spuds and adding dextrose, antibiotics, and agar powder. They filled test tubes with the homebrew and set them in a slope to maximize the surface area for culturing fungi, some possibly new to science, that they collected in Bhutan's high country. It would have been better to keep the fungi frozen in suspended animation, but for now that's not an option, says Hywel-Jones, who is waiting for a −80°C freezer to arrive.

The challenges of carrying out high-caliber science are daunting in an isolated country known for tracking its standard of living with a Gross National Happiness index. Hywel-Jones, a lab chief at the National Center for Genetic Engineering and Biotechnology (BIOTEC) in Bangkok, arrived here last September to help a biotech company take root in a land with a mere handful of Ph.D. scientists. "I was ready for a new challenge," he says.

Hywel-Jones, on a temporary assignment from BIOTEC, is serving as an adviser to Bhutan Pharmaceuticals Private Ltd. (BPPL), a company founded by local entrepreneur Wangdi Jamyang. Besides prospecting for fungi that attack insects and culturing isolates that may have medicinal value, Hywel-Jones is crafting a business model for biotech in the kingdom. There is no dearth of raw materials. Bhutan's highlands are a prime habitat for at least one prized commodity: an insect fungus, *Cordyceps sinensis*, that fetches outrageous prices as a Chinese medicine. Hywel-Jones believes that Bhutan, a biodiversity hot spot, may harbor a wealth of novel compounds for Western medicine, too. "There's fantastic potential," he says. Wangdi puts it this way.

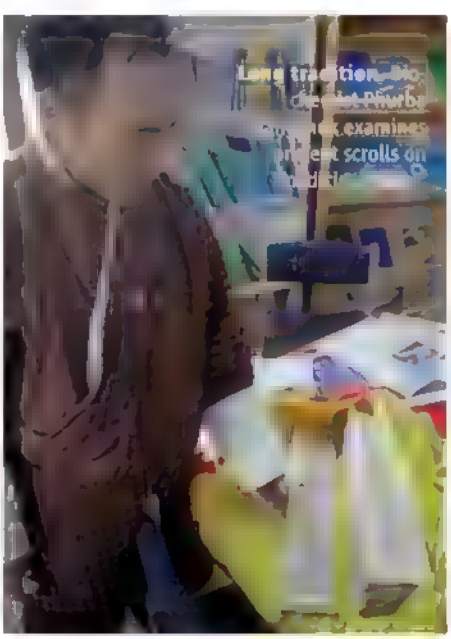

"No one knows much about Bhutan, and that's a selling point. Brand Bhutan."

The duo insists that they are not embarking on a biological Gold Rush. For starters, BPPL is collaborating with the government's National Biodiversity Centre and has approval for now to collect only *Cordyceps* and related species. (The company hopes to expand to other fungi and plants after Bhutan develops expertise in these areas.) Wangdi emphasizes that their activities will be guided by a Buddhist reverence for the environment enshrined in Bhutan's 2008 constitution, which calls for preserving 65% of the country as forest. "We want to set an example for future generations," says Wangdi. "Look, just because we got approval to start exploring, we should not go in and exploit."

Some scientists commend the new venture. "It is generally the case that big pharma has stopped its search for anti-infectious drugs," says Gary Strobel, a plant scientist at Montana State University, Bozeman, who travels the globe in search of fungi of potential commercial value. "There are promising life forms out there, but few people seem to be interested in finding and utilizing them," he says.

Blazing a trail for the pharmaceutical industry carries a moral responsibility to protect Bhutan's interests, Wangdi says: "We'd like to open Bhutan to the world—the right way."

Biological Shangri-La

After a half-hour hike into a mixed broadleaf and pine forest in Dodena, north of Thimpu, Hywel-Jones and Wangdi break for lunch at a makeshift camp 2800 meters above sea level, the first station on an arduous 5-day trek to a *Cordyceps* research site nestled in a valley more than 5000 meters high. The fungus is used in China to treat many ailments, from flu to impotence; in Bangkok, Hywel-Jones and colleagues have isolated novel *Cordyceps* metabolites, including an anti-tuberculosis agent that they have patented. Wangdi passes out sandwiches and hands Hywel-Jones his "diet": a bottle of Druk 11000, a local beer.

They make an odd couple. Wangdi, 41, trim with short black hair and an easy smile, opened his latest money-spinner, a laminate factory near the border with India, last December. Long-haired and irreverent, Hywel-Jones, 51, has gained renown in Bhutan's upland villages for trekking in sandals through snow to his research site and surviving for days on crackers and Marmite. The two enjoy a playful, wry rapport.

CREDITS: R. STONE/SCIENCE

Long before their improbable partnership began, Hywel-Jones had been coming to Bhutan on brief research stints. He first came in 2002, invited by Tshitila (like some Bhutanese, he goes by one name), an agronomist with the agriculture ministry's Renewable Natural Resources Research Centre in Yusipang. Tshitila had asked Hywel-Jones to consult on an urgent fungal problem.

Every spring, Himalayan villagers fan out by the thousands to dig up the few-centimeter-long fruiting bodies of *C. sinensis*, along with the husks of the ghost moth caterpillars that the fungus ghoulishly devours. Known as *yartsa guenbub* in Bhutan, the finest *Cordyceps* fetches several thousand dollars per kilogram (*Science*, 21 November 2008, p. 1182).

Going once. ... Buyers examine Cordyceps before an auction; prime specimens fetch astronomical prices.

In 1995, a royal decree declared *Cordyceps* a protected species and forbade its collection. Research was permitted, however, and a decade ago, when Tshitila and his colleagues were out in the field, they increasingly encountered poachers from Tibet coming across the porous northern border to collect *Cordyceps*. Not surprisingly, that left Bhutanese villagers fuming. "I remember Tshitila's first e-mail asking if I could help with this problem," says Hywel-Jones, a self-described "old-style, traditional taxonomist" who has named nearly 3 dozen fungal species. "I wrote back that I needed to see it firsthand. When he said 'Sure,'" Hywel-Jones says, pumping his fist, "I said, 'YES!'" He then had to consult an atlas to find out where precisely Bhutan is located.

In their initial survey in the spring of 2002 in the Soe Valley, Hywel-Jones, Tshitila, and colleagues logged ample *Cordyceps*. They recommended that the government establish a research program on sustainable collection and legalize the harvest before the fruiting bodies shoot spores. "Our idea was that if locals were allowed to collect, they would put pressure on their Tibetan cousins not to collect," Hywel-Jones says. In 2004, the ban on *Cordyceps* collection was lifted for 1 month every year, in June. That decision, says Wangdi, has pulled many rural Bhutanese out of poverty: Their earnings from *Cordyceps* can exceed a year's income from yak herding.

With support from the U.K. government's Darwin Initiative, in 2005 Hywel-Jones and Tshitila established research plots at Nam Nha, in western Bhutan, that are monitored each year to track population levels and the effects of collecting. Meanwhile, BIOTEC has hosted Bhutanese researchers for training stints in Bangkok. In 2008, Hywel-Jones says, he met Wangdi, "and the rest is history."

Branding Bhutan

In the library of the Institute of Traditional Medicine Services (ITMS) here, a young man wearing a *gho*, Bhutan's national dress, carefully unwraps a canary-yellow cotton cloth. Inside are long and narrow rectangular scrolls in jagged Dzongkha script. The ancient manuscript is a kind of medieval *Merck Manual* compiled when Bhutan was known as *Lho Men Jong*, or "Southern Land of Medicinal Herbs."

To Phurba Wangchuk, an ITMS biochemist who earned a master's degree in natural product chemistry from the Australian National University in Canberra, these scrolls are the guiding principles of Bhutan's health care strategy, which is to ensure access to high-quality, traditional Bhutanese medicine. ITMS trains practitioners and produces more than 100 preparations, including CordyPlus, a concoction based on *Cordyceps* and "other health-promoting ingredients," says Phurba. ITMS's preparations include several dozen medicinal plants found only in Bhutan organisms that are largely terra nova for Western scientists.

One aim of BPPL is to zero in on active compounds. Phurba says that approach does not threaten ITMS, which focuses solely on traditional medicines for the Bhutanese market. In the long run, developing Western medicines by synthesizing compounds could prevent unsustainable exploitation of biological resources. For that reason, Phurba says, BPPL "is on the right track."

The road ahead is not easy. Phurba is one of a rare breed of Bhutanese with credentials in this field, notes Hywel-Jones, whose two assistants have no previous lab experience. "It's going to take time to build a research base," he says. Toward that end, BPPL, in collaboration with the government, plans to send top students overseas to earn bachelor's degrees in areas such as biochemistry and mycology, in which expertise would benefit the company and the nation. Hywel-Jones envisions that 15 years from now, BPPL could have 200 or more research staff

In the short term, survival will require cutting deals with foreign companies. "They will be getting access to biodiversity that's never been opened up before," says Hywel-Jones, honing his sales pitch. "Only 500 species of fungi have been described in Bhutan, compared to 6000 species of higher plants. We know that there is six times more fungal biodiversity as there is in plants. So there are many thousands of fungal species here that have not been characterized." Hywel-Jones is "passionate and sincere" and knows his stuff, says Roger Shivas, curator of Agri-Science Queensland's plant pathology herbarium in Indooroopilly, Australia.

BPPL is in talks with Novozymes, a top producer of commercial enzymes in Bagsværd, Denmark, to sell isolates of insect fungi for operating cash and a potential royalty if an isolate were to have commercial value. Hywel-Jones hopes that in a few years, BPPL will have sufficient in-house expertise to screen isolates itself. That game plan suits Wangdi. "I'm investing in Dr. Nigel," he says. "Bad mistake!" Hywel-Jones says with a grin.

Back in the forest, Hywel-Jones, in the mode most people in Bhutan encounter him wearing a T-shirt and sandals and downing a Druk 11000—says the adventure of launching a biotech industry in Bhutan came at just the right moment in his career. "In Thailand, I was stuck in the lab, writing reports and proposals for bean counters and stuff like that. Yet, this is where I'm happiest and most productive," he says. "The best ideas come when you're in the forest." He and Wangdi hope that more than a few new drugs will emerge from Bhutan's forests as well **–RICHARD STONE**

CREDIT: N. HYWEL-JONES

Politics as (Un)usual

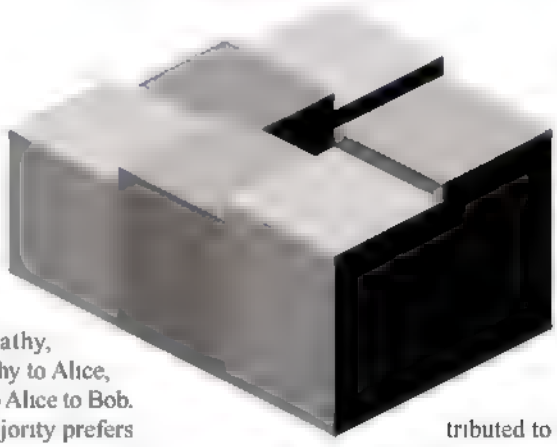

Politics, it's said, is the art of the possible. And for decades, mathematical voting theorists have pointed to the possibility that different voting systems—from simple plurality to instant run-off to the rank-ordered Borda count—could produce vastly different results Donald Saari, director of the Institute for Mathematical Behavioral Sciences at the University of California, Irvine, and a leading voting theorist, likes to boast that if you tell him the result you want (say, for a textbook selection or a new hire for your department) and your voters' actual preferences, he'll find a perfectly fair way of guaranteeing the desired result.

But how common are such paradoxes in practice? Not very, if a recent case study is typical In a session on voting theory at the joint meeting of the American Mathematical Society and the Mathematical Association of America, Anna Popova, a graduate student in psychology at the University of Illinois, Urbana-Champaign, described an analysis of ranked ballots from 8 years of voting for the presidency of the American Psychological Association (APA). She and her adviser, Michel Regenwetter, found that different voting methods gave the same result much more often than not

One classic voting paradox is known as a Condorcet cycle. An extreme example occurs when a third of the voters prefer Alice to Bob to Cathy, another third prefer Bob to Cathy to Alice, and a final third prefer Cathy to Alice to Bob. In such a case, an outright majority prefers Alice to Bob, a different outright majority prefers Bob to Cathy, and yet another outright majority prefers Cathy to Alice. Subtler examples, with the numbers not exactly equal, produce cases in which a reasonable argument can be made—and a voting system adopted—for electing any of the candidates.

Popova and Regenwetter obtained data sets from APA elections from 1998 to 2005, each with upward of 20,000 voters giving full or partial rankings to five candidates for president. (APA uses a form of instant-runoff voting, in which candidates with the fewest first-place votes are successively eliminated and their supporters' ballots are redistributed to those voters' second-place selections.) The research, which compared seven different voting methods, turned up no examples of Condorcet cycles and found only one case in which one method (plurality vote) produced a different winner from the others.

Steven Brams, a voting theory expert at New York University in New York City, questions the generality of the psychologists' findings, noting that balloting in professional societies is often heavily influenced by the process of selecting nominees. "I don't allege that its nominating committees pick some preferred candidate and then fill in the rest of the ballot with weak opponents," he says.

Perfection in a Box

Here's a good way to keep mathematicians busy for centuries: Make up an object, call it "perfect," and then try to find out if it exists. Take so-called perfect numbers: whole numbers such as 6 or 28, which equal the sum of their divisors ($6 = 1 + 2 + 3$; $28 = 1 + 2 + 4 + 7 + 14$). It's hard enough to find ones that are even, but no one has ever spotted a single one that's odd.

Things are even worse with "perfect cuboids": rectangular bricks whose three different edges and four different diagonals (three on faces of the brick and one angling through its "body") all have lengths that are exact integers. Nobody knows whether they exist at all. But something similar has just turned up: At the meeting, researchers reported the first sightings of "perfect parallelepipeds"

A parallelepiped is basically a brick whose sides are allowed to be parallelograms rather than strict 90° rectangles. Like a cuboid, a parallelepiped has three different edges, but it has 10 different diagonals: two on each of its three different sides, and four crisscrossing the body. Perfection is achieved if all 13 of these numbers are exact integers.

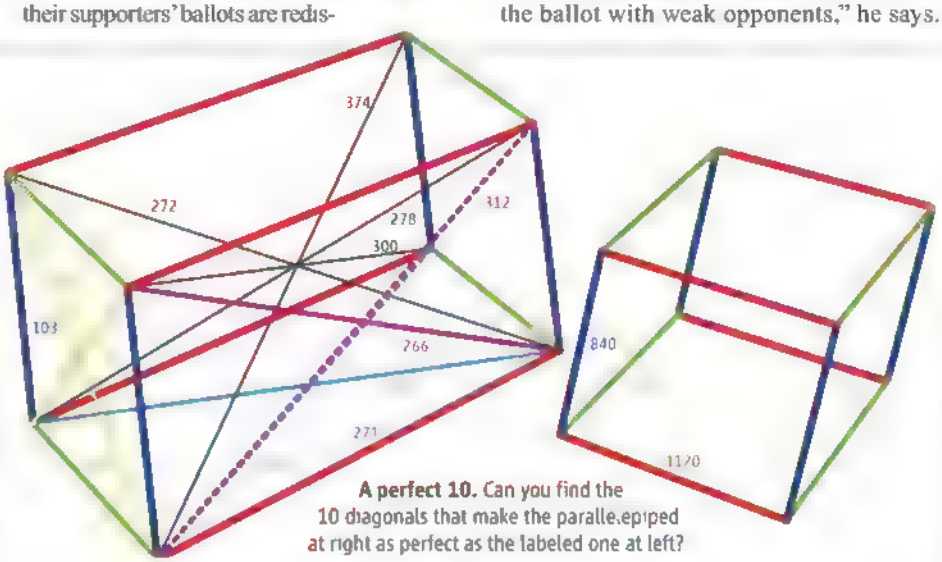

A perfect 10. Can you find the 10 diagonals that make the parallelepiped at right as perfect as the labeled one at left?

Now Clifford Reiter of Lafayette College in Easton, Pennsylvania, and Jorge Sawyer, an undergraduate at Lafayette, have found the first examples of perfect parallelepipeds Their search depended on a simple property of all parallelograms, established by simple algebra: The sum of the squares of a parallelogram's two diagonals is twice the sum of the squares of its two edges. With that formula and a bit of number theory to guide them, Reiter and Sawyer could easily run a systematic search for all parallelograms with edges of "short" integer length, say, into the thousands, whose diagonals are also integers. They then looked for combinations

CREDITS (TOP TO BOTTOM): © AKIYOSHI KITAOKA 2009; SOURCE: CLIFF REITER AND JORGE SAWYER

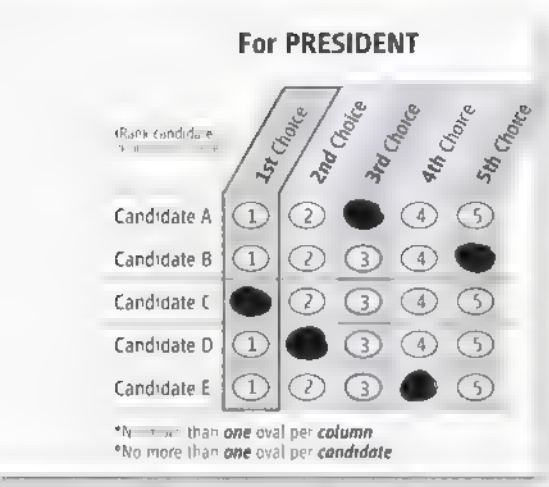

Who's on first? Optical illusion (*left*) mimics a paradoxical "everybody wins" outcome that can actually occur in ranked-choice voting.

"But it may be more than coincidence that one candidate almost always handily beats four opponents." Saari is similarly unsure. "The only way such an empirical result can happen is if people have remarkably similar preferences, much more so than we would expect in general society," he says.

Regenwetter agrees there's a lot left to be explained. But it's becoming clear, he says, that "the empirical world is highly different from the picture that has generally emerged out of the mathematical theory of social choice."

of these "perfect parallelograms" to serve as sides of candidate parallelepipeds and devised a computer algorithm to pick out the perfect ones.

"The biggest surprise for me was how quickly we got results," Sawyer says. Their first example has edges of length 271, 106, and 103 (see figure, left). In all, the computer search found 30 perfect parallelepipeds, with edge lengths up to 3920. Some are tantalizingly close to being cuboids, with one or two rectangular sides. Such findings "may spark even more interest in the perfect cuboid problem," Sawyer says.

Ezra Brown, a number theorist at Virginia Polytechnic Institute and State University in Blacksburg, agrees. "The size of Reiter and Sawyer's smallest solution is very surprising," he says. "Apparently, easing the restrictions that the faces be rectangles is more crucial than anyone thought." Nonetheless, he notes, perfect cuboids, if they exist at all, are a long way off: Computers have looked at all possible bricks with edge lengths up to 10 billion without finding a single one that's perfect.

CREDIT: PHOTO: SUSANNA CAYLER

What Comes Next?

One of mathematicians' most beloved Web sites is getting ready for a makeover. The Online Encyclopedia of Integer Sequences, established by Neil Sloane at AT&T Labs Research in 1996 and run largely as a one-man shop, is poised to go "wiki," with 50 associate editors taking over much of the workload.

The OEIS, or simply "Sloane" as it's known to sequence fanatics, is a database of nearly 200,000 lists of numbers—a mathematical equivalent to the FBI's voluminous fingerprint files. Much as fingerprints give police a quick way to link a new crime to earlier ones, sequences enable researchers to make connections between mathematical problems that might otherwise go unnoticed. The innocuous-seeming sequence 1, 2, 5, 14, 42, 132, ..., for example, arises in a huge number of different contexts, from counting the arrangements of nonintersecting chords inside a circle to enumerating secondary structure possibilities of RNA. To sequence fanatics, such "Catalan numbers," as they're known, are even more famous than the ubiquitous Fibonacci sequence 1, 1, 2, 3, 5, 8, 13, ...

Sloane began compiling sequences in 1965 as a graduate student at Cornell University. By 1973 he had 2372 of them, which he published as *A Handbook of Integer Sequences*. An updated edition, with 5487 sequences, appeared in 1995, with the help of Simon Plouffe of the University of Quebec, Montreal. But by then, Sloane was already moving online. The OEIS made its debut a year later, with a database of 10,000 sequences.

The OEIS "is one of the most useful tools available online for the working mathematician," says Doron Zeilberger, a combinatorialist at Rutgers University, New Brunswick. "It also is a great tool for determining the novelty of a new sequence. If it is not in Sloane, it is most likely to be new!"

The Web site invites users to submit new sequences or comment on existing ones. Such contributions have fueled the database's steady growth. In 2009 alone, the total increased by 18,709 sequences, or more than 50 a day. "Sequences are still pouring in," Sloane says.

Even as he edits the constant stream of new sequences, Sloane takes time to admire some of the contributions. His latest favorite is the "toothpick sequence," added in 2008 by Omar Pol, an OEIS contributor from Buenos Aires. The toothpick sequence registers the increasing size of a geometric arrangement of toothpicks, in which a new batch is added at each stage, centered on and at right angles to the exposed tips of the previous batch (see figure). The picture that emerges displays surprising fractal growth. "It's got beautiful structure," Sloane says. He and his AT&T colleague David Applegate have written a paper on the sequence's mathematical properties, and Applegate has contributed a movie of its geometric growth, linked to its entry in the OEIS.

Sloane set up the OEIS Foundation last year and transferred intellectual-property rights to the nonprofit organization. With Applegate's help, he plans to move the data-

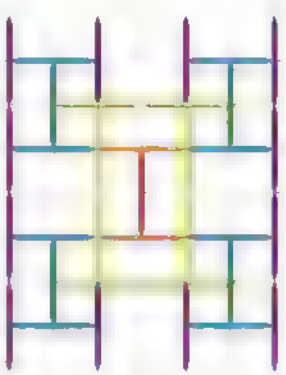

Chewy. Database managed by Neil Sloan (*top*) includes the "toothpick" sequence (1, 3, 7, 11, 15, 23, 35,...), shown here in color-coded steps.

base to a wiki format, giving each sequence its own Web page, with new submissions moderated by a board of editors. The transition has hit a snag, however: Search-engine software in the "wikiverse" can't yet handle sequences of numbers.

Once that technicality is overcome, Sloane expects the wiki format to be an improvement. "It's the correct mechanism for handling the database," he says. As for his anticipated reduced workload, "it'll mostly be a relief. On the other hand, I'll miss all the e-mails."

–BARRY CIPRA

New Mexico Center for Spatiotemporal Modeling of Cell Signaling,
Los Alamos Center for Nonlinear Studies, and
Santa Fe Complex announce:

"The Art and Science of Systems Biology"

March 26 & 27, 2010

The first public display of the winners of the National Science Foundation

Exhibits and all events are free and open to the public. There will be a reception with scientists and artists followed by a public science lecture on Friday and Saturday.

The show will also feature contributed scientific visualizations and artistic expressions relevant to the theme of systems biology, including immersive projections and interactive exhibits.

Santa Fe Complex
632 Agua Fria, Santa Fe, NM 87501

Please call 505-216-7562 to register and visit sfcomplex.org/sysbio for a detailed event schedule.

[illegible]mc.health.unm.edu
[illegible]lanl.gov

Summer Internships
Students with Disabilities

To meet the challenge of the competitive economy in the new millennium, private industry and government research agencies must expand the pool of technical talent. AAAS started Entry Point!, a program that offers students with disabilities competitive internship opportunities in science, engineering, mathematics, computer science and many fields of business. And this is just one of the ways that AAAS [illegible] a more diverse, inclusive, and prosperous world. Join us. Together we can make [illegible]

AAAS

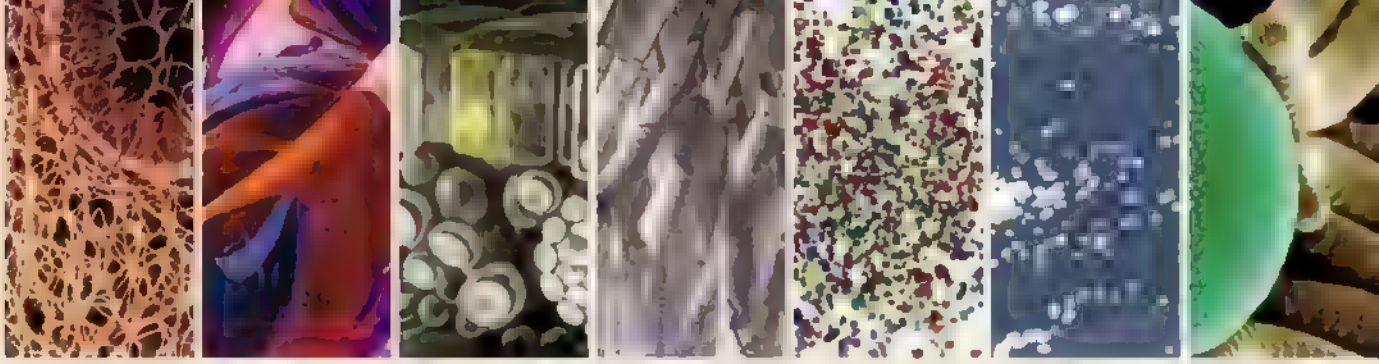

Visualization Challenge

SOMETIMES SCIENTIFIC INFORMATION CAN BE VIVIDLY REPRESENTED WITH commonplace materials. Take the illustration on the cover of this issue of *Science*. It is a three-dimensional art installation made from 75,000 cable zip ties depicting the dynamic relationships between endothelial cells and their surrounding microenvironment. Or turn to page 950 for a description of how cotton batting, a clothesline, and sewing pins are used in a video to illustrate the impact of the environment on gene expression. The sculpture and video are among the awardees in this year's International Science & Engineering Visualization Challenge.

Online

sciencemag.org

Slideshow and podcast interview

Clearly, the convergence of art and science can successfully convey complex phenomena in spectacular ways.

For the past 7 years, *Science* and the U.S. National Science Foundation (NSF) have co-sponsored annual challenges to promote cutting-edge efforts to visualize scientific data, principles, and findings. The visualization challenge is intended to showcase and encourage this kind of work.

This year's entries present a bold and unique look at life, from the broad view of planet Earth, to a more intimate picture of activity inside the human brain. We received 130 entries from 14 countries, 23 U.S. states, and the District of Columbia. A committee of staff members from *Science* and NSF screened the entries, and an outside panel of experts in scientific visualization reviewed the finalists and selected the winners. The winning entries appear on the following pages.

We encourage you to submit applications for next year's challenge, details of which will be available at www.nsf.gov/news/scivis, and to join us in celebrating this year's winners.

Tarri Joyner of NSF organized this year's challenge. Michael Torrice of *Science*'s news staff wrote the text that accompanies the images in this special section, and Martyn Green, Tara Marathe, and Andrew Whitesell put together a special Web presentation at www.sciencemag.org/special/vis2009/.

– JEFF NESBIT, DIRECTOR, OFFICE OF LEGISLATIVE AND PUBLIC AFFAIRS, NSF
MONICA BRADFORD, EXECUTIVE EDITOR, *SCIENCE*

Judges

Donna Cox
University of Illinois
Urbana, IL

Thomas Lucas
Thomas Lucas Productions Inc
Ossining, NY

Alisa Zapp Machalek
National Institute of General Medical Sciences
Bethesda, MD

Corinne Sandrone
Johns Hopkins School of Medicine
Baltimore, MD

Tierney Thys
National Geographic Emerging Explorer
Carmel, CA

Thomas Wagner
Cryosphere Science Program, NASA
Washington, DC

Science

CREDITS: SEE FOLLOWING PAGES

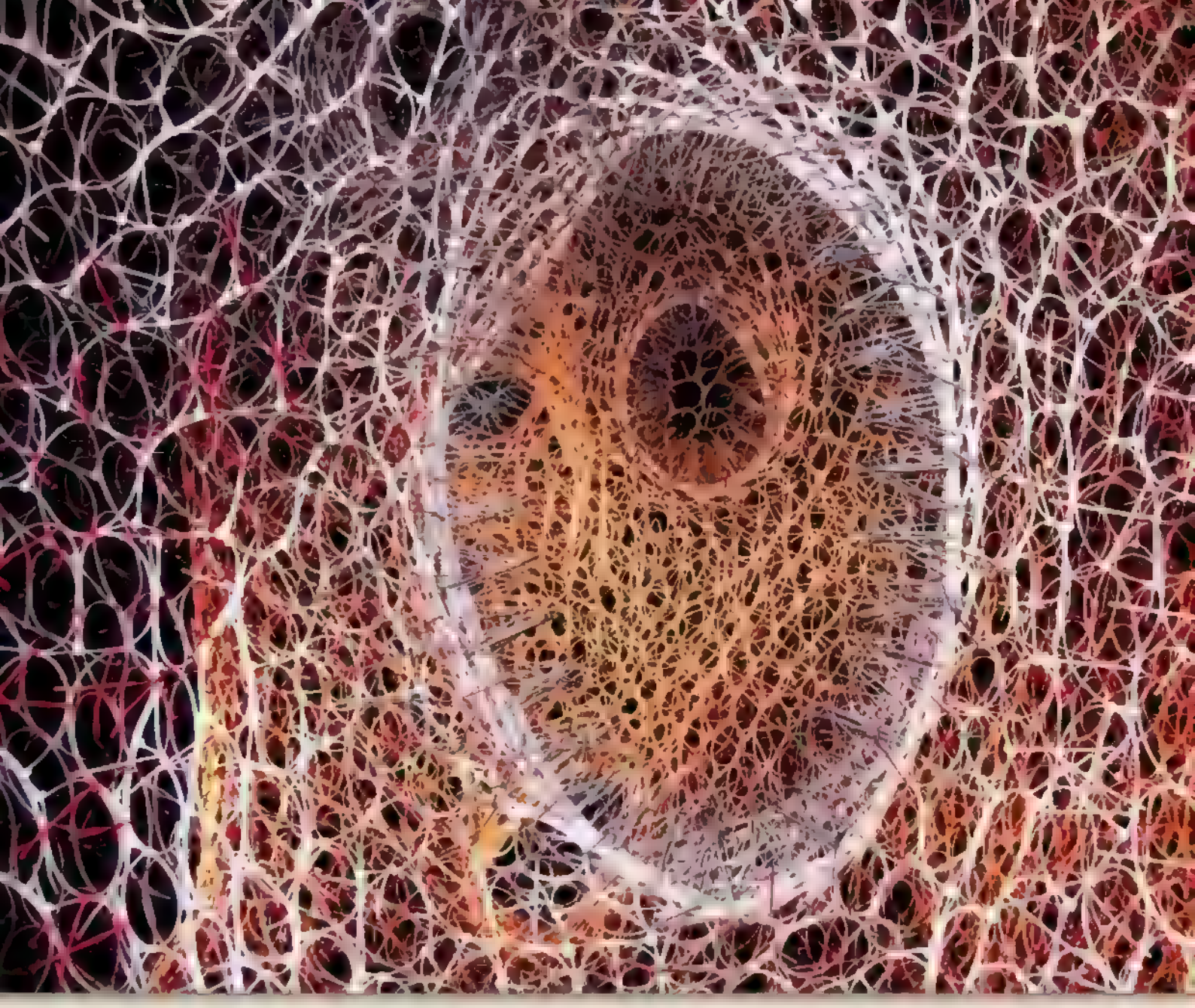

Branching Morphogenesis

Peter Lloyd Jones, Andrew Lucas, and Jenny E. Sabin,
University of Pennsylvania's Sabin + Jones LabStudio

Forget about staring at data on a computer screen; try walking through those statistics and touching them. With this illustration of the forces lung cells exert as they form capillaries, scientists and museumgoers can do just that. The 3.5-meter-tall, three-dimensional art installation is one of several projects by biologist Peter Lloyd Jones and architect Jenny E. Sabin of the University of Pennsylvania's Sabin + Jones LabStudio that depict large, complex data sets in new ways. "Sometimes graphing data won't tell you about its intricacies," Jones says. "This makes the whole process exciting and interactive."

The sculpture depicts five snapshots from a computer simulation of lung endothelial cells pushing against and pulling on the protein matrix that surrounds them. Using the simulation data as a template, the team connected 75,000 cable zip ties, each representing a single data point, into five 4.5-meter-wide hanging curtains for each time point. The designers built zip-tie tunnels between the curtains, so viewers could peer through them and watch how the cells' forces changed over time. The sculpture acts like a time-lapsed movie of the data, Sabin says. "Gallery visitors are encouraged to walk around and in between the layers and immerse themselves in this newly created datascape," she says.

The members of the panel of judges felt that the illustration captivated viewers' attention with the imaginative use of zip ties and its mesmerizing tunnels. "It literally drew you in, because you could walk through it and examine it," says panel of judges member Thomas Lucas. And "you can interact with it with more than just your eyeballs," says judge Alisa Zapp Machalek.

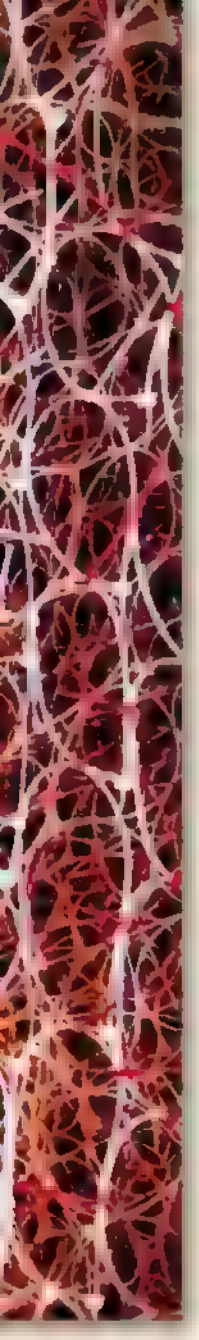

Illustration

First-Place Winners

Kuen's Surface: A Meditation on Euclid, Lobachevsky, and Quantum Fields

Richard Palais and Luc Benard,
University of California, Irvine

Sketch a line and then draw a point off it. How many lines parallel to the first line can you draw through that point? The Greek mathematician Euclid said just one, but for more than 2000 years after his death, mathematicians struggled to prove that he was right based on his other geometric rules. Then the 19th century Russian mathematician Nikolai Lobachevsky showed that you couldn't: In some circumstances, you can sketch an infinite number of lines through that point and not violate any of Euclid's other axioms. Mathematician Dick Palais of the University of California, Irvine, and digital artist Luc Benard wanted to convey the history of Lobachevsky's solution to this mathematical puzzle with their illustration

Lobachevsky's work "caused a big stir, as you can imagine," Palais says. Other mathematicians began building on the discovery and created new kinds of geometry. (Albert Einstein used these geometries when he developed his general theory of relativity.) One important discovery they made was that surfaces called pseudospheres, which violate Euclid's parallel postulate, could be described simply from solutions to an equation called sine-Gordon.

In this illustration, a sheet of paper shows sketches of one of these surfaces, called Kuen's surface, and the expression, called a soliton, that describes it. "We wanted to talk about these equations in a way that nonmathematicians could understand," Palais says. "So we took a symbolic approach: The surface itself stands as a symbol for that equation." Benard rendered Kuen's surface to resemble a glass sculpture, reflecting light bouncing off the paper and into the shape's many folds—a process that required more than 200 hours of computer time.

The judges appreciated how the page on the table connected the stunning glass shape with mathematical theory. The illustration made me "feel like I was being asked to sit down at the table and engage with the math," says panel of judges member Corinne Sandone.

Illustration
Honorable Mentions

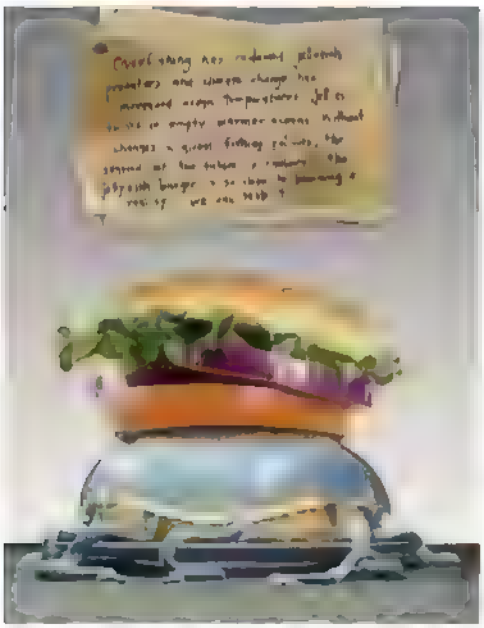

Jellyfish Burger

Dave Beck, Clarkson University, and Jennifer Jacquet, University of British Columbia

Fast-food diners don't expect stringy tentacles or a gelatinous blob when they bite into their burger. But marine scientist Jennifer Jacquet of the University of British Columbia in Canada and digital artist Dave Beck's illustration uses this absurd, grotesque image to make their point: Overfishing and climate change have significant consequences for marine ecosystems. As the numbers of larger fish dwindle and ocean temperatures rise, the sea becomes more and more ideal for the floating creatures, Jacquet says.

Jacquet's adviser, Daniel Pauly, first dreamt up the jellyfish burger as an absurd metaphor for where overfishing was leading us. To illustrate the idea, Jacquet contacted Beck, whom she's known since the fifth grade. Beck set up a fake burger shoot with buns, tomatoes, and lettuce from the market. He then digitally added the computer-generated jellyfish, adjusting it for just the right amount of rubbery gooeyness. "I wanted it to be both funny and scary," Beck says. "My ultimate goal is to reel viewers in so that they're no longer interested in the image, but they're now thinking about the larger issue." Along with the burger, Jacquet has also imagined a series of follow-up illustrations to create a possible exhibit of seafood of the future, including krill chowder and squid and chips.

Back to the Future

Mario De Stefano, Antonia Auletta, and Carla Langella, The Second University of Naples

Nature has been building microscopic cellular solar panels for almost 200 million years. So let's follow her lead, says marine biologist Mario De Stefano of the Second University of Naples in Italy. De Stefano and his collaborators have been studying diatoms, microscopic algae, and they believe the organisms' cellular structures could inspire the design of solar panels. This illustration demonstrates the principles of biomimeticism, which involves looking "to natural organisms to see our future," De Stefano says. In the foreground, a scanning electron microscope image shows the blue fans of diatom colonies from the species *Licmophora flabellata* that have attached themselves to a sand grain with a long, gelatinous anchor, called a peduncle. Each cell is a flat wedge with a glasslike wall shaped to maximize its surface area and absorb sunlight more efficiently for photosynthesis. Behind the sand grain, the team presents computer drawings of their bio-inspired solar panels, which would stand 3 meters tall with a span of 50 meters. De Stefano and his collaborators have started building these panels and believe that they could be used to create solar-powered street lamps.

Interactive Media

First-Place Winner

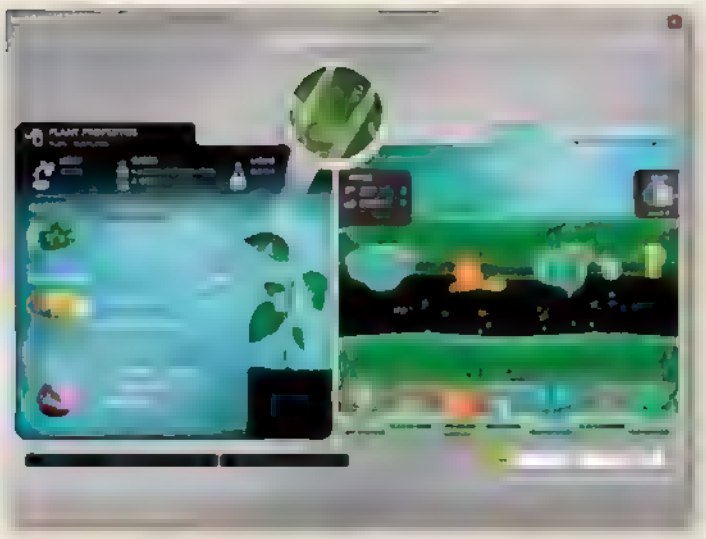

Genomics Digital Lab: Cell Biology

Jeremy Friedberg and Andrea Bielecki,
Spongelab Interactive

Video games allow players to rock out like Jimi Hendrix or hurl touchdown passes like Peyton Manning. In this interactive media entry, they can turn sunlight into electrons and convert sugar into energy like a plant cell. Jeremy Friedberg and his team at Spongelab Interactive in Toronto, Canada, designed this Web-based game to teach high school students about the intricate cycles and pathways that keep the cell alive by generating and burning energy.

At the start of each game, the camera zooms into the cross section of a leaf and focuses on a glowing cell. Then the students must play the role of that cell, building and maintaining its cycles and pathways to score energy points. In one game, players have to manage glycolysis, the pathway that breaks down the sugar glucose, by shooting enzymes at molecules marching on tracks to convert them into new chemicals that the cell can use. The final games focus on transcribing genes and synthesizing proteins—processes on which cells spend much of their energy. Similar to Guitar Hero, players transcribing a gene must hit the appropriate RNA base letter as the DNA template scrolls down the screen. Too many mistakes and the cell becomes sick.

Games can be important educational tools that go beyond rote memorization, Freidberg says. "I want to know if my students can think critically and be creative and figure out ways through problems," he says. "That's what games can do: They can create scenarios that make students problem-solve."

The judges "were impressed with the incredible attention to detail and accurate representation of cell structures … as well as the use of story lines to draw in and sustain the users' attention," says panel of judges member Tierney Thys. "My only wish is that I'd had more time to play it!"

Noninteractive Media

First-Place Winners

The Epigenetics of Identical Twins

Harmony Starr and Molly Malone, University of Utah

As children, identical twins are indistinguishable. But as they reach adulthood, physical differences develop. One twin may go gray earlier or the other's facial features may seem more youthful. This short video from the Genetic Science Learning Center at the University of Utah explains that one reason for this phenomenon is epigenetics, the chemical changes cells make to chromosomes.

The A, T, C, and G letters of our genetic code are familiar enough. But enzymes write another message onto the nucleotides of our DNA and our chromosome's proteins to control how our genes turn on and off.

Harmony Starr and Molly Malone tell the story of how two twins' epigenetic codes change with their different environments and life choices. The video starts with tubes of cotton batting clipped onto a clothesline to depict the chromosomes the twins inherit from their parents. Red-topped sewing pins pushed into each tube represent the chemical tags of each chromosome's epigenetic code. As the twins grow from infant to adult—visualized by a scroll unraveling from a rolling pin—hands place objects that symbolize environmental differences next to clothes baskets filled with each twins' chromosome tubes. With each new factor, such as an ashtray for smoking or a jump rope for exercise, the hands push more pins into the white tubes. By the end of the video, corresponding chromosomes from each twin have visibly different pin patterns dotting them.

This low-tech approach to explaining a technical topic was intentional: "Because there is so much use of computer graphics [in science videos], we hoped the style of this piece would catch people's attention with its simplicity and quirkiness," says the center's director, Louisa Stark. The judges agreed. "It was a delightful way to present an extraordinarily detailed scientific concept that is accessible and entertaining to an audience," says panel of judges member Alisa Zapp Machalek. "You could tell that the producers had a tremendous amount of fun conceiving and making it," says judge Thomas Lucas.

Follow the Money: Human Mobility and Effective Communities

Christian Thiemann and Daniel Grady,
Northwestern University

Ever wonder where your dollar bills travel after you plop them down for a cup of coffee? The Web site Where's George? allows you to do just that: Record your bill's serial number and then track its journeys as other people spend it across the country. But it's more than just a game. Because every time a dollar is spent in a new place, it means someone moved it there. Christian Thiemann and Daniel Grady of Northwestern University in Evanston, Illinois, have been using the Web site's data to study how people move within the United States.

They produced this video to explain their project and animate the results. Tiny bills stretch out from county to county on a map of the contiguous United States. Some places, such as Los Angeles, California, have many bills passing through it from across the nation, while others, such as Anderson County in Tennessee—Grady's home—have just a few that mainly cycle locally. From this travel data, the team ran computer algorithms to find what they call effective communities within the United States. People tend to travel more within these invisible boundaries than outside them. In the video, counties flash and wiggle as the computer algorithm tries to decide which counties belong in the right community. "Normally, … you just push a button and wait for 2 hours and then all you get are numbers, which is really boring," Thiemann says. "But [the animation] makes the process visible and shows you how interesting it can be."

Grady hopes the video will stimulate other people to think up new ideas about what to do with these data. They've already started using it to study how diseases, such as H1N1, spread, and linguistics professors want to compare these travel boundaries to dialect boundaries.

Panel of judges member Corinne Sandone thought the video had a whimsical, quirky appeal, like that of independent films. "I liked the extreme geekiness of it and how it made me want to watch it again to absorb it all," says judge Thomas Lucas. "It was so rich."

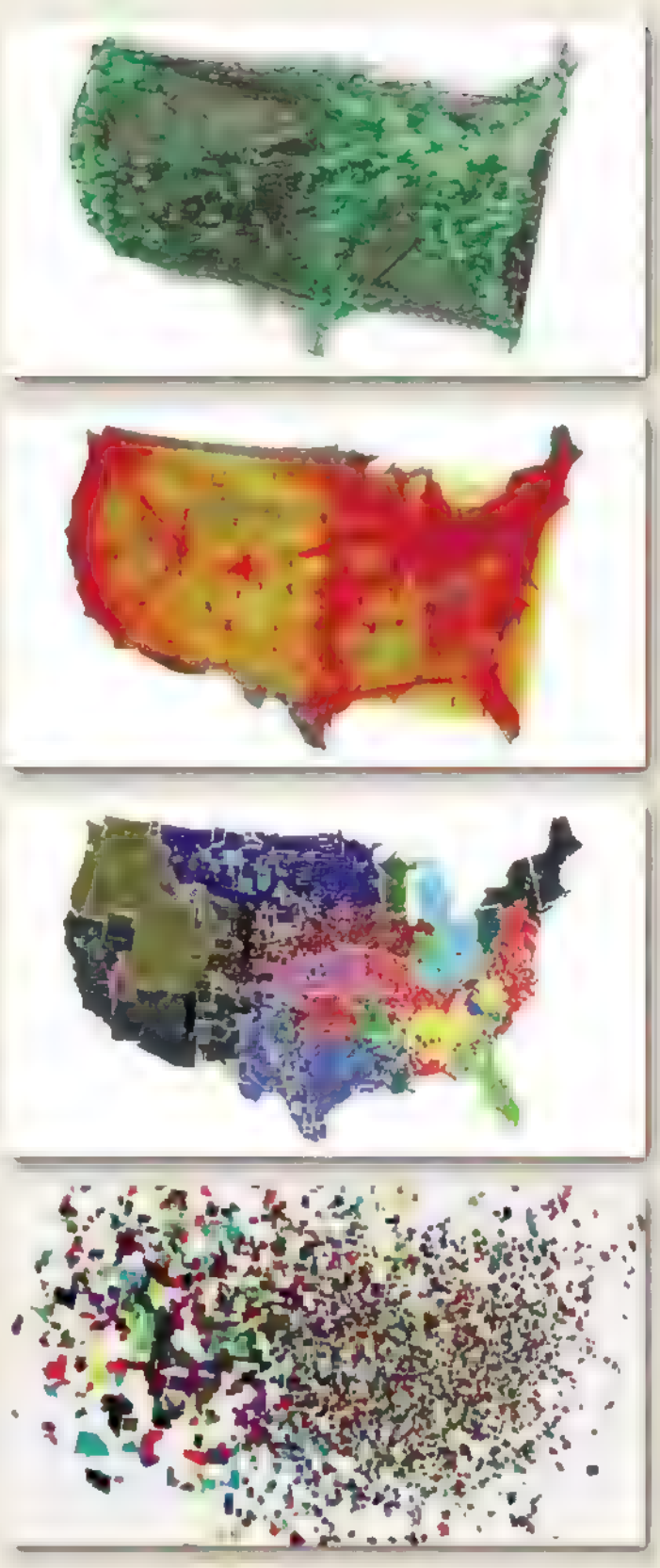

Noninteractive Media

Honorable Mentions

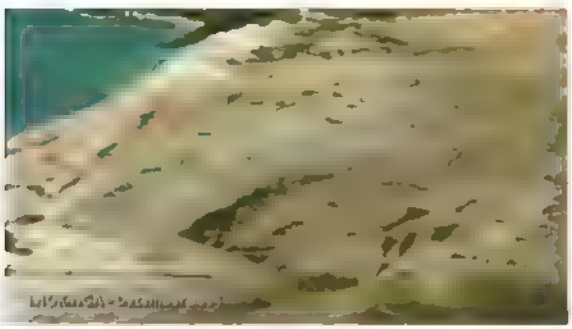

Decision Support System for Tsunami Early Warning

Gregor Hochleitner, Christian Gredel, and Nils Sparwasser, German Aerospace Center (DLR)

After the 2004 Indian Ocean earthquake triggered a devastating tsunami that killed more than 200,000 people, Germany and Indonesia designed a new system to warn people when a tidal wave is about to strike. Nils Sparwasser and his collaborators at the German Aerospace Center produced this video to explain how the new German Indonesian Tsunami Early Warning System combines data from underwater probes, orbiting global positioning system satellites, and floating buoys to better detect a coming tidal wave. Starting with a hypothetical earthquake off the coast of Sumatra, the video's animations show how the different components relay their information to a central decision-making center and how computers there then predict which areas should be evacuated. "We wanted to explain that the new system works with much more information [than previous systems]," Sparwasser says. "So if it generates a warning, they have a really good reason to evacuate."

Inside the Brain: Unraveling the Mystery of Alzheimer's Disease

Stacy Jannis, William Dempsey, and Rebekah Fredenburg, Jannis Productions

In a brain riddled with Alzheimer's disease, protein tangles grow and connections between nerve cells shrivel. This video by Stacy Jannis and her team at Jannis Productions in Silver Spring, Maryland, animates these microscopic damages to explain how the disease starts. The team produced the movie for the National Institute on Aging to depict scientists' most current understanding of what happens inside cells during the disease. The video's computer graphics animate the molecules that start the trouble: Enzymes snip amyloid precursor protein in the wrong spot to create fragments that form long, destructive plaques; meanwhile, tau proteins go awry and tangle up with other proteins in the cell. "A lot of people have a sense of how the disease affects a person's personality and mental functioning," Jannis says. "But we wanted to show that there are specific cellular reasons behind all of that."

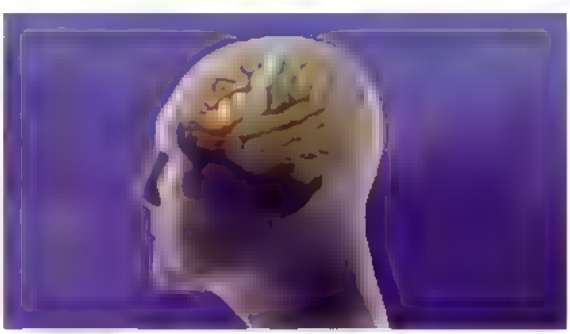

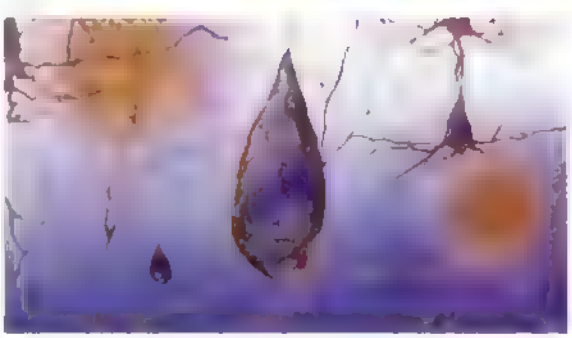

Informational Graphics

First-Place Winner

Brain Development

Dwayne Godwin, Wake Forest University School of Medicine, and Jorge Cham, www.phdcomics.com

Some comic strips tell stories about caped superheroes saving their city or obese cats tormenting dogs. But this strip tells the tale of how the most complex object in the universe—your brain—develops.

Neuroscientist Dwayne Godwin of Wake Forest University School of Medicine in Winston-Salem, North Carolina, and cartoonist Jorge Cham hope to tap into people's curiosity about how their brains become complex computational machines. They explain that our brains start when cells in a 4-week-old embryo fold up into a tube. They then zoom in to describe how individual nerve cells form connections by reaching out and firing chemical signals at each other, a process that continues even after birth. Fast-forward to the teenage years and the brain is still developing—especially the frontal lobe, which is the judgment and decision-making center. "Which might explain a lot," the team writes in a frame with a woman pointing at her boyfriend's high-school yearbook and laughing at his embarrassing wardrobe choices.

Godwin and Cham—who developed the strip *Piled Higher and Deeper (PhD)*—started working on neuroscience-themed comic strips together in 2007. To design their cartoons, which now appear in *Scientific American Mind*, Godwin begins by reviewing the latest literature on their chosen topic and outlines a story. "Each comic could have a bibliography attached to it," Godwin says. Then Cham boils that outline down to visuals and sprinkles in some humor.

The team hopes that a few laughs will help the concepts stick in the readers' brains. The judges felt that it worked and found the cartoon to be engaging. Although many high-school students probably think brain development "is intimidating or dry, … the medium of cartooning makes it come alive," says panel of judges member Alisa Zapp Machalek. Middle and high school students would enjoy it, because "it's different from what they'd find in their textbooks," says judge Corinne Sandone.

Honorable Mention

Regulation of the Cell Cycle and DNA Damage-Induced Checkpoint Activation

Erin Olson, Daphne Orlando, and Tim Manning, R&D Systems Inc

Inside a cell's nucleus, some proteins act like quality-control auditors, ensuring that it's safe for the cell to copy its DNA and divide. This informational graphic from Erin Olson and her team at R&D Systems in Minneapolis, Minnesota, sketches how these proteins seek out DNA damage during checkpoints as the cell moves between the four stages of its cycle. In the purple circles, they juxtapose the actions of the checkpoint proteins with the normal events inside the cell's nucleus. Some of these checkpoint proteins detect DNA damage, while others sit on the broken site and recruit new proteins to send out the call for DNA-repair enzymes to fix the problem. Olson hopes the poster will serve as a quick reference for researchers and biology students.

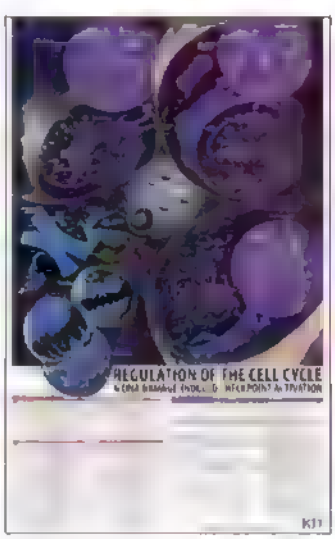

Photography

First-Place Winner

Save Our Earth, Let's Go Green

Sung Hoon Kang, Boaz Pokroy, and Joanna Aizenberg, Harvard University

Noodlelike fibers stretch to latch onto a green sphere. Alone each fiber is powerless, but together they grip and support the orb, embodying cooperation at a microscopic scale. This electron microscope photograph catches self-assembling polymers in action, but it could also represent people's cooperative efforts to save Earth, says materials scientist Joanna Aizenberg of Harvard University. "Each hair represents a person or an organization," she says. "It shows our collaborative effort to hold up the planet and keep it running."

Aizenberg and her colleagues design self-assembling polymers in hopes of creating energy-efficient materials. They have snapped many similar photos of micrometer-scale cooperation. This image shows hairlike fibers of epoxy resin assembling around a polystyrene sphere, which is about 2 micrometers in diameter. When the scientists added a drop of water containing these spheres, the hairs were standing straight up. But when the liquid began to evaporate, the fibers wound around the sphere. The hairs aren't attracted to the sphere chemically or magnetically; instead, capillary action glues them to it. (These same forces make wet hair clump.) "We're trying to make the process reversible and potentially use it in drug release or self-cleaning materials," Aizenberg says. She envisions polymer fingers that grab dust particles or floating bacteria and then later release them to flush the contaminants away.

The judges enjoyed how the photograph wove together a gorgeous image with an important message. "This image simply sprang forth from the page as the most arresting, aesthetic, and provocative image in this category," says panel of judges member Tierney Thys.

Microbe vs. Mineral—A Life-or-Death Struggle in the Desert

Michael P. Zach, University of Wisconsin, Stevens Point

Although the bursts of rainbow colors in this photograph are mesmerizing, microbes fight for their lives in the background. Chemist Michael P. Zach of the University of Wisconsin, Stevens Point, snapped this image of a salt sample he collected in a hot, arid valley near Death Valley National Park in California. He crushed the salt, placed it under a microscope slide, and added a drop of water. Suddenly a slew of microbes came to life as the salt crystals dissolved. Then when the water started evaporating, he took the picture. (The colors come from light passing through the growing crystals, which act like prisms.) The microbes evolved to live in this salty, scorching landscape by excreting molecules that halt crystal growth, which helps them avoid getting trapped in the salt. Zach was drawn to the photograph because it captures "the intrigue of a life-and-death struggle in just one drop of water."

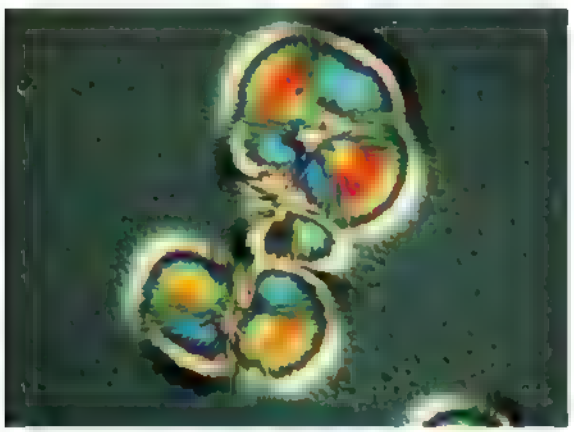

Self-Fertilization

Heiti Paves and Birger Ilau, Tallinn University of Technology

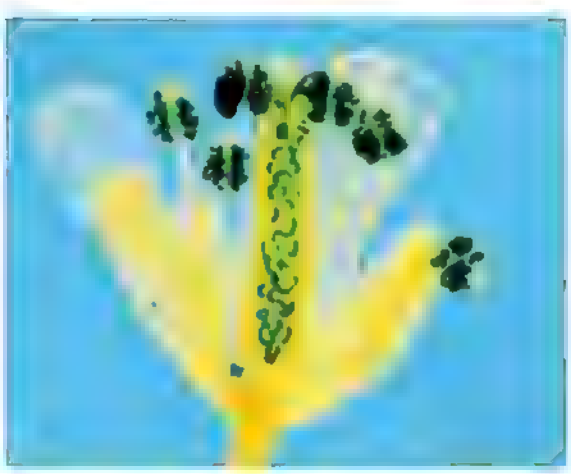

Within its tiny white flowers, thale cress (*Arabidopsis thaliana*) does what most plants avoid: It fertilizes itself. Heiti Paves of Tallinn University of Technology in Estonia took this photograph of the flower with its pollen grains and ovaries stained blue to show the process in action. From the six pollen heads, the grains grow thin tubes toward the bean-shaped ovaries in the flower's stigma to fertilize them. Because of the microscope technique used, polarized light turns the normally white flower yellow and the background blue. Scientists have used *A. thaliana* in many genetic studies because its self-fertilization makes experiments clearer. Gregor Mendel used a self-fertilizer, the pea, to build his genetic theories, Paves notes.

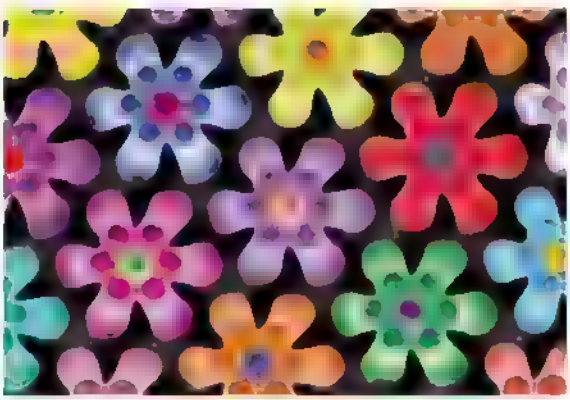

Flower Power

Russell Taylor, Briana K. Whitaker, and Briana L. Carstens, University of North Carolina, Chapel Hill

Accidents can sometimes be beautiful. Briana Whitaker and Briana Carstens of the University of North Carolina, Chapel Hill, snapped this photograph as a quality-control step in their experiments to study the forces that cells, such as those that stitch together skin wounds, exert. They visualize these forces by watching how forests of 10-micrometer-tall polymer pillars bend when they place the cells on top of them. Ideally, the pillars should stand straight up, but on this occasion most of the pillars had fallen over. Amazingly, though, they'd all collapsed into a flower-petal-like pattern. "If you zoom out, you can see a whole field of view of these pillars collapsed in the same pattern," Carstens says. Usually the rods twist around each other and form an unappealing mess. So when the scientists saw this repeating pattern, they decided to color them in pastels and create this paisley photo.

The Cure for Poor Resolution

MeltDoctor™ HRM Reagents

Improve the health of your HRM experiments
www.appliedbiosystems.com/hrm

applied biosystems™

LETTERS

edited by Jennifer Sills

Sustainable Foresting: Easier Said Than Done

IT IS COMMONLY HELD THAT PLANTING FORESTS HELPS TO MITIGATE CLIMATE CHANGE, because forests sequester carbon dioxide into long-lived biomass and soils (*1*). However, our personal experience shows that managed forests are unlikely to increase the land carbon sink unless foresters are paid a fair price for the ecosystem services they provide

Six years ago, we bought 200 ha of mountain spruce forest and 35 ha of deciduous forest from the German government, under the condition that we would use the forest to grow and sell wood in a sustainable manner and that we would employ local labor. The spruce forest was a monoculture; the deciduous forest contained a rich flora of about 15 tree species.

The first obstacle we ran into was deer. To convert the spruce forest from a monoculture to a mixed forest, we supported the early successional rowan trees, but the deer ate the rowan tree bark. The resulting wood rot caused the trees to break. At that point, we had to choose between returning to a less environmentally friendly spruce monoculture or upsetting the public by clearing, replanting, and fencing in our mixed forest to keep out the deer. Fencing is unpopular with the German public, who are entitled to use private forest for recreation.

Clearing requires permission by German forest law; permits are granted after wind or pest damage We opted for clearcutting in a few cases, but found that the more environmentally friendly approach of doing so prevented recovery of the forest. Leaving slash on site was well received by nature conservationists because of the habitats provided by the dead wood, but the spruce slash stimulated nitrification, and tall thickets of nettle prevented tree regeneration. When slash was removed and sold to a power station, the cost of collecting the slash was as high as the income received. Our action also upset the nature conservationists However, the forest did regenerate.

An attempt to return to a more natural vegetation at a mountain site also met with a mixed response from conservationists When wind damage forced us to clearcut an old spruce stand, we planted a mix of beech, sycamore, and fir. Landscape conservationists (who want to preserve the original spruce) complained that we had changed the appearance of the mountain, whereas nature conservationists applauded the fact that the new habitat supports rare insects, bats, and birds. Yet, sycamore and fir are susceptible to deer browsing and must be fenced for about 50 years. Given the carbon cost of fencing and the soil carbon loss after clearing, the climate mitigation potential of this clearcut will likely be negative over the next 60 years (*1*).

We also found that selling our wood was not as easy as we had envisioned. A 150-year beech could not pass through the saw mill and was not perfect for veneers; it went as cheap firewood. The price for spruce peaks at a breast-height diameter of 20 to 25 cm (typical of a 60-year-old tree) because modern construction beams are glued compound woods, not solid cuts from big trees. The forest carbon pool will fall in response to this demand for small trees Such trees can be logged selectively with modern harvesting machines, but the machines require a 4-m-wide skidder trail every 20 m; the resulting 20% loss of forested land diminishes the capacity of the forest to absorb carbon

Furthermore, maintaining biodiversity turns out to be a commercially risky management strategy. Industry demands uniform pieces of wood of the same species, mainly beech or spruce. The only way to maintain our 15-species mix is to sell to the niche market for high-quality stems of rare woods.

These observations show that in Germany, and likely elsewhere, there is little incentive to manage land in a climate-friendly manner. Only when ecosystem services such as mitigating climate, biodiversity, and recreation create income will they be able to compete with the market for wood as timber, pulp, or an energy source

E. DETLEF SCHULZE* AND INGE SCHULZE

Max Planck Institute for Biogeochemistry, Jena, Germany.

*To whom correspondence should be addressed. E-mail: dschulze@bgc-jena.mpg.de

References and Notes

1. A. Thuille, E. D. Schulze, *Glob. Change Biol.* **12**, 325 (2006)

2 We thank J. Gash for editorial help and discussion

Responsible Researchers Required

THE NEWS OF THE WEEK STORY "A DARK TALE behind two retractions" (R. F. Service, 18 December 2009, p. 1610) omitted important issues regarding the training of young scientists. Students and postdocs involved in this debacle may have learned excellent experimental protocols and techniques, but did any of them have training in responsible conduct of research? And if so, how did that training influence their actions? When co-workers present research results, we trust them to be open, honest, and forthright. The high stakes of losing two papers in top-tier journals for all involved, including a pretenure faculty member whose tenure decision may have been affected by the retractions, remind us that we should pursue science for the sake of discovery and self-actualization rather than less savory goals such as power, financial gain, and prestige.

Disappointingly, the News story did not discuss subsequent action that could preclude this type of situation from arising again. Challenging results that cannot be reproduced requires substantial courage. At what point do we draw the line between results that "have

not yet been reproduced" and those that "cannot be reproduced"? Without guidance about responsible conduct of research, students lack the tools and experience to question protocols or recognize potentially risky situations. Both the National Institutes of Health (*1*) and the National Science Foundation (*2*) have written new guidelines for required training in responsible conduct of research. These changes suggest that the scientific community now acknowledges that training young scientists means more than teaching them how to design and perform experiments and interpret data. We hope that high-profile laboratories, such as Peter Schultz's, will lead by example and will endorse the concept that real-time, face-to-face, responsible-conduct training by qualified professionals is not only desirable but necessary to help avert horror stories like this in the future.

NANCY E. LEVINGER* AND ELLEN R. FISHER

Department of Chemistry, Colorado State University, Fort Collins, CO 80523–1872, USA

*To whom correspondence should be addressed. E-mail levinger@lamar.colostate.edu

References

1. NIH, "Update on the Requirement for Instruction in the Responsible Conduct of Research" (http://grants.nih.gov/grants/guide/notice-files/NOT-OD-10-019.html)
2. NSF, Responsible Conduct of Research (http://edocket.access.gpo.gov/2009/E9-19930.htm)

Letters to the Editor

Letters (~300 words) discuss material published in *Science* in the previous 3 months or issues of general interest. They can be submitted through the Web (www.submit2science.org) or by e-mail (1200 New York Ave., NW, Washington, DC 20005, USA). Letters are not acknowledged upon receipt, nor are authors generally consulted before publication. Whether published in full or in part, letters are subject to editing for clarity and space.

Oil and Water Do Mix

IN THE 20 NOVEMBER 2009 SECTION OF This Week in *Science* (p. 1040), the piece "Methane's path to captivity" invoked a widespread scientific misconception: the idea that oil and water repel each other. In fact, water molecules and hydrophobic substances—including oil—attract one another, although only weakly. The false belief in repulsion traces to the original use of the misleading descriptive term "hydrophobic." In this case, the summary refers to a Report by M. R. Walsh *et al.* (*1*), but nowhere does this Report assert that hydrophobic substances repel or are repelled by water. A valid exposition of the interaction of water with hydrophobic substances can be found in an article in *Nature* by D. Chandler (*2*). Chandler states that "the term hydrophobic (water-fearing) is commonly used to describe substances that, like oil, do not mix with water. Although it may

CREDIT: ISTOCKPHOTO.COM

look as if water repels oil, in reality the separation of oil and water in ambient conditions is not due to repulsion…but to particularly favorable hydrogen bonding between water molecules." Also widely in current use is the term "superhydrophobic," referring to surfaces that often are described, erroneously, as repelling water. A paper by L. Zhai *et al.* (*3*) deals with this topic. The authors explain, "Water repellant in the context of our work simply means that water droplets placed on the surface will roll off freely at a small angle. This is how we and many others define the superhydrophobic state (contact angle greater than 150° coupled with a small rolling angle)." Not surprisingly, the forces involved—cohesion, adhesion, and gravity—are all attractive

J. LEE KAVANAU

Department of Ecology and Evolutionary Biology, University of California, Los Angeles, CA 90095–1606, USA. E-mail: kavanau@biology.ucla.edu

References

1. M. R. Walsh, C. A. Koh, E. D. Sloan, A. K. Sum, D. T. Wu, *Science* **326**, 1095 (2009); published online 8 October 2009
2. D. Chandler, *Nature* **417**, 491 (2002)
3. L. Zhai *et al.*, *Nano Lett.* **6**, 1213 (2006)

CORRECTIONS AND CLARIFICATIONS

News Focus: "The little wasp that could," by E. Pennisi (15 January, p. 260). The caption, "Eaten Alive," should read: Larvae of *Euplectrus wolteri* (inset) ingest blood from a caterpillar. They develop attached to the outside of the caterpillar's body.

Perspectives: "Explaining Bird Migration" by O. Gilg and N. G. Yoccoz (15 January, p. 276). The second affiliation for Olivier Gilg should have been as follows: Lab Biogeosciences, UMR CNRS 5561, Eq Eco Evo, Universite de Bourgogne, 21000 Dijon, France.

This week in *Science*: "Targeting DNA gyrase" (4 December 2009, p. 1317). In the fifth line, "DNA gyrase GTPase activity" should have read "DNA gyrase ATPase activity."

Reports: "Broad and potent neutralizing antibodies from an African donor reveal a new HIV-1 vaccine target" by L. M. Walker *et al.* (9 October 2009, p. 289). Sequence information for the variable domains of the neutralizing antibodies was not provided at the time of publication; GenBank accession numbers are GU272043 to GU272052. Patents have been filed related to the work on the method of isolation of the broadly HIV-neutralizing human antibodies, the neutralization profile for multiple clades and strains of HIV viruses that demonstrates the breadth and potency of activity, and the epitope on V2 and V3 loops that PG9 and PG16 recognize (U.S. provisional patent application numbers USSN 61/161,010; USSN 61/165,829; and USSN 61/224,739, respectively).

Reports: "Activation of the cellular DNA damage response in the absence of DNA lesions" by E. Soutoglou and T. Misteli (13 June 2008, p. 1507). The horizontal panels in rows 1 and 6 of Fig. 1A were inadvertently duplicated during figure production. The correct row 6 panel is reproduced here. The conclusion that tethering of LacR-Chk1 does not lead to accumulation of γ-H2AX at the tethering site is not affected and is supported by the quantitation shown in the original Fig. 1B.

TECHNOLOGY

Under Microscope and Macroscope

Michael N. Alexander

Although we are all familiar with "technology," how many of us would try to define it and describe the principles that govern its workings? In *The Nature of Technology*, W. Brian Arthur does that and more: Besides offering a coherent depiction of technology's underlying attributes and inner structure, he seeks to demonstrate that its historical development is a form of (non-Darwinian) evolution, describe how engineering and invention function, and elucidate the ways by which technology prompts change in economic structures. His account is almost always enlightening, stimulating, and thought-provoking.

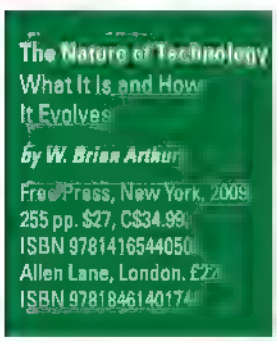

Arthur (an economist, complexity theorist, and mathematician at the Santa Fe Institute and Palo Alto Research Center) provides a highly structured analysis that proceeds from three "fundamental principles." First, all technologies are combinations. This may seem self-evident to readers of *Science*, especially those who employ instruments in their own work. Spectrometers, for example, are composed of parts that are technology products (lenses, mirrors, gratings, actuators, etc.). But on reflection, one realizes that the parts are themselves miniature technologies; so are their subparts, sub-subparts, and so on (Arthur's second principle). Moreover, each "technology is a phenomenon captured and put to use" (his third principle).

It follows that technologies have hierarchical structures and that "[t]echnologies at a higher level direct or 'program' (as in a computer program) technologies at lower levels" to fulfill human purposes. Their interacting constituents, especially in complex, composite technologies like jet engines, can even have properties akin to metabolism. A naval aircraft carrier group becomes, via this reasoning, a technology composed of ships and their multiple levels of constituent technologies. This is a novel and powerful perspective, for we rarely if ever regard organizational arrangements as technologies.

However, the perspective can also be problematic. Where is the dividing line between technology and not-technology? Arthur's logic leads to the conclusion that a symphony by Gustav Mahler is a technology—an acoustic one whose constituent parts are string, woodwind, brass, etc., technologies. Arthur finds this discomfiting, yet he accepts symphonies as technologies. Extending his line of reasoning, one could regard painters (da Vinci, Monet, Picasso, *et al.*) as visual technologists. Doing so creates intriguing links among technology, science, and fine arts [compare (*1*)].

Suppose, further, that one relaxes the stipulation that a technology's base phenomenon is physical. Arthur argues plausibly that legal codes, institutions, and organizations should then be regarded as akin to technologies. But placing them in the same category as laser printers or even naval flotillas would unduly strain the concept of technology. Therefore, Arthur assigns these social technologies to a new category, "purposed systems." Making a distinction between technologies and purposed systems may seem like medieval scholasticism, but in fact it is astute. This distinction opens the way to an original and penetrating description, toward the end of the book, of how structural changes in the economy are generated by the interactions of technology (as a collective enterprise) with purposed systems.

Arthur's portrayal of technologies as composed of subtechnologies, the book's logical foundation, also constitutes a template for his depictions of the heart of the technological enterprise—invention and innovation (which Arthur treats as synonymous). He begins by analyzing the easiest form of innovation to comprehend, "standard engineering," which solves problems by combining well-accepted, usually well-known, technologies. The new technologies created through these combinations may be important and complex (jet aircraft and bridges, for example) even though the underlying inventive principles may not be novel. The resultant knowledge diffuses through engineering professions, adding to the corpus of "building blocks that can be [combined to create] further technologies."

In a similar vein, Arthur argues that radically novel innovations also result from problem-solving and combination—but that novel innovations combine principles, concepts, or functionalities, not only existing technologies. E. O. Lawrence, for example, invented the cyclotron by combining the physics of charged particles in a magnetic field with acceleration of the particles by a radio frequency electric field. "The principle [of the cyclotron] was constructed from existing pieces—existing functionalities." Arthur holds that "[a]t the creative heart of invention lies appropriation, some sort of mental borrowing that comes in the form of a half-conscious suggestion." Furthermore, "What is common to originators [i.e., inventors] is . . . the possession of a very large quiver of functionalities and principles. Originators are steeped in the practice and theory of the principles or phenomena they will use."

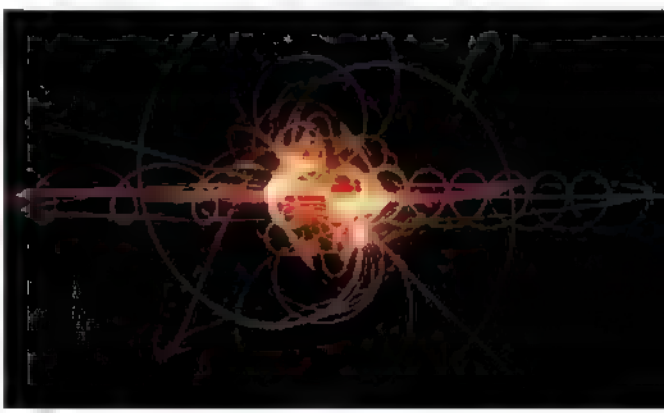

These are important, potent insights. But Arthur pushes them so hard that he almost devalues the usual concept of novelty. He claims, for example, that the perception of novelty arises because connections among the most important principles underlying an invention are initially apparent only to the originators. He repeatedly attributes invention to "human agency," and employs growth of a coral reef as a metaphor for the way technology grows through accretion of know-how and concepts. To demonstrate how technology can grow by "combinatorial evolution," he describes a computer experiment in which elementary electronic logic circuits combined randomly to create circuits that became more and more complex. He avers, "I do not believe there is any such thing as genius" but he does believe in a large quiver.

A large, full quiver is irrelevant unless the archer espies targets and aims accurately. Just as archers rarely score bull's-eyes by shooting in random directions, radically novel inventions rarely result from ran-

CREDIT: SHUTTERSTOCK/COURTESY FREE PRESS

The reviewer is at the Electromagnetics Technology Division, Sensors Directorate, Air Force Research Laboratory, 80 Scott Drive, Hanscom Air Force Base, MA 01731–2909, USA. E-mail: mna41@eee.org

dom sampling. Could it be that individual and group human agency improve convergence to successful solutions, thereby making inventive processes and the evolution of technology more efficient?

One does not have to be a romantic to agree with mathematician Mark Kac that Richard Feynman was a "magician," rather than an "'ordinary' genius" (*2*). And even though I understand the principles and origins of, for example, the quantum cascade laser (*3*), I cannot expunge the belief that it is an awesomely brilliant creation.

Such observations, however, scarcely detract from Arthur's achievement. Systematic, multifaceted, enlightening, and stimulating, *The Nature of Technology* is enhanced by a remarkable diversity of historical examples. Although a relatively brief account, this review could only partially distill its richness. The book invites comparisons with work by Thomas Kuhn (*4*) and Joseph Schumpeter (*5*, *6*). Economists, social scientists, engineers, and scientists all may come to regard it as a landmark.

References and Notes

1. J. Bronowski, *Science and Human Values* (Harper and Row, New York, ed. 2, 1965)
2. M. Kac, *Enigmas of Chance: An Autobiography* (Harper and Row, New York, 1985)
3. J. Faist *et al.*, *Science* **264**, 553 (1994).
4. T. S. Kuhn, *The Structure of Scientific Revolutions* (Univ. Chicago Press, Chicago, 1962)
5. J. A. Schumpeter, *Theorie der wirtschaftlichen entwicklung* (Dunker and Humblot, Leipzig, 1912)
6. J. A. Schumpeter, *Capitalism, Socialism, and Democracy* (Harper, New York, 1942)

10.1126/science.1187156

EXHIBITIONS: MEDICINE AND ART

The Human Body as a Meeting Point

Perched 53 stories above the streets of midtown Tokyo, atop the Roppongi Hills skyscraper, the Mori Art Museum offers spectacular views of the surrounding city. Through the end of the month, visitors will also find an unusual exhibition, *Medicine and Art: Imagining a Future for Life and Love*. Organized in collaboration with Britain's Wellcome Trust and the Japanese newspaper *Yomiuri Shimbun*, the show brings together 150 medical and art objects from the Wellcome Collection, three anatomical sketches by Leonardo da Vinci from the British Royal Collection, and about 30 works of contemporary art.

The exhibit is divided into three sections. The first, "Discovering the Inner World of the Body," explores our fascination with the human body and its innards. As Nanjo Fumio, the museum's director, notes, "The body can be seen as the meeting point between medicine and art and as the point of departure for journeys into these two different worlds." The section presents anatomical models and diagrams; traditional Japanese art by Maruyama Ōkyo and Kawanabe Kyosai; and contemporary works by Andy Warhol, Magnas Wallin, and Bai Yilao. It also includes beautifully delicate and detailed drawings of cranium, liver, and cerebral ventricles by Leonardo da Vinci. The section "Fighting Against Death and Disease" displays many devices constructed to fight the effects of disease along with a variety of classical and modern works of memento mori, which convey the warning that we are all mortal. (Contemporary artists here include Damien Hirst, Marc Quinn, and Yanagi Miwa.) The third section, dauntingly named "Towards Eternal Life and Love," looks at the effects of aging and recent advances in genetics, biotechnology, and neuroscience.

Jan Fabre's *Ik men mijn eigen brein II* [*I Drive My Own Brain II*] (2008).

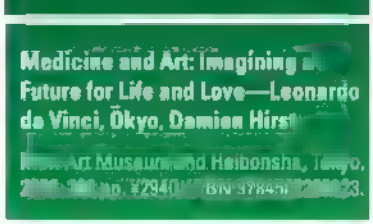

The works presented within the sections are not arranged historically but in ways that are clearly meant to generate thought-provoking juxtapositions. As a result, a 19th-century model of a skull used for phrenology is placed across from a brainwave-powered wheelchair, and anatomical sketches from a variety of cultures and historical periods turn up at odd moments. There was a warning in front of one small room that it contained "graphic and anatomic drawings and figures that some visitors might find disturbing," but that was not the case for me. Instead, what left me most emotionally moved was a room dominated by five pairs of several-feet-wide photographs by Walter Schels that depicted people before and just after they died. There was also a work by Alvin Zafra that seems to be a long splotch of white streaked on wooden panels but which is actually the remains of a human skull that was scraped and rubbed onto the wood for 14 days. These and other displays effectively depict the fragility and power of life and death.

There is humor as well, as in a wedding dress that was made from 6500 oral contraceptive packets and in the depictions of aging superheroes. And there are surprises—for example, Lee Byung Ho's *Vanitas Bust*, a seemingly standard sculpture of a young woman's head, is actually made of silicon and, through the use of compressed air, ages before your eyes. Having grown up with the see-through "Visible Man," I found it interesting to encounter something similar in a miniature 17th- or 18th-century model, made of ivory. I was also struck by Magnus Wallin's *Exercise Parade*, a walk-in video installation that places the observer in the entry of a hallway where a leapfrogging figure and a skeleton dodge an enormous pinball.

There are too many noteworthy pieces to mention them all. Because so many of these evoke personal reactions, visitors will probably not always agree with interpretations that accompany the works—these sometimes stretch points. The Wellcome Collection (www.wellcomecollection.org/), begun in the 1890s by pharmaceutical entrepreneur Henry Wellcome, prides itself on being more than a collection of "things" (extraordinary preservations of history that they are). It also amasses ideas as a way to make new links between disciplines and cultures. That goal has been accomplished quite successfully in this exhibition.

—Barbara R. Jasny

10.1126/science.1187798

RESEARCH ETHICS

NIH Guidelines for Stem Cell Research and Gamete Donors

Rather than informed consent, dispositional authorization may be the preferred strategy in obtaining gamete donations for embryonic stem cell research.

Bernard Lo,[1,2,3]* Lindsay Parham,[1] Marcelle Cedars,[4] Susan Fisher,[3,5] Elena Gates,[3,4] Linda Giudice,[3,4] Dina Gould Halme,[6] William Hershon,[7] Arnold Kriegstein,[3,8] Radhika Rao,[9] Clifford Roberts,[10] Richard Wagner[11]

Recent National Institutes of Health (NIH) guidelines regarding human embryonic stem cell (hESC) lines created from embryos remaining after infertility treatment (*1*) are expected to increase substantially the number of hESC lines eligible for U.S. federal funding. Although the guidelines require informed consent from embryo donors for derivation of hESC lines, such consent is not required from third-party donors (not an intended parent) whose gametes were used to create the embryos. This is in contrast to many state, national, and international recommendations (*2*–*8*). We argue that dispositional authorization after disclosure regarding hESC research should be obtained from third-party gamete donors, but that the requirements may be more flexible and less complex than for informed consent.

Need for Gamete Donor Authorization

Gamete donors for in vitro fertilization (IVF) programs sign a form giving the IVF patient legal authority to determine the disposition of embryos created with their gametes after infertility treatment has been completed. The unrestricted legal power of such blanket dispositional authorization includes options that were not specifically mentioned to the donor. However, such legal authority may be ethically problematic if the gamete donor was not told—and therefore may not appreciate—what options the IVF patient might choose, including hESC research. Some donors may object to research using embryos made from their gametes (*9*). One reason underlying such objections may be that some donors may regard gametes as having special status compared with somatic cells because of their reproductive potential, with reproduction being a highly personal and private matter. However, gametes are not typically granted the same special status as embryos, which may be perceived to have the moral status of persons (*10*). Using embryos for research without permission of third-party oocyte donors could fail to respect donors as persons (*11*), breaching a fundamental principle of bioethics (*12*).

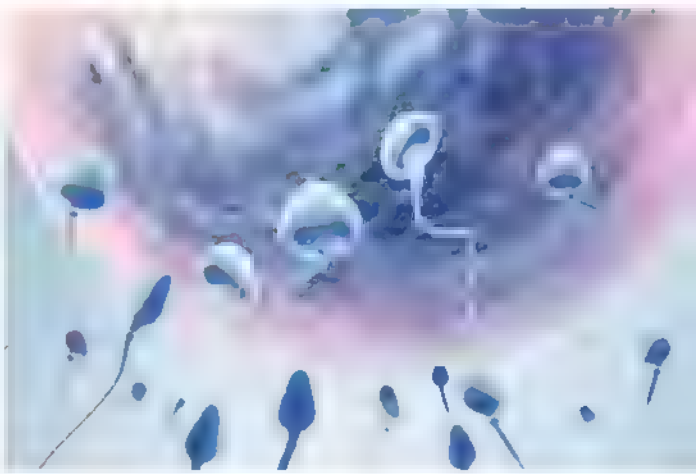

We analyze below two other models for gamete donors to allow IVF patients to make decisions about embryos remaining after completion of infertility treatment.

Informed Consent

Informed consent is an "opt-in" process; individuals are not required to participate as patients or research participants and agree to only those procedures specified in the consent form. For instance, oocyte donors give informed consent to the clinical procedures of ovarian stimulation and oocyte retrieval (*13*). However, detailed consent forms are not required for many important, very private decisions currently made by third-party gamete donors during dispositional authorization (e.g., forgoing parental rights to children conceived with their gametes and allowing the IVF patient to donate embryos to another infertility patient). It would be unfair to require gamete donors to follow stricter standards to authorize the donation of embryos to hESC research than to authorize these other major decisions.

There are also pragmatic barriers to requiring informed consent from gamete donors for hESC research. Stem cell researchers typically get involved with embryo donation only after an IVF patient inquires about it; they do not interact with gamete donors or write forms for granting dispositional authority. Considerable efforts by IVF clinicians to obtain consent from oocyte donors for potential future research may raise concerns about conflicts of interest (*14*) and could compromise the informed consent process for the complex medical procedures of ovarian stimulation and oocyte retrieval (*15*). Recontacting gamete donors after the IVF patient has completed infertility treatment to seek consent for embryo research may be viewed as an invasion of privacy and also may not be feasible.

A Modified Approach

We conclude that informed consent from third-party gamete donors should not be required for hESC research. Instead, we recommend a model of dispositional authorization after options for embryo disposition have been disclosed, including hESC research, discarding embryos, and donation to another IVF patient. Informing gamete donors of options respects the donors by making the decision to grant disposition rights to the IVF patient more informed. Most gamete donors grant blanket dispositional authority to the IVF patient. Some gamete donors may not be willing to accept some dispositional options, such as hESC research. An IVF patient should consider such preferences at the beginning of infertility treatment when selecting a gamete donor. However, IVF patients are free to

[1]Program in Medical Ethics, University of California, San Francisco (UCSF), San Francisco, CA 94143, USA. [2]Department of Medicine, UCSF, San Francisco, CA 94143, USA. [3]The Eli and Edythe Broad Center for Regeneration Medicine and Stem Cell Research, UCSF, San Francisco, CA 94143, USA. [4]Department of Obstetrics, Gynecology, and Reproductive Sciences, UCSF, San Francisco, CA 94143, USA. [5]Department of Anatomy, UCSF, San Francisco, CA 94143, USA. [6]Office of the Dean of the School of Medicine, UCSF, San Francisco, CA 94143, USA. [7]Disability Rights California, Oakland, CA 94612, USA. [8]Program in Developmental and Stem Cell Biology, UCSF, San Francisco, CA 94143, USA. [9]University of California, Hastings College of the Law, San Francisco, CA 94102, USA. [10]Office of the Vice Chancellor for Research, UCSF, San Francisco, CA 94143, USA. [11]Human Research Protection Program, UCSF, San Francisco, CA 94143, USA

*Author for correspondence. E-mail: berme@medicine.ucsf.edu

choose another donor who will grant unrestricted dispositional authority; thus, the gamete donor cannot control the dispositional decisions of the IVF patient.

At present, disclosure of dispositional options to gamete donors may be carried out as a clinical best practice and is recommended by many legal advisors to IVF practices, although it is not required. For frozen embryos created years ago, disclosure is even more variable.

The standards for disclosing information about hESC research should be comparable to disclosure of information about other dispositional options. It would be desirable to inform gamete donors about features of disposition options that may be pertinent to decisions about disposition but may not be common knowledge (*16*) [e.g., the possibility of patents on hESC discoveries and what provisions, if any, will be in place for sharing royalties (*17*)]. Donors should have the opportunity to ask questions or obtain additional information about disposition options.

But information given to gamete donors about hESC research need not include all the basic elements required in consent forms for human subjects research (*13*). For example, it would be misleading to say that refusal to participate in research will involve no loss of benefits; a prospective gamete donor who is unwilling to grant blanket dispositional authorization may not be selected as a donor and would then not receive compensation.

In this context, the ethical rationale—respect for gamete donors and their preferences—may be satisfied by more flexible procedures and documentation than those for informed consent for research. Disclosing the option of hESC research, along with other available options for embryo disposition, might be done in several ways. Documentation would be unambiguous if the form granting legal dispositional authority listed hESC research as an option. Alternatively, dispositional options, including hESC research, could be described in a separate document, and the form granting dispositional authority need not explicitly mention hESC research, provided that the IVF practice, oocyte donor agency, or sperm bank documents or attests that they provided information about disposition options and that research was given as an option.

Recommended Policy Changes

NIH guidelines should be revised. For hESC lines derived from embryos created after the date of the revised guidelines, dispositional authorization after disclosure from third-party gamete donors should be required. This may be documented by evidence that the donor (i) was told hESC research was an option for the disposition of frozen embryos remaining after the IVF patient had completed treatment, and (ii) then granted the IVF patient dispositional authority over embryos created with the donor's gametes. Gamete donors still must provide informed consent for medical procedures.

Exceptions to dispositional authorization after disclosure may be justified on a case-by-case basis (for example, as determined by NIH). hESC lines already in existence at the time revised guidelines are issued may be used (*18*) if the following three criteria are met: (i) the gamete donor granted dispositional authority to the IVF patient, even without documentation that the gamete donor was told research was an option, (ii) there are strong scientific reasons to use them, and (iii) other legal requirements are met (*19*). For example, the particular hESC line may be the only line that has been derived under good manufacturing process standards or that matches a specific phenotype (*20*).

A more thorough consent process for embryo donors is warranted than for third-party gamete donors, given the special moral status ascribed to embryos (*10*). IVF patients donating embryos for hESC derivation should still give informed consent, consistent with new NIH guidelines (*1*) and other policies (*21*).

For stem cell science to continue to progress, it would be highly desirable to have consistency among standards and regulations (*1*, *8*). If such harmonization is achieved, many IRBs and oversight bodies will likely allow NIH-eligible hESC lines to be used for any otherwise acceptable hESC research.

References and Notes

1. NIH, National Institutes of Health Guidelines on Human Stem Cell Research (NIH, Bethesda, MD, 2009); http://stemcells.nih.gov/policy/2009guidelines.htm.
2. National Research Council and Institute of Medicine, *2007 Amendments to the National Academies' Guidelines for Human Embryonic Stem Cell Research* (National Academies Press, Washington, DC, 2007), www.nap.edu/catalog.php?record_id=11871.
3. California Institute for Regenerative Medicine, CIRM MES Regulations Title 17, California Code of Regulations Section 100010–100110 (CIRM, San Francisco, CA, 2009) www.cirm.ca.gov/reg/pdf/Reg100100_SM_Acct_Standards.pdf.
4. International Society for Stem Cell Research (ISSCR), *Guidelines for the Conduct of Human Embryonic Stem Cell Research* (ISSCR, Deerfield, IL, 2006); www.isscr.org/guidelines/index.htm.
5. Human Fertilisation and Embryo Authority (HFEA), Guidance: Consent to use and storage of gametes and embryos, Note 5A, Interpretation of mandatory requirements (HFEA, London, 1991); www.hfea.gov.uk/336.html#guidanceSection3718.
6. Australian Government National Health and Medical Research Council, Prohibition of Human Cloning for Reproduction Act of 2002 (Attorney General's Department, Australian Government, Canberra, 2002), www.nhmrc.gov.au/publications/synopses/prohibitsyn.htm.
7. Parliament of Canada, Assisted Human Reproduction Act, SC 2004, chap. 2; http://laws.justice.gc.ca/PDF/Statute/A/A-13.4.pdf.
8. European Group on Ethics in Science and New Technologies to the European Commission, *The Ethics Review of hESC FP7 Research Projects* (European Communities, 2007); http://ec.europa.eu/european_group_ethics/avis_index_en.htm.
9. About 25% of women who provided oocytes to patients in infertility clinics said they would not want their oocytes to be used for research (*22*). In an IVF program, 13% of oocyte donors would not be willing to donate embryos created from their eggs for research, and 5% were unsure (*23*). Among prospective (not actual) oocyte donors, 10% would not be comfortable if embryos made using their oocytes were donated for research (*24*).
10. National Bioethics Advisory Commission (NEBAC), *Ethical Issues in Human Stem Cell Research* (NEBAC, Rockville, MD, 1999).
11. B. Lo *et al.*, *Science* **301**, 921 (2003).
12. National Commission for the Protection of Human Subjects of Biomedical and Behavioral Research, *The Belmont Report. Ethical Principles and Guidelines for the Protection of Human Subjects of Biomedical and Behavioral Research* (Office of Human Subjects Research, NIH, Bethesda, MD, 1979).
13. For research, informed consent forms must be approved by an Institutional Review Board and should contain specific required elements, including the risks and benefits of research participation and its alternatives (*25*). U.S. regulations on human subjects research do not apply to research with existing biological materials that investigators cannot link to the donors. The ethical justification for this exception is that few patients would object if a leftover tube of blood or surgical specimen were de-identified and used for research. Nonetheless, because hESC research is sensitive, NIH requires consent from embryo donors even if the materials are de-identified, a policy consistent with other standards (*21*).
14. G. P. Lomax, Z. W. Hall, B. Lo, *PLoS Med.* **4**, e114 (2007).
15. The primary concerns of IVF physicians and oocyte donor agencies are (i) that donors appreciate that the medical procedures present risks (requiring donor consent), and (ii) that they will have no parental rights regarding children produced from their oocytes, and that the IVF patient may choose to donate frozen embryos to another IVF patient or destroy them (requiring donor dispositional authority). These issues may be more thoroughly discussed and documented than potential downstream hESC research, which some IVF physicians and donor agencies may regard as a secondary issue.
16. J. W. Berg, C. W. Lidz, P. S. Appelbaum, *Informed Consent. Legal Theory and Clinical Practice* (Oxford Univ. Press, New York, ed. 2, 2001).
17. R. Korobkin, S. R. Munzer, *Stem Cell Century: Law and Policy for a Breakthrough Technology* (Yale Univ. Press, New Haven, CT, 2007).
18. J. Sugarman, A. W. Siegel, *Science* **322**, 379 (2008).
19. B. Lo *et al.*, *Cell Stem Cell* **4**, 115 (2009).
20. Exceptions may also be permitted for frozen embryos already in existence when the guidelines are revised if it is uncertain whether third-party gamete donors were told that hESC research was a dispositional option. Because it is not known before hESC lines are derived whether they will have significant scientific advantages over other lines, stricter standards should be applied for such exceptions than in the case of hESC lines already in existence.
21. R. Streiffer, *Hastings Cent. Rep.* **38**, 40 (2008).
22. A. L. Kalfoglou, G. Geller, *Fertil. Steril.* **74**, 660 (2000).
23. R. Klitzman, M. V. Sauer, *Reprod. Biomed. Online* **18**, 603 (2009).
24. N. Adsuar *et al.*, *Fertil. Steril.* **84**, 1513 (2005).
25. Department of Health and Human Services, Protection of Human Subjects, **45** Code of Federal Regulations, part 46 (2005); www.dhhs.gov/ohrp/humansubjects/guidance/45cfr46.htm.

10.1126/science.1180725

CELL BIOLOGY

Rise of the Rival

Amanda Norvell[1] and Steven B. McMahon[2]

Widespread acetylation of metabolic enzymes suggests a modification that is as important as protein phosphorylation in controlling cell function

Like protein phosphorylation, the posttranslational addition of acetyl groups to lysine residues of eukaryotic and prokaryotic proteins has been known for decades (*1*). The discovery that eukaryotic enzymes implicated in transcriptional regulation can acetylate or deacetylate lysines in chromatin-associated proteins (histones) raised the possibility that dynamic changes in lysine acetylation might provide an important regulatory switch in complex cellular processes (*2*, *3*). A decade ago, Kouzarides made the bold prediction that acetylation might "rival phosphorylation" as a regulator of cell function (*4*). With proteomics, thousands of mammalian proteins with acetylated lysines have indeed been identified (*5*, *6*), and one of the surprising findings has been that, along with chromatin proteins, metabolic enzymes are highly represented among acetylation substrates. This suggested that changes in acetylation status might alter enzymatic activity to allow the cell to respond to changes in metabolic demands by adjusting flux through critical nodes in the relevant pathways. Reports by Zhao *et al.* and Wang *et al.* on pages 1000 and 1004 of this issue, respectively, now validate this hypothesis in the prokaryote *Salmonella enterica* and in human liver cells (*7*, *8*).

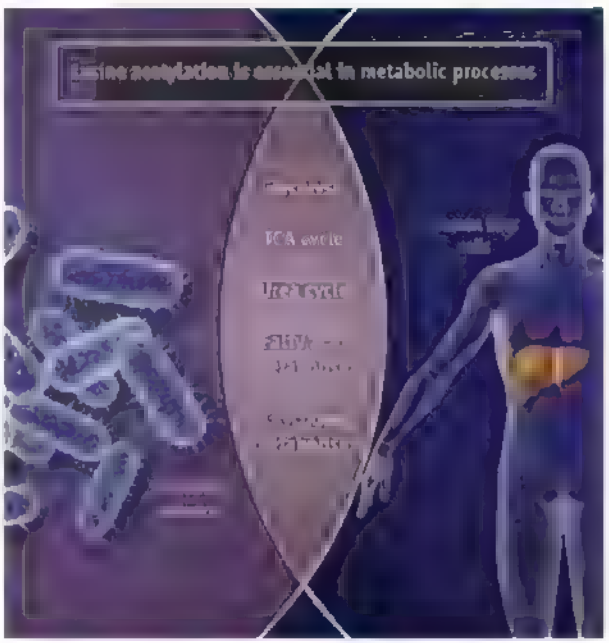

Ubiquitous and conserved in metabolism. In bacteria and human cells, dynamic acetylation of nearly all metabolic enzymes regulates their activities to modulate flux through specific metabolic pathways.

These two studies report a number of fundamental similarities betwen bacteria and humans. The first is the sheer pervasiveness of lysine acetylation on metabolic enzymes. Zhao *et al.* found that 90% of the *S. enterica* proteins involved in central metabolism are acetylated, and Wang *et al.* likewise found acetylation of essentially every enzyme involved in glycolysis, fatty acid and glycogen metabolism, and the tricarboxylic acid (TCA) and urea cycles (see the figure). Both groups also found that changing the carbon source available to either the prokaryotic or eukaryotic cells altered the total profile of acetylated metabolic enzymes.

Zhao *et al.* and Wang *et al.* conducted elegant biochemical studies on a handful of enzymes from *S. enterica* and humans and showed that acetylation has multiple effects, increasing the activity of some metabolic enzymes while inhibiting the activity of others. Furthermore, the effects of acetylation appear to be coordinated to simultaneously shunt metabolic flux down specific pathways and away from others. Remarkably, this flux can be reversed by changes in metabolic state or carbon source availability. However, not all aspects of this process are conserved. In *S. enterica*, the changes in metabolic enzyme acetylation result in part from changes in the relative expression of the major acetylase and deacetylase, a feature that has not been widely observed for eukaryotic counterparts. Indeed, only a few cases exist in which we understand the mechanisms regulating mammalian acetylases and deacetylases (*9*). When Zhao *et al.* compared proteins acetylated in human liver cells to those identified in earlier studies, they found 70% overlap with the acetylated proteins identified in mouse liver but only 14% overlap with the acetylated proteins found in a human leukemia cell line, which suggests that acetylation patterns vary widely between cell lineages.

In protein phosphorylation, adenosine triphosphate (ATP) serves as the major phosphoryl group donor. Lysine acetylation relies on acetyl coenzyme A (CoA) as the acetyl group donor. Like ATP, acetyl-CoA lies at the core of a number of critical cellular pathways, and its intracellular concentration is therefore a potential readout of the processes involved. Changes in the availability of acetyl-CoA could directly affect the acetylation status of critical substrates, as observed for the core histone proteins H2A, H2B, H3, and H4 (*10*). Thus, a model emerges in which changes in cellular pools of acetyl-CoA, which fluctuate in response to a myriad of metabolic pathways, could provide the rheostat by which the acetylation status, and hence the activity, of metabolic enzymes can be modulated.

Understanding the control of lysine acetylation, as well as the effect of altered protein acetylation on specific cellular pathways, has clear implications for human disease. (Verinostat, a deacetylase inhibitor, received approval by the U.S. Food and Drug Administration in 2006 as a treatment for cutaneous T cell lymphoma.) Given the renewed appreciation of cancer as a partly metabolic disease (*11*), the studies by Zhao *et al.* and Wang *et al.* raise the question of how much the success of deacetylase inhibitors depends on their ability to change transcriptional profiles versus reprogramming cancer cell metabolism. Beyond cancer, as we learn more about the role of acetylation in regulating flux through metabolic pathways, drugs that modulate acetylation might be of benefit to patients with specific metabolic disorders. And as the proteomic data on protein acetylation are mined further, and the methodology is refined, we should come to understand whether there are cellular processes beyond those linked to chromatin or metabolism—where dynamic lysine acetylation plays a global regulatory role.

The importance of phosphorylation is broadly accepted, but the importance of pathways related to dynamic protein acetylation has received little recognition since the 1964 Nobel Prize in Physiology or Medicine to Konrad Bloch and Feodor Lynen for their discoveries linking acetyl-CoA to fatty acid metabolism. Although dynamic protein phos-

[1]Department of Biology, College of New Jersey, Ewing, NJ 08628, USA. [2]Department of Cancer Biology, Thomas Jefferson University, Philadelphia, PA 19107, USA. E-mail: steven.mcmahon@jci.tju.edu

CREDIT: C. BICKEL/SCIENCE

phorylation unquestionably provides a major regulatory switch in cells, it is now clear from studies like those of Zhao *et al.* and Wang *et al.* that lysine acetylation is an equally important and evolutionarily conserved control mechanism (*7*, *8*). Phosphorylation appears indeed to have found its "rival" in lysine acetylation

References

1. V. G. Allfrey, R. Faulkner, A. E. Mirsky, *Proc. Natl. Acad. Sci. U.S.A.* **51**, 786 (1964).
2. J. E. Brownell *et al.*, *Cell* **84**, 843 (1996).
3. J. Taunton, C. A. Hassig, S. L. Schreiber, *Science* **272**, 408 (1996).
4. T. Kouzarides, *EMBO J.* **19**, 1176 (2000).
5. C. Choudhary *et al.*, *Science* **325**, 834 (2009).
6. S. C. Kim *et al.*, *Mol. Cell* **23**, 607 (2006).
7. S. Zhao *et al.*, *Science* **327**, 1000 (2010).
8. Q. Wang, Y. Zhang, C. Yang, H. Xiong, Y. Lin, *Science* **327**, 1004 (2010).
9. H. S. Mellert, S. B. McMahon, *Trends Biochem. Sci.* **34**, 571 (2009).
10. K. E. Wellen *et al.*, *Science* **324**, 1076 (2009).
11. C. B. Thompson, *N. Engl. J. Med.* **360**, 813 (2009).

10.1126/science.1187159

CHEMISTRY

Cooperativity Tames Reactive Catalysts

A fast catalyst that forms undesired side products is made more selective through its strong interactions with a second catalyst.

Peter R. Schreiner

When chemists use more than one catalyst to speed up a chemical reaction, it is almost always the case that overall increase in reaction rate is greater than that for either catalyst alone. For example, for acid-catalyzed reactions, combinations of "designer acids"—combinations of organic and inorganic molecules bearing acidic groups—can result in higher reactivity, selectivity, and versatility than the use of individual catalysts (*1*). However, there can be advantages to adding a second catalyst that actually slows down the rate of an already catalyzed reaction, especially if the goal is suppressing unwanted side reactions. This strategy is similar to that used by a coach of a relay team, who may pair a slower but sure-handed runner with a faster but less agile one. Speed is sacrificed to avoid losing by dropping the baton. On page 986 of this issue, Xu *et al.* (*2*) report the use of two catalysts that cooperate to control stereochemistry, that is, to pick between different spatial arrangements of the same product. The initial catalyst is fast but produces an unwanted mixture of stereoisomers; adding the second catalyst suppresses one of these pathways and selects for the desired product.

These cooperative effects were demonstrated with organocatalysts, which are small organic molecules used in a wide variety of chemical transformations (*3*). The challenge in creating cooperative catalysts lies in controlling the competition of the two catalysts for the reactants as well as their mutual interaction. In this case, hydrogen-bond donors (*4*), such as urea and thiourea derivatives (*5*–*7*), were used that should hydrogen-bond their NH groups to basic atoms or groups in one of the reactants, which is similar to the way a weak Lewis acid would interact (*8*).

Xu *et al.* envisioned that the ability for urea and thiourea catalysts to recognize anions (*9*–*11*) could be exploited as well to coordinate to another catalyst that is a strong Brønsted acid (*12*). In this case, the anion is the counterion of the Brønsted acid, which forms a salt bridge (*13*) to the protonated amine group of the urea catalyst. A second functionality on the urea catalyst, a sulfinamide, then additionally coordinates with the protonated substrate to form a chiral complex (see the figure). Hence, the urea catalyst tames the activity of the acid catalyst through enforcing its cooperativity in the activation of the substrate.

The authors chose to apply their concept to ring-forming reactions in which a reactant with two adjacent double bonds and a reactant with one double bond form a six-

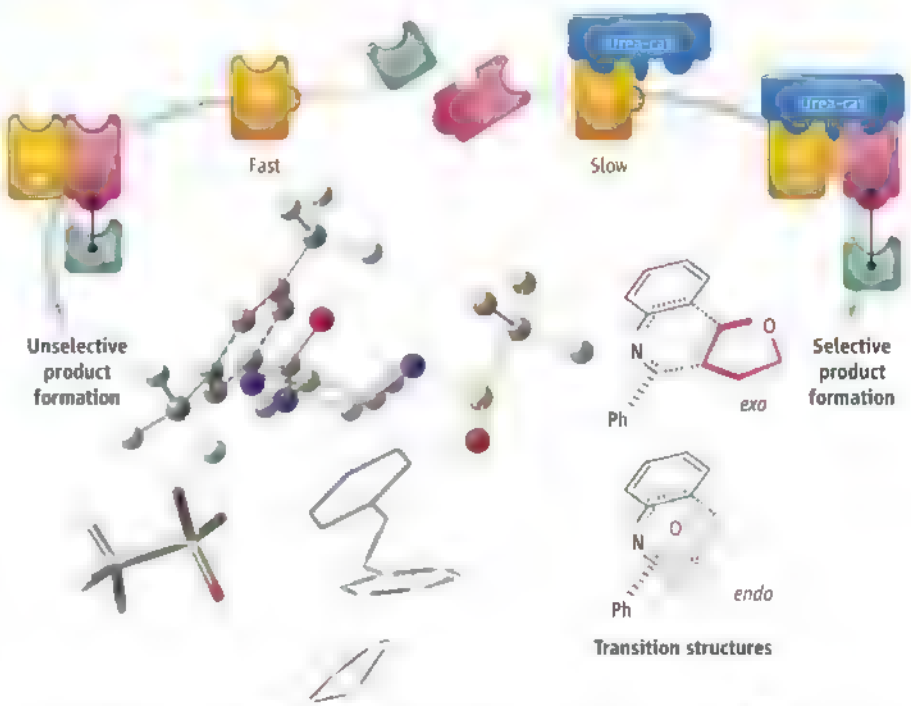

A careful hold by two catalysts. The "puzzle pieces" illustrate how two organic molecules cooperate as catalysts for the reaction between molecules A and B. On the pathway to the left, a Brønsted acid (Acid-cat) binds to reactant A, and product formation is fast but unselective—B can react at two sites. The pathway on the right shows the effect of adding a urea derivative (Urea-cat), which binds to Acid-cat and also interacts with A. The reaction is slowed down, and by surrounding part of reactant A, B is forced to react at one site, which favors one stereoproduct. The center shows a rendering of the transition structure for the urea (as balls and sticks) and the Brønsted acid (tubes), which together catalyze ring formation by benzylidene aniline and 2,3-dihydrofuran (wireframe); hydrogen atoms are omitted for clarity. The favored exo and unfavored endo transition states are also illustrated

Institute of Organic Chemistry, Justus-Liebig University, Heinrich-Buff-Ring 58, 35392 Giessen, Germany. E-mail: prs@org.chemie.uni-giessen.de

member ring. Formally, these are [4+2] cycloadditions of *N*-aryl imines to electron-rich olefins, the so-called Povarov reaction (*14*). It is desirable that this reaction is enantioselective, which in this case means producing tetrahydroquinoline derivatives with control over the spatial arrangement of substituents around three of the atoms that can form different stereoisomers. This reaction is potentially useful because it provides direct access to some important biologically active compounds.

Several bifunctional ureas and thioureas equipped with sulfinamido groups, depicted as Urea-cat in the figure, were particularly suitable to control the activity of *ortho*-nitrobenzenesulfonic or trifluoromethansulfonic as the acid catalyst (Acid-cat), which otherwise promote the rapid unselective reaction. This combination provides the products with up to 92% yield with diastereomeric ratios higher than 20:1 and up to 99% enantiomeric excess of the favored exo products. The validity of the cooperativity concept was supported by proton nuclear magnetic resonance studies and density functional theory computations. Both experiment and theory provide convincing evidence that complex formation occurs between the two catalysts and the substrates in the critical stages of the reaction.

Cooperatively operating catalytic systems are highly useful in both homogeneous (*15*) and heterogeneous transformations (*16*). The fruitful interplay between organocatalysis and catalysis in natural systems is just beginning but is very likely to be highly beneficial for both. The work of Xu *et al.* is an impressive demonstration of the precise control of a cooperatively catalyzed reaction with noncovalent interactions alone. It is likely to become a general strategy for asymmetric catalysis because it mimics enzymes, where multiple sites are in charge of fine-tuning their catalytic activity.

References and Notes

1. H. Yamamoto, K. Futatsugi, *Angew. Chem. Int. Ed.* **44**, 1924 (2005).
2. H. Xu *et al.*, *Science* **327**, 986 (2010).
3. A. Berkessel, H. Gröger, *Asymmetric Organocatalysis* (Wiley-VCH, Weinheim, 2005).
4. P. M. Pihko, *Hydrogen Bonding in Organic Synthesis* (Wiley-VCH, Weinheim, 2009).
5. P. R. Schreiner, *Chem. Soc. Rev.* **32**, 289 (2003).
6. A. G. Doyle, E. N. Jacobsen, *Chem. Rev.* **107**, 5713 (2007).
7. M. S. Taylor, E. N. Jacobsen, *Angew. Chem. Int. Ed.* **45**, 1520 (2006).
8. P. R. Schreiner, A. Wittkopp, *Org. Lett.* **4**, 217 (2002).
9. P. R. Schreiner, M. Kotke, *Synthesis* **2007**, 779 (2007).
10. I. T. Raheem, P. S. Thiara, E. A. Peterson, E. N. Jacobsen, *J. Am. Chem. Soc.* **129**, 13404 (2007).
11. Z. Zhang, P. R. Schreiner, *Chem. Soc. Rev.* **38**, 1187 (2009).
12. S. Mayer, B. List, *Angew. Chem. Int. Ed.* **45**, 4193 (2006).
13. M. Rueping *et al.*, *Synlett* **2007**, 1441 (2007).
14. L. S. Povarov, *Russ. Chem. Rev.* **36**, 656 (1967).
15. G. J. Rowlands, *Tetrahedron* **57**, 1865 (2001).
16. E. L. Margelefsky, R. K. Zeidan, M. E. Davis, *Chem. Soc. Rev.* **37**, 1118 (2008).

17. Our work on organocatalysis was generously supported by the Deutsche Forschungsgemeinschaft (Priority Program 1179).

10.1126/science.1186764

CELL BIOLOGY

When the Beginning Marks the End

An acetylated amino terminus represents a degradation signal for eukaryotic proteins.

Axel Mogk and Bernd Bukau

Acetylation of the amino terminus (Nt-acetylation) of a protein is one of the most common modifications, occurring in about 50% of yeast proteins and more than 80% of human proteins (*1*). It is catalyzed by N-terminal acetyltransferases, occurs predominantly on a nascent polypeptide chain as it is synthesized, and seems to be irreversible. So far, the biological role of Nt-acetylation has been enigmatic; only in a few cases has it been reported to affect protein functionality [for instance, nonacetylated actin is less efficient at assembling microfilaments (*2*)]. Controlling the activity of individual proteins cannot, however, explain the massive Nt-acetylation of bulk proteins. On page 973 in this issue, Hwang *et al.* (*3*) demonstrate that acetylation of the amino terminus of a protein can function as a degration signal (degron), revealing an entirely unexpected role of acetylation in protein turnover and possibly homeostasis.

Protein degradation in eukaryotic cells is highly specific; the majority of proteins are protected from being destroyed, whereas those with signaling functions or aberrant proteins are often subjected to regulated and general proteolysis, respectively. The latter are covalently labeled at internal lysine residues with chains of ubiquitin molecules (catalyzed by E3 ligases) that serve as a signal for protein degradation by the 26*S* proteasome (*4*, *5*).

One of the first protein degradation signals to be identified was defined by residues at the amino termini of proteins, and led to the N-end rule (*6*), which is conserved from eubacteria to humans. The rule states that the half-life of a protein is determined by its amino-terminal amino acid, which is either stabilizing (Met, Cys, Gly, Ala, Ser, Thr, Val, Pro) or destabilizing (Phe, Leu, Trp, Tyr, Ile, Arg, Lys, His) (*7*, *8*). Almost 25 years later, Hwang *et al.* have revisited the N-end rule by assessing the influence of residues in the penultimate position at the amino terminus. Their astonishing observation is that some residues that were initially characterized as stabilizing (Ala, Ser, Thr, Val) are destabilizing as well, provided that a basic residue (Lys, Arg, or His) is not present in the penultimate position.

It was a striking correlation between the amino-terminal sequences that cause protein destabilization and the substrate specificity of N-terminal acetyltransferases, that unexpectedly placed Nt-acetylation at the center of the investigation by Hwang *et al.* Genetic studies in the yeast *Saccharomyces cerevisiae* and biochemical studies revealed that Nt-acetylation is indeed a prerequisite for the degradation of model substrates. The authors further validated the role of Nt-acetylation in protein degradation by identifying in vivo substrates in yeast. An acetylated amino terminus therefore represents a degradation tag (Ac-N-degron). Similarity in the pattern of amino-terminal acetylation and the conservation of N-terminal acetyltransferases between yeast and human suggest that Nt-acetylation–dependent protein degradation also operates in higher eukaryotes (*9*). In this context, it should be stressed that the role of Nt-acetylation is not restricted to controlling protein stability. For example, it also regulates tropomyosin-actin interactions (*10*), which cannot be explained by this new N-end rule.

The Ac-N-degron is different from the "classical" N-degron in major aspects. Ac-N-degrons are recognized by the E3 ligase Doa10, whereas the E3 ligase Ubr1 ubiquitinates "classical" N-degrons (see the figure). Hwang *et al.* found that Doa10 specifically recognizes acetylated amino termini, and proteins harboring Ac-N-degrons are at least partially stabilized in mutant yeast cells lacking Doa10. Although Doa10 localizes to the endoplasmic reticulum (ER) membrane and inner nuclear membrane and targets aberrant ER membrane proteins, it also

Zentrum für Molekulare Biologie der Universität Heidelberg (ZMBH), DKFZ-ZMBH Alliance, Im Neuenheimer Feld 282, Heidelberg 69120, Germany. E-mail: bukau@zmbh.uni-heidelberg.de

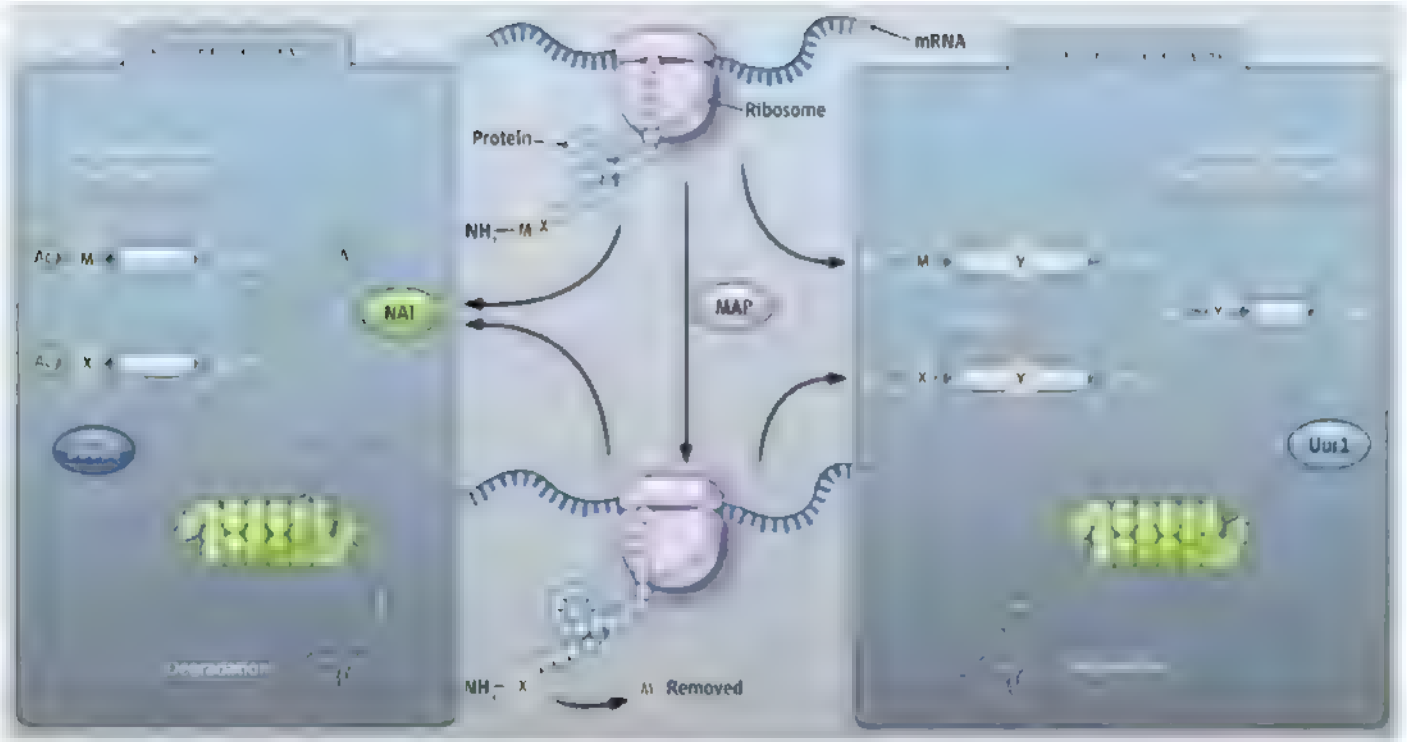

Tags for destruction. Nascent polypeptide chains are cotranslationally processed by ribosome-associated methionine aminopeptidases (MAP) and *N*-acetyltranferases (NAT), generating conditional Ac-N-degrons that can be targeted by the E3 ligase Doa10 for degradation. Classical N-degrons are generated from full-length proteins by cleavage and enzymatic modifications and are degraded in a Ubr1-dependent manner. The accessibility of acetylated amino termini to Doa10 might link the stability of proteins to their folding or assembly state. Amino acid residues: A, Ala; C, Cys; F, Phe; H, His; I, Ile; K, Lys; L, Leu; M, Met; R, Arg; S, Ser; T, Thr; V, Val; and W, Trp.

marks cytosolic and nuclear proteins for degradation (*11*).

Another difference is that a "classical" N-degron can only be produced from a pre-N-degron sequence, requiring either cleavage to generate a new amino-terminal residue or enzymatic modification of the amino terminus to produce a destabilizing residue. The generation of such N-degrons represents regulatory entry points to control protein stability. By contrast, Ac-N-degrons are generated constantly during protein synthesis. Nt-acetylation can occur at an amino-terminal methionine residue, however, methionine is frequently removed by a methionine aminopeptidase, leading to Nt-acetylation of the residue placed originally in the penultimate position. Methionine aminopeptidase does not remove methionine if a "classical" destabilizing residue is in the penultimate position, thus restricting aminopeptidase activity to Ac-N-degrons (*12*). Here, a methionine aminopeptidase might either allow Ac-N-degrons of different strengths to be generated, or protect the nascent polypeptide chain from Nt-acetylation in case glycine and proline residues, which are rarely acetylated, become positioned at the amino terminus.

What might be the physiological function of Ac-N-degrons? Because Nt-acetylation is largely cotranslational, seemingly irreversible, and occurs in bulk proteins, it is unlikely to play a role in specific regulatory circuits. Comparing the total proteins expressed in wild-type and in mutant yeast cells lacking individual N-terminal acetyltransferase enzymes did not reveal global differences (*13*); thus, the presence of an Ac-N-degron does not automatically target a protein for proteasomal degradation. Accordingly, a general correlation between Nt-acetylation and protein stability does not exist. Instead, Hwang *et al.* propose that an acetylated amino terminus represents a conditional N-degron, which results in protein degradation only when it is accessible for recognition by Doa10. Such accessibility could link the folding or assembly state of a protein to its stability by allowing an aberrant protein to be removed and stoichiometries of protein complexes to be correctly adjusted by degrading nonassembled subunits. This would not lead to vast and nonspecific protein degradation but rather would use a built-in quality-control mechanism to ensure high specificity of protein removal and to control protein homeostasis. However, the authentic substrates of the Ac-N degradation pathway that have been identified so far do not yet clarify whether such a link to protein quality control exists.

It is unclear why for some proteins, only a fraction of their cellular pool is amino-terminally acetylated. It is also not yet known whether chaperone proteins that assist in protein folding and assembly might control the accessibility of acetylated amino termini to Doa10, potentially adding another layer of complexity to this degradation pathway. Nt-acetylation and protein degradation might also be controlled by different intracellular amounts of acetyl–coenzyme A, the cosubstrate of N-terminal acetyltransferases, thus allowing additional stimuli to be integrated into the degradation pathway. The identification of Ac-N-degrons sets the stage for an entire new research field.

CREDIT: Y. GREENMAN/SCIENCE

References

1. T. Arnesen *et al.*, *Proc. Natl. Acad. Sci. U.S.A.* **106**, 8157 (2009).
2. B. Polevoda *et al.*, *J. Biol. Chem.* **278**, 30686 (2003).
3. C.-S. Hwang, A. Shemorry, A. Varshavsky, *Science* **327**, 973 (2010); published online 28 January 2010 (10.1126/science.1183147).
4. T. Ravid, M. Hochstrasser, *Nat. Rev. Mol. Cell Biol.* **9**, 679 (2008).
5. A. Varshavsky, *Trends Biochem. Sci.* **30**, 283 (2005).
6. A. Bachmair, D. Finley, A. Varshavsky, *Science* **234**, 179 (1986).
7. A. Varshavsky, G. Turner, F. Du, Y. Xie, *Biol. Chem.* **381**, 779 (2000).
8. A. Mogk, R. Schmidt, B. Bukau, *Trends Cell Biol.* **17**, 165 (2007).
9. B. Polevoda, F. Sherman, *J. Mol. Biol.* **325**, 595 (2003).
10. J. M. Singer, J. M. Shaw, *Proc. Natl. Acad. Sci. U.S.A.* **100**, 7644 (2003).
11. R. Swanson, M. Locher, M. Hochstrasser, *Genes Dev.* **15**, 2660 (2001).
12. F. Frottin *et al.*, *Mol. Cell. Proteomics* **5**, 2336 (2006).
13. J. I. Garrels *et al.*, *Electrophoresis* **18**, 1347 (1997).

10.1126/science.1187274

PALEONTOLOGY

On Giant Filter Feeders

Massive filter-feeding vertebrates have roamed the world's oceans for the past 170 million years.

Lionel Cavin

The largest living marine vertebrates—baleen whales and several lineages of sharks and rays—feed directly on very small organisms (such as plankton and small fishes). Planktivorous sharks and rays collect food by filtering seawater through gill rakers (fingerlike projections on gill arches), whereas mysticete whales sieve small animals from seawater through whalebone or baleen (comblike keratin structures in their upper jaws) (*1*, *2*). On page 990 of this issue, Friedman *et al.* show that the first known large pelagic filter feeders, a group of ray-finned fishes, persisted between 170 and 65 million years ago (*3*). And on page 993, Marx and Uhen show that in the Tertiary (65 to 2.5 million years ago), the diversity of mysticete whales was linked to the diversity of diatoms and to climatic variations (*4*).

Department of Geology and Paleontology, Natural History Museum, Geneva, Switzerland. E-mail: lionel.cavin@ville-ge.ch

In the Jurassic (200 to 145 million years ago) and the Cretaceous (145 to 65 million years ago), ray-finned fishes called pachycormiforms lived in the oceans. These extinct fishes are regarded as primitive teleosts, the group to which most living bony fishes belong (*5*). A giant representative from the Middle Jurassic, *Leedsichthys*, was up to 9 m long and has been interpreted as a filter feeder (*6*). This massive filter-feeding fish has been regarded as an isolated and fleeting evolutionary experiment. By reinterpreting old findings, analyzing new fossils, and running phylogenetic analyses, Friedman *et al.* show that this and other fossil fishes form a clade of massive marine filter feeders that lived from 170 to 65 million years ago. As today's planktivorous sharks and rays do (*1*), these fishes engulfed water by swimming with an open mouth and sieved food while water escaped through the gill arches.

Giant reptiles roamed the Jurassic and Cretaceous oceans, and some huge ray-finned fishes—the ichthyodectiforms (bulldog fish and relatives)—emerged at the end of the Cretaceous. But all these beasts were apex predators that fed on large preys, and none had a filter-feeding diet. The newly discovered clade of massive filter-feeding fishes thus fills a large ecological niche.

Marx and Uhen reveal how the taxonomic diversity of another, younger type of massive filter feeder, the Tertiary baleen whales, was controlled by biological and environmental factors, rather than by the amount of rock in which we might find their fossils. Modern cetaceans (whales, dolphins, and porpoises) fall into two groups: the baleen whales (Mysteceti) and the toothed whales

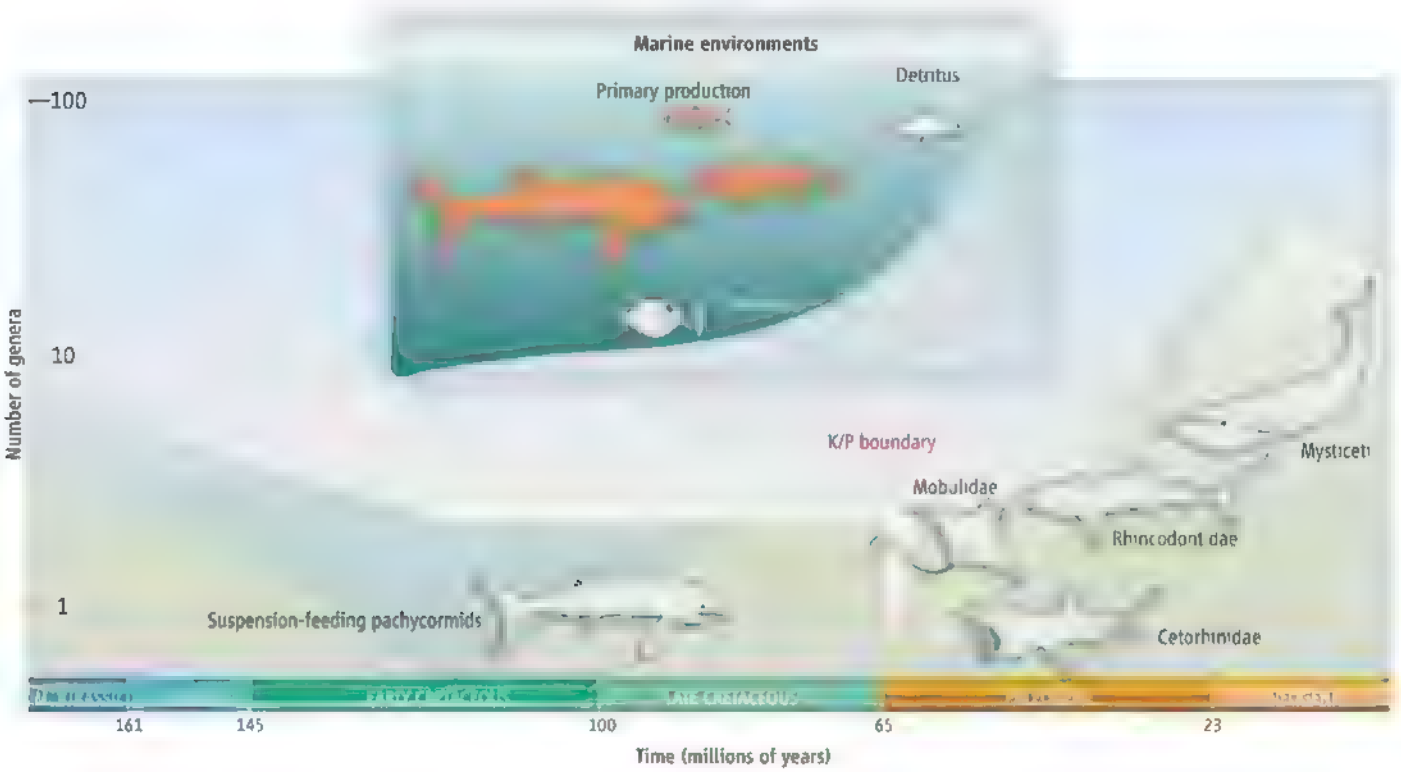

Past diversity of large filter feeders. The diversity of filter-feeding pachycormids is from (*3*); the dotted line shows the diversity, including ghost lineages (which have no fossil record but are inferred to exist to comply with a phylogenetic tree) [see supporting online material of (*3*)]. The diversity of rays and sharks (Mobulidae, Cetorhinidae, Rhincodontidae) is from (*10*) and that of mysticete whales from (*4*). **(Inset)** At the Cretaceous–Paleogene boundary, the food chains based on primary production collapsed, leading to the extinction of large suspension feeders and large fish-eating fishes (red), whereas costal and deep-ocean fishes that relied more on detritus survived.

(Odontoceti). The authors show that the diversity of both groups can be explained by diatom diversity in conjunction with variations in climate, as indicated by oxygen stable isotope records. The results add to previous observations that have stressed the importance of environmental parameters (both geographic and oceanographic) in the evolution of modern cetaceans (*7*).

The two papers change our view of the natural history of these evolutionary distant organisms, which share similar trophic resources (see the figure), and raise new questions about their evolutionary drivers. For instance, it has been shown that marine ray-finned fish diversity was positively correlated with sea surface temperature in the Cretaceous, and that the Cretaceous fossil fish record corresponds to a genuine biological radiation (*8*). Further evolutionary studies will help to determine whether the diversity of the Jurassic/Cretaceous filter-feeder clade was related to climatic factors and the diversity of primary producers, and/or whether it was controlled by paleogeographical factors.

What caused the gap between the Jurassic/Cretaceous and the Tertiary episodes of the natural history of giant filter feeders? It is probably linked with the same event that caused a mass extinction at the Cretaceous-Paleogene boundary on land. This event affected only specific food chains, mainly those based on fresh plants (*9*). In the oceans, the phytoplankton-based food chains collapsed, whereas coastal and deep-ocean organisms that fed more on detritus survived (see the figure, inset). The filter-feeding pachycormiforms, relying for food on small organisms low in the trophic chain, had the perfect profile of a victim and became extinct. The trophic niche was later refilled, first with sharks and rays from ~56 million years ago and then with modern cetaceans from ~34 million years ago (see the figure).

The two studies also show that phylogenetic reconstructions can be the starting point for investigating major events in the history of life (*3*)—and not only an aim per se, as happens too often with fossil fish studies—and that variations in the diversity of life can be read directly from the fossil record if precautions are taken (*4*).

References

1. S. L. Sanderson, R. Wassersug, in *The Skull, vol. 3*, J. Hanken, B. K. Hall, Eds. (Univ. Chicago Press, Chicago, IL, 1993), pp. 37–112
2. T. A. Demére, M. R. McGowen, A. Berta, J. Gatesy, *Syst. Biol.* **57**, 15 (2008)
3. M. Friedman *et al.*, *Science* **327**, 990 (2010)
4. F. G. Marx, M. D. Uhen, *Science* **327**, 993 (2010)
5. J. Liston, in *Mesozoic Fishes 3—Systematics, Paleoenvironments and Biodiversity*, G. Arratia, A. Tintori, Eds. (Friedrich Pfeil, München, 2004), pp. 379–390
6. D. M. Martill, N. Jahrb. Geol. *Paläontol.* **1988**, 670 (1988)
7. M. E. Steeman *et al.*, *Syst. Biol.* **58**, 573 (2009).
8. L. Cavin, P. L. Forey, C. Lécuyer, *Palaeog. Palaeoc. Palaeoec.* **245**, 353 (2007)
9. E. Buffetaut, *Nature* **310**, 276 (1984)
10. H. Cappetta, in *Handbook of Paleoichthyology, vol. 3B*, H.-P. Schultze, Ed. (Friedrich Pfeil, München, 1987)

10.1126/science.1186904

PHYSICS

The Lowdown on Heavy Fermions

Layer-by-layer growth provides a route to control the properties of complex interacting electron systems.

Piers Coleman

One of the quests of condensed matter physics is to discover materials with new types of collective electronic properties, such as the giant magnetoresistance materials (*1*) now used for memory storage or high-temperature superconductors (*2*). Such "strongly correlated electron" materials challenge our understanding and provide the grist for future technologies. However, identifying new kinds of electronic behavior is still serendipitous, largely because the materials structures of greatest interest do not crystallize to order. On page 980 of this issue, Shishido *et al.* (*3*) introduce a systematic approach based on molecular beam epitaxy for the preparation of complex interacting electron materials, thus opening up the possibility of making available many new structures not currently accessible to direct chemical synthesis.

It is the Coulomb repulsion between electrons that drives the development of new kinds of electronic behavior. When the repulsion energy between electrons is small compared with their kinetic energy, electrons move independently, but when the interactions are large, electron motions become highly correlated, and may develop unexpectedly new types of collective behavior in order to try and lower the Coulomb energy.

Two strategies have proven particularly successful in preparing strongly correlated electron materials. The first is to find layered materials where the confinement of electrons to two dimensions enhances their interactions. The other is to tune the material by some external parameter (e.g., pressure, magnetic or electric field) to the brink of magnetic instability, a point in the phase diagram called a "quantum phase transition" (*4*, *5*). Interactions between electrons inside materials are

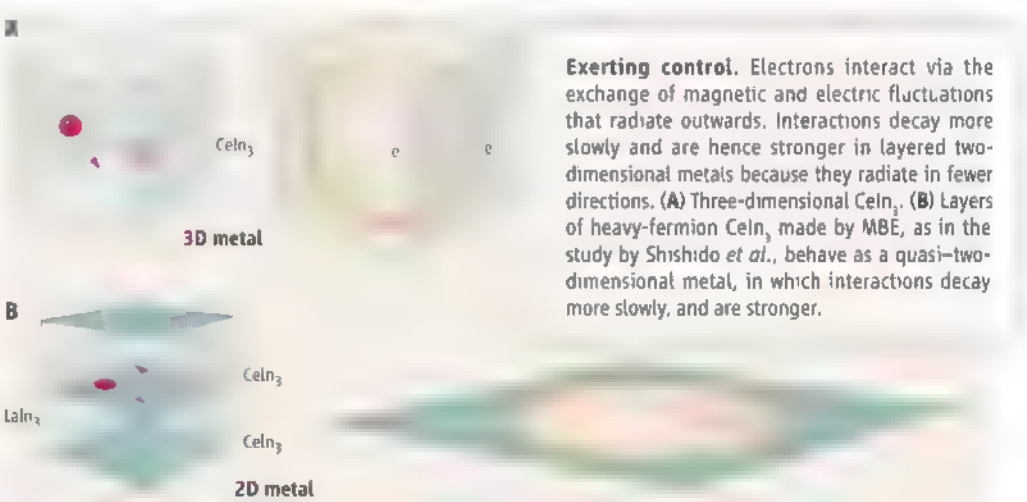

Exerting control. Electrons interact via the exchange of magnetic and electric fluctuations that radiate outwards. Interactions decay more slowly and are hence stronger in layered two-dimensional metals because they radiate in fewer directions. (**A**) Three-dimensional $CeIn_3$. (**B**) Layers of heavy-fermion $CeIn_3$ made by MBE, as in the study by Shishido *et al.*, behave as a quasi–two-dimensional metal, in which interactions decay more slowly, and are stronger.

Center for Materials Theory, Rutgers University, Piscataway, NJ 08854–8019, USA. E-mail: coleman@physics.rutgers.edu

transmitted by quantum mechanical fluctuations that radiate out from each particle (see the figure). In two dimensions these fluctuations decay more slowly with distance, resulting in stronger interactions. The fluctuations also become more intense near a quantum phase transition. Many of the superconductors discovered in the past decade are indeed layered compounds close to a quantum phase transition (*6*, *7*).

Rather than using direct chemical synthesis, Shishido *et al.* turn to a method used commonly to fabricate semiconductor devices molecular beam epitaxy (MBE), a technique involving the direct deposition of atoms from an atomic beam onto a substrate, slowly building an ordered crystal, layer by layer (*8*, *9*). They apply the MBE method to a class of strongly correlated metals called heavy-fermion compounds, materials that contain arrays of rare earth atoms that trap electrons tightly inside f orbitals where they experience strong interactions ("heavy fermion" refers to the very large effective mass of the charge carriers in these metals).

Shishido *et al.* start with a three-dimensional heavy-fermion compound, $CeIn_3$. In three dimensions, the f electrons in this material are localized and arrange their magnetic properties to form an antiferromagnet. Earlier experiments showed that under high pressure (*4*), the magnetism could be suppressed, driving the material to a quantum critical point where superconductivity developed. Layered derivatives of this material in which the magnetism was sometimes absent and superconductivity developed spontaneously were later discovered (*6*). Could one systematically reproduce these effects using MBE methods?

By successfully identifying the conditions and substrate needed to lay down layers of heavy-electron material, Shishido *et al.* systematically lower the dimensionality of $CeIn_3$. They do this by introducing alternating layers of magnetic $CeIn_3$ and nonmagnetic $LaIn_3$, which is a weakly interacting metal. They have prepared a family of such compounds containing variable thicknesses of cerium layers. With eight cerium layers the material behaved like three-dimensional $CeIn_3$, with a magnetic phase transition, but as they reduced the number of cerium layers, they found that the reduced dimensionality suppressed the temperature of the magnetic phase transition, driving it to absolute zero (0K) by the time they had reached the two-layer system.

Two fascinating properties developed in the two-layer system, suggesting that it lies right at a quantum phase transition. First, Shishido *et al.* found that the resistance of this material is very sensitive to magnetic fields, an indication of scattering of electrons off the soft magnetic fluctuations around a magnetic quantum phase transition. Second, the temperature (T) dependence of the resistivity changed qualitatively as the dimensionality of the crystal decreased, shifting from a T^2 dependence expected in conventional metals to a linear dependence on temperature behavior characteristic of inelastic scattering off spin fluctuations

These experiments are a milestone in the application of MBE methods to layered intermetallic materials, showing that these methods can be successfully used to tune the dimensionality and increase the electron interactions in these kinds of materials. Although the current experiments did not observe any emergent superconductivity at the magnetic quantum phase transition, this next milestone may not be far away. In the current samples, the resistivity of the most two-dimensional samples is large, an effect the authors attribute to interdiffusion of lanthanum and cerium between layers (*3*). The scattering this creates is well known to break up the electron pairs needed for superconductivity. Future experiments, replacing the lanthanum with smaller transition metal ions, may well be able to solve this problem.

References and Notes

1. W. P. McCray, *Nat. Nanotechnol.* **4**, 2 (2009)
2. See, e.g., http://en.wikipedia.org/wiki/High-temperature_superconductivity
3. H. Shishido *et al.*, *Science* **327**, 980 (2010)
4. N. D. Mathur *et al.*, *Nature* **394**, 39 (1998)
5. P. Coleman, A. J. Schofield, *Nature* **433**, 226 (2005)
6. J. L. Sarrao, J. D. Thompson, *J. Phys. Soc. Jpn.* **76**, 051013 (2007)
7. H. Hosono *et al.*, *N. J. Phys.* **11**, 025003 (2009)
8. M. B. Panish, *Science* **208**, 916 (1980)
9. B. A. Joyce, *Rep. Prog. Phys.* **48**, 1637 (1985).

10. Supported by NSF grant NSF-DMR 0907179

10.1126/science.1186253

ATMOSPHERIC SCIENCE

Can We Understand Clouds Without Turbulence?

Advances at the interface between atmospheric and turbulence research are helping to elucidate fundamental properties of clouds.

E. Bodenschatz,[1,2] S. P. Malinowski,[3] R. A. Shaw,[4] F. Stratmann[5]

Just over 50 years ago, Henry Houghton published an essay in *Science* entitled "Cloud physics: Not all questions about nucleation, growth, and precipitation of water particles are yet answered" (*1*). Since then, understanding of cloud processes has advanced enormously, yet we still face some of the basic questions Houghton drew attention to. The interest in finding the answers, however, has steadily increased, largely because clouds are a primary source of uncertainty in projections of future climate (*2*). Why is our understanding of cloud processes still so inadequate, and what are the prospects for the future?

Clouds are dispersions of drops and ice particles embedded in and interacting with a complex turbulent flow. They are highly nonstationary, inhomogeneous, and intermittent, and embody an enormous range of spatial and temporal scales. Strong couplings across those scales between turbulent fluid dynamics and microphysical processes are integral to cloud evolution (see the figure).

Turbulence drives entrainment, stirring, and mixing in clouds, resulting in strong fluctuations in temperature, humidity, aerosol concentration, and cloud particle growth and decay (*3*). It couples to phase transition processes (such as nucleation, condensation, and freezing) as well as particle collisions and breakup (*4*). All these processes feed back on the turbulent flow by buoyancy and drag forces and

[1]Max Planck Institute for Dynamics and Self-Organization, 37073 Göttingen, Germany. [2]Laboratory of Atomic and Solid State Physics, Cornell University, Ithaca, NY 14853, USA. [3]Institute of Geophysics, University of Warsaw, 02-093 Warsaw, Poland. [4]Department of Physics, Michigan Technological University, Houghton, MI 49931, USA. [5]Leibniz Institute for Tropospheric Research, 04318 Leipzig, Germany. E-mail: frank.stratmann@tropos.de

CREDIT (MICROPHYSICS) F. STRATMANN; (TRAJECTORIES) E. BODENSCHATZ, SCIENCE MAGAZINE TABLE OF CONTENTS 19 FEBRUARY 2006; (MIXING) S. MALINOWSKI; (ENTRAINMENT AND CLOUDS) R. A. SHAW; (GLOBAL) NASA EARTH OBSERVATORY

affect cloud dynamical processes up to the largest scales (*5*–*7*).

To a large extent, understanding of clouds has come through the study of two phenomena: cloud microphysical processes in nonturbulent fluids, and large-scale cloud circulation and dynamics. At the same time, understanding of the physics of fully developed turbulent flows has advanced rapidly. For example, sophisticated laboratory apparatus now allows the study of nucleation and growth of cloud particles under well-controlled conditions (*8*). Computational models ranging from the cloud to the global scale elucidate detailed interactions between aerosols and cloud dynamics (*9*). And three-dimensional particle tracking and fully resolved turbulence simulations have substantially advanced our understanding of turbulent transport and mixing (*10*).

The frontier in cloud physics, and the challenge in understanding cloud processes, lies at the intersection of these two fields (*11*). For example, high-resolution measurements of temperature, liquid water content, aerosol properties, and airflow reveal fascinating small-scale cloud structures, invisible with earlier technology (*3*, *12*). Laboratory experiments and numerical simulations are providing detailed information on cloud microphysics (*8*), turbulent dynamics (*13*), and interactions and collisions between droplets (*14*, *15*). Scale-resolving simulations that merge methods from the cloud and turbulence communities are elucidating the wide variety of circulation regimes (*16*). These tools allow the full complexity of microphysical and fluid-dynamical interactions in clouds to be explored (see the figure).

Two examples illustrate this further. First, computational, laboratory, and field studies (*17*, *18*) have explored two fundamentally different regimes for the interplay between turbulent mixing and droplet growth and evaporation. At large scales, mixing occurs at sharp fronts and fields are inhomogeneous, whereas at small scales, mixing is smooth and homogeneous. These regimes strongly affect spatiotemporal droplet growth and evaporation, with implications for precipitation initiation and radiative properties of clouds.

Second, recent research has changed our understanding of rain formation. Rain formation has long been attributed to collisions and subsequent coalescence resulting from cloud particles falling at different terminal speeds in a quiescent fluid. This view neglected the fact that clouds are turbulent. Turbulence provides a random acceleration term to compete with the gravitational sedimentation, resulting in complex particle trajectories that cross fluid streamlines and lead to spatially clustered particle distributions (see the figure). This process substantially enhances collision rates, thus reducing the time required to form precipitation in clouds (*15*, *19*).

With these advances we can better address some of Houghton's persistent questions (*1*). Laboratory facilities are being developed for studying droplet activation, ice nucleation, and condensational growth in flows with realistic turbulence and thermodynamics conditions. Lagrangian particle tracking can elucidate cloud particle dynamics in the laboratory as well as in real clouds. Scale-resolving numerical simulations have begun to capture the interplay of turbulent mixing and nonlinear phase transitions. The resulting insights will enable the development of hierarchies of models for predicting how small-scale processes couple to the larger scales and how this coupling affects weather and climate

A matter of scale. Turbulence on scales from hundreds of meters to fractions of millimeters affects the formation and dynamics of clouds, with consequences extending to the scale of weather and global climate. CCN, cloud condensation nuclei.

References and Notes

1. H. G. Houghton, *Science* **129**, 307 (1959).
2. J. Heintzenberg, R. J. Charlson, Eds., *Clouds in the Perturbed Climate System* (MIT Press, Cambridge, MA, 2009).
3. H. Siebert *et al.*, *Bull. Am. Meteorol. Soc.* **87**, 1727 (2006).
4. R. A. Shaw, *Annu. Rev. Fluid Mech.* **35**, 183 (2003).
5. B. Stevens *et al.*, *Mon. Weather Rev.* **133**, 1443 (2005).
6. I. M. Held, M. Zhao, B. Wyman, *J. Atmos. Sci.* **64**, 228 (2007).
7. C. Stan *et al.*, *Geophys. Res. Lett.* **37**, L01702 (2010).
8. F. Stratmann, O. Moehler, R. Shaw, H. Wex, in *Clouds in the Perturbed Climate System*, J. Heintzenberg, R. J. Charlson, Eds. (MIT Press, Cambridge, MA, 2009), pp. 149–172.
9. B. Stevens, G. Feingold, *Nature* **461**, 607 (2009).
10. F. Toschi, E. Bodenschatz, *Annu. Rev. Fluid Mech.* **41**, 375 (2009).
11. Z. Warhaft, *Fluid Dyn. Res.* **41**, 011201 (2009).
12. K. E. Haman, S. P. Malinowski, M. J. Kurowski, H. Gerber, J.-L. Brenguier, *Q. J. R. Meteorol. Soc.* **133**, 213 (2007).
13. M. Bourgoin *et al.*, *Science* **311**, 835 (2006).
14. J. Chun, D. L. Koch, S. L. Rani, A. Ahluwalia, L. R. Collins, *J. Fluid Mech.* **536**, 219 (2005).
15. L.-P. Wang, O. Ayala, B. Rosa, W. W. Grabowski, *N. J. Phys.* **10**, 075013 (2008).
16. O. Pauluis, J. Schumacher, *Comm. Math. Sci.* **8**, 295 (2010).
17. K. Lehmann, H. Siebert, R. A. Shaw, *J. Atmos. Sci.* **66**, 3641 (2009).
18. S. P. Malinowski *et al.*, *N. J. Phys.* **10**, 075020 (2008).
19. M. Pinsky, A. Khain, H. Krugliak, *J. Atmos. Sci.* **65**, 357 (2008).

20. We thank O. Moehler, J. Schumacher, H. Siebert, and B. Stevens for important comments.

10.1126/science.1185138

RETROSPECTIVE

Marshall Warren Nirenberg (1927–2010)

Passion and curiosity spurred a soft-spoken biologist to lead the fierce race to crack the code of life

Philip Leder

Of all the astonishing advances and discoveries of 20th-century biology, few compare to the elucidation of the genetic code in terms of importance and universal impact. The code is the Rosetta Stone of life, specifying how genetic information in the form of a linear array of four nucleotides in RNA directs the incorporation of each of the 20 amino acids into proteins.

By the mid-1950s, researchers understood enough about the role of RNA and DNA to realize that some mechanism must translate genetic information in the form of messenger RNA (mRNA) into its final form as protein. This mechanism was called the "genetic code," and, coming after the determination of the double helical structure of DNA, it became the target of intense speculation and even some experimental probing. Such was the scientific world into which a young Marshall Nirenberg entered, fascinated by the advances in protein synthesis and eager to try his hand in an experimental approach.

Nirenberg was prepared and motivated for the work. Born in New York City in 1927, but raised in central Florida, he loved tramping through swamps, catching all sorts of creatures, in particular, snakes. One photograph from that era shows the teenager in waders, holding a 6-foot snake and smiling mischievously.

Later, Nirenberg would matriculate in the Department of Zoology at the University of Florida, where his master's thesis was on caddisflies. Hoping for a more molecular orientation in his work, Nirenberg entered the University of Michigan, where he earned a Ph.D. There, James Hogg, whom he often referred to as a wonderful teacher and friend, mentored him in biochemistry. In another and final move, Nirenberg came to the National Institutes of Health (NIH) as a postdoctoral fellow in 1957, ultimately achieving an independent staff position. Finally, he had the opportunity to pursue his studies of protein synthesis

Nirenberg realized that development of a cell-free protein synthetic system would be a valuable tool in detecting mRNA. First working by himself, and later with a postdoctoral fellow, Heinrich Matthaei, they labored, literally day and night, to develop conditions under which the system was stabilized. Their work resulted in the famous polyU experiment, in which a synthetic RNA polymer consisting entirely of uradylic acid (U) residues directed the incorporation of only 1 of the 20 amino acids (phenylalanine) into protein. Therefore, the codon or code word, the informational unit, for phenylalanine is a stretch of U's, probably a triplet as other genetic evidence suggested.

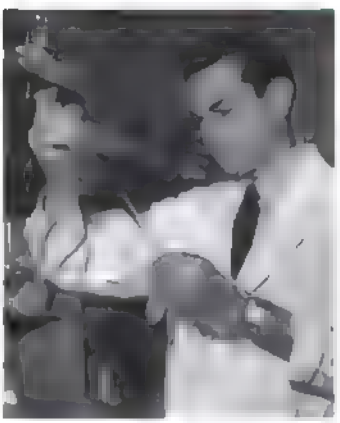

Nirenberg presented the work in August 1961 at the International Congress of Biochemistry in Moscow. Coming from an unknown, it initially received scant attention until Francis Crick, codiscoverer of the structure of DNA and a leading figure in molecular biology, organized a repeat performance in a larger hall.

Nirenberg had taken the first step toward elucidating the genetic code, and it invited intense competition. Severo Ochoa, a distinguished Nobel Laureate who directed a large and very able group of biochemists at New York University, seized the opportunity and a veritable horse race to work out the complete code ensued. At NIH, friends and colleagues dropped what they were doing to help Nirenberg. Papers from the two labs seemed to appear almost monthly, and by 1962 the composition, but not the sequence of nucleotides of each codon, was largely determined. The first phase of the race, the compositional code, was complete, but the sequence of nucleotides in each codon remained to be determined.

This last phase depended on the development of a simple assay devised by the Nirenberg group to observe the binding of aminoacyl tRNA (transfer RNA) to a ribosomal complex in response to synthetic triplet codons. The success of this approach was announced at the 1964 International Congress of Biochemistry, in New York City, before a large and very excited crowd of biochemists. Using this approach, the Nirenberg group, now joined in the race by the chemist Har Gobind Khorana, had largely completed all the codon assignments. Further studies revealed that the code was virtually universal, that is, the same code words were used in almost all animal and plant species. In 1968, Nirenberg, Khorana, and Robert Holley (who worked on tRNA) shared the Nobel Prize in Physiology or Medicine

Although interesting details remained to be worked out, the coding problem was essentially solved. Nirenberg, among several other distinguished molecular biologists seeking important challenges in the 1970s, turned to the study of the nervous system. The field advanced slowly pending the development of recombinant DNA and other technologies. These eventually made this area one of the most rapidly advancing fields of biology, thus vindicating Nirenberg's decision to move.

While Nirenberg's tenure at NIH for his entire career suggests that he was averse to teaching, nothing could be further from the truth. He was a wonderful and generous one-on-one teacher and a great supporter of his associates, many of whom have gone on to distinguished careers. Soft spoken, he would patiently listen to a younger colleague and give serious thought to his or her question or idea, no matter how off-beat. Colleagues were invariably greeted by a cheery, "So what's new?" And he really wanted to hear what was going on in the lab. Science was clearly his all-consuming passion. Conversations with him were always stimulating. He retained that gleeful enthusiasm he exhibited as a teenager, catching snakes in a Florida swamp.

Sadly, Marshall Warren Nirenberg died of cancer on 15 January 2010. He was predeceased by his wife of 40 years, the Brazilian chemist, Perola Zaltzmann, and is survived by his present wife, Myrna Weissman, professor of Epidemiology and Psychiatry at Columbia University, College of Physicians and Surgeons

CREDIT: NLM/NIH

Department of Genetics, Harvard Medical School, 77 Avenue Louis Pasteur, Boston, MA 02115, USA. E-mail: leder@genetics.med.harvard.edu

10.1126/science.1187484

N-Terminal Acetylation of Cellular Proteins Creates Specific Degradation Signals

Cheol-Sang Hwang, Anna Shemorry, Alexander Varshavsky*

The retained N-terminal methionine (Met) residue of a nascent protein is often N-terminally acetylated (Nt-acetylated). Removal of N-terminal Met by Met-aminopeptidases frequently leads to Nt-acetylation of the resulting N-terminal alanine (Ala), valine (Val), serine (Ser), threonine (Thr), and cysteine (Cys) residues. Although a majority of eukaryotic proteins (for example, more than 80% of human proteins) are cotranslationally Nt-acetylated, the function of this extensively studied modification is largely unknown. Using the yeast *Saccharomyces cerevisiae*, we found that the Nt-acetylated Met residue could act as a degradation signal (degron), targeted by the Doa10 ubiquitin ligase. Moreover, Doa10 also recognized the Nt-acetylated Ala, Val, Ser, Thr, and Cys residues. Several examined proteins of diverse functions contained these N-terminal degrons, termed ^{Ac}N-degrons, which are a prevalent class of degradation signals in cellular proteins.

Many eukaryotic proteins are acetylated at the α-amino group of their N-terminal residues (fig. S1A) (*1*). Previous studies of N^{α}-terminal acetylation (Nt-acetylation) have characterized Nt-acetylated proteins and N^{α}-terminal acetyltransferases (Nt-acetylases) that catalyze this cotranslational modification (*2*–*7*). Owing to the design of the genetic code, nascent proteins contain N-terminal Met. A retained N-terminal Met that is followed by "acetylation-permissive" residues is usually Nt-acetylated (fig. S1A) (*5*–*7*). Met-aminopeptidases cleave off the N-terminal Met if the residue at position 2 has a small enough side chain, resulting in N-terminal Ala, Val, Ser, Thr, Cys, Gly, or Pro (fig. S1B) (*8*). With the near-exception of Gly and Pro, these N-terminal residues are often Nt-acetylated, similarly to N-terminal Met (*5*–*7*). In cell extracts, some Nt-acetylated proteins can be degraded by the ubiquitin (Ub) system (*9*). However, no cognate Ub ligases have been identified, and it has been assumed that the relevant degradation signals were internal (not N-terminal) (*9*). Currently, the prevalent view of Nt-acetylation is that this modification protects proteins from degradation. To the contrary, we report here that Nt-acetylation creates specific degradation signals (degrons) that are targeted by a branch of the Ub-dependent N-end–rule pathway.

Destabilizing N-terminal sequences. The N-end rule relates the in vivo half-life of a protein to the identity of its N-terminal residue (*10*–*20*). N-terminal degradation signals of the N-end–rule pathway are called N-degrons. Their main determinant is a destabilizing N-terminal residue of a protein (fig. S1C). Recognition components of the N-end–rule pathway are called N-recognins. An N-recognin is an E3 Ub ligase that can target for polyubiquitylation at least a subset of N-degrons (*13*, *15*, *18*, *19*). The N-end rule of the yeast *S. cerevisiae* comprises 12 destabilizing, unacetylated N-terminal residues (out of the fundamental set of 20 amino acids) (*12*–*15*, *18*, *19*). Among these residues, eight are primary destabilizing residues; that is, recognized directly by the Ubr1 N-recognin, whereas the other four N-terminal residues, called secondary or tertiary destabilizing residues, must be modified through deamidation and/or arginylation before the corresponding proteins can be targeted by Ubr1 (fig. S1C).

In mammalian cells, the N-terminal Cys of N-end rule substrates can be oxidized, by nitric oxide (NO) and oxygen, and thereafter arginylated by an arginyl-transferase. The resulting N-terminal Arg is recognized by Ubr1-type N-recognins (*15*, *16*). In contrast, N-terminal Cys appeared to be a stabilizing residue in *S. cerevisiae*, which lacks NO synthases (*11*). That study also classified N-terminal Met, Ala, Val, Ser, and Thr as stabilizing residues in *S. cerevisiae* (*11*). One caveat in these assignments is the possible influence of sequences downstream of the reporter's N terminus. To determine whether N-terminal Cys can be destabilizing in yeast, we performed a screen in *ura3 S. cerevisiae* with Cys-Z-e^{K}-Ura3 reporters, produced by deubiquitylation (*10*, *21*) of Ub-Cys-Z-e^{K}-Ura3. Z denotes a varied residue at position 2, and e^{K} [extension (e) containing lysine (K)] denotes a ~40-residue sequence upstream of Ura3. The e^{K}

Fig. 1. Destabilizing N-terminal residues. (**A**) CHX chases, for 0, 1, and 2 hours in wild-type *S. cerevisiae* expressing CK-e^{K}-Ura3 (lanes 1 to 3) or CL-e^{K}-Ura3 (lanes 4 to 6). Cell extracts were fractionated by SDS–polyacrylamide gel electrophoresis, followed by immunoblotting with anti-Ha and anti-tubulin, the latter a loading control. (**B**) As in (A) but chases for 0 and 2 hours with XZ-e^{K}-Ura3 (X = Cys, Met, or Ser; Z = Trp, Val, or Leu) in wild-type versus *ubr1*Δ cells. (**C**) As in (A) but with MZ-e^{K}-Ura3 (Z = Leu or Lys) in wild-type cells. (**D**) As in (A) but chases for 0, 0.5, and 1.5 hours with XL-e^{K}-Ura3 (X = Gly, Val, Ala, or Thr) in wild-type cells. (**E**) As in (A) but with CL-e^{K}-Ura3 in wild-type cells (lanes 1 to 3) versus *doa10*Δ cells (lanes 4 to 6). (**F**) As in (E) but chases for 0, 0.5, 1, and 2 hours with ML-e^{K} Ura3. (**G**) Lanes 1 and 2, short-lived ML-e^{K}-Ura in the MG132-sensitive *pdr5*Δ *S. cerevisiae*, in the absence and presence of MG132, respectively. Lanes 3 and 4, same as lanes 1 and 2 but with long-lived MK-e^{K}-Ura3.

Division of Biology, California Institute of Technology, Pasadena, CA 91125, USA.

*To whom correspondence should be addressed. E-mail: avarsh@ca-tech.edu

extension (fig. S1D) has the technically valuable property of lacking internal degrons while containing "ubiquitylatable" Lys residues (*10*–*12*). This screen identified Cys-Z-e^K-Ura3 fusions (Z = Leu, Val, or Pro) with low Ura3 activity. We examined these fusions using a cycloheximide (CHX)–chase assay, in which a protein is analyzed by immunoblotting as a function of time after the inhibition of translation by CHX (*18*, *19*). The above three reporters were short-lived in vivo [half-life ($t_{1/2}$) < 1 hour], in contrast to GL-e^K-Ura3 (N-terminal Gly) and CK-e^K-Ura3 (Lys at position 2), which were long-lived (Fig. 1, A, B, and D; fig. S2B, and fig. S3, A and D). Other nonbasic residues at position 2 also yielded short-lived CZ-e^K-Ura3 (Z = Trp, Glu, Gly, or Ile) (Fig. 1B and fig. S3A).

Several other XL-e^K-Ura3 reporters (X = Met, Ser, Val, Ala, or Thr) were also short-lived in vivo, like CL-e^K-Ura3 and in contrast to long-lived MK-e^K-Ura3 (Lys at position 2), MR-e^K-Ura3 (Arg at position 2), GL-e^K-Ura3 (N-terminal Gly), and PL-e^K-Ura3 (N-terminal Pro) (Fig. 1, A to D; fig. S2, A and B; and fig. S3, B, C, and E). We also performed ^{35}S-pulse chases (*18*, *19*) with CL-e^K-Ura3 and ML-e^K-Ura3 versus CK-e^K-Ura3 and MK-e^K-Ura3 (fig. S4, A to C). The techniques of CHX chases and ^{35}S-pulse chases are complementary, because the former method monitors the degradation of all molecules of a specific protein, whereas the latter assay measures the degradation of newly formed (pulse-labeled) molecules. ^{35}S-pulse chases confirmed the instability of XL-e^K-Ura3 (X = Cys or Met) and stability of XK-e^K-Ura3 (X = Cys or Met) (Fig. 1, A and C; fig. S2, A and B; and fig. S4, A to C). The degradation of ML-e^K-Ura3 was proteasome-dependent, because the MG132 proteasome inhibitor significantly increased the level of the normally short-lived ML-e^K-Ura3 but not of the long-lived MK-e^K-Ura3, whose levels were high both in the presence and absence of MG132 (Fig. 1G).

The Doa10 ubiquitin ligase recognizes acetylated N-terminal residues. To search for a Ub ligase or ligases that mediate the degradation of XL-e^K-Ura3 (X = Met, Ala, Val, Ser, Thr, or Cys), we expressed CL-e^K-Ura3 in *S. cerevisiae* mutants that lacked specific E3 or E2 enzymes (fig. S4D). CL-e^K-Ura3 became long-lived in the absence of Doa10 (Fig. 1E and fig. S4, D and E). Moreover, other short-lived XL-e^K-Ura3 proteins (Z = Met, Ser, or Val) were also stable in *doa10*Δ cells (Fig. 1F and fig. S4, F and G). Doa10 is a transmembrane E3 Ub ligase that functions with the Ubc6/Ubc7 E2s and resides in the endoplasmic reticulum (ER) and inner nuclear membrane (INM) (*22*–*24*). To address the above results, we focused on MATα2, a physiological substrate of Doa10.

The 24-kD MATα2 contains more than one degradation signal and has an in vivo half-life of 5 to 10 min (*13*, *25*, *26*). MATα2 represses transcription of **a**-specific genes in α-cells, whereas in **a**/α diploids the MATα2-MATa1 complex represses haploid-specific genes (*27*, *28*). The 67-residue N-terminal region of MATα2, termed Deg1, has been shown to harbor a Doa10-dependent degron (*22*–*24*). MATα2 is absent from databases of Nt-acetylated proteins (*5*, *6*), possibly because of its short in vivo half-life. We expressed full-length MATα2 in *doa10*Δ *ubc4*Δ yeast and analyzed purified MATα2 using liquid chromatography–tandem mass spectrometry (LC-MS/MS). The results (fig. S5A) indicated virtually complete Nt-acetylation of MATα2 (no MATα2 that lacked Nt-acetylation could be detected), in agreement with Nt-acetylation of other proteins containing the N-terminal Met-Asn (*5*–*7*). Similar LC-MS/MS of the Doa10-targeted, purified **ML**-e^K-Ura3 (fig. S5, B and C) indicated the Nt-acetylation of this reporter, in agreement with Nt-acetylation of other proteins containing the N-terminal Met-Leu (*5*–*7*). We also observed Nt-acetylation of a Deg1-bearing reporter that was purified from *E. coli* and incubated with *S. cerevisiae* extracts (fig. S6A).

In addition, we produced an antibody, termed anti-^{AcNt}MATα2, that recognized the Nt-acetylated N-terminal sequence of MATα2 (Fig. 2C) and was specific for the Nt-acetylated, hemagglutinin (HA)–tagged, MATα2-derived, MN-α2$^{3-67}$-e^K-Ura3 reporter, denoted MNα2 (Fig. 2, A and B). Anti-^{AcNt}MATα2 and anti-Ha (the latter antibody recognized both Nt-acetylated and unacetylated

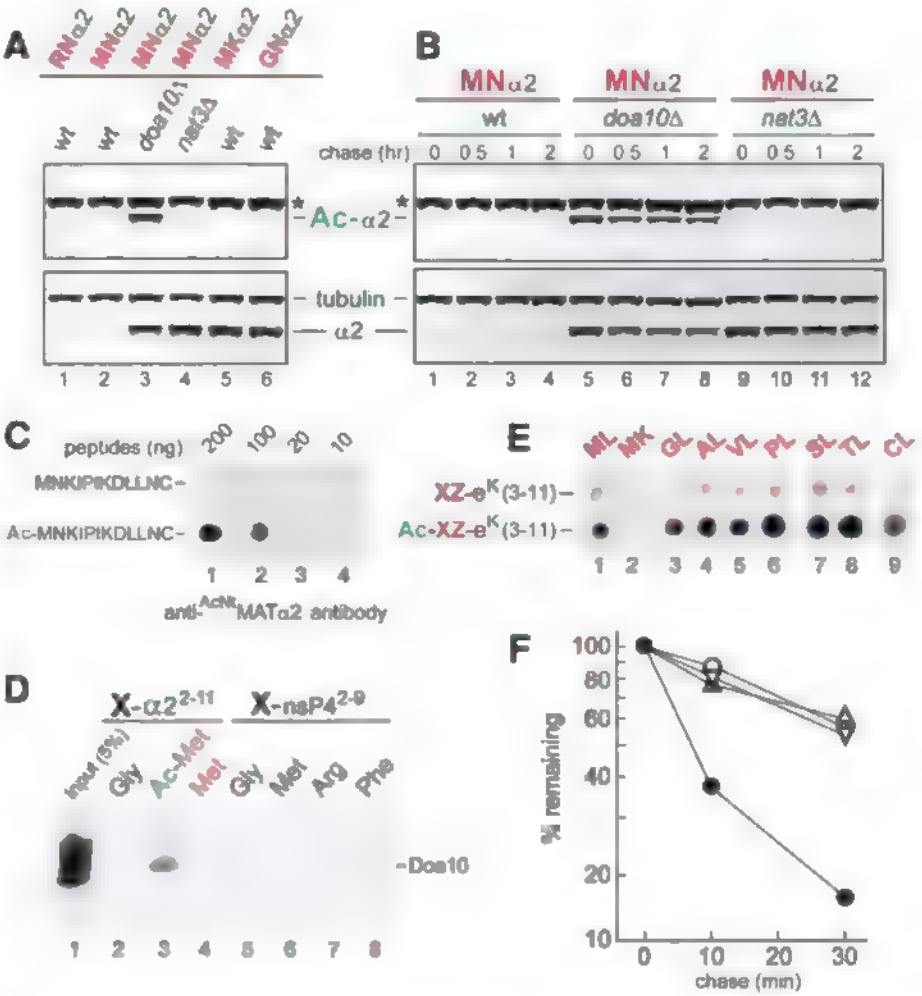

Fig. 2. Doa10 as an N-recognin. (**A**) Extracts from wild-type, *doa10*Δ, and *nat3*Δ *S. cerevisiae* that expressed XZ-α2$^{3-67}$-e^K-Ura3 (XZα2) (X = Met, Arg, or Gly; Z = Asn or Lys) were immunoblotted with anti-^{AcNt}MATα2 (which selectively recognized Nt-acetylated MNα2) or (separately) with anti-Ha, which recognized both Nt-acetylated and unacetylated MNα2, or with anti-tubulin. XZα2 ("α2"), Nt-acetylated XZα2 ("Ac-α2"), and tubulin are indicated. Asterisks denote a protein cross-reacting with anti-^{AcNt}MATα2. (**B**) As in (A) but CHX chases for 0, 0.5, 1, and 2 hours with MNα2, in wild-type, *doa10*Δ, and *nat3*Δ cells. (**C**) Indicated amounts of the Nt-acetylated Ac-MNKIPIKDLLNC peptide versus its unacetylated counterpart were spotted onto membrane and assayed for their binding to anti-^{AcNt}MATα2. (**D**) X-peptide pulldown with peptides XNKIPIKDLLNC (X = Met, ^{Ac}Met, or Gly) (lanes 2 to 4) or XIFSTDTGPGGC (X = Gly, Met, Arg, or Phe) (lanes 5 to 8) and extract of *S. cerevisiae* that expressed Doa10$_{myc13}$. Lane 1, input extract (5%). (**E**) SPOT assay with purified, flag-tagged Doa10$_f$ and spot-arrayed synthetic peptides XZ-e$^{K(3\text{-}11)}$ (X = Gly, Ala, Val, Pro, Ser, Thr, or Cys; Z = Leu or Lys) and their Nt-acetylated X2-e$^{K(3\text{-}11)}$ counterparts. XZ residues are indicated at the top of the membrane. (**F**) Quantitation, using a PhosphorImager, of ^{35}S-pulse chases with MATα2$_f$ and its mutant derivatives (fig. S6, B and C). Solid circles, ^{MN}MATα2$_f$; open circles, ^{MK}MATα2$_f$; upright triangles, ^{GN}MATα2$_f$ (initially ^{MGN}MATα2$_f$) in *ubc4*Δ cells; inverted triangles, ^{MN}MATα2$_f$ in *ubc4*Δ *doa10*Δ cells.

MNα2) were used to immunoblot extracts of cells that expressed MNα2. Wild-type cells contained barely detectable steady-state levels of either total or Nt-acetylated MNα2 (Fig. 2A), owing to its rapid degradation. In contrast, *nat3*Δ cells, which lacked the cognate NatB Nt-acetylase, contained high levels of unacetylated MNα2 (detected by anti-Ha) and almost no Nt-acetylated MNα2 (Fig. 2A). Similar patterns were observed in wild-type cells that expressed MKα2 (Lys at position 2) or GNα2 (N-terminal Gly) (Fig. 2A). As shown by proteome-scale analyses, *S. cerevisiae* proteins containing Lys at position 2 are virtually never Nt-acetylated, and few proteins that bear N-terminal Gly are Nt-acetylated (*5*–*7*). Most importantly, high levels of Nt-acetylated MNα2 were present in *doa10*Δ cells (Fig. 2A), owing to metabolic stabilization of Nt-acetylated MNα2 in the absence of Doa10. These data (Fig. 2A) were in agreement with the LC-MS/MS results showing that MATα2 was Nt-acetylated (fig. S5A).

To determine whether the Doa10 Ub ligase recognizes the Nt-acetylated Met (^{AcNt}Met), we used the X-peptide assay (*15*) with synthetic peptides XNKIPIKDLLNC (X = Met, ^{Ac}Met, or Gly) (*39*). Except for C-terminal Cys and the varied N-terminal residues, these peptides were identical to the N-terminal region of MATα2. Immobilized peptides were incubated with extract from yeast that expressed myc_{13}-tagged Doa10, followed by elution of the bound proteins and immunoblotting with antibody to myc. $Doa10_{myc13}$ bound to the MATα2 peptide with N-terminal ^{AcNt}Met but not to the otherwise identical peptides with unmodified N-terminal Met or with N-terminal Gly (Fig. 2D). Additional controls, which did not bind to $Doa10_{myc13}$, were peptides XIFSTDTGPGGC (X = Gly, Met, Arg, or Phe) derived from the N terminus of nsP4, a Sindbis viral protein (*13*) (Fig. 2D). Thus, Doa10 recognizes the ^{AcNt}Met residue and does not have a significant affinity for downstream sequences of MATα2 or nsP4.

Doa10 specificity was also analyzed with the synthetic peptide arrays on membrane support (SPOT) technique, in which synthetic XZ-$e^{K(3-11)}$ peptides and their Nt-acetylated ^{Ac}XZ-$e^{K(3-11)}$ counterparts were C-terminally linked to a membrane as "dots" in equal molar amounts. SPOT peptides were identical to the N-terminal region of e^K (fig. S1D), with varied residues at positions 1 and 2. A SPOT assay with C-terminally flag-tagged $Doa10_f$ indicated the recognition of ^{AcNt}Met by Doa10, in agreement with the results of the X-peptide assay (Fig. 2, D and E). SPOT also indicated a highly preferential binding of $Doa10_f$ to other Nt-acetylated (versus unacetylated) ^{Ac}XZ-$e^{K(3-11)}$ peptides (X = Gly, Ala, Val, Pro, Ser, Thr, or Cys), including Nt-acetylated Gly and Pro (Fig. 2E). Thus, Gly and Pro are (largely) stabilizing in the N-end rule (Fig. 1D and fig. S3E) because N-terminal Gly and Pro are Nt-acetylated in relatively few proteins (*5*–*7*). Doa10 did not bind to N-terminal ^{AcNt}Met if it was followed by Lys at position 2 (Fig. 2E). Thus, the metabolic stability of XK-e^K-Ura3 (X = Met or Cys) containing Lys at position 2 (Fig. 1, A and C) stems not only from the absence of Nt-acetylation (*5*–*7*) but also from the rejection, by Doa10, of Lys at position 2 (Fig. 2E).

The Doa10-dependent ^{Ac}N-degron of MATα2. Taking advantage of the specificity of anti-^{AcNt}MATα2 for Nt-acetylated MNα2, we performed CHX chases as well, in addition to steady-state assays (Fig. 2, A and B). MNα2 was short-lived in wild-type cells. Even "time-zero" samples, at the time of addition of CHX, contained barely detectable levels of either Nt-acetylated or total MNα2 (Fig. 2B). In contrast, MNα2 was a long-lived protein in *doa10*Δ and *nat3*Δ cells, but for different reasons: In *doa10*Δ cells, which lacked the cognate Ub ligase, MNα2 was long-lived despite its Nt-acetylation; whereas in *nat3*Δ cells, which lacked the cognate Nt-acetylase, the largely unacetylated MNα2 was long-lived because the targeting by Doa10 required Nt-acetylation (Fig. 2B).

MATα2 contains yet another degradation signal, targeted by an unknown E3 in conjunction with the Ubc4 and (to a minor extent) Ubc5 E2s (*25*, *26*). This degron is nearly inactive in *ubc4*Δ cells (*23*, *26*). In contrast, the Doa10 Ub ligase functions with the Ubc6/Ubc7 E2s and remains active in *ubc4*Δ cells (*22*). In ^{35}S-pulse chases with C-terminally flag-tagged full-length $MAT\alpha2_f$, the rapid degradation of wild-type $^{MN}MAT\alpha2_f$ in *ubc4*Δ cells ($t_{1/2} \approx$ 9 min) was substantially decreased in *doa10*Δ *ubc4*Δ cells ($t_{1/2} \approx$ 35 min) (Fig. 2F and fig. S6, B and C). A Lys residue at position 2 in a polypeptide chain is known to preclude Nt-acetylation in *S. cerevisiae*, and few proteins that bear N-terminal Gly are Nt-acetylated (*5*, *6*). The absence of Nt-acetylation in $^{MK}MAT\alpha2_f$ (Lys at position 2) or $^{GN}MAT\alpha2_f$ (Gly at position 1) decreased the rate of MATα2 degradation in wild-type cells (Fig. 2F

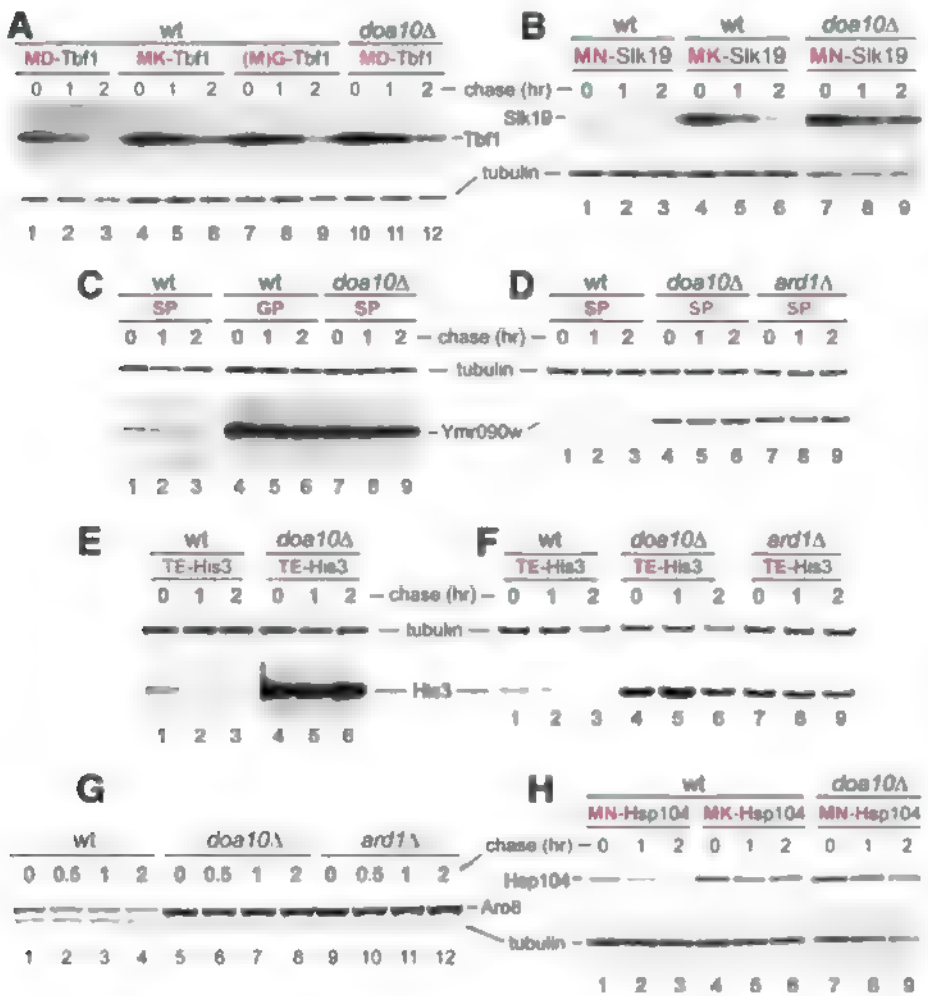

Fig. 3. ^{Ac}N-degrons in yeast proteins. (**A**) Lanes 1 to 3, CHX chase for 0, 1, and 2 hours in wild-type *S. cerevisiae* expressing $Tbf1_{ha}$. Lanes 4 to 6, 7 to 9, and 10 to 12, analogous patterns but in *doa10*Δ cells with $^{MK}Tbf1_{ha}$ (Lys at position 2), $^{G}Tbf1_{ha}$ (initially $^{MG}Tbf1_{ha}$), and wild-type $Tbf1_{ha}$, respectively. (**B**) As in (A) but with wild-type $Slk19_{ha}$ and its mutant derivatives in wild-type versus *doa10*Δ cells. (**C**) As in (A) but with wild-type $Ymr090w_{ha}$ and its mutant derivatives in wild-type versus *doa10*Δ cells. (**D**) As in (C) but with wild-type $Ymr090w_{ha}$ in wild-type versus *doa10*Δ and *ard1*Δ cells. (**E**) As in (A) but with wild-type $His3_{ha}$ in wild-type versus *doa10*Δ cells. (**F**) As in (E), with wild-type $His3_{ha}$ in wild type versus *doa10*Δ and *ard1*Δ cells. (**G**) As in (A) but CHX chases for 0, 0.5, 1, and 2 hours with wild-type $Aro8_{ha}$ in wild-type versus *doa10*Δ and *ard1*Δ cells. (**H**) As in (A) but with wild-type $Hsp104_{ha}$ and its mutant derivatives in wild-type versus *doa10*Δ cells.

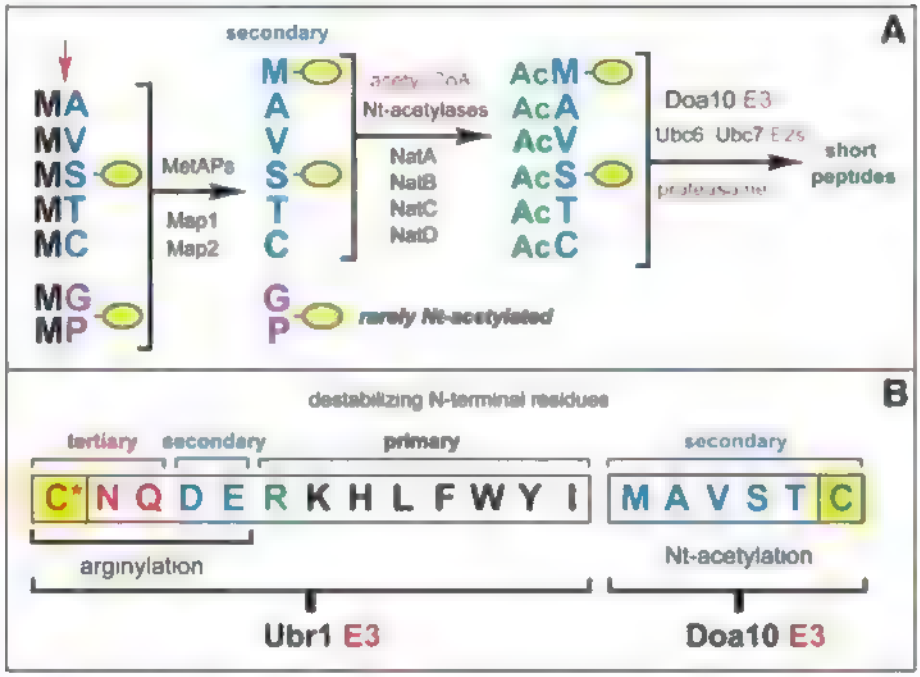

Fig. 4. N^{α}-terminal acetylases, Met-aminopeptidases, and the Doa10 branch of the N-end–rule pathway. (**A**) The Doa10-mediated branch of the *S. cerevisiae* N-end–rule pathway (see fig. S1C for the Ubr1-mediated branch of this pathway). The red arrow on the left indicates the MetAP-mediated removal of N-terminal Met. This Met is retained if a residue at position 2 is nonpermissive (too large) for MetAPs. If the retained N-terminal Met or N-terminal Ala, Val, Ser, Thr, and Cys are followed by acetylation-permissive residues, the above N-terminal residues are usually Nt-acetylated (*5*–*7*). The resulting N-degrons are termed ^{Ac}N-degrons. The term "secondary" refers to the necessity of modification (Nt acetylation) of a destabilizing N-terminal residue before a protein can be recognized by a cognate Ub ligase (fig. S1C). Proteins containing ^{Ac}N-degrons are targeted for ubiquitylation (and proteasome-mediated degradation) by the Doa10 E3 Ub ligase. Although Gly or Pro can be made N-terminal by MetAPs, and although Doa10 can recognize Nt-acetylated Gly and Pro (Fig. 2E), few proteins with N-terminal Gly or Pro are Nt-acetylated (*5*–*7*). (**B**) The Ubr1 and Doa10 branches of the N-end–rule pathway. Both branches target, through different mechanisms, the N-terminal Cys residue (yellow rectangles), with oxidized Cys marked by an asterisk.

and fig. S6, B and C). The extent of this decrease, in comparison to degradation of Nt-acetylated ^{MN}MATα2$_f$ in wild-type cells, was indistinguishable from the decrease of ^{MN}MATα2$_f$ degradation in *doa10*Δ cells, which lacked the Doa10 Ub ligase (Fig. 2F and fig. S6, B to E). In addition to indicating that the sole degron targeted by Doa10 in MATα2 is its ^{Ac}N-degron, these results were also in agreement with technically independent evidence that used the anti-^{AcNt}MATα2 to prove that the Nt-acetylation of MNα2 was required for its targeting by Doa10 (Fig. 2, A to C).

^{Ac}N-degrons in cellular proteins. As expected, given the presence of the ^{Ac}N-degron in MATα2, both full-length MATα2$_f$ and MNα2 were strongly stabilized in *nat3*Δ cells, which lacked the cognate NatB Nt-acetylase (Fig. 2, A and B, and fig. S6, D and E). Besides MATα2, our survey of *S. cerevisiae* proteins has encompassed, thus far, Tbf1, a regulator of telomeres; Slk19, a regulator of chromosome segregation; Ymr090w, a cytosolic protein of unknown function; His3, an enzyme of histidine biosynthesis; Pop2, a subunit of mRNA-deadenylating complexes; Hsp104, a chaperone; Tho1, an RNA-binding regulator; Ubp6, a deubiquitylating enzyme; and Aro8, an aromatic aminotransferase (Fig. 3, fig. S2, C and D, and fig. S7) (*30*).

Wild-type Tbf1, Slk19, Pop2, Hsp104, Tho1, Ubp6, and Aro8 are known to be Nt-acetylated (*5*, *6*). In contrast, the testing of His3 and Ymr090w stemmed from our two-dimensional electrophoretic analyses, including ^{35}S-pulse chases. The resulting patterns contained a number of protein spots with significantly higher levels of ^{35}S in samples from *doa10*Δ versus wild-type cells (fig. S8). We examined three of these spots using matrix-assisted laser desorption/ionization MS fingerprinting techniques and identified His3, Ymr090w, and Aro8 as putative substrates of Doa10 (fig. S8). The testing for ^{Ac}N-degrons in Tbf1, Slk19, Ymr090w, His3, Pop2, Hsp104, Tho1, Ubp6, and Aro8 (this analysis included second-residue mutants of some of these proteins) involved CHX chases in the presence or absence of a cognate Nt-acetylase or the Doa10 Ub ligase. As shown in Fig. 3; fig. S2, C and D; and fig. S7, we identified ^{Ac}N-degrons in all of these proteins (in addition to MATα2), except Pop2 and Tho1 [see also (*30*)].

Discussion. Our results, summarized in Fig. 4, revealed the function of Nt-acetylation, producing the largest increase in the scope of the N-end–rule pathway since its discovery more than two decades ago (*10*–*13*). At present, only ~10 proteins in all eukaryotes have been identified that require, or are inferred to require, Nt-acetylation for their in vivo roles, which are unrelated to protein degradation [(*30*) and references therein]. In contrast, the creation of degradation signals by Nt-acetylation (Fig. 4) is relevant, in principle, to all Nt-acetylated proteins. N-terminal Met, Ala, Val, Ser, Thr, and Cys are shown here to function as secondary destabilizing residues in the N-end–rule pathway, in that they must be Nt-acetylated before their recognition by the *S. cerevisiae* Doa10 Ub ligase as N-degrons, termed ^{Ac}N-degrons, that require Nt-acetylation (Fig. 4). Out of 20 amino acids in the genetic code, 18 are now known to function as destabilizing N-terminal residues in the N-end–rule pathway (Fig. 4 and fig. S1C). More than 50% of proteins in *S. cerevisiae* and more than 80% of proteins in human cells are Nt-acetylated (*5*–*7*). Thus, remarkably, the majority of eukaryotic proteins harbor a specific degradation signal from the moment of their birth. Putative metazoan counterparts of the yeast Doa10 Ub ligase (*22*–*24*) include human TEB4 (*31*), indicating the likely relevance of our results to all eukaryotes.

The Nt-acetylation is largely cotranslational, apparently irreversible, and involves a majority of cellular proteins. What functions are subserved by such a massive production of degradation signals (^{Ac}N-degrons) in nascent proteins if many of these proteins are destined for long half-lives? We suggest that a major role of these degradation signals involves quality-control mechanisms and the regulation of protein stoichiometries in a cell. A key feature of such mechanisms would be conditionality of ^{Ac}N-degrons. If a nascent Nt-acetylated protein can fold its N-terminal domain rapidly enough, or if this protein either interacts with a "protective" chaperone such as Hsp90 or becomes assembled into a cognate multisubunit complex, the cotranslationally created ^{Ac}N-degron of this protein may become inaccessible to the Doa10 Ub ligase. Consequently, the degradation of this protein would be decreased or precluded. In contrast, delayed or defective folding of a protein's N-terminal domain (because of oxidative, heat, or other stresses; or a conformation-perturbing mutation; or nonstoichiometric levels of cognate protein ligands) would keep an ^{Ac}N-degron exposed (active) and thereby increase the probability of the protein's destruction.

The discovery that Nt-acetylation is a part of the N-end–rule pathway (Fig. 4) has also revealed the physiological functions of Nt-acetylases and Met-aminopeptidases. Nt-acetylases produce ^{Ac}N-degrons, whereas the upstream Met-aminopeptidases make possible these degradation signals, all of them except the one mediated by Nt-acetylated Met (Fig. 4). Nt-acetylases and Met-aminopeptidases are universally present, extensively characterized, and essential enzymes whose physiological roles were largely unknown. These enzymes are now functionally understood components of the N-end–rule pathway (Fig. 4 and fig. S1C).

Although the bulk of Nt-acetylation is cotranslational (*4*), posttranslational Nt-acetylation is likely to be extensive as well. A number of proteases can specifically cleave a variety of

intracellular proteins, resulting in C-terminal fragments that often bear destabilizing N-terminal residues of the Ubr1-mediated branch of the N-end–rule pathway (fig. S1C). Such fragments are often short-lived in vivo, thereby regulating specific circuits [reviewed in (*13*)]. Given the major expansion of the N-end rule in the present work (Fig. 4), most in vivo–produced C-terminal fragments of intracellular proteins should now be viewed, a priori, as putative targets of the Doa10 or Ubr1 branches of the N-end–rule pathway.

The topologically unique location of N-terminal residues, their massive involvement in proteolysis, and their extensive modifications make N-degrons a particularly striking example of the scope and subtlety of regulated protein degradation (Fig. 4 and fig. S1C).

References and Notes

1. H. Jörnvall, *J. Theor. Biol.* **55**, 1 (1975).
2. J. R. Mullen *et al.*, *EMBO J.* **8**, 2067 (1989).
3. E. C. Park, J. W. Szostak, *EMBO J.* **11**, 2087 (1992).
4. M. Gautschi *et al.*, *Mol. Cell. Biol.* **23**, 7403 (2003).
5. B. Polevoda, F. Sherman, *J. Mol. Biol.* **325**, 595 (2003).
6. T. Arnesen *et al.*, *Proc. Natl. Acad. Sci. U.S.A.* **106**, 8157 (2009).
7. S. Goetze *et al.*, *PLoS Biol.* **7**, e1000236 (2009).
8. F. Frottin *et al.*, *Mol. Cell. Proteomics* **5**, 2336 (2006).
9. A. Mayer, N. R. Siegel, A. L. Schwartz, A. Ciechanover, *Science* **244**, 1480 (1989).
10. A. Bachmair, D. Finley, A. Varshavsky, *Science* **234**, 179 (1986).
11. A. Bachmair, A. Varshavsky, *Cell* **56**, 1019 (1989).
12. A. Varshavsky, *Proc. Natl. Acad. Sci. U.S.A.* **93**, 12142 (1996).
13. A. Varshavsky, *J. Biol. Chem.* **283**, 34469 (2008).
14. A. Mogk, R. Schmidt, B. Bukau, *Trends Cell Biol.* **17**, 165 (2007).
15. T. Tasaki, Y. T. Kwon, *Trends Biochem. Sci.* **32**, 520 (2007).
16. R.-G. Hu *et al.*, *Nature* **437**, 981 (2005).
17. R.-G. Hu, H. Wang, Z. Xia, A. Varshavsky, *Proc. Natl. Acad. Sci. U.S.A.* **105**, 76 (2008).
18. C.-S. Hwang, A. Varshavsky, *Proc. Natl. Acad. Sci. U.S.A.* **105**, 19188 (2008).
19. C.-S. Hwang, A. Shemorry, A. Varshavsky, *Proc. Natl. Acad. Sci. U.S.A.* **106**, 2142 (2009).
20. H. Wang, K. I. Piatkov, C. S. Brower, A. Varshavsky, *Mol. Cell* **34**, 686 (2009).
21. A. Varshavsky, *Methods Enzymol.* **399**, 777 (2005).
22. R. Swanson, M. Locher, M. Hochstrasser, *Genes Dev.* **15**, 2660 (2001).
23. M. Deng, M. Hochstrasser, *Nature* **443**, 827 (2006).
24. T. Ravid, S. G. Kreft, M. Hochstrasser, *EMBO J.* **25**, 533 (2006).
25. M. Hochstrasser, A. Varshavsky, *Cell* **61**, 697 (1990).
26. P. Chen, P. Johnson, T. Sommer, S. Jentsch, M. Hochstrasser, *Cell* **74**, 357 (1993).
27. A. D. Johnson, *Curr. Opin. Genet. Dev.* **5**, 552 (1995).
28. O. A. Zill, J. Rine, *Genes Dev.* **22**, 1704 (2008).
29. Single-letter abbreviations for the amino acid residues are as follows: A, Ala; C, Cys; D, Asp; E, Glu; F, Phe; G, Gly; H, His; I, Ile; K, Lys; L, Leu; M, Met; N, Asn; P, Pro; Q, Gln; R, Arg; S, Ser; T, Thr; V, Val; W, Trp; and Y, Tyr.
30. Materials and methods are available as supporting material on *Science* Online.
31. G. Hassink *et al.*, *Biochem. J.* **388**, 647 (2005).

32. We thank J. Zhou (Caltech) for MS analyses and C. Brower for comments on the paper. We are grateful to members of the Varshavsky laboratory for their advice in the course of this study and particularly thank O. Batygin for her technical assistance. This work was supported by grants from NIH and the March of Dimes Foundation to A.V.

Supporting Online Material

www.sciencemag.org/cgi/content/full/science.1183147/DC1
Materials and Methods
SOM Text
Figs. S1 to S9
Tables S1 to S3
References

9 October 2009; accepted 12 January 2010
Published online 28 January 2010;
10.1126/science.1183147
Include this information when citing this paper.

REPORTS

Kepler Planet-Detection Mission: Introduction and First Results

William J. Borucki,[1]* David Koch,[1] Gibor Basri,[2] Natalie Batalha,[3] Timothy Brown,[4] Douglas Caldwell,[5] John Caldwell,[17] Jørgen Christensen-Dalsgaard,[6] William D. Cochran,[7] Edna DeVore,[5] Edward W. Dunham,[8] Andrea K. Dupree,[10] Thomas N. Gautier III,[9] John C. Geary,[10] Ronald Gilliland,[11] Alan Gould,[18] Steve B. Howell,[15] Jon M. Jenkins,[5] Yoji Kondo,[29] David W. Latham,[10] Geoffrey W. Marcy,[2] Søren Meibom,[10] Hans Kjeldsen,[6] Jack J. Lissauer,[1] David G. Monet,[12] David Morrison,[1] Dimitar Sasselov,[10] Jill Tarter,[5] Alan Boss,[19] Don Brownlee,[21] Toby Owen,[20] Derek Buzasi,[22] David Charbonneau,[10] Laurance Doyle,[5] Jonathan Fortney,[24] Eric B. Ford,[13] Matthew J. Holman,[10] Sara Seager,[25] Jason H. Steffen,[26] William F. Welsh,[27] Jason Rowe,[1] Howard Anderson,[2] Lars Buchhave,[10] David Ciardi,[28] Lucianne Walkowicz,[2] William Sherry,[15] Elliott Horch,[23] Howard Isaacson,[2] Mark E. Everett,[14] Debra Fischer,[16] Guillermo Torres,[10] John Asher Johnson,[28] Michael Endl,[7] Phillip MacQueen,[7] Stephen T. Bryson,[1] Jessie Dotson,[1] Michael Haas,[1] Jeffrey Kolodziejczak,[30] Jeffrey Van Cleve,[5] Hema Chandrasekaran,[5] Joseph D. Twicken,[5] Elisa V. Quintana,[5] Bruce D. Clarke,[5] Christopher Allen,[31] Jie Li,[5] Haley Wu,[5] Peter Tenenbaum,[5] Ekaterina Verner,[32] Frederick Bruhweiler,[32] Jason Barnes,[33] Andrej Prsa[34]

The Kepler mission was designed to determine the frequency of Earth-sized planets in and near the habitable zone of Sun-like stars. The habitable zone is the region where planetary temperatures are suitable for water to exist on a planet's surface. During the first 6 weeks of observations, Kepler monitored 156,000 stars, and five new exoplanets with sizes between 0.37 and 1.6 Jupiter radii and orbital periods from 3.2 to 4.9 days were discovered. The density of the Neptune-sized Kepler-4b is similar to that of Neptune and GJ 436b, even though the irradiation level is 800,000 times higher. Kepler-7b is one of the lowest-density planets (~0.17 gram per cubic centimeter) yet detected. Kepler-5b, -6b, and -8b confirm the existence of planets with densities lower than those predicted for gas giant planets.

Since the first discoveries of planetary companions around pulsars (*1*, *2*) and normal stars (*3*), more than 400 such planets have been detected. Most of these are giant planets, often more massive than Jupiter. Many have a semimajor axis (mean star/planet separation) of less than 1 astronomical unit (AU, the distance between Earth and the Sun) and/or high eccentricity. These surprisingly small semimajor axes suggest that many planets form at

[1]NASA Ames Research Center, Moffett Field, CA 94035, USA. [2]University of California, Berkeley, CA 94720, USA. [3]San Jose State University, San Jose, CA 95192, USA. [4]Las Cumbres Observatory Global Telescope, Goleta, CA 93117, USA. [5]SETI Institute, Mountain View, CA 94043, USA. [6]Aarhus University, Aarhus, Denmark. [7]McDonald Observatory, University of Texas at Austin, Austin, TX 78712, USA. [8]Lowell Observatory, Flagstaff AZ 86001, USA. [9]Jet Propulsion Laboratory, California Institute of Technology, Pasadena, CA 91109, USA. [10]Harvard-Smithsonian Center for Astrophysics, Cambridge, MA 02138, USA. [11]Space Telescope Science Institute, Baltimore, MD 21218, USA. [12]United States Naval Observatory, Flagstaff, AZ 86001, USA. [13]University of Florida, Gainesville, FL 32611, USA. [14]Planetary Science Institute, Tucson, AZ 85719, USA. [15]National Optical Astronomy Observatory, Tucson, AZ 85719, USA. [16]Yale University, New Haven, CT 06520, USA. [17]York University, North York, M3J 1P3 Ontario, Canada. [18]Lawrence Hall of Science, Berkeley, CA 94720, USA. [19]Carnegie Institute of Washington, Washington, DC 20015 USA. [20]University of Hawaii, Hilo, HI 96720 USA. [21]University of Washington, Seattle, WA 98195, USA. [22]Eureka Scientific, Oakland, CA 94602, USA. [23]Southern Connecticut State University, New Haven, CT 06515, USA. [24]University of California, Santa Cruz, CA 95064, USA. [25]Massachusetts Institute of Technology, Cambridge, MA 02139, USA. [26]Fermilab, Batavia, IL 60510, USA. [27]San Diego State University, San Diego, CA 92182, USA. [28]Exoplanet Science Institute/Caltech, Pasadena, CA 91125, USA. [29]NASA Goddard Space Flight Center, Greenbelt, MD 20025, USA. [30]Marshall Space Flight Center, Huntsville, AL 35805, USA. [31]Orbital Sciences, Mountain View, CA 94043, USA. [32]Catholic University of America, Washington, DC 20064 USA. [33]University of Idaho, Moscow, ID 83844, USA. [34]Villanova University, Villanova, PA 19085, USA.

*To whom correspondence should be addressed. E-mail: William.J.Borucki@nasa.gov

several astronomical units from their stars before migrating to their current locations. The processes that terminate the inward migration and the fraction of planets that fall into their stars are not known. Although the inward migration of a giant planet is expected to remove inner, smaller planets by scattering them into the star or out of the planetary system, a second generation of planets might reaccrete in the wake of the migrating planet (*4*). Because it is difficult to predict or detect terrestrial planets, their frequency and distributions are unknown.

Kepler includes a differential photometer with a wide (115 square degrees) field of view (FOV) that continuously and simultaneously monitors the brightness of approximately 150,000 main-sequence stars. The photometer is based on a modified Schmidt telescope design that uses a corrector with a 0.95-m aperture and a 1.4-m diameter *f*/1 primary mirror. The aperture is sufficient to reduce the Poisson noise to the level that is required to obtain a 4σ detection for a single transit from an Earth-sized planet passing in front of a 12th-magnitude G2 dwarf (that is, a Sun-like star) with a 6.5-hour transit. The mission was launched on 6 March 2009 into an Earth-trailing orbit. Its design, characteristics, selection of target stars, on-orbit performance, data processing pipeline, data characteristics, and mission operations can be found in the supporting online material (SOM) text, section 1, and (*5*–*11*).

Here we describe the detection of five new exoplanets of varying size and orbital period based on the first two data segments taken at the start of the mission, and we provide some comparisons with previous detections. The first segment is a 9.7-day period (Q0) starting on 2 May 2009 universal time (UT) during the commissioning phase. The second is a 33.5-day period (Q1) taken at the beginning of science operations on 13 May 2009 UT. For Q0, oversized apertures were used to image each star, because the point-spread function and geometry of the focal plane were not yet known precisely. During this period, nearly all stars brighter than $V = 13.6$ magnitude in the FOV were observed (52,496 in total). Analysis of these data sets also led to a series of astrophysical discoveries, including oscillations of giant stars and two examples of planet-sized objects that are hotter than the stars they orbit (*12*–*21*).

The Q1 observations used smaller apertures, which allowed 156,097 objects to be observed. Targets were chosen to maximize the number of stars that were both bright and small enough to show detectable transit signals for small planets in and near the habitable zone (HZ) [SOM text 2 (*11*)].

Planets orbiting close to hot stars can reach temperatures in excess of 2000 K and can emit enough light for Kepler to detect their thermal radiation in the range of visible wavelengths. Kepler's first observations detected thermal emission from exoplanet HAT-P-7b (*22*, *23*). The phase curve of the emission provided information about the planetary albedo, the depth of absorption in the planet's atmosphere, and the lack of redistribution of the energy to the night side of the planet. Analysis of the first data set led to the discovery of ellipsoidal variations in the host star (*24*).

Several planetary candidates that passed the tests to remove false-positive events (SOM text 3) were observed with radial velocity (RV) spectrometers to determine their masses. (See SOM text 4 for the approach used to determine the characteristics of the planets from the observations.) Modeling was performed to establish the system characteristics and uncertainties (*25*). Each target has a Kepler identification number (KIC no.) from the Kepler Input Catalog (KIC), but each confirmed exoplanet is also assigned a convenient abbreviation (Kepler-number-letter) (Tables 1 and 2). The numbering begins with 4b, because the designations 1b, 2b, and 3b are used to refer to previously known exoplanets in the Kepler FOV: TrES-2 (*26*), HAT-P-7b (*22*), and HAT-P-11b (*27*), respectively.

Table 1. Properties of the exoplanets detected by Kepler. The state of the current observations is insufficient to support claims of nonzero eccentricity. Therefore, parameter estimates are based on the assumption of a circular orbit. Calculations of the equilibrium temperatures assume a Bond albedo = 0.1 and efficient transport of heat to the night side. Epoch = HJD-2454900.0. R_J is the Jupiter equatorial radius. M_J is the mass of Jupiter. Errors are ± 1σ and represent formal errors only.

Identification	KIC no.	Period (days)	Epoch	Radius (R_J)	Mass (M_J)	Density (g/cm^3)	Equilibrium temperature (K)	Semimajor axis (AU)	Inclination (degrees)	Reference
Kepler-4b	11853905	3.21346 ± 0.00022	56.6127 ± 0.0015	0.357 ± 0.021	0.077 ± 0.012	1.91 ± 0.41	1650 ± 200	0.04558 ± 0.00087	89.76 ± 1.17	(*25*)
Kepler-5b	8191672	3.548460 ± 0.000032	55.90122 ± 0.00021	1.431 ± 0.048	2.114 ± 0.064	0.894 ± 0.079	1868 ± 284	0.05064 ± 0.00070	86.3 ± 0.6	(*30*)
Kepler-6b	10874614	3.234723 ± 0.000017	54.48636 ± 0.00014	1.323 ± 0.026	0.669 ± 0.027	0.352 ± 0.019	1500 ± 200	0.04567 ± 0.00050	86.8 ± 0.3	(*29*)
Kepler-7b	5780885	4.885525 ± 0.000039	67.27567 ± 0.00014	1.478 ± 0.051	0.433 ± 0.040	0.166 ± 0.019	1540 ± 200	0.06224 ± 0.00127	86.5 ± 0.4	(*28*)
Kepler-8b	6922244	3.52254 ± 0.00004	54.1182 ± 0.0003	1.419 ± 0.055	0.603 ± 0.154	0.261 ± 0.071	1764 ± 200	0.0483 ± 0.0008	84.07 ± 0.33	(*31*)

Table 2. Characteristics of the stars hosting Kepler planets. *Kp* is the stellar magnitude calculated for the Kepler band pass. The values are similar to those produced by an R filter (*7*) for most star types. Right ascension (RA) and declination (dec) refer to the J2000.0 equinox. For three of the stars (Kepler-4, -5, and -7), the model fits give two peaks in the distributions of the mass and radius. The values listed here are thought to be the best estimate (*25*, *28*–*31*). log(*g*) values are calculated from model fit based on stellar density and temperature. T_{eff}, effective temperature. M^* and R^* are the mass and radius of the host stars, respectively. M_{Sun} and R_{Sun} are the mass and radius of the Sun, respectively.

Identification	M^* (M_{Sun})	R^* (R_{Sun})	log(*g*) (cgs)	[Fe/H]	T_{eff} (K)	*Kp* (mag)	RA, dec (hour, degree)
Kepler-4	1.223 + 0.068	1.487 + 0.084	4.165 + 0.037	+0.17 + 0.06	5857 + 60	12.21	19.04102, 50.13575
Kepler-5	1.374 ± 0.056	1.793 ± 0.053	4.067 ± 0.020	+0.04 ± 0.06	6297 ± 60	13.4	19.96047, 44.03505
Kepler-6	1.209 ± 0.040	1.391 + 0.024	4.236 + 0.011	+0.34 ± 0.06	5647 + 44	13.3	19.78915, 48.23994
Kepler-7	1.347 ± 0.080	1.843 ± 0.057	4.030 ± 0.018	+0.11 ± 0.03	5933 ± 44	12.9	19.23877, 41.08981
Kepler-8	1.213 ± 0.063	1.486 ± 0.056	4.174 ± 0.026	-0.055 ± 0.033	6213 ± 75	13.6	18.75254, 42.45108

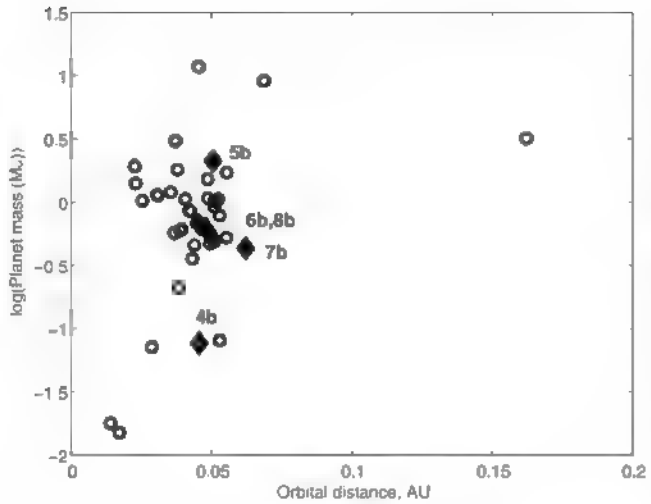

Fig. 1. Comparison of mass versus semimajor axes for Kepler planets. Circles represent transiting planets listed in the Extrasolar Planets Encyclopedia (*37*).

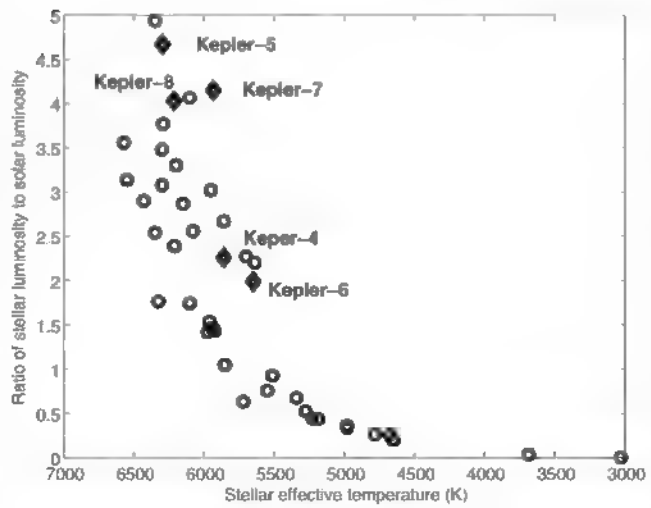

Fig. 2. Comparison of stars associated with the Kepler exoplanets with those associated with the planets in the Extrasolar Planet Encyclopedia. The parameter plotted on the vertical axis is the ratio of the area of the star multiplied by its effective temperature to the fourth power divided by solar values.

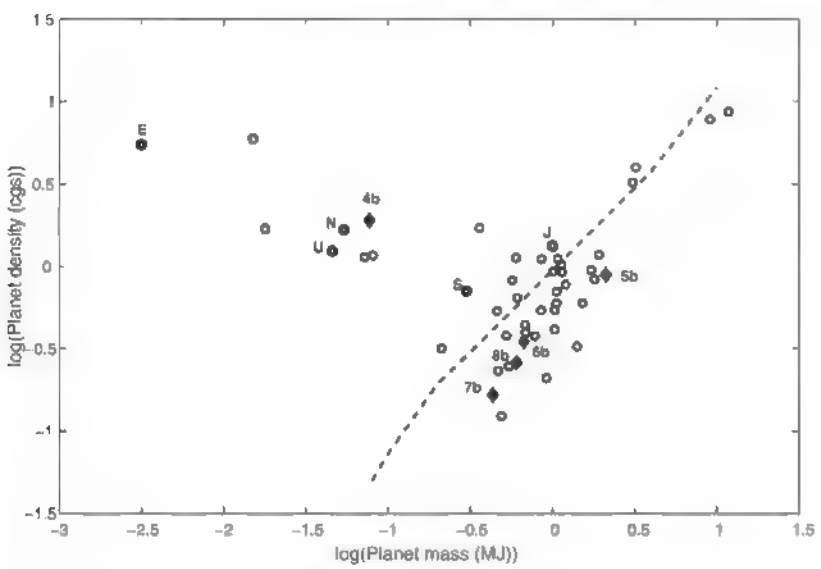

Fig. 3. Planet density versus mass. Kepler planets are shown as diamonds. Letter symbols represent solar system planets. Placement of the Kepler exoplanets on mass-radius diagrams can be found in (*25*, *28*). Circles represent transiting planets listed in the Extrasolar Planet Encyclopedia. The data to the right show planet density increasing with mass. The dashed line is the prediction for planets composed only of H and He and receiving irradiation associated with a Sun-like star at a distance of 0.045 AU (*34*). Rocky planets similar to Earth without atmospheres that contribute substantially to the mass of the planet are at the left. In between are ice giants, which are mixtures of H/He and rocky material (*36*).

Light curves and RV curves can be found in SOM text 5 and (*25*, *28*–*31*). The results presented in the Tables 1 and 2 are based on time series of photometry and radial velocity data that can be retrieved from the Space Telescope Science Institute's Multimission Archive at STScI high-level science products (MAST/HLSP) data archive (*32*).

Kepler-4b is an exoplanet that is very similar in size, density, and mass to Neptune (the most probable estimates are 1.03 times the size, 1.09 times the density, and 1.43 times the mass) and is similar in mass and radius to GJ 436b (*33*). A major difference between Kepler-4b and Neptune is that the irradiance level for Kepler-4b is over 800,000 times larger than that of Neptune. However, the large difference in irradiance levels appears to make little difference to the sizes of the planets. The result implies a difference in bulk composition (*34*), with either a higher rock-to-water ratio or less H/He in Kepler-4b as compared with Neptune (and GJ 436b). The latter degeneracy cannot be resolved at this time.

The Kepler results did not find planets with very small values of semimajor axes (Fig. 1), even though such planets would have a larger probability of alignment than those with larger values. The stars associated with the Kepler exoplanets are generally larger than those shown in the Exoplanet Encyclopedia for transiting planets (Fig. 2). The difference could be due to the Malmquist bias or to the preferential selection of stars with sharp spectral lines for the Kepler follow-up, that is, slightly evolved stars.

The data add to the evidence for three planet populations (Fig. 3) and the separation between ice giants and gas giants. The scatter in the data might be explained by differing fractions of heavy elements and H/He envelopes (*35*, *36*). However, it is surprising that Kepler exoplanets 5b, 6b, 7b, and 8b, as well as many other transiting planets shown in Fig. 3, also lie below the curve for a pure H/He planet (*34*). The radii of Uranus, Neptune, GJ 436b, HAT-P-11b, and Kepler-4b have been shown to lie below the predicted irradiated and nonirradiated radius-mass curves (*25*, *35*).

References and Notes

1. A. Wolszczan, D. A. Frail, *Nature* **355**, 145 (1992).
2. A. Wolszczan, *Science* **264**, 538 (1994).
3. M. Mayor, D. Queloz, *Nature* **378**, 355 (1995).
4. S. N. Raymond, A. M. Mandell, S. Sigurdsson, *Science* **313**, 1413 (2006).
5. D. Koch *et al.*, *Astrophys. J.*, preprint available at http://xxx.lanl.gov/abs/1001.0268
6. W. J. Borucki *et al.*, *Proc. IAU Symp.* **253**, 289 (2008).
7. R. L. Gilliland *et al.*, *Astrophys. J.*, preprint available at http://xxx.lanl.gov/abs/1001.0142
8. D. A. Caldwell *et al.*, *Astrophys. J.*, preprint available at http://xxx.lanl.gov/abs/1001.0216
9. J. M. Jenkins *et al.*, *Astrophys. J.*, preprint available at http://xxx.lanl.gov/abs/1001.0256
10. M. R. Haas *et al.*, *Astrophys. J.*, preprint available at http://xxx.lanl.gov/abs/1001.0437
11. N. M. Batalha *et al.*, *Astrophys. J.*, preprint available at http://xxx.lanl.gov/abs/1001.0349

12. R. L. Gilliland *et al.*, *Publ. Astron. Soc. Pacific*, preprint available at http://xxx.lanl.gov/abs/1001.0139
13. J. Christensen-Dalsgaard *et al.*, *Astrophys. J.*, preprint available at http://xxx.lanl.gov/abs/1001.0032
14. W. J. Chaplin *et al.*, *Astrophys. J.*, preprint available at http://xxx.lan .gov/abs/1001 0506
15. G. Basri *et al.*, *Astrophys. J.*, preprint available at http://xxx.lanl.gov/abs/1001 0414.
16. D. Stello *et al.*, *Astrophys. J.*, preprint available at http://xxx.lanl.gov/abs/1001.0026
17. T. R. Bedding *et al.*, *Astrophys. J.*, preprint available at http://xxx.lan..gov/abs/1001 0229
18. S. Hekker *et al.*, *Astrophys. J.*, preprint available at http://xxx.lanl.gov/abs/1001 0399
19. K. Kolenberg *et al.*, *Astrophys. J.*, preprint available at http://xxx.lan..gov/abs/1001 0417
20. A. Gingachcene *et al.*, *Astrophys. J.*, preprint available at http://xxx.lan..gov./1001 0747.
21. J. F. Rowe *et al.*, *Astrophys. J.*, preprint available at http://xxx.lan..gov/abs/1001 3420
22. A. Pál *et al.*, *Astrophys. J.* **680**, 1450 (2008)
23. W. J. Borucki *et al.*, *Science* **325**, 709 (2009)
24. W. F. Welsh *et al.*, *Astrophys. J.*, preprint available at http://xxx.lanl.gov/abs/1001 0413
25. W. J. Borucki *et al.*, *Astrophys. J.*, preprint available at http://xxx.lanl.gov/abs/1001 0604v1
26. F. T. O'Donovan *et al.*, *Astrophys. J.* **651**, L61 (2006)
27. G. A. Bakos *et al.*, *Astrophys. J.*, preprint available at http://xxx.lanl.gov/abs/0901 0282
28. D. W. Latham *et al.*, *Astrophys. J.*, preprint available at http://xxx.lanl.gov/abs/1001 0190
29. E. W. Dunham *et al.*, *Astrophys. J.*, preprint available at http://xxx.lanl.gov/abs/1001 0333
30. D. G. Koch *et al.*, *Astrophys. J.*, preprint available at http://xxx.lanl.gov./abs/1001 0913
31. J. M. Jenkins *et al.*, *Astrophys. J.*, preprint available at http://xxx.lanl.gov/abs/1001 0416
32. The MAST/HLSP data archive is available at http://archive.stsci.edu/prepds/kepler_hlsp
33. M. Gillon *et al.*, *Astron. Astrophys.* **472**, L13 (2007)
34. J. J. Fortney, in *ASP Conference Series 398: Extreme Solar Systems*, D. Fischer *et al.*, Eds. (Astronomical Society of the Pacific, San Francisco, 2008) pp. 405–418
35. I. Baraffe, G. Chabrier, T. Barman, *Astron. Astrophys.* **482**, 315 (2008)
36. E. R. Adams, S. Seager, L. Elkins-Tanton, *Astrophys. J.* **673**, 1160 (2008)
37. The Extrasolar Planets Encyclopedia is available at http://exoplanet.eu
38. Kepler was competitively selected as the 10th Discovery mission. Funding for this mission is provided by NASA's Science Mission Directorate.

Supporting Online Material

www.sciencemag.org/cgi/content/full/science.1185402/DC1
SOM Text
Fig. S1
References

1 December 2009; accepted 28 December 2009
Published online 5 January 2010;
10.1126/science.1185402
Include this information when citing this paper

Tuning the Dimensionality of the Heavy Fermion Compound $CeIn_3$

H. Shishido,[1,2] T. Shibauchi,[1] K. Yasu,[1] T. Kato,[1] H. Kontani,[3] T. Terashima,[2] Y. Matsuda[1]*

Condensed-matter systems that are both low-dimensional and strongly interacting often exhibit unusual electronic properties. Strongly correlated electrons with greatly enhanced effective mass are present in heavy fermion compounds, whose electronic structure is essentially three-dimensional. We realized experimentally a two-dimensional heavy fermion system, adjusting the dimensionality in a controllable fashion. Artificial superlattices of the antiferromagnetic heavy fermion compound $CeIn_3$ and the conventional metal $LaIn_3$ were grown epitaxially. By reducing the thickness of the $CeIn_3$ layers, the magnetic order was suppressed and the effective electron mass was further enhanced. Heavy fermions confined to two dimensions display striking deviations from the standard Fermi liquid low-temperature electronic properties, and these are associated with the dimensional tuning of quantum criticality.

Heavy fermion materials are metallic compounds with extremely large effective electron masses, and they typically contain a rare-earth element. In these materials, the electrons populating the 4f orbitals are, at high temperatures, essentially localized with well-defined magnetic moments. As the temperature is lowered, the localized moments are screened by conduction electrons (s, p, and d orbitals), forming a nonmagnetic state by virtue of the Kondo effect (*1*). At yet lower temperatures, the f-orbital electrons dressed by conduction electron clouds (Kondo clouds) become itinerant, forming a very narrow conduction band that is characterized by a heavy effective quasiparticle mass. On the other hand, the Ruderman-Kittel-Kasuya-Yosida (RKKY) interaction, which is an intersite exchange interaction between the localized f-orbital moments, promotes magnetic ordering. Thus, the ground state of these compounds is either a nonmagnetic metal or a magnetically ordered state, as determined by the competition of the above two effects. Generally, in reduced spatial dimensions, many-body correlation effects due to the Coulomb interaction between electrons become more relevant. Moreover, thermal and quantum fluctuations are significantly enhanced, extending critical regimes with no long-range ordering to a wide temperature range. Therefore, many-body effects that are not observed in three dimensions are expected to arise in two-dimensional (2D) heavy fermion systems.

Quantum criticality is a central research issue in the physics of highly correlated matter (*2*, *3*). In conventional metals, interacting electrons (quasiparticles) are well described by Landau's Fermi liquid theory. Near the quantum critical point (QCP), where a second-order phase transition occurs at zero temperature, low-lying spin fluctuations give rise to a serious modification of the quasiparticle mass and the scattering cross section of the Fermi liquid. This results in a strong deviation of physical properties from the standard Fermi liquid behavior. In heavy fermion metals, quantum criticality can be tuned by external parameters, such as doping, pressure, and magnetic fields (*2*). Fabricating superlattice heterostructure provides another way to control the quantum criticality through "dimensional tuning"; however, the epitaxial growth of heavy fermion thin films has been challenging (*4*–*6*).

There have been attempts to realize heavy fermion systems with low dimensions. One is the bulk crystals of $CeTIn_5$ (where T = Rh, Co, or Ir), whose crystal structure yields alternating layers of $CeIn_3$ and TIn_2 (*7*, *8*). However, the largely corrugated Fermi surface (*9*), the small anisotropy of upper critical fields (*10*), and the strong deviations from 2D antiferromagnetic spin fluctuations (*11*) all indicate that the electronic and magnetic properties of $CeTIn_5$ are anisotropic 3D rather than 2D. Another example is the bilayer 2D films of ^{3}He fluid (*12*), where the mass enhancement is observed near a QCP. Here the controlled parameter is the ^{3}He density of the second layer. However, the dimensional tuning from 3D to 2D heavy fermions is still lacking.

The heavy fermion compound $CeIn_3$ appears to be a good candidate for addressing the key issues of QCP physics. Bulk cubic $CeIn_3$ exhibits a 3D antiferromagnetic ordering at Neel temperature T_N = 10 K (*13*, *14*) that is destroyed in a quantum phase transition accessed by applying pressure. Near the critical pressure of $p_c \sim 24$ kbar, in the vicinity of the QCP, $CeIn_3$ undergoes a transition into an unconventional superconducting state, and a remarkable deviation from the Fermi liquid behavior is reported (*14*–*16*). To adjust the dimensionality in a controllable way, we used molecular beam epitaxy to grow the $CeIn_3/LaIn_3$ superlattices (Fig. 1A): m layers of $CeIn_3$ and n layers of isomorphic $LaIn_3$ were grown alternately, forming an (m:n) heterostruc-

[1]Department of Physics, Kyoto University, Kyoto 606-8502, Japan. [2]Research Center for Low Temperature and Materials Sciences, Kyoto University, Kyoto 606-8501, Japan. [3]Department of Physics, Nagoya University, Nagoya 464-8602, Japan

*To whom correspondence should be addressed. E-mail: matsuda@scphys.kyoto-u.ac.jp

ture, where m and n are integers. The clearly observed streak pattern of the reflection high-energy electron diffraction (RHEED) (Fig. 1B) indicates the epitaxial growth of each layer with atomic-scale flatness. The cross-sectional transmission electron microscope (TEM) image (Fig. 1C, lower panel), which shows bright spots corresponding to Ce atoms, demonstrates that the $CeIn_3$ layers are continuous even for the m =

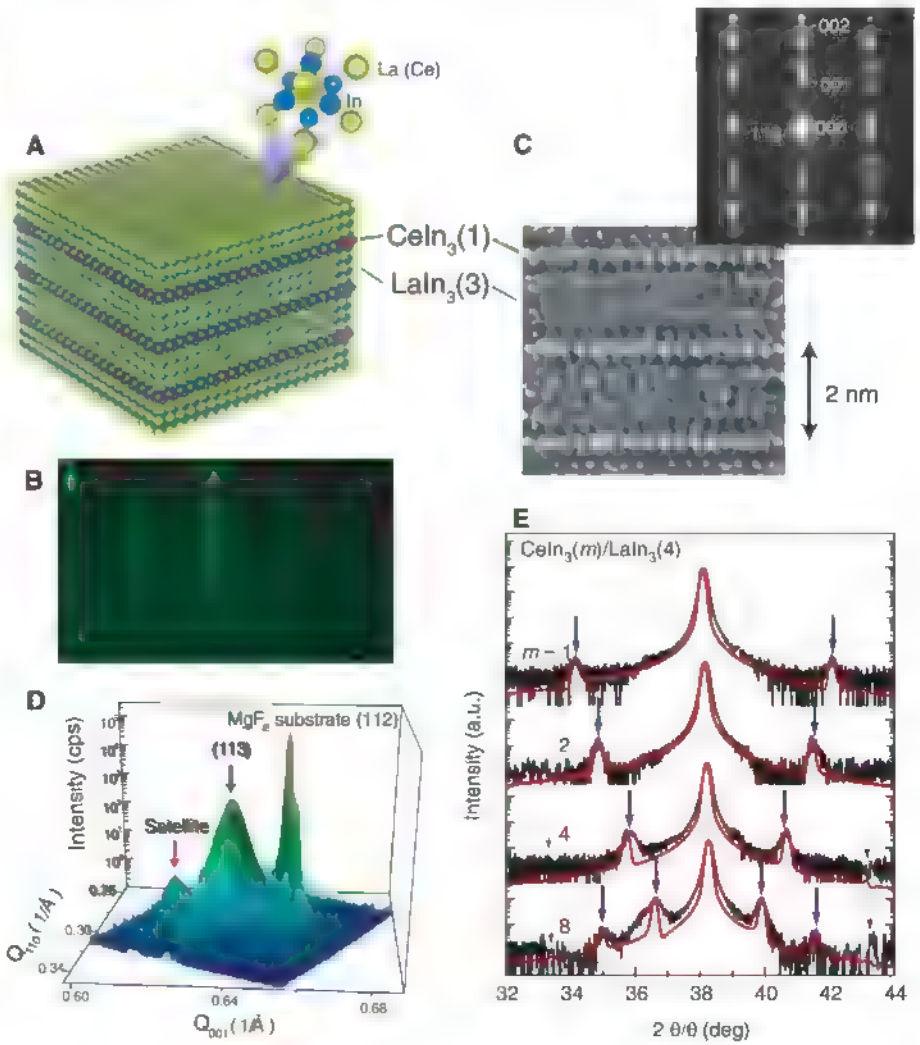

Fig. 1. Superlattice heterostructure of $CeIn_3$ and $LaIn_3$. (**A**) Illustration of the artificial superlattice (m:n) composed of m unit cell–thick layers of $CeIn_3$ and n unit cell–thick layers of $LaIn_3$. (**B**) Streak patterns of the RHEED image during the crystal growth. (**C**) Cross-sectional TEM image of the (1:3) superlattice. The Ce atoms can be identified as brighter spots than the La and In atoms (lower left). The diffraction pattern of the electron beam incident along the [110] direction is shown (upper right). (**D**) X-ray reciprocal lattice mapping for the (8:4) superlattice. A satellite peak is observed around the fundamental (113) peak along the Q_{001} direction. (**E**) Diffraction patterns using a monochromatized Cu $K_{\alpha 1}$ x-ray (black line) around the (002) main peaks of (m:4) superlattices for m = 1, 2, 4, and 8, with typical superlattice thickness of 200 nm. The step-model simulations (red line), which neglect interface and layer-thickness fluctuations (*25*), reproduce both the intensities and the positions of the satellite peaks (solid arrows). Some higher-order peaks are below the experimental resolutions (dotted arrows). Each curve is shifted vertically for clarity

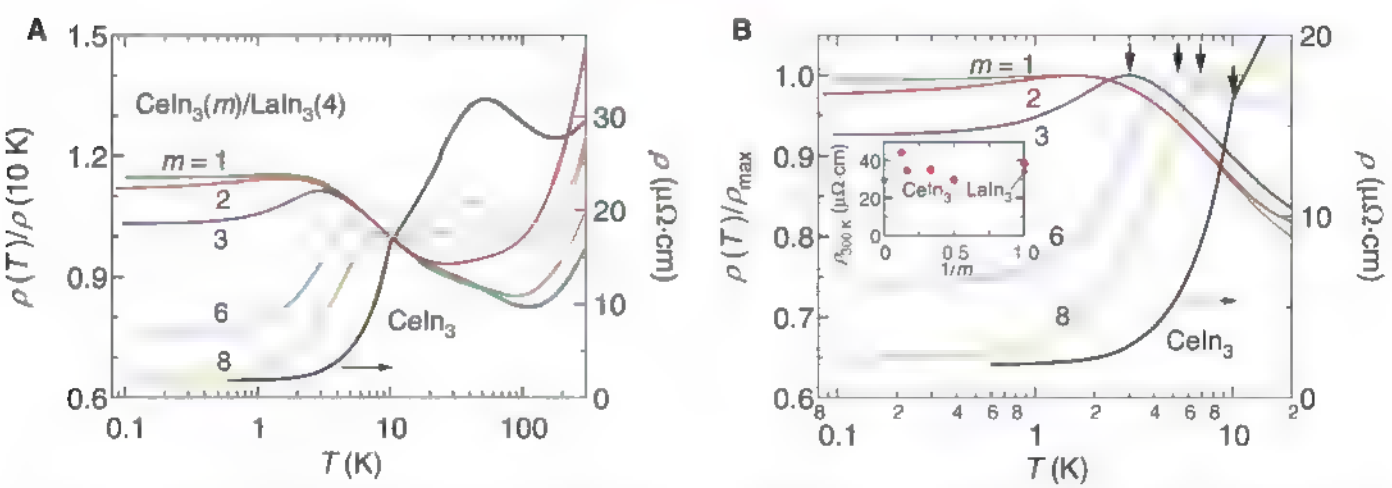

Fig. 2. Temperature dependence of the resistivity in (m:4) superlattices for m = 1 (green), 2 (red), 3 (dark blue), 6 (light blue), and 8 (yellow). Each data set is normalized by its value at 10 K (**A**) and the maximum value ρ_{max} (arrows) at low temperatures (**B**) to compensate for the slight differences in resistivity at room temperature between the films [inset in (B)]. The data for the 200-nm-thick $CeIn_3$ (blue square) and $LaIn_3$ thin films (black square) are also shown. The $\rho(T)$ of the $CeIn_3$ film coincides well with that of bulk single crystals.

l structures (*17*) The electron diffraction pattern with clear superspots (Fig 1C, upper panel), the x-ray diffraction pattern (Fig 1D), and the simulation results (Fig. 1E) all demonstrate the realization of an epitaxial superlattice structure These indicate the successful confinement of f-orbital electrons to the 2D spaces.

We investigated the transport properties of the (m 4) superlattices by varying m Because the RKKY interaction decays as 1 r^3, where r is the distance between the interacting magnetic

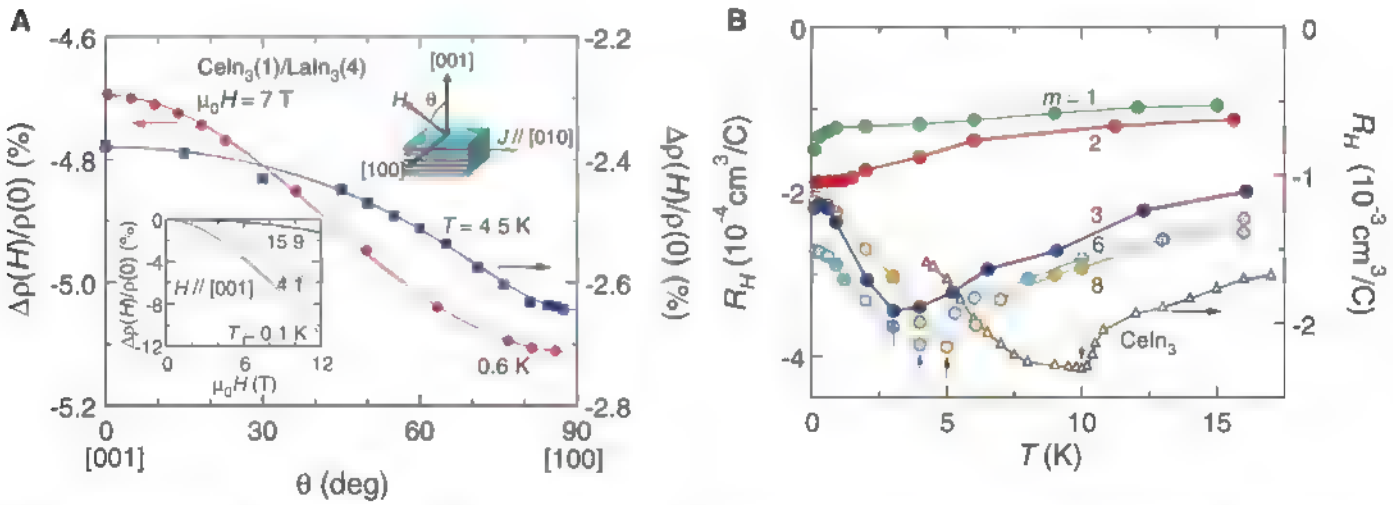

Fig. 3. Magnetotransport of the superlattices. (**A**) Transverse magnetoresistance $\Delta\rho(H)/\rho(H=0)$ of the (1:4) superlattice in magnetic field H rotated within the ac plane at 0.6 K (red) and 4.5 K (blue). The current is applied along the b axis. Here the c axis is perpendicular to the layers. θ is the angle between H and the c axis. The inset shows $\Delta\rho(H)/\rho(0)$ for $H//c$ at several temperatures (**B**) Temperature dependence of the Hall coefficient R_H for the superlattices and for $CeIn_3$. $R_H(T)$ shows a cusplike minimum (arrows) for m = 8, 6, and 3 as well as for $CeIn_3$.

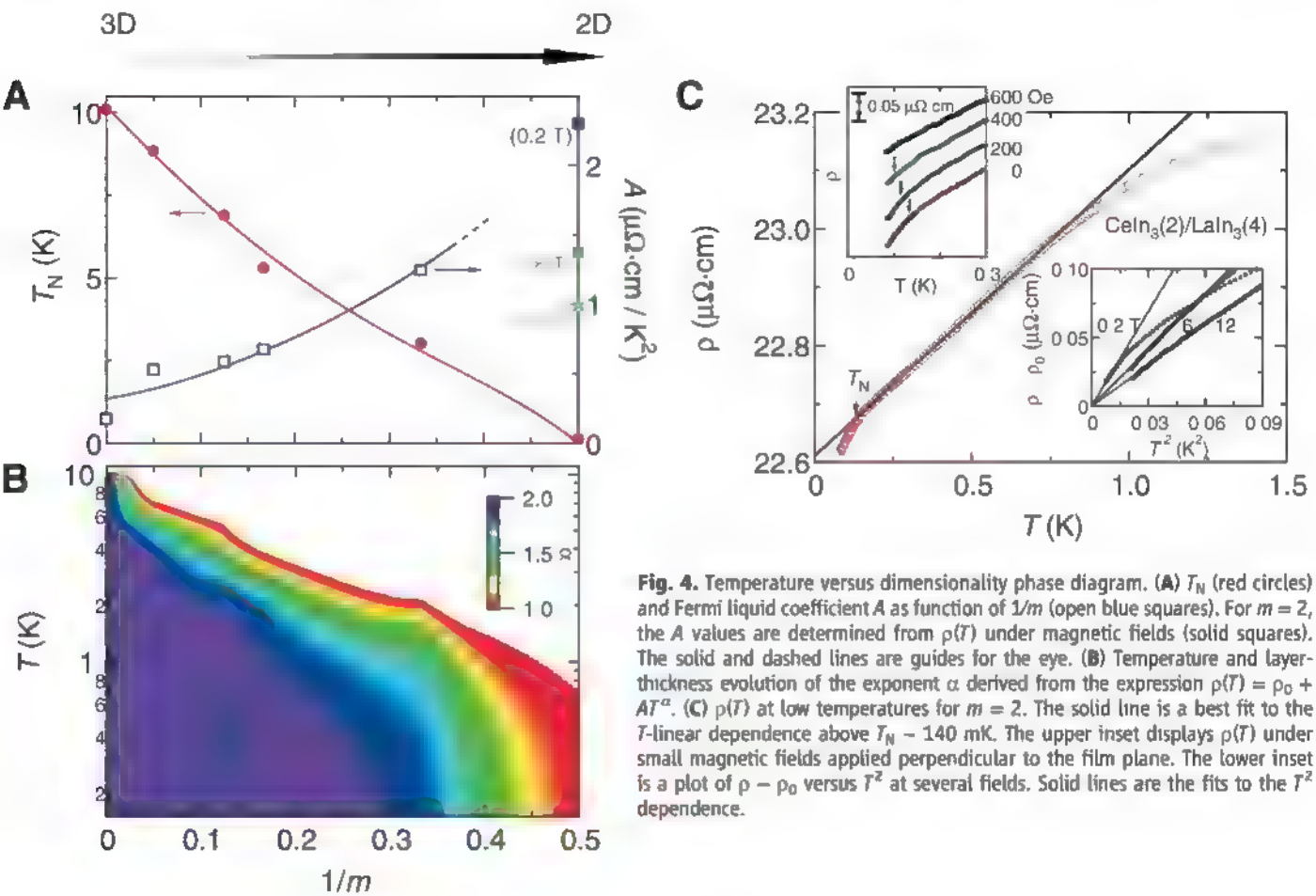

Fig. 4. Temperature versus dimensionality phase diagram. (**A**) T_N (red circles) and Fermi liquid coefficient A as function of $1/m$ (open blue squares). For m = 2, the A values are determined from $\rho(T)$ under magnetic fields (solid squares). The solid and dashed lines are guides for the eye. (**B**) Temperature and layer-thickness evolution of the exponent α derived from the expression $\rho(T) = \rho_0 + AT^{\alpha}$. (**C**) $\rho(T)$ at low temperatures for m = 2. The solid line is a best fit to the T-linear dependence above T_N ~ 140 mK. The upper inset displays $\rho(T)$ under small magnetic fields applied perpendicular to the film plane. The lower inset is a plot of $\rho - \rho_0$ versus T^2 at several fields. Solid lines are the fits to the T^2 dependence.

moments, the magnetic interaction between the Ce ions in different layers reduces to less than 1% of that between the neighboring Ce ions within the same layer. Therefore, the interlayer magnetic interactions are negligible. Resistivity ρ of the superlattices at room temperature is of the same order as for $CeIn_3$ (Fig. 2B, inset). $CeIn_3$ exhibits a $\rho(T)$ behavior that is typical of heavy fermion compounds. Below ~200 K, $\rho(T)$ increases because of the Kondo scattering and shows a maximum $\rho(T)$ at $T_{peak} \sim 50$ K. At $T_N = 10$ K, $\rho(T)$ shows a distinct cusp, below which it decreases rapidly as the magnetic scattering is suppressed. In the superlattices, the hump structure of $\rho(T)$ at $T_{peak} \sim 50$ K becomes less pronounced with decreasing m (Fig. 2A). Below T_{peak}, $\rho(T)$ increases again with decreasing temperature. Such behavior is caused by the interplay of the Kondo interaction with the crystal field effect (*18*), whose energy scale is 123 K in $CeIn_3$ (*19*). At lower temperatures, $\rho(T)$ shows a pronounced peak structure, as indicated by arrows for $m = 8$, 6, and 3 (Fig. 2B). For $m = 2$ and 1, $\rho(T)$ decreases gradually without exhibiting a pronounced peak below a characteristic temperature $T_{coh} \sim 1.6$ K, which marks the onset of coherent electron conduction.

The residual resistivity ρ_0 of the superlattices is larger than that of $CeIn_3$ (Fig. 2A). This is probably due to the inevitable scattering at the interfaces between the $CeIn_3$ and $LaIn_3$ layers, where Kondo holes that were created by possible Ce/La disorder act as strong impurity-scattering centers. Residual resistivity in the 2D planes can be enhanced with small impurity concentration by quantum fluctuations via enlarged effective cross section of local impurity scattering (*20*, *21*).

The observed distinct anisotropy in the magnetoresistance (Fig. 3A) indicates the substantial contribution from the 2D electrons confined within the layers, which is in sharp contrast to the 3D isotropic Ce(La)In_3. The negative magnetoresistance (Fig. 3A, inset) is consistent with the view that antiferromagnetic fluctuations that are responsible for the scattering can be suppressed by the magnetic field. The Hall coefficient $R_H(T)$ exhibits a cusp-like minimum in bulk $CeIn_3$ and superlattices for $m = 8$, 6, and 3 (Fig. 3B). These cusp temperatures coincide with the temperatures at which $\rho(T)$ exhibit cusps (Fig. 2B, arrows). Therefore, we surmise that the observed transport anomalies for $m = 8$, 6, and 3 appear as a result of magnetic ordering, as in $CeIn_3$. The low-temperature behavior of the transport properties for $m = 2$ and 1 are essentially different from those for $m > 2$. For $m \leq 2$, $\rho(T)$ does not exhibit a pronounced peak, and $R_H(T)$ decreases monotonically with decreasing temperature without showing the upturn. These results indicate that the magnetic order is suppressed when the $CeIn_3$ layer thickness decreases, and is vanishing near $m = 2$. This conclusion is reinforced by the results shown in Fig. 4A, where T_N decreases nearly linearly with $1/m$ and goes to zero in the vicinity of $m = 2$. Therefore, it is natural to conclude that the enhanced antiferromagnetic fluctuations associated with two-dimensionality are responsible for destroying the magnetic order.

The vanishing magnetic order implies that a quantum phase transition occurs close to $m = 2$. Close to a QCP, the resistivity strongly deviates from the Fermi liquid behavior $\rho(T) - \rho_0 + AT^{\alpha}$, with $\alpha = 2$, where A is the Fermi liquid coefficient. In Fig. 4B, the exponent α is mapped in the T versus $1/m$ diagram. The T^2-dependence is observed at low temperatures for $m > 2$. In contrast, for $m = 2$, a marked deviation from such behavior is observed (Fig. 4C): A T-linear dependence with $\alpha = 1.01 \pm 0.02$ is seen below 0.5 T_{coh}, which corresponds to the Fermi temperature of heavy fermions. At even lower temperatures, below ~140 mK, $\rho(T)$ shows a faster-than-linear decrease, which is suppressed by small magnetic fields (Fig. 4C, upper inset). We conclude that for $m = 2$, the lowered dimensionality suppresses the magnetic order down to $T_N \sim 140$ mK, which can be further suppressed by a small field (*17*). The T-linear behavior is consistent with scattering by the 2D antiferromagnetic fluctuations (*22*) that are enhanced by the QCP. This is in contrast to the 3D case, where $\alpha = 1.5$ is expected (*22*), and indeed $\alpha \sim 1.6$ is observed near the pressure-induced QCP in the bulk $CeIn_3$ (*14*, *15*).

Even for $m > 2$, where T^2 behavior is observed, the initial slope of $\rho - \rho_0$ as T approaches 0 K becomes larger with decreasing m, and A is enhanced toward $m = 2$ (Fig. 4A). Because A is related to the Sommerfeld coefficient of specific heat γ as $A = a_0\gamma^2$, with a_0 close to the universal value of 10^{-5} μΩ-cm (K-mol/mJ)^2 (*14*, *21*), the large A immediately indicates the enhanced quasiparticle mass. At temperatures below ~1 K, the resistivity of $LaIn_3$ is much smaller than that of superlattices, and its temperature dependence is negligible. Thus the observed large A values indicate that the temperature-dependent part of the resistivity is governed by the 2D heavy fermion layers. In fact, the γ value estimated from A is enhanced from the bulk $CeIn_3$ value of ~120 mJ/(K^2 mol) and reaches ~350 mJ/(K^2 mol) for $m = 3$, which corresponds to a quasiparticle mass at least several hundred times larger than the free electron mass. Because the T-linear behavior observed for $m = 2$ suggests further enhancement of A, it is tempting to associate this result with diverging quasiparticle mass because of the quantum fluctuations enhanced upon approaching a QCP. For $m = 1$, the determination of A is ambiguous because of the weak temperature dependence of ρ. The diverging behavior of γ near a QCP is also reported in bilayer films of ^{3}He systems (*12*).

Quantum criticality is reported to be strongly modified by magnetic fields in strongly correlated electron systems (*2*, *9*, *23*, *24*). The quantum criticality for $m = 2$ is removed by strong magnetic fields, and the Fermi-liquid properties with $\alpha = 2$ are recovered (Fig. 4C, lower inset). Simultaneously, the A value is quickly suppressed with increasing magnetic field H (Fig. 4A). Thus, both temperature and field dependencies of the transport properties provide strong support for the presence of the quantum phase transition in the vicinity of $m = 2$, which is tuned by the dimensionality parameter. The successful growth of epitaxial Ce-based superlattices promises to provide a setting in which to explore the fundamental physics of strongly correlated electron systems such as the 2D Kondo lattice and, potentially, 2D superconductivity near a QCP.

References and Notes

1. A. C. Hewson, *The Kondo Problem to Heavy Fermions* (Cambridge Univ. Press, Cambridge, 2003)
2. P. Gegenwart, Q. Si, F. Steglich, *Nat. Phys.* **4**, 186 (2008)
3. S. Sachdev, *Quantum Phase Transition* (Cambridge Univ. Press, Cambridge, 2000)
4. M. Jourdan, M. Huth, H. Adrian, *Nature* **398**, 47 (1998)
5. D. Groten, G. J. C. van Baarle, J. Aarts, G. J. Nieuwenhuys, J. A. Mydosh, *Phys. Rev. B* **64**, 144425 (2001)
6. M. Izaki *et al.*, *Appl. Phys. Lett.* **91**, 122507 (2007)
7. H. Hegger *et al.*, *Phys. Rev. Lett.* **84**, 4986 (2000)
8. C. Petrovic *et al.*, *Cond. Matt* **13**, L337 (2001)
9. H. Shishido, R. Settai, H. Harima, Y. Onuki, *J. Phys. Soc. Jpn.* **74**, 1103 (2005).
10. Y. Ida, R. Settai, Y. Ota, F. Honda, Y. Onuki, *J. Phys. Soc. Jpn.* **77**, 084708 (2008)
11. G. Zheng *et al.*, *Phys. Rev. Lett.* **86**, 4664 (2001)
12. M. Neumann, J. Nyéki, B. Cowan, J. Saunders, *Science* **317**, 1356 (2007).
13. J. M. Lawrence, S. M. Shapiro, *Phys. Rev. B* **22**, 4379 (1980)
14. N. D. Mathur *et al.*, *Nature* **394**, 39 (1998)
15. G. Knebel, D. Braithwaite, P. C. Canfield, G. Lapertot, J. Flouquet, *Phys. Rev. B* **65**, 024425 (2001).
16. S. Kawasaki *et al.*, *J. Phys. Soc. Jpn.* **73**, 1647 (2004)
17. See supporting material on *Science* Online
18. S. Kashiba, S. Maekawa, S. Takahashi, M. Tachiki, *J. Phys Soc. Jpn.* **55**, 1341 (1986)
19. W. Knafo *et al.*, *Cond. Matt* **15**, 3741 (2003).
20. Y. Nakajima *et al.*, *J. Phys. Soc. Jpn.* **76**, 024703 (2007)
21. H. Kontani, *Rep. Prog. Phys.* **71**, 026501 (2008)
22. T. Moriya, K. Ueda, *Adv. Phys.* **49**, 555 (2000)
23. A. Bianchi, R. Movshovich, I. Vekhter, P. G. Pagliuso, J. L. Sarrao, *Phys. Rev. Lett.* **91**, 257001 (2003)
24. T. Shibauchi *et al.*, *Proc. Natl. Acad. Sci. U.S.A.* **105**, 7120 (2008)
25. E. E. Fullerton, I. K. Schuller, H. Vanderstraeten, Y. Bruynseraede, *Phys. Rev. B* **45**, 9292 (1992)

28. We thank M. Izaki, N. Kawakami, H. Kurata, K. Miyake, and A. Tanaka for discussion. This work was supported by Grants-in-Aid for Scientific Research (KAKENHI) from the Japan Society for the Promotion of Science and by a Grant-in-Aid for the Global Centers of Excellence program "The Next Generation of Physics, Spun from Universality and Emergence" from the Ministry of Education, Culture, Sports, Science and Technology

Supporting Online Material

www.sciencemag.org/cgi/content/full/327/5968/980/DC1
Materials and Methods
SOM Text
Figs. S1 to S5

15 October 2009; accepted 7 January 2010
10.1126/science.1183376

The Silicate-Mediated Formose Reaction: Bottom-Up Synthesis of Sugar Silicates

Joseph B. Lambert,* Senthil A. Gurusamy-Thangavelu,† Kuangbiao Ma†

Understanding the mechanism of sugar formation and stabilization is important for constraining theories on the abiotic origin of complex biomolecules. Although previous studies have produced sugars from small molecules through the formose and related reactions, the product mixtures are complex and unstable. We have demonstrated that simple two- and three-carbon molecules (glycolaldehyde and glyceraldehyde), in the presence of aqueous sodium silicate, spontaneously form silicate complexes of four- and six-carbon sugars, respectively. Silicate selects for sugars with a specific stereochemistry and sequesters them from rapid decomposition. Given the abundance of silicate minerals, these observations suggest that formose-like reactions may provide a feasible pathway for the abiotic formation of biologically important sugars, such as ribose.

Sugars are essential elements of biochemistry, including energy processing (e.g., glycogen and starch), structure (e.g., cellulose and cell walls), and genetics (e.g., DNA and RNA). The synthesis of sugars in a prebiotic world therefore plays a key role in any theory of the origin of life. The formose reaction (*1*, *2*) is a possible process whereby sugars form abiotically (*3*, *4*). This reaction converts formaldehyde (HCHO; C1) to a variety of sugars, in the presence of strong bases (*5*), organic bases (*6*), or minerals (*7*–*11*). The generally accepted mechanism (fig. S1) (*12*) involves conversion of formaldehyde to higher sugars, with autocatalysis by glycolaldehyde [$(CHO)CH_2OH$; C2] (*13*, *14*). Aldol reactions then sequentially produce glyceraldehyde [$(CHO)CH(OH)CH_2OH$; C3] and higher sugars.

Despite the effectiveness of an autocatalytic reaction, the current prebiotic formose model has limitations (*7*, *15*, *16*). Most notably, the reaction generates a plethora of unstable sugars, of which the key sugar, ribose, is present in a very small proportion (*17*–*19*). Although the problem of sugar instability is unresolved, some molecules, such as borates, phosphates, and cyanamide, select for the synthesis of certain sugars (*20*–*24*). All these reactions require alkaline conditions such as those found naturally in hydrothermal vents, in some lakes, and at the surfaces of aluminosilicate minerals (*25*–*27*). An additional drawback is that the products from the formose mechanism (*13*) are racemic, whereas sugars under terrestrial biological conditions are homochiral. Recent results suggest that the aluminosilicate environment of certain clays (*28*, *29*) may provide this chirality.

C5 and C6 sugars react with aqueous sodium silicate to form stable complexes (*30*–*32*). Silicate minerals constitute the major component of Earth's crust and mantle, as well as those of the moon, asteroids, and other rocky planets. Amorphous silica is readily soluble in aqueous solution at pH 9, and its solubility rises appreciably at higher alkalinity (*33*). Here, we report simple reactions under these same conditions at room temperature with only C1, C2, or C3 as the reactants (*12*). Formaldehyde by itself does not oligomerize readily when placed in sodium silicate solution, as it does not possess an alpha hydrogen required to initiate the base-catalyzed reaction (*4*, *13*, *14*). Glycolaldehyde at room temperature is in equilibrium with its hydrate [$HOCH_2CH(OH)_2$] and several dioxane dimers (*34*). Within 20 min after exposure to aqueous sodium silicate, new peaks in the ^{13}C nuclear magnetic resonance (NMR) spectrum replaced all former peaks except those from the hydrate (fig. S2). The ^{29}Si spectrum recorded after 30 min contained several peaks in the region δ-102 to δ-100, indicative of negatively charged silicon in its pentacoordinated form (fig. S3) (*12*). After conversion of the sugar silicate products of C2 by hydrolysis to the free sugars (no longer complexed with silicate), the ^{13}C spectrum was composed almost entirely of peaks attributable to the C4 sugars erythrose and threose (Fig. 1A), in the approximate ratio of 75/25 (fig. S4). These are the expected products of a simple aldol reaction between two moles of glycolaldehyde (Fig. 1B). The simplicity of the product mixture contrasts with past formose results (*17*, *19*, *35*).

Previous work indicated that sugar silicates, with some exceptions, exist as 2:1 sugar-silicate complexes and can form only when the sugar exists as the furanose (five-membered) form with an unsubstituted anomeric hydroxy group cis to a hydroxy group on the adjacent carbon (*24*, *31*, *32*). The C4 sugars do not have enough carbons to form pyranose (six-membered) rings and are the smallest sugars that can form furanose rings. Thus, C1, C2, and C3 sugars cannot form silicate complexes because four carbons are required to close the ring. As a result, C2 dimerizes to C4, which sodium silicate sequesters as the silicate complex. Three stereoisomers are possible for these 2:1 complexes, in which both sugar rings are syn to the uncomplexed hydroxy group (Fig. 1B), both are anti, or one is syn while the other is anti. Multiple tetrose silicate stereoisomers, plus the possibility of regioisomers and some hexose silicates, supply the observed multiplicity of ^{29}Si resonances (fig. S3).

Electrospray ionization (ESI) mass spectra of the silicate complexes confirmed these results. After 30 min, only 2:1 sugar-silicate complexes were present, primarily C4 with some C6 (Fig. 2A). After 12 hours, C6 complexes were the primary product, with some C4 and C8 (Fig. 2B). Products lacking the ability to form silicate complexes, such as the anomers (C1 stereoisomers) of the structures in Fig. 1A, can isomerize to complex-forming products or can oligomerize further. The reaction also was carried out under the normal formose conditions of

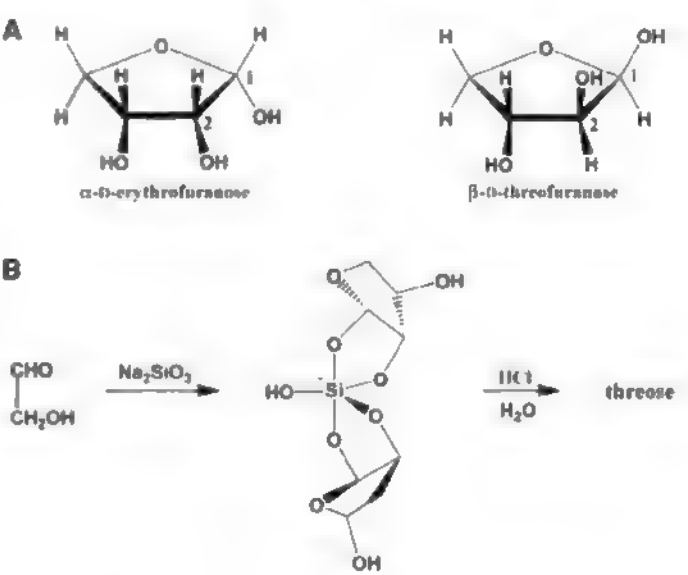

Fig. 1. **(A)** The preferred structures of erythrose and threose for reaction with sodium silicate, in which the 1- and 2-hydroxy groups are cis. **(B)** The bottom-up synthesis of threose from glycolaldehyde. In the presence of sodium silicate, the aldol dimer is sequestered as its 2:1 silicate complex. Hydrolysis liberates the free sugar.

Department of Chemistry, Northwestern University, Evanston, IL 60208, USA.

*To whom correspondence should be addressed. E-mail: j-lambert@northwestern.edu

†These authors contributed equally to this work.

aqueous NaOH (*3*, *5*), at the same pH but without sodium silicate. Even after 30 min, the C4 products constitute less than half the total (Fig. 2C), and, after 12 hours, a preponderance of higher oligomers and nonsugars indicates an almost fully decomposed product set (Fig. 2D). Thus silicate provides selection and stabilization of the sugars formed, compared with solutions containing only hydroxide as base.

The same experiments with glyceraldehyde (C3) produced even simpler and stabler product mixtures. The NMR spectrum of C3 in neutral water indicates a mixture of its many forms, including the aldehyde, the hydrate, dimer dioxolanes, and dimer dioxanes (*36*). Reaction with sodium silicate at room temperature immediately replaces almost all carbon peaks (fig. S5). The observation of several ^{29}Si peaks in the region δ-102 to δ-100 confirms the pentacoordinated nature of the sugar silicates (fig. S6). The aldol reactions of glyceraldehyde and its keto isomer give branched aldohexoses and straight-chain ketohexoses (fig. S7). The ^{13}C chemical shifts are consistent with ketohexose products such as sorbose and tagatose (*37*), but assignments are not yet certain. The ESI mass spectrum after 12 hours was almost unchanged from that after 30 min (Fig. 3, A and B). In contrast, the ESI mass spectrum of the products of reaction of C3 under classic formose conditions (aqueous sodium hydroxide without silicate) indicates rapid decomposition to nonsugars after 12 hours (Fig. 3, C and D).

We also studied the solutions in which two different, small sugars reacted in basic conditions in the presence of silicate (*12*). Reaction of an equimolar mixture of formaldehyde and glyceraldehyde (C1+C3) in the presence of sodium silicate produced primarily C4 products, resembling those from C2 alone. Not surprisingly on steric grounds, the anion of glyceraldehyde reacts more rapidly with formaldehyde to form C4 products than with another glyceraldehyde molecule to form C6 isomers (fig. S8). Reaction of an equimolar mixture of glycolaldehyde and glyceraldehyde (C2+C3) under the same conditions yielded a complex mixture of sugar silicates containing 30 to 40% pentoses (the single largest component), with smaller amounts of tetroses, hexoses, and higher sugars. The ratios remain nearly constant from 30 min to 12 hours (fig. S9). The reaction mixture decomposes rapidly under classic formose conditions, in the absence of silicate (fig. S10). The aldol reaction of the enolate of glycolaldehyde with glyceraldehyde can give all four of the straight-chain aldopentoses directly (fig. S11). Reaction in the opposite sense gives branched aldopentoses (fig. S12). Isomerization of glyceraldehyde to its ketose isomer (dihydroxyacetone) and reaction with glycolaldehyde can give the straight-chain ketopentoses ribulose and xylulose (fig. S13). Individual hexose structures remain unidentified.

Because formaldehyde, glycolaldehyde, and glyceraldehyde (C1 to C3) have too few carbon atoms to complex with sodium silicate, they oligomerize through base-catalyzed reactions to C4 to C6 sugars, and the first-formed sugar with the appropriate stereochemistry reacts immediately with silicate at room temperature. This bottom-up synthesis of sugar silicates is a plausible prebiotic process. In contrast, C5 and C6 sugars form silicate complexes directly, in a top-down synthesis, and consequently resist base-catalyzed reactions under the same conditions. Furthermore, the C5 and C6 sugar silicates formed in the bottom-up synthesis oligomerize very slowly (Fig. 3, A and B, and fig. S9), the C4 products somewhat faster (Fig. 2, A and B). In the absence of sodium silicate, the uncomplexed higher sugars decompose rapidly under alkaline conditions (Fig. 2, C and D, Fig. 3, C and D, and fig. S10). Only certain structures are selected because of stereo control of silicate formation. Moreover, silicate mediation ameliorates one of the primary impediments to a possible role of the formose reaction in prebiotic sugar synthesis: product instability. The rationale is similar to that proposed for a borate-mediated formose reaction (*23*), with the advantage here of the much wider availability of

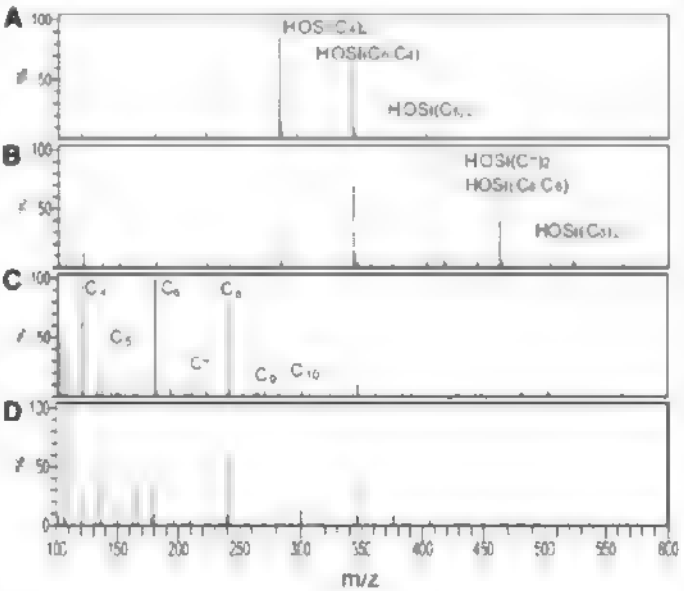

Fig. 2. (**A**) The negative ion ESI mass spectrum of the sugar silicate products of the reaction of glycolaldehyde with aqueous sodium silicate after 30 min at room temperature. The symbol $HOSi(C4)_2$ identifies the mass of any 2:1 sugar-silicate complex containing two C4 sugars. (**B**) The same spectrum after 12 hours. (**C**) ESI mass spectrum of the free sugar products of the reaction of glycolaldehyde with aqueous sodium hydroxide after 30 min at room temperature (classic formose conditions). Carbon numbers (e.g., C4 for all tetroses) identify specific sugar structures. (**D**) The same spectrum after 12 hours.

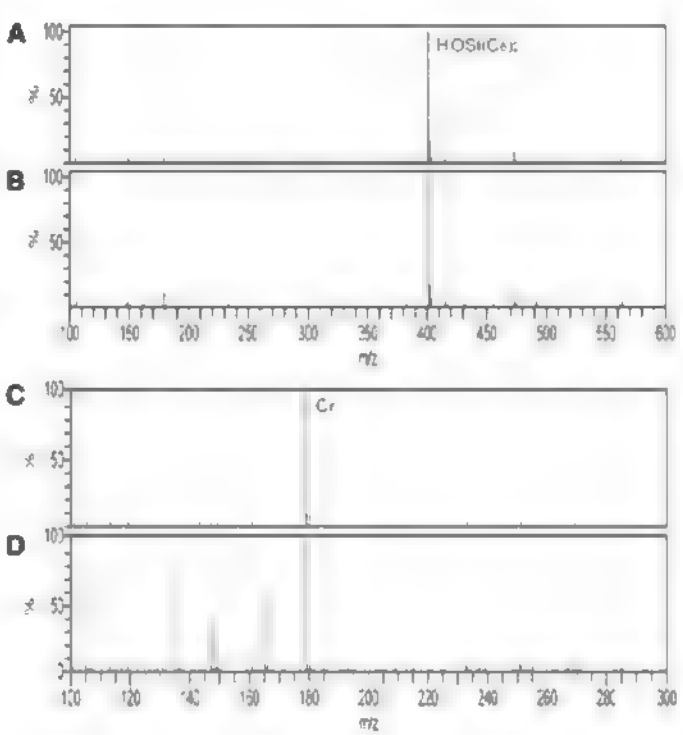

Fig. 3. (**A** and **B**) The negative ion ESI mass spectra of the sugar silicate products of the reaction of glyceraldehyde with aqueous sodium silicate after 30 min and after 12 hours at room temperature. (**C** and **D**) ESI mass spectra of the free sugar products of the reaction of glyceraldehyde with aqueous sodium hydroxide after 30 min and after 12 hours at room temperature.

silicate minerals and hence readily available silicate ions.

References and Notes

1. A. Butlerow, *Justus Liebigs Ann. Chem.* **120**, 295 (1861)
2. O. Loew, *J. Prakt. Chem.* **34**, 51 (1886)
3. N. W. Gabel, C. Ponnamperuma, *Nature* **216**, 453 (1967)
4. L. E. Orgel, *Crit. Rev. Biochem Mol. Biol.* **39**, 99 (2004)
5. R. Breslow, *J. Am. Chem. Soc.* **80**, 3719 (1958)
6. T. Matsumoto, S. Inoue, *J. Chem. Soc. Perkin Trans. 1* **1982**, 1975 (1982)
7. A. W. Schwartz, R. M. de Graaf, *J. Mol. Evol.* **36**, 101 (1993)
8. A. G. Cairns-Smith, P. Ingram, G. L. Walker, *Theor. Biol.* **35**, 601 (1972)
9. L. E. Orgel, *Proc. Natl. Acad. Sci. U.S.A.* **97**, 12503 (2000)
10. R. Krishnamurthy, S. Pitsch, G. Arrhenius, *Orig. Life Evol. Biosph.* **29** 139 (1999)
11. S. Pitsch, R. Krishnamurthy, G. Arrhenius, *Helv. Chim. Acta* **83**, 2398 (2000)
12. Materials and methods are available as supporting material on *Science* Online
13. R. Breslow, *Tetrahedron Lett.* **1**, 22 (1959)
14. R. F. Socha, A. H. Weiss, M. M. Sakharov, *J. Catal.* **67**, 207 (1981)
15. G. O. Arrhenius, *Helv. Chim. Acta* **86**, 1569 (2003)
16. R. Shapiro, *Orig. Life Evol. Biosph.* **18**, 71 (1988)
17. P. Decker, H. Schweer, R. Pohlmann, *J. Chromatogr. A* **244**, 281 (1982)
18. V. M. Kolb, J. P. Dworkin, S. L. Miller, *J. Mol. Evol.* **38**, 549 (1994)
19. R. Larralde, M. P. Robertson, S. L. Miller, *Proc. Natl. Acad. Sci. U.S.A.* **92** 8158 (1995)
20. Y. Shigemasa, S. I. Akagi, E. Waki, R. Nakashima, *J. Catal.* **69**, 58 (1981)
21. Y. Shigemasa *et al.*, *Carbo. Res.* **134**, C4 (1984)
22. G. Springsteen, G. F. Joyce, *J. Am. Chem. Soc.* **126**, 9578 (2004)
23. A. Ricardo, M. A. Carrigan, A. N. Olcott, S. A. Benner, *Science* **303**, 196 (2004)
24. A. N. Simonov *et al.*, *Adv. Space Res.* **40**, 1634 (2007)
25. D. S. Kelley *et al.*, *Science* **307**, 1428 (2005)
26. N. G. Holm, M. Dumont, M. Ivarsson, C. Konn, *Geochem. Trans.* **7**, 7 (2006)
27. W. Stumm, J. J. Morgan, *Aquatic Chemistry* (Wiley-Interscience, New York, ed. 3, 1996)
28. J. Washington, *Orig. Life Evol. Biosph.* **30**, 53 (2000)
29. R. M. Hazen, D. S. Sholl, *Nat. Mater.* **2**, 367 (2003)
30. S. D. Kinrade, R. J. Hamilton, A. S. Schach, C. T. B. Knight, *J. Chem. Soc., Dalton Trans.* (7) 961 (2001)
31. J. B. Lambert, G. Lu, S. R. Singer, V. M. Kolb, *J. Am. Chem. Soc.* **126**, 9611 (2004)
32. K. Kästele, P. Klüfers, F. Kopp, J. Schuhmacher, M. Vogt, *Chem. Eur. J.* **11**, 6326 (2005)
33. K. Yang, P. Roonasi, A. Holmgren, *J. Colloid Surf. Sci.* **328**, 41 (2008)
34. G. C. S. Collins, W. O. George, *J. Chem. Soc. B* **1971** 1352 (1971)
35. M. Z. Iqbal, S. Novalin, *J. Chromatogr. A* **1216**, 5116 (2009)
36. F. García-Jiménez, O. Collera Zuñiga, Y. Castells García, J. Cárdenas, G. Cuevas, *J. Braz. Chem. Soc.* **16**, (3a) 467 (2005)
37. L. Que, G. R. Gray, *Biochem.* **13**, 146 (1974)

38. This research was supported by the National Science Foundation, Dow Corning Corp., and Schlumberger Ltd.

Supporting Online Material

www.sciencemag.org/cgi/content/full/327/5968/984/DC1
Materials and Methods
Figs. S1 to S13

30 September 2009; accepted 5 January 2010
10.1126/science.1182669

Asymmetric Cooperative Catalysis of Strong Brønsted Acid–Promoted Reactions Using Chiral Ureas

Hao Xu, Stephan J. Zuend, Matthew G. Woll, Ye Tao, Eric N. Jacobsen*

Cationic organic intermediates participate in a wide variety of useful synthetic transformations, but their high reactivity can render selectivity in competing pathways difficult to control. Here, we describe a strategy for inducing enantioselectivity in reactions of protio-iminium ions, wherein a chiral catalyst interacts with the highly reactive intermediate through a network of noncovalent interactions. This interaction leads to an attenuation of the reactivity of the iminium ion and allows high enantioselectivity in cycloadditions with electron-rich alkenes (the Povarov reaction). A detailed experimental and computational analysis of this catalyst system has revealed the precise nature of the catalyst-substrate interactions and the likely basis for enantioinduction.

The proton (H^+) is the simplest, and arguably the most versatile, catalyst for organic reactions, mediating an extraordinary range of biological and synthetic transformations (*1*). Although a proton cannot be rendered chiral, enantioselective Brønsted acid catalysis is attainable through the influence of the acid's conjugate base and through medium effects. The former strategy, involving the use of chiral acids, has proven particularly useful, as demonstrated in the design and application of chiral phosphoric acids (*2*–*4*), *N*-triflyl phosphoramides (*5*), aryl sulfonic acids (*6*), and Lewis acid– (*7*, *8*) or thiourea-assisted Brønsted acids (*9*, *10*). The use of medium effects has been less straightforward, and chiral solvents have been investigated in asymmetric catalysis with comparatively limited success (*11*). The recent discovery of anion-binding pathways (*12*, *13*) in reactions catalyzed by chiral, small-molecule, H-bond donor catalysts such as urea and thiourea derivatives (*14*) suggests an alternative strategy that combines elements of both approaches. In this scenario, a chiral catalyst might associate with a protonated substrate through the counteranion and induce enantioselectivity in nucleophilic addition reactions to the cationic electrophile through specific secondary interactions with the charged species.

This idea was explored in the context of the formal [4+2] cycloaddition of *N*-aryl imines and electron-rich olefins, also known as the Povarov reaction (*15*). This Brønsted acid–catalyzed reaction affords tetrahydroquinoline derivatives with the concomitant generation of up to three contiguous stereogenic centers, and enantioselective Lewis acid– or phosphoric acid–catalyzed variants have been identified recently (*16*–*18*). The acid-catalyzed Povarov reaction between benzylidene aniline **2a** and 2,3-dihydrofuran **3** was selected as a model reaction (Fig. 1A), and a broad range of chiral urea and thiourea derivatives that were developed and studied previously in our laboratory, as well as several different Brønsted acids, were evaluated as catalysts for this transformation (table S1) (*19*). With this approach, we found that the combination of the bifunctional sulfinamido urea derivative **1a** (*20*) and *ortho*-nitrobenzenesulfonic acid (NBSA) catalyzed the model reaction with high enantioselectivity (Fig. 1, B and C, entry 1). The importance of both the urea and sulfinamide groups in the catalyst became evident in structure-reactivity/enantioselectivity studies. Thiourea derivative **1b** is an efficient catalyst, but it induced lower enantio- and diastereoselectivity (Fig. 1C, entry 2), whereas the diastereoisomeric (*R*,*R*,*S*)-sulfinamido urea **1c** promoted a much slower and poorly selective reaction (Fig. 1C, entry 3). In addition, reactions catalyzed by phosphinic amide urea **1d** displayed a modest selectivity, and pivalamide urea **1e** and amino urea **1f** both induced low reactivity and selectivity (Fig. 1C, entries 4 to 6). These results suggest a cooperative role for the urea and sulfinamide groups of **1a** in the rate- and enantioselectivity-determining steps of the catalytic reaction.

Under optimized conditions, the Povarov reaction that is catalyzed by **1a** was found to be applicable to different nucleophiles and a wide variety of *N*-aryl imines (Fig. 2, A and B). The highest enantioselectivities were observed in reactions that were carried out under cryogenic conditions with a 2:1 ratio of **1a** to NBSA, which was used to ensure complete suppression of the racemic pathway catalyzed by NBSA alone. Lactam-substituted tetrahydroquinoline derivatives $\mathbf{6}_{exo}$ were obtained in high enantio- and diastereoselectivities by reaction of benzaldimines **2** with vinyllactam **5**. Tricyclic hexahydropyrrolo-[3,2-*c*]quinoline derivatives $\mathbf{8}_{exo}$ were generated in an analogous manner by the cyclization of *N*-Cbz–protected 2,3-dihydropyrrole **7** with **2**.

Department of Chemistry and Chemical Biology, Harvard University, Cambridge, MA 02138, USA.

*To whom correspondence should be addressed. E-mail: jacobsen@chemistry.harvard.edu

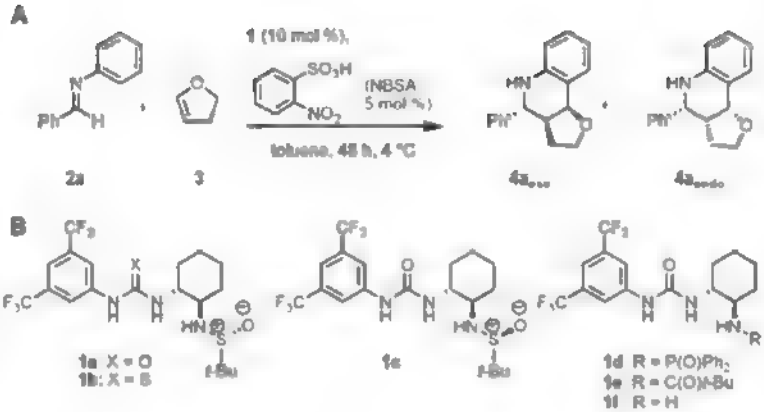

C

entry	catalyst	conversion (%)	dr (4_{exo} 4_{endo})	4_{exo} ee (%)
1	1a	92	4.0	91
2	1b	95	1.4	83
3	1c	82	0.3	2
4	1d	20	1.0	50
5	1e	8	0.25	<5
6	1f	0	ND	ND

Fig. 1. (**A**) Model Povarov reaction cocatalyzed by *o*-nitrobenzenesulfonic acid and chiral ureas/thioureas. (**B**) Some of the chiral catalysts evaluated in optimization studies. (**C**) Results of catalyst structure-reactivity/enantioselectivity studies. dr, diastereomeric ratio;. Both dr and ee were determined by supercritical fluid chromatography analysis using commercially available chiral columns (*19*).

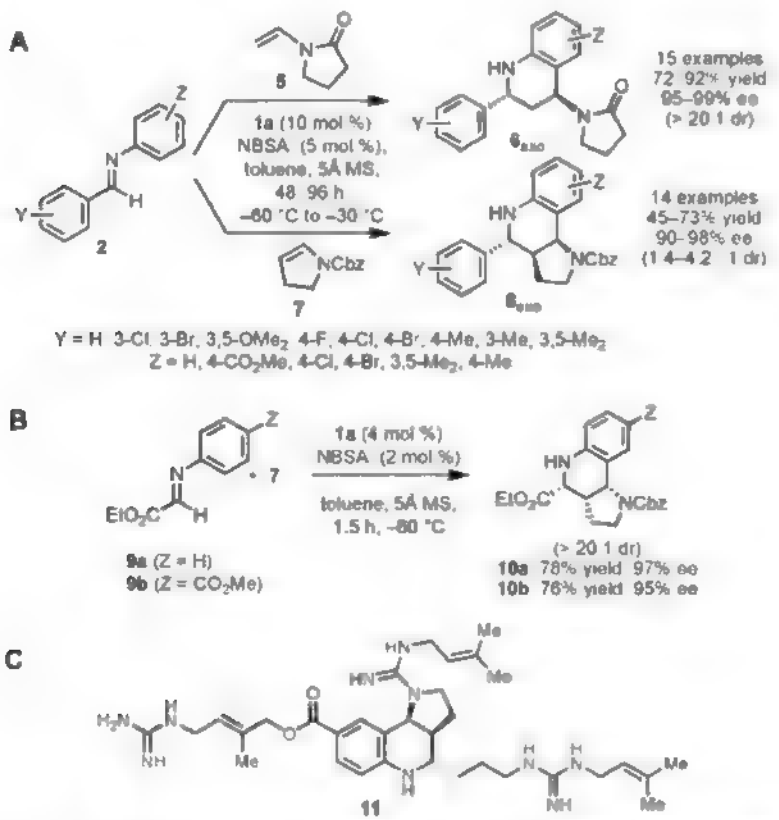

Fig. 2. (**A** and **B**) Asymmetric Povarov reactions catalyzed by **1a**/NBSA with enamide **5** and enecarbamate **7** as the nucleophilic reacting partners. Molecular sieves (5 Å) serve to sequester water introduced with the hygroscopic NBSA reagent, thereby preventing competing imine hydrolysis pathways. See tables S2 and S3 for yields and selectivities obtained with each substrate. (**C**) Martinelline (**11**), a natural-product inhibitor of bradykinin B1 and B2 G protein-coupled receptors (median inhibitory concentration IC_{50} = 6.4 and 0.25 μM, respectively). A previous study demonstrated that a racemic form of ester **10b** could be converted to (+)**11** after epimerization of the corresponding aldehyde, so the enantioselective synthesis of **10b** described here constitutes a formal enantioselective synthesis of martinelline (*25*).

Although moderate diastereoselectivities favoring the exo diastereomer were obtained in this case ($8_{exo}/8_{endo}$ = 1.4 to 4.2:1), this product was also generated in high enantiomeric excess (ee) (90 to 98% ee) and could be isolated in diastereomerically pure form in useful yields (45 to 73%). In general, imines derived from electron-deficient aldehydes—especially imines derived from glyoxylate esters—underwent reaction more rapidly in the Povarov reaction, but uniformly high enantioselectivities were obtained despite these reactivity differences.

Povarov reactions between glyoxylate imines **9a** or **9b** with 2,3-dihydropyrrole **7** provide the endo products in high enantioselectivity. This represents a direct route to the core tetrahydroquinoline structure of a variety of important, biologically active compounds (*21*–*23*), including martinelline (**11**, Fig. 2C), a naturally occurring nonpeptide natural product that has been identified as a bradykinin B1 and B2 receptor antagonist (*24*). The enantioselective catalytic Povarov method provides an efficient enantioselective route to this natural product and its analogs (*25*), thereby solving a longstanding synthetic challenge.

The cooperative activity of an acid and a chiral organic molecule may represent a general strategy for asymmetric catalysis (*9*, *10*), and we thus undertook a detailed experimental and computational study to elucidate the mechanism of catalysis in the Povarov reaction and the basis for the high levels of stereoselectivity induced by **1a**. Similar enantioselectivities were achieved with a variety of sulfonic acids under homogeneous conditions, and we selected the **1a**/HOTf cocatalyzed reaction between **2a** and **3** as a model for mechanistic analysis (HOTf, triflic acid, HO_3SCF_3). The reaction between **2a** (0.2 to 0.8 M) and **3** (0.4 to 1.6 M) promoted by catalytic quantities of HOTf (0.2 to 2.0 mM) alone in toluene was monitored by reaction calorimetry and ^{1}H nuclear magnetic resonance (NMR) spectroscopy (table S4). Kinetic analysis of reactions carried out at 28°C revealed a first-order dependence on [**3**] and [HOTf], and a zeroth-order dependence on imine [**2a**] (Eq. 1). These data indicate that imine **2a** undergoes quantitative protonation by HOTf under the reaction conditions, and that protioiminium triflate **2a**•**HOTf** represents the resting state of the achiral acid catalyst under the reaction conditions.

$$\text{Rate} = d[\mathbf{4}]/dt = k_{rac}[\text{imine}]^0[\mathbf{3}]^1[\text{HOTf}]^1_{tot} \quad (1)$$

Here, t is time and k_{rac} is the second-order rate constant for the nonenantioselective cycloaddition of **2a**•**HOTf** and **3**.

Consistent with this conclusion, the reaction of imine **2a** with one equivalent of HOTf resulted in the quantitative formation of protioiminium triflate **2a**•**HOTf** as a moisture-sensitive salt that is sparingly soluble in nonpolar solvents

(~2.0 mM in C_6D_6). The solubility of **2a•HOTf** increases by a factor of 4 in the presence of achiral urea **12** through the formation of the 1:1 complex (Fig. 3A). ^{1}H NMR chemical shifts of the formyl proton are sensitive probes of charge separation in iminium ions (*26*). We observed that the 1:1 complex of **2a•HOTf** with achiral urea **12** exhibits a 0.14 parts per million (ppm) up-field shift of the ^{1}H NMR resonance of the formyl proton of **2a•HOTf**, consistent with increased charge separation. These observations can be attributed to a hydrogen-bonding interaction between **12** and the triflate anion of **2a•HOTf** that leads to both solubilization and greater charge separation between the immium ion and the triflate anion.

Markedly different effects are observed when **2a•HOTf** is treated with solutions of bifunctional sulfinamidourea **1a**, which increases the solubility of **2a•HOTf** by more than one order of magnitude; however, dissolution is accompanied by a 0.92-ppm down-field shift of the ^{1}H NMR resonance of the formyl proton of **2a•HOTf**, which is consistent with a less charge-separated

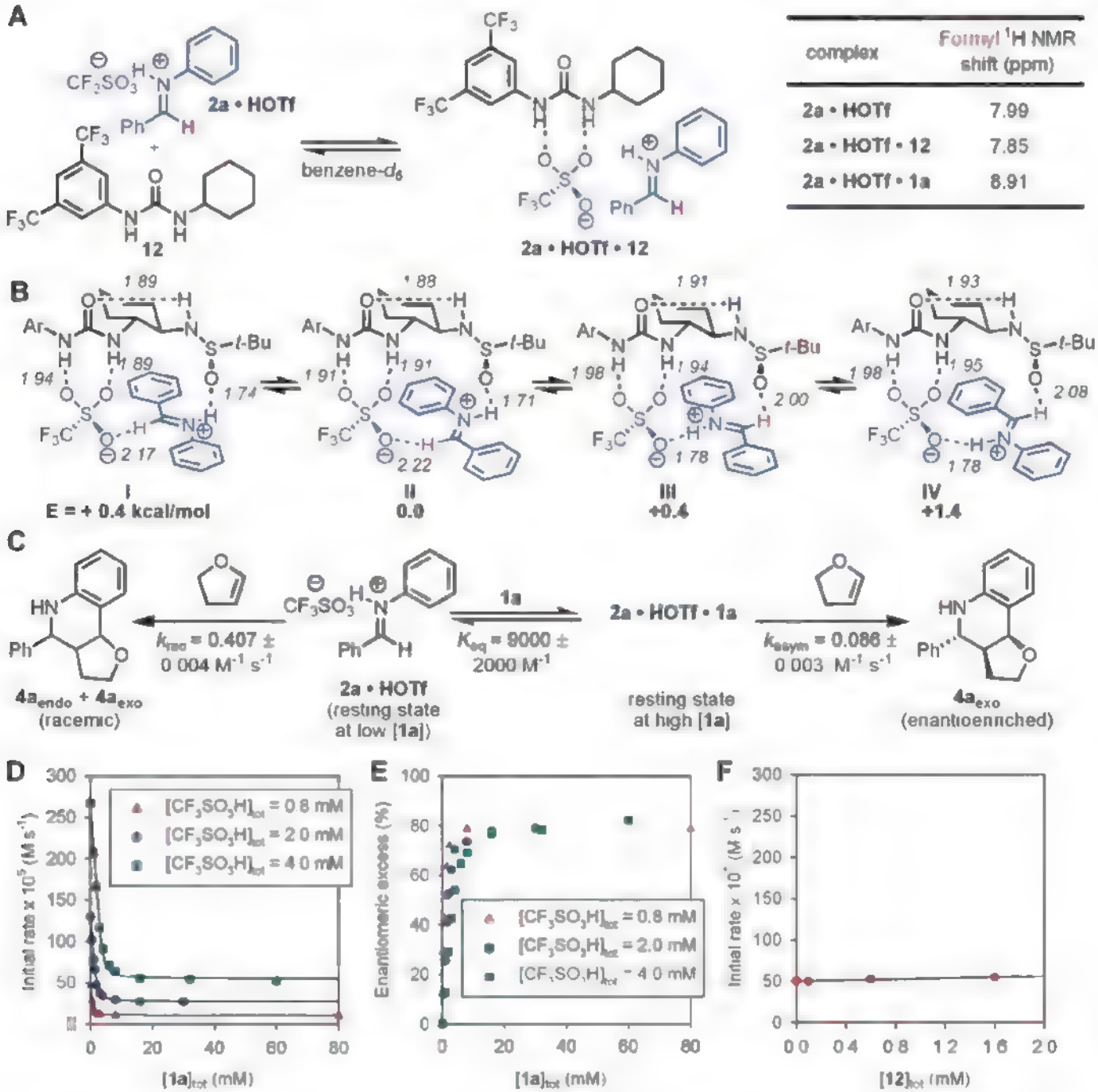

Fig. 3. (**A**) Formation of a complex between urea **12** and iminium sulfonate **2•HOTf**. ^{1}H NMR chemical shifts of the formyl proton of **2a** as free and urea-bound salts. (**B**) Geometry and energy-minimized structures of **2a•HOTf•1a** calculated at the B3LYP/6-31G(d) level of density functional theory. Ar = 3,5-$(CF_3)_2C_6H_3$. Selected bond distances are shown in angstroms. (**C**) Kinetic parameters of racemic and enantioselective Povarov reaction of **2a** and **3** cocatalyzed by **1a** and HOTf. (**D**) Plot of initial rate of the Povarov reaction versus [**1a**] at three different concentrations of HOTf. [**2a**] = 0.2 or 0.4 M, [**3**] = 1.6 M. The black curves represent least-squares fits to the rate law derived from the kinetic scheme depicted in (C). (**E**) Plot of ee of $\mathbf{4a}_{exo}$ versus [**1a**] at three different concentrations of HOTf. (**F**) Plot of initial rate of the racemic Povarov reaction cocatalyzed by achiral urea **12** and HOTf versus [**12**] with HOTf = 0.80 mM, [**2a**] = 0.2 M, [**3**] = 1.6 M.

iminium ion. Computational analysis (*27*) of the ternary **2a•HOTf•1a** complex suggests the basis for the observed effect. Four energetic minima of comparable stability were identified (Fig. 3B), with the **1a**-triflate complex acting as a dual H-bond acceptor through the triflate and sulfinamide groups, and the iminium ion acting as a dual H-bond donor through the iminium nitrogen and formyl protons (*28*).

The additional stabilizing interactions involving the catalyst-sulfinamide group and iminium ion formyl proton group have a pronounced effect on the rate of the Povarov reaction. Kinetic analysis of the reaction between **2a** and **3** that was cocatalyzed by HOTf and chiral sulfinamidourea **1a** under homogeneous conditions revealed that **1a** induces a substantial decrease in reaction rate (Fig. 3D). In contrast, the simple achiral urea **12** has a slight accelerating effect (Fig. 3F). In the presence of **1a**, the reaction rate can be expressed by a two-term rate law in which the pathway catalyzed by HOTf alone dominates at low [**1a**], and a HOTf/**1a** cocatalyzed pathway dominates at high [**1a**] (Eq. 2). A binding constant of $K = 9000 \pm 2000\ M^{-1}$ for the interaction between **1a** and **2a•HOTf** can be determined from the kinetic data (Fig. 3D and fig. S11). This relatively high value stands in sharp contrast to the much weaker binding between chiral H-bond donors and neutral substrates (*29*, *30*), but is consistent with binding constants determined between tetraalkylammonium salts and ureas and thioureas (*31*, *32*).

$$\text{Rate} = d[\mathbf{4}]/dt = k_{\text{rac}}[\text{imine•HOTf}][\mathbf{3}] + k_{\text{asym}}[\text{imine•HOTf•}\mathbf{1a}][\mathbf{3}] \quad (2)$$

Here, k_{asym} is the second-order rate constant for the enantioselective cycloaddition between **2a•HOTf•1a** and **3**.

The observation of tight binding between protio-iminium triflate **2a•HOTf** and sulfinamido urea **1a** serves to explain how high enantioselectivity is obtained during the formation of **4a**, even under conditions where the HOTf-catalyzed racemic pathway is several times more rapid than the enantioselective pathway (Fig. 3, C and E). The equilibrium constant for complex formation is sufficiently high that virtually no free iminium ion exists, and the reaction is thus channeled through the asymmetric pathway. The enantioselectivity in the formation of $\mathbf{4a}_{\text{exo}}$ is increased further to synthetically useful levels by carrying out the reaction at lower temperatures (that is, 55°C, 97% ee).

To glean insight into the basis for stereoinduction in the Povarov reaction by sulfinamidourea catalyst **1a**, we carried out a full experimental and computational analysis of the mechanism of addition of dihydrofuran **3** to the protoiminium sulfate **2•HOTf•1a**. In principle, any of several elementary steps in this process may represent the rate- and enantioselectivity-determining event (Fig. 4A, steps a to d). The absence of a primary kinetic isotope effect on the ortho hydrogens of the aniline group of **2** indicates that rearomatization (step d) is kinetically rapid (Fig. 4B). A positive Hammett correlation was obtained in the analysis of the effect of anilino substituents on the rate of reaction ($\rho = +1.96 \pm 0.06$, fig. S17). This result indicates that either the first step of a stepwise process (step a) or a concerted cycloaddition (step c) may be rate-limiting, but it is inconsistent with the cyclization step of a stepwise process (step b) representing the slow step. Definitive distinction between steps a and c is more challenging (*33*), but the kinetic isotope effect data suggest that partial rehybridization of the ortho-carbon of the aniline occurs in the rate-limiting step (*34*), and this is indicative of a concerted, albeit highly asynchronous [4+2] cycloaddition. This conclusion was supported by a computational analysis of the reaction leading to $\mathbf{4}_{\text{exo}}$, which predicts that the lowest-energy pathway involves an endothermic cycloaddition and a comparatively rapid deprotonation/rearomatization step (fig. S19).

The catalyst-bound iminium ions depicted in Fig. 3B each have one π face exposed to solvent

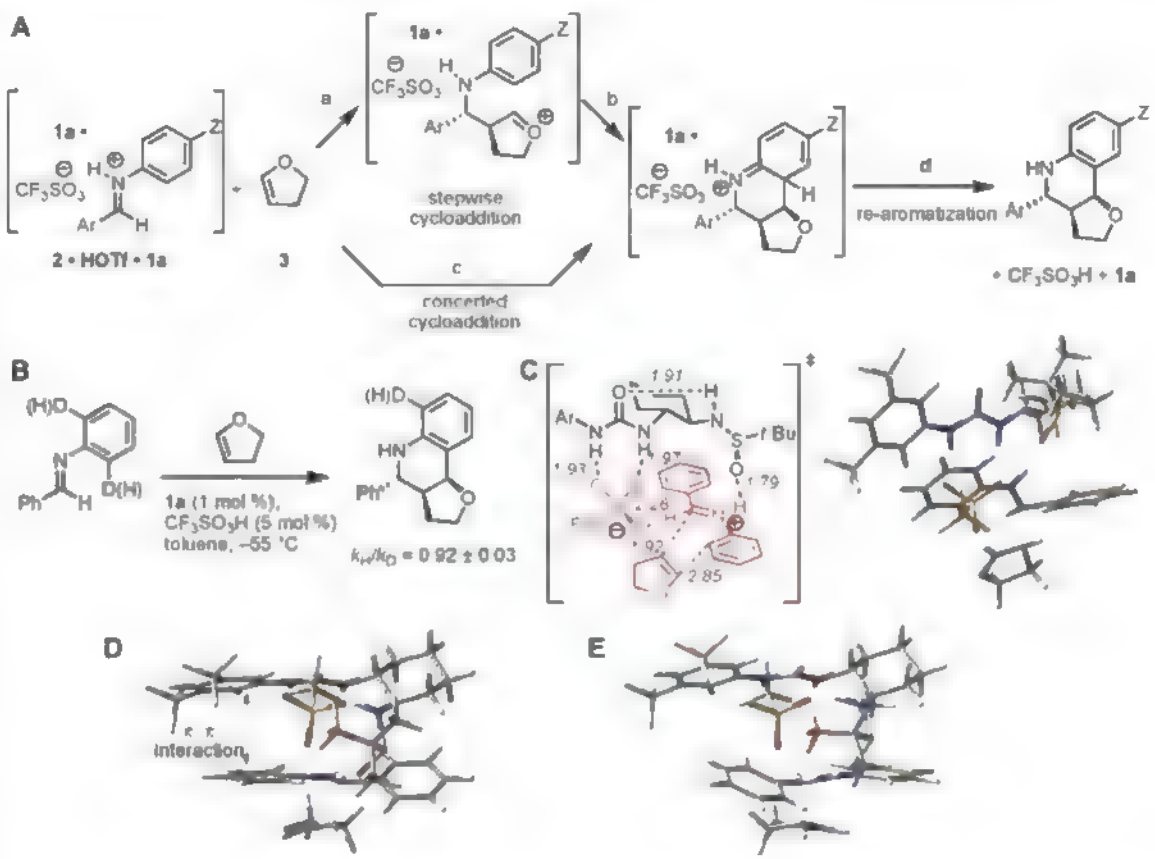

Fig. 4. (**A**) Possible mechanisms and rate-limiting steps in the asymmetric Povarov reaction. Z, an electron-donating or withdrawing substituent. (**B**) Kinetic isotope-effect experiments to distinguish between different possible rate-limiting steps. (**C**) Geometry and energy-minimized lowest-energy transition structure for cycloaddition calculated at the B3LYP/6-31G(d) level of density functional theory. Selected bond distances are shown in angstroms. Ar, 3,5-$(CF_3)_2C_6H_3$. (**D**) Alternate view of the structure in (C) highlighting the stabilizing π–π interaction between the aryl groups of the catalyst and the imirmum ion undergoing cycloaddition. (**E**) Analogous view of the transition structure leading to the minor enantiomer of product. This transition structure lacks stabilizing π–π interactions and is disfavored relative to the structure in (D) by 1.3 kcal/mol in calculations using the B3LYP/6-31G(d) method, and by 3.6 to 3.9 kcal/mol using M05-2X/6-31+G(d,p) or MP2/6-31G(d) single-point calculations. See table S17 for further details.

and the other π face shielded by the catalyst, and are all expected to be energetically accessible under the reaction conditions. Computational analyses using either density functional theory or ab initio methods (Fig. 4, C to E) predict that the enantioselectivity-determining cycloaddition occurs preferentially with complex **I**, leading to the experimentally observed (*R*)-enantiomer of product $\mathbf{4a}_{exo}$. The lowest-energy cycloaddition transition structure displays iminium N–H···$O_{sulfinamide}$ and formyl C–H···$O_{sulfonate}$ hydrogen bonds (Fig. 4C), and is predicted to have ≥1.3-kcal mol lower energy than alternatives arising from complexes **II** to **IV**, which is consistent with the experimental data. The basis for enantioselectivity may be ascribed to a stabilizing π–π interaction between the $(CF_3)_2$-C_6H_3N component of the catalyst and the cationic aniline moiety of the substrate. This interaction is evident in transition structures leading to the major enantiomer of $\mathbf{4a}_{exo}$ (Fig. 4D), but it is absent in transition structures leading to the minor enantiomer (Fig. 4E).

Enantioselective catalysis by **1a** of a strong Brønsted acid–catalyzed Povarov reaction thus involves tight binding to a highly reactive cationic intermediate through multiple, specific H-bonding interactions, and these noncovalent interactions are maintained in the subsequent stereodetermining cycloaddition event. One of the four energetically accessible ground-state complexes undergoes reaction with the nucleophile preferentially, illustrating the ability of bifunctional catalyst **1a** to control precisely the outcome of this reaction through noncovalent interactions alone. Given the known ability of urea and thiourea derivatives to bind a wide range of anions, the strategy demonstrated here is applicable, in principle, to cationic intermediates with a variety of counterion structures.

References and Notes

1. M. Eigen, *Angew. Chem. Int. Ed. Engl.* **3**, 1 (1964).
2. T. Akiyama, J. Itoh, K. Yokota, K. Fuchibe, *Angew. Chem. Int. Ed.* **43**, 1566 (2004).
3. D. Uraguchi, K. Sorimachi, M. Terada, *J. Am. Chem. Soc.* **126**, 11804 (2004).
4. T. Akiyama, *Chem. Rev.* **107**, 5744 (2007).
5. D. Nakashima, H. Yamamoto, *J. Am. Chem. Soc.* **128**, 9626 (2006).
6. M. Hatano, T. Maki, K. Moriyama, M. Arinobe, K. Ishihara, *J. Am. Chem. Soc.* **130**, 16858 (2008).
7. K. Ishihara, M. Kaneeda, H. Yamamoto, *J. Am. Chem. Soc.* **116**, 11179 (1994).
8. H. Yamamoto, K. Futatsugi, *Angew. Chem. Int. Ed.* **44**, 1924 (2005).
9. T. Weil, M. Kotke, C. M. Kleiner, P. R. Schreiner, *Org. Lett.* **10**, 1513 (2008).
10. R. S. Klausen, E. N. Jacobsen, *Org. Lett.* **11**, 887 (2009).
11. D. Seebach, H. A. Oei, *Angew. Chem. Int. Ed. Engl.* **14**, 634 (1975).
12. I. T. Raheem, P. S. Thiara, E. A. Peterson, E. N. Jacobsen, *J. Am. Chem. Soc.* **129**, 13404 (2007).
13. Z. Zhang, P. R. Schreiner, *Chem. Soc. Rev.* **38**, 1187 (2009).
14. A. G. Doyle, E. N. Jacobsen, *Chem. Rev.* **107**, 5713 (2007).
15. V. V. Kouznetsov, *Tetrahedron* **65**, 2721 (2009).
16. H. Ishitani, S. Kobayashi, *Tetrahedron Lett.* **37**, 7357 (1996).
17. T. Akiyama, H. Morita, K. Fuchibe, *J. Am. Chem. Soc.* **128**, 13070 (2006).
18. H. Liu, G. Dagousset, G. Masson, P. Retailleau, J. P. Zhu, *J. Am. Chem. Soc.* **131**, 4598 (2009).
19. Materials and methods are available as supporting material on *Science* Online.
20. K. L. Tan, E. N. Jacobsen, *Angew. Chem. Int. Ed.* **46**, 1315 (2007).
21. P. D. Leeson *et al.*, *J. Med. Chem.* **35**, 1954 (1992).
22. R. A. Batey, P. D. Simoncic, D. Lin, R. P. Smyj, A. J. Lough, *Chem. Commun. (Camb.)* (7): 651 (1999).
23. M. Takamura, K. Funabashi, M. Kanai, M. Shibasaki, *J. Am. Chem. Soc.* **123**, 6801 (2001).
24. K. M. Withenup *et al.*, *J. Am. Chem. Soc.* **117**, 6682 (1995).
25. C. F. Xia, L. S. Heng, D. W. Ma *Tetrahedron Lett.* **43** 9405 (2002).
26. H. Mayr, A. R. Ofial, E. U. Wurthwein, N. C. Aust, *J. Am. Chem. Soc.* **119**, 12727 (1997).
27. M. J. Frisch *et al.*, Gaussian 03, Revision E.01 (Gaussian, Wallingford, CT, 2004).
28. G. R. Elia, R. F. Childs, J. F. Britten, D. S. C. Yang, B. D. Santarsiero, *Can. J. Chem.* **74**, 591 (1996).
29. P. Vachal, E. N. Jacobsen, *J. Am. Chem. Soc.* **124**, 10012 (2002).
30. P. R. Schreiner, A. Wittkopp, *Org. Lett.* **4**, 217 (2002).
31. J. L. Sessler, P. A. Gale, W.-S. Cho, *Anion Receptor Chemistry* (RSC Publishing, Cambridge, UK, 2006).
32. T. R. Kelly, M. H. Kim, *J. Am. Chem. Soc.* **116**, 7072 (1994).
33. J. González, K. N. Houk, *J. Org. Chem.* **57**, 3031 (1992).
34. N. Isaacs, In. *Physical Organic Chemistry*, (Wiley, New York, 1995), pp. 296–301.

35. This work was supported by NIH (grants GM-43214 and P50 GM-69721) and by fellowship support from the Dreyfus Foundation (to H.X.), the American Chemical Society and Roche (to S.J.Z.), and the American Chemical Society through the Irving S. Sigal Postdoctoral Fellowship (to M.G.W.) We thank L. P. C. Nielsen for helpful discussions. Metrical parameters for a derivative of compound $\mathbf{4a}_{exo}$ are available free of charge from the Cambridge Crystallographic Data Centre.

Supporting Online Material

www.sciencemag.org/cgi/content/full/327/5968/986/DC1
Materials and Methods
SOM Text
Figs. S1 to S19
Tables S1 to S17
References

5 October 2009; accepted 13 January 2010
10.1126/science.1182826

100-Million-Year Dynasty of Giant Planktivorous Bony Fishes in the Mesozoic Seas

Matt Friedman,[1]* Kenshu Shimada,[2,3] Larry D. Martin,[4] Michael J. Everhart,[3] Jeff Liston,[5] Anthony Maltese,[6] Michael Triebold[6]

Large-bodied suspension feeders (planktivores), which include the most massive animals to have ever lived, are conspicuously absent from Mesozoic marine environments. The only clear representatives of this trophic guild in the Mesozoic have been an enigmatic and apparently short-lived Jurassic group of extinct pachycormid fishes. Here, we report several new examples of these giant bony fishes from Asia, Europe, and North America. These fossils provide the first detailed anatomical information on this poorly understood clade and extend its range from the lower Middle Jurassic to the end of the Cretaceous, showing that this group persisted for more than 100 million years. Modern large-bodied, planktivorous vertebrates diversified after the extinction of pachycormids at the Cretaceous-Paleogene boundary, which is consistent with an opportunistic refilling of vacated ecospace.

The largest vertebrates—fossil or living—are marine suspension feeders. Modern clades adopting this ecological strategy diversified in the Paleogene (66 to 23 million years ago) (*1*–*3*) and include baleen whales and four independent lineages of cartilaginous fishes (sharks and rays) (*4*). In striking contrast to the array of giant suspension feeders found in Cenozoic marine environments, this guild has appeared to be absent during most of the Mesozoic, an interval that is marked by the ecological ascendance of modern plankton groups (*5*, *6*). Possible candidates have been proposed (*7*, *8*), but the clearest examples of large-bodied planktivores in the Mesozoic seas have been a handful of bony fishes confined to a brief 20-million-year window during the Jurassic (Callovian-Tithonian, 165 to 145 million years ago) and known almost exclusively from European deposits (*9*–*12*). These enigmatic taxa belong to the extinct family †Pachycormidae (the dagger symbol indicates extinct groups), a stem-teleost clade that is otherwise composed of pelagic predators convergent upon tunas and billfishes (*10*). Giant †pachycormids include the largest bony fish of all time (the ~9 m †*Leedsichthys*) (*9*, *13*), but their short stratigraphic range had implied that they were an inconsequential component of

[1]Department of Earth Sciences, University of Oxford, Parks Road, Oxford OX1 3PR, UK. [2]Environmental Science Program and Department of Biological Sciences, DePaul University, 2325 North Clifton Avenue, Chicago, IL 60614, USA. [3]Sternberg Museum of Natural History, Fort Hays State University, 3000 Sternberg Drive, Hays, KS 67601, USA. [4]Natural History Museum and Biodiversity Research Center, University of Kansas, 1345 Jayhawk Boulevard, Lawrence, KS 66045, USA. [5]Division of Ecology and Evolutionary Biology, Faculty of Biomedical and Life Sciences, University of Glasgow University Avenue, Glasgow G12 8QQ, UK. [6]Triebold Paleontology and Rocky Mountain Dinosaur Resource Center, 201 South Fairview Street, Woodland Park, CO 80863, USA.

*To whom correspondence should be addressed. E-mail: mattf@earth.ox.ac.uk

Mesozoic marine ecosystems and a minor—and ultimately unsuccessful—experiment in suspension feeding at large body sizes.

Here, we report newly recognized remains of suspension-feeding †pachycormids ranging from the lower Middle Jurassic to the Upper Cretaceous and discuss the implications of our discoveries for Mesozoic marine ecosystems. With the exception of one recently discovered specimen, these fossils were housed in museum collections in which they were either unstudied or had been described but incorrectly identified in the 19th century. Further preparation and examination, combined with an existing systematic framework (*10*, *12*), led us to revise previous interpretations of this material.

The fossils reported here include a generically indeterminate cranium from the lower Middle Jurassic (Bajocian, 172 to 168 million years ago) Inferior Oolite of Dorset, UK (Fig. 1); the nearly complete skull of †*Rhinconichthys taylori* gen. et sp. nov. (*14*) from the lower Upper Cretaceous (Cenomanian, 100 to 94 million years ago) Lower Chalk of Kent, UK (Fig. 1); a similar fish from the Upper Cretaceous (Cenomanian) Middle Yezo Group of Hokkaido, Japan (*15*); and multiple specimens of †*Bonnerichthys gladius* gen. nov. (*16*) from mid-upper Upper Cretaceous (Coniacian-Maastrichtian, 89 to 66 million years ago) deposits of the Western Interior Seaway and Coastal Plain in the United States (Fig. 2) (*15*, *17*, *18*).

These specimens reveal the anatomy of suspension-feeding †pachycormids, previously known exclusively from poorly understood Jurassic fossils. Material of †*Leedsichthys* is crushed, fragmented, and disarticulated (*9*, *11*), and detailed structure is obscure in rare articulated examples of †*Asthenocormus* (*10*) and †*Martillichthys* (*12*). We base our description on †*Bonnerichthys* (Fig. 2).

The snout is covered by a median rostrodermethmoid, which is a †pachycormid synapomorphy (*10*, *15*, *19*). Two lateral projections along the oral margin are unknown in other forms, but their position suggests that they might be coossified premaxillae. Thickened ridges trace the lateral margins of the rostrodermethmoid, mark the position of the supraorbital canal, and imply that the rostrodermethmoid of †*Bonnerichthys* also incorporates the nasals. The rectangular frontal bears a ridge on its visceral surface, marking the course of the supraorbital sensory canal. The hook-shaped dermosphenotic lies lateral to the frontal, defines the dorsal margin of the orbit, and bears the anastomosis between the infraorbital and otic sensory canals. A triradiate canal-bearing ossification is identified as a dermopterotic. There is no indication of sutural contacts between the dermosphenotic, dermopterotic, and frontal, or between the frontal and the rostrodermethmoid. The condition in †*Bonnerichthys* is derived relative to all other †pachycormids, in which dermal bones of the skull roof are tightly linked.

As in many suspension-feeding fishes (*4*), the dentary of the lower jaw and the maxilla of the upper jaw are elongate and edentulous. Absence of dentition even extends to the prearticular, which lines the inner surface of the mandible, and the parasphenoid, which forms much of the roof of the oral chamber. The parasphenoid is pierced by paired foramina for the internal carotid arteries, a derived feature of teleosts (*15*).

Members of the operculogular series recovered for †*Bonnerichthys* include the opercle, subopercle, and gular plate. The hyoid arch is represented by large, imperforate hyomandibulae with well-developed opercular processes and rod-shaped ceratohyals. Gill-arch remains include hypo- and infrapharyngobranchials with complex articular surfaces, plus long and deeply grooved cerato- and epibranchials. Enlarged gill rakers bearing long, needle-like projections are found in †*Asthenocormus*, †*Leedsichthys*, and †*Rhinconichthys* (*9*, *10*, *12*, *15*). These probable suspension-feeding structures have not yet been recovered for †*Bonnerichthys*.

Typical of †pachycormids, the pectoral fins are scythe-shaped. The leading edge of the fin is fused, with an irregular margin that contrasts with the precisely patterned serrations in some species of †*Protosphyraena* (*10*, *17*, *19*, *20*). Distally, the fin-rays bifurcate in the "Y" pattern characteristic of †pachycormids (*10*, *19*). The pectoral endoskeleton of †*Bonnerichthys* agrees closely with those of †*Orthocormus* (*21*) and †*Protosphyraena* (*20*). The second radial is "C"-shaped, makes two independent articulations with the primary shoulder girdle, and is trailed by a series of paddle-shaped radials (*15*).

The skull of †*Bonnerichthys* specimen KUVP 60692 measures roughly 1 m from the tip of the snout to the rear of the pectoral girdle (Fig. 2C). Isometric scaling relative to articulated fossils of †*Asthenocormus* and †*Martillichthys* (*12*) suggests a total length of approximately 4 m for this specimen. Other less complete remains of †*Bonnerichthys* (associated skeleton University of Nebraska State Museum UNSM 88507 and pectoral fins and girdles KUVP 465) are over 20% larger than equivalent elements of KUVP 60692, indicating that the genus is likely to have reached at least 5 m in length. This is smaller than revised length estimates for †*Leedsichthys* (*13*) but approaches the size of some modern planktivorous chondrichthyans (*4*, *22*).

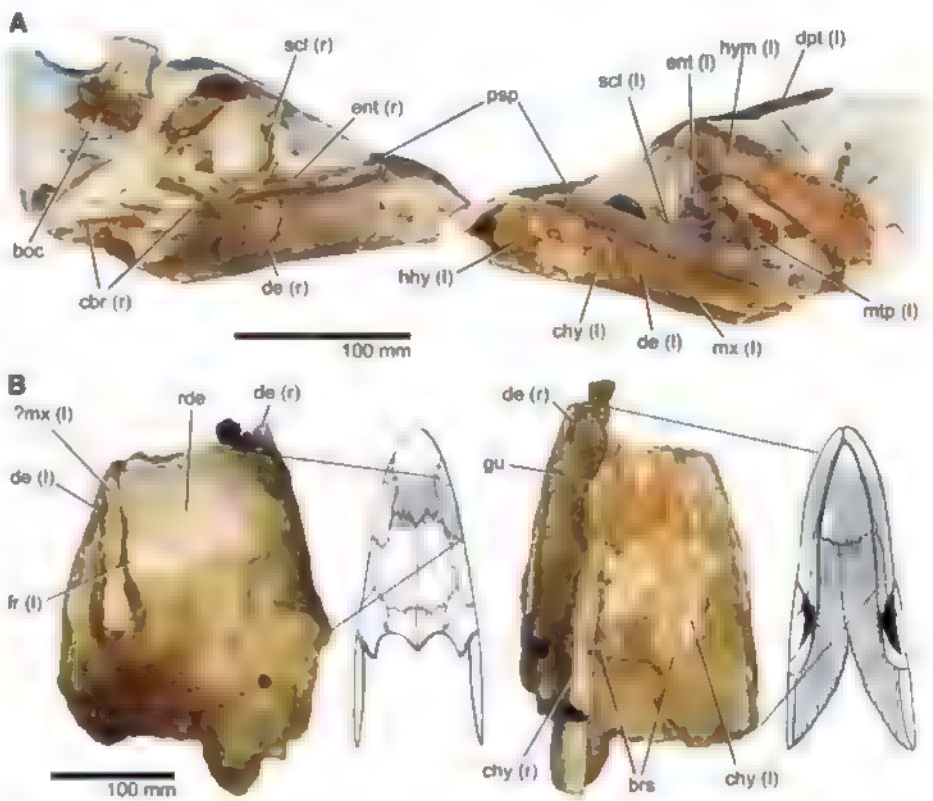

Fig. 1. Newly recognized fossils of giant Mesozoic suspension-feeding bony fishes. (**A**) †*Rhinconichthys taylori* gen. et sp. nov., BMNH 219, from the lower Upper Cretaceous (Cenomanian) Lower Chalk of Kent, UK, in right- and left-lateral views. (**B**) Indeterminate edentulous †pachycormid, BMNH P.41669, from the lower Middle Jurassic (Bajocian) Inferior Oolite of Dorset, UK, in dorsal and ventral view (anterior is toward the top). Matrix has been digitally masked so as to enhance contrast, and preserved bone that would have been visible externally in the ventral and dorsal views is shaded in tentative reconstruction based on †*Martillichthys* and †*Pachycormus*. Scale bars apply only to fossils. boc, basioccipital; brs, branchiostegal rays; cbr, certobranchials, chy, anterior ceratohyal; de, dentary; dpt, dermopterotic; ent, entopterygoid, fr, frontal; gu, median gular; hhy, hypohyal; hym, hyomandibula; mtp, metapterygoid; mx, maxilla; psp, parasphenoid; rde, rostrodermethmoid; and scl, sclerotic ring. Paired bones are listed as right (r) or left (l).

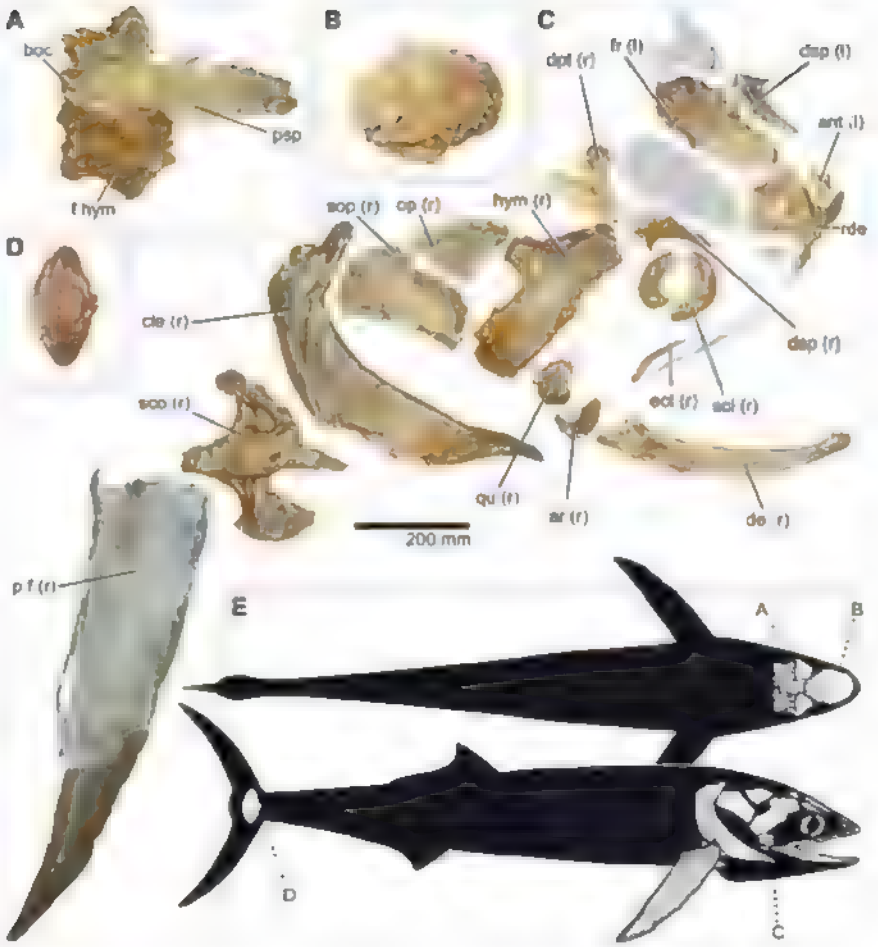

Fig. 2. †*Bonnerichthys gladius* gen. nov., a giant suspension-feeding bony fish from the Upper Cretaceous of the United States. (**A**) Neurocranium and parasphenoid in ventral view. (**B**) Gular plate in ventral view. (**C**) Cranial and pectoral skeleton, shown in right-lateral view. Bones that were reconstructed from other specimens are shown in gray. (**D**) Hypural plate in right-lateral view. Scale bar in (C) applies to (A) to (D). (A) to (C) show specimen KUVP 60692; (D) shows specimen FHSM (Sternberg Museum, Hays, Kansas) VP-17428. (**E**) Tentative reconstruction in ventral (top) and lateral (bottom) views, indicating life position of bones shown in (A) to (D). ant, antorbital; ar, articular; cle, cleithrum; dsp, dermosphenotic; ect, ectopterygoid; f.hym, hyomandibular facet of neurocranium; op, opercle; p.f, pectoral fin; qu, quadrate; sco, scapulocoracoid; and sop, subopercle. Other abbreviations are as in Fig. 1.

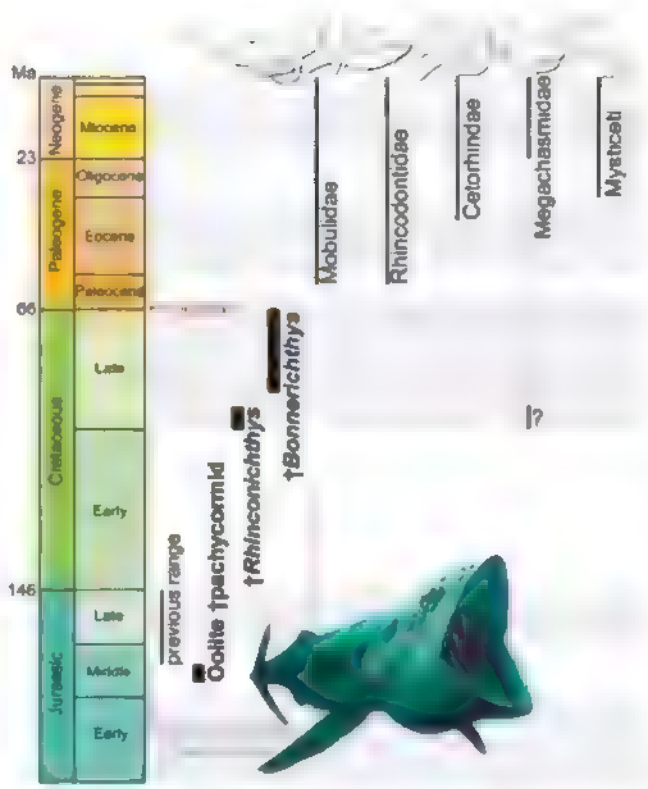

Fig. 3. Stratigraphic distribution of giant †pachycormid fishes and modern planktivorous whales and chondrichthyans (icons of living groups are not shown to scale). Previous occurrences of suspension-feeding †pachycormids were confined to a short interval in the Jurassic (shown as a thin line representing †*Leedsichthys*, †*Martillichthys*, and †*Asthenocormus*), but occurrences reported here (shown as thick lines) expand this group's stratigraphic range to approximately 100 million years. Convincing records of modern large-bodied planktivorous vertebrates only appear in the Paleogene, after the extinction of giant †pachycormids.

A cladistic analysis provides robust support for the monophyly of a clade comprising †*Bonnerichthys* plus other large edentulous †pachycormids and reinforces the interpretation of †pachycormids as stem teleosts (*15*). This subset of †pachycormids is a unique example of suspension feeding at massive body sizes within the teleost total group (*23*), which is a diverse radiation that otherwise contains a bewildering array of bodyplans and whose living representatives are taxonomic dominants in marine vertebrate faunas (*22*). With lengths between 5 and 9 m, †*Bonnerichthys* and †*Leedsichthys* are comparable in size with some modern suspension-feeding sharks (*4*, *22*). Even the more modestly sized †*Martillichthys* and †*Asthenocormus* are ecological giants in comparison with extant planktivorous teleosts. At over 2 m, these †pachycormid genera are an order of magnitude longer—and by extension several orders of magnitude more massive—than living teleost suspension feeders, most of which are on the order of 10 cm long (*23*). The only moderately large planktivorous actinopterygian (the more extensive bony fish clade that contains teleosts) is the paddlefish *Polyodon*. This sturgeon relative is confined to the freshwaters of North America and rarely exceeds 2 m in length despite a greatly elongated rostrum (*24*).

The discovery of early Middle Jurassic and Late Cretaceous †pachycormids with anatomical features that are consistent with suspension feeding (*4*) alters the picture of the evolution of this ecological guild in the Mesozoic and afterward. Oceans during much of this interval have been viewed as devoid of large-bodied suspension feeders (*25*), but we now recognize that †pachycormids occupied this ecological role for much of the Mesozoic (Fig. 3). Marine reptiles diversified prolifically during this geological interval, attaining massive sizes and evolving specializations attributed to suction and ram feeding (*26*), but there is no clear evidence that they ever adopted planktivory. This observation, coupled with the perceived absence of large-bodied planktivores during most of the Mesozoic, led to suggestions that anatomical constraints prevented these otherwise diverse marine amniote clades from exploiting suspension feeding (*25*). Our findings suggest that marine reptiles might have been excluded from this trophic strategy by incumbent †pachycormids.

The first fossil occurrences of modern large-bodied suspension feeders are confined to the Cenozoic: manta rays and whale sharks in the late Paleocene (*1*), basking sharks in the mid-Eocene (*2*), and plankton-feeding whales near the Eocene-Oligocene boundary (*3*). The only example with a possible Mesozoic record is the megamouth shark *Megachasma*, but there is a 75-million-year interval between a few isolated Late Cretaceous teeth and the next oldest occurrence, which dates to the late Oligocene–early Miocene (*27*). The radiation of large-bodied suspension-feeding chondrichthyans and whales in the Paleogene follows the disappearance of †*Bonnerichthys* and many other large-bodied marine teleosts (*28*, *29*) during the end-Cretaceous extinction, suggesting that familiar modern groups of planktivores diversified into the ecospace vacated by giant †pachycormids.

References and Notes

1. H. Cappetta, C. Duffin, J. Zidek, in *The Fossil Record 2*, M. Benton, Ed. (Chapman & Hall, London, 1993), pp. 593–609
2. A. L. Cione, M. A. Reguero, *Antarct. Sci.* **10**, 83 (1998)
3. E. M. G. Fitzgerald, *Proc. Biol. Sci.* **273**, 2955 (2006)
4. S. L. Sanderson, R. Wassersug, in *The Skull*, vol. 3, J. Hanken, B. K. Hall, Eds. (Univ. of Chicago Press, Chicago, IL, 1993), pp. 37–112
5. S. N. Jarman, *Biol. J. Linn. Soc. Lond.* **73**, 199 (2001)
6. P. G. Fakowski *et al.*, *Science* **305**, 354 (2004)
7. A. Bartholomai, *Mem. Queensl. Mus.* **49**, 521 (2004)
8. L. Cavin, P. L. Forey, in *Mesozoic Fishes 4—Homology and Phylogeny*, G. Arratia, H.-P. Schultze, M. V. H. Wilson, Eds. (Verlag Dr. Friedrich Pfeil, München, 2008) pp. 199–216
9. D. M. Martill, N. Jahrb. *Geol. Palaeontol.* **1988**, 670 (1988)
10. P. Lambers, thesis, Rijksuniversiteit Groningen, Groningen, Netherlands (1992)
11. J. Liston, in *Mesozoic Fishes 3—Systematics, Paleoenvironments and Biodiversity*, G. Arratia, A. Tintori, Eds. (Verlag Dr. Friedrich Pfeil, München, 2004), pp. 379–390
12. J. Liston, in *Mesozoic Fishes 4—Homology and Phylogeny*, G. Arratia, H.-P. Schultze, M. V. H. Wilson, Eds. (Verlag Dr. Friedrich Pfeil, München, 2008), pp. 181–198
13. J. J. Liston, L. F. Noè, *Arch. Nat. Hist.* **31**, 236 (2004)
14. Etymology: The generic name is a homophone of an unpublished name by G. Martell (*"Rhynchonichthys"*) and evokes the whale shark *Rhincodon*. The specific name honors H. W. Taylor, collector of the type. Systematics: Osteichthyes Huxley, 1880; Actinopterygii Woodward, 1891, Teleostei Müller, 1846 (*sensu* de Pinna 1996), †Pachycormidae Woodward, 1895; and †*Rhinconichthys taylori* gen. et sp. nov. Holotype: BMNH (The Natural History Museum, London) 219, nearly complete three-dimensional skull lacking anterior skull roof and posterior portions of lower jaws. Diagnosis of genus and species: Edentulous †pachycormid differing from other members of that group in having exceptionally elongated posterior processes of the dermopterotics and a proximal head of hyomandibula rounded rather than laterally compressed. Locality and age: Lower Chalk (Late Cretaceous, Cenomanian), Burham, Kent, UK.
15. Materials and methods are available as supporting material on *Science* Online.
16. Etymology: The generic name honors the Bonner family, Scott City, Kansas, which has made many important discoveries in the Niobrara Formation, including KUVP (University of Kansas Natural History Museum, Lawrence, Kansas) 60692. Systematics: Osteichthyes Huxley, 1880; Actinopterygii Woodward, 1891, Teleostei Müller, 1846 (*sensu* de Pinna 1996); †Pachycormidae Woodward, 1895; †*Bonnerichthys* nov. gen., and †*Bonnerichthys gladius* (Cope, 1874), comb. nov. Holotype: AMNH (American Museum of Natural History, New York) FF 1849, incomplete pectoral fin. Diagnosis of genus and species: Edentulous †pachycormid differing from other members of that group in having a rostrodermethmoid with ventrolateral processes, basioccipital with deep aortic groove, dermal bones of skull unsutured, and anterior margins of pectoral fins irregularly crenellated. Locality and age: Type from Niobrara Formation (Late Cretaceous, Coniacian-Campanian), Kansas, USA.
17. J. D. Stewart, in *Geology, Paleontology and Biostratigraphy of Western Kansas*, M. E. Nelson Ed. (Fort Hays State Univ., Hays, KS, 1988), pp. 80–94.
18. D. C. Parris, B. S. Grandstaff, W. B. Gallagher, *Spec. Pap. Geol. Soc. Am.* **427**, 99 (2007)
19. A. J. Mainwaring, thesis, Westfield College, University of London, London, UK (1978)
20. A. S. Woodward, *The Fossil Fishes of the English Chalk* (Palaeontographical Society, London, UK, 1902)
21. H. L. Jessen, *Fossils Strata* **1**, 1 (1972)
22. J. S. Nelson, *Fishes of the World* (Wiley, Hoboken, NJ, 2006)
23. J. A. Freedman, D. L. G. Noakes, *Rev. Fish Biol. Fish.* **12**, 403 (2002)
24. L. M. Page, B. M. Burr, *A Field Guide to Freshwater Fishes of North America and North of Mexico* (Houghton Mifflin, Boston, 1991)
25. R. Colin, C. M. Janis, in *Ancient Marine Reptiles*, J. M. Callaway, E. L. Nicholls, Eds. (Academic Press, San Diego, CA, 1997), pp. 451–466
26. E. M. Nicholls, M. Manabe, *J. Vertebr. Paleontol.* **24**, 838 (2004)
27. K. Shimada, *J. Vertebr. Paleontol.* **27**, 512 (2007)
28. L. Cavin, in *Geological and Biological Effects of Impact Events*, E. Buffetaut, C. Koeberl, Eds. (Springer Verlag, Berlin, 2001), pp. 141–158
29. M. Friedman, *Proc. Natl. Acad. Sci. U.S.A.* **106**, 5218 (2009)

30. M.F. was funded by an Environmental Protection Agency Science to Achieve Results Fellowship (award FP916730). We thank T. Uyeno and M. Manabe for provenance data for the Japanese pachycormid, S. Moore-Fay for exacting specimen preparation, R. Nicholls for his reconstruction of †*Bonnerichthys*, and M. Brazeau, L. Sallan, and three anonymous reviewers for their constructive comments.

Supporting Online Material

www.sciencemag.org/cgi/content/full/327/5968/990/DC1
SOM Text
Figs. S1 to S15
References

16 November 2009; accepted 25 January 2010
10.1126/science.1184743

Climate, Critters, and Cetaceans: Cenozoic Drivers of the Evolution of Modern Whales

Felix G. Marx[1,2]* and Mark D. Uhen[3]

Modern cetaceans, a poster child of evolution, play an important role in the ocean ecosystem as apex predators and nutrient distributors, as well as evolutionary "stepping stones" for the deep sea biota. Recent discussions on the impact of climate change and marine exploitation on current cetacean populations may benefit from insights into what factors have influenced cetacean diversity in the past. Previous studies suggested that the rise of diatoms as dominant marine primary producers and global temperature change were key factors in the evolution of modern whales. Based on a comprehensive diversity data set, we show that much of observed cetacean paleodiversity can indeed be explained by diatom diversity in conjunction with variations in climate as indicated by oxygen stable isotope records ($\delta^{18}O$).

Modern cetaceans (Neoceti), the mysticetes and odontocetes, show a number of mass-feeding adaptations beyond the immediate demands of an aquatic existence (*1*). Whereas mysticetes have become edentulous and rely on baleen to filter food from the water, odontocetes have evolved the ability to search for prey by means of echolocation. What unites these two different adaptive strategies is their effectiveness in terms of mass feeding: Whereas mysticetes obtain enormous amounts of small prey by filtering vast quantities of water, odontocetes may be able to use their biosonar to locate the vertically migrating layers of plankton with their associated grazers and predators known as deep scattering layers (*1*). To support such large and abundant apex predators, the ecosystems exploited by cetaceans must be extremely productive, and the energy captured by primary producers must be transmitted very efficiently

through the food web (*2*). Compared with photosynthetic bacteria and nannoplankton, diatoms, the dominant marine producers of today, are relatively large organisms (*3*) and are thus likely to be at the base of a food web with relatively fewer intermediate consumers (*1*, *2*). This shortening of the food web reduces the amount of trophic fractionation between the original photosynthetic event and the final consumption by apex predators, such as cetaceans, thus allowing the latter to forage more efficiently and grow larger, more abundant, and more diverse as a result (*1*).

We investigated whether the rise of diatoms to dominance may have triggered the radiation of neocetes (*1*) by fitting a set of a priori models (Table 1) to a comprehensive genus-level cetacean diversity data set ($n = 204$) downloaded from the Paleobiology Database (*4*), as well as by assessing the explanatory power of the different models using the second-order Akaike's Information Criterion (AIC_c) and Akaike weights (w_i) (*5*, *6*). Apart from diatom and nannoplankton species diversity, which we downloaded from the Neptune database (*7*) (comparable dinoflagellate data were unavailable), our set of potential predictors also comprised oxygen isotope records (expressed as $\delta^{18}O$ values), a proxy reflecting both temperature and global ice volume (*8*). These records allowed us to test for the effect of primary production (*1*) and climate change (*9*), respectively. In addition, we included two measures of global marine rock abundance to account for the potentially biasing effect of the variable amount of preserved sedimentary rock on our cetacean diversity data (*10*). Our first estimate consisted of the total number of fossiliferous marine formations; our second estimate was a subset of the former and included only those formations that have produced any vertebrate fossils, to account for potential preservational biases. Both were downloaded from the Paleobiology Database (*4*).

In addition to the sampled-in-bin cetacean diversity data, we also included a biologically adjusted diversity estimate in our analysis to investigate whether this would result in a strengthening of any observed relationships between the diversity and environmental data. For this adjusted estimate, taxa were ranged through time bins in which they had not actually been sampled, provided that the taxon in question had already been recorded in at least one earlier and one later bin. We accounted for variations in stage length by including stage duration as a nonoptional predictor in all our models. Furthermore, we accounted for non-normality and nonconstant variances, which are often associated with count data like ours, by square-root-transforming cetacean diversity in all analyses, and for temporal autocorrelation by fitting autoregressive models to our original data and using generalized least squares where appropriate (*4*). We ran two sets of models based on our two estimates of rock abundance. However, because the results of both sets were similar, we decided to focus on the total number of marine formations [see (*4*) for further details].

Out of our models, the combination of diatom species diversity and $\delta^{18}O$ values was most strongly associated with cetacean diversity (Fig. 1 and Table 1). This was true for the sampled-in-bin data both for the whole of Neoceti and for mysticetes and odontocetes viewed separately, with mysticete diversity being particularly well predicted by this model (Tables 1 and 2). By contrast, we could not clearly distinguish between the model including diatom diversity and $\delta^{18}O$ only and the model including diatom diversity, $\delta^{18}O$, and rock abundance as far as the ranged-through data were concerned, the latter model having an Akaike weight of nearly 0.1. Because the diatom and $\delta^{18}O$ model is nested within the latter, we were able to test whether the more parameter-rich model explained our data significantly better by using a likelihood ratio test. This test showed a significant improvement of the model also including rock abundance over the model including just diatom diversity and $\delta^{18}O$ for the neocete ranged-through data ($\chi^2 = 6.50$, $P = 0.011$) but not for the sampled-in-bin data ($\chi^2 = 0.02$, $P = 0.879$). Interestingly, in all of the favored models the link between phytoplankton and cetacean diversity was restricted to diatoms only, as nannoplankton failed to explain much of the variance in the cetacean data both on its own and in combination with diatoms.

The link between diatom diversity and observed cetacean diversity supports the hypothesis that diatom-based primary production has been an important driver of neocete evolution (*1*). Similarly, the observation that climate change also has a role to play is not surprising in light of recent research that has demonstrated substantial temperature-dependent variations in the diversity of extant cetaceans (*9*). Finally, the observation that the model including diatom diversity and $\delta^{18}O$ seems to explain mysticete diversity relatively better than odontocete diversity is reasonable, consid-

[1]Department of Geology, University of Otago, 360 Leith Walk, Post Office Box 56, Dunedin, Otago 9016, New Zealand. [2]Department of Earth Sciences, University of Bristol, Wills Memorial Building, Queen's Road, Bristol BS8 1RJ, UK. [3]Department of Atmospheric, Oceanic, and Earth Sciences, George Mason University, MS 5F1, Fairfax, VA 22030, USA.

*To whom correspondence should be addressed. E-mail: f.g.marx@bristol.ac.uk

Table 1. Comparison of a number of a priori models attempting to explain cetacean paleodiversity based on the PaleoDB diversity data as sampled per bin. $\delta^{18}O$, oxygen isotope records used as proxy for climate change (*8*); diatom, diatom species diversity (Neptune database) (*7*); nanno, nannoplankton species diversity (Neptune database) (*7*); rock, total number of fossiliferous marine formations as downloaded from the PaleoDB (*4*). All models also included geologic stage duration as a nonoptional predictor to account for the potentially biasing effect of unequal Cenozoic stage durations. The R^2 shown is the generalized R^2 proposed by (*26*) and (*27*). The preferred models are shown in bold.

Model	R^2	P	AIC_c	ΔAIC	w_i	Model	R^2	P	AIC_c	ΔAIC	w_i
	Neoceti sampled-in-bin						Neoceti ranged-through				
Rock	0.05	0.753	53.37	12.37	<0.01	Rock	0.07	0.681	51.06	14.13	<0.01
Diatom	0.28	0.169	50.38	9.38	<0.01	Diatom	0.50	0.057	46.30	9.38	<0.01
Nanno	0.07	0 686	53.18	12.18	<0.01	Nanno	0.33	0.214	49 35	12.43	<0.01
Diatom, nanno	0.35	0.191	56.51	15.51	<0.01	Diatom, nanno	0.50	0.104	53 47	16 54	<0.01
Rock, diatom	0.36	0.179	56.36	15.36	<0.01	Rock, diatom	0.58	0.024	49.69	12.76	<0.01
Rock, $\delta^{18}O$	0.09	0.801	60.27	19.27	<0.01	Rock, $\delta^{18}O$	0.07	0.857	58.39	21.47	<0.01
Diatom, $\delta^{18}O$	**0.84**	**<0.001**	**41.00**	**0.00**	**0.98**	Diatom, $\delta^{18}O$	**0.87**	**<0.001**	**36.93**	**0.00**	**0.89**
Rock, diatom, $\delta^{18}O$	0.84	<0.001	51.98	10.98	<0.01	Rock, diatom, $\delta^{18}O$	**0.93**	**<0.001**	**41.43**	**4.50**	**0.09**
	Mysticeti sampled-in-bin						Odontoceti sampled-in-bin				
Rock	0.01	0.971	43.00	32.18	<0.01	Rock	0.06	0.700	50.76	11.34	<0.01
Diatom	0.67	0.017	35.00	24.18	<0.01	Diatom	0.26	0.193	48 18	8.76	0 01
Nanno	0.11	0.516	41.74	30.91	<0.01	Nanno	0.06	0.704	50.77	11.35	<0.01
Diatom, nanno	0.76	0.008	38.76	27.94	<0.01	Diatom, nanno	0.39	0.141	53.34	13.92	<0.01
Rock, diatom	0.84	0.001	34.13	23.31	<0.01	Rock, diatom	0.34	0.210	54.29	14.86	<0.01
Rock, $\delta^{18}O$	0.03	0.945	50.02	39.20	<0.01	Rock, $\delta^{18}O$	0.09	0.787	57.75	18.32	<0.01
Diatom, $\delta^{18}O$	**0.98**	**<0.001**	**10.82**	**0.00**	**0.99**	Diatom, $\delta^{18}O$	**0.86**	**<0.001**	**39.42**	**0.00**	**0.98**
Rock, diatom, $\delta^{18}O$	0.98	<0.001	21.38	10.56	<0.01	Rock, diatom, $\delta^{18}O$	0.86	<0.001	50.41	10.99	<0.01

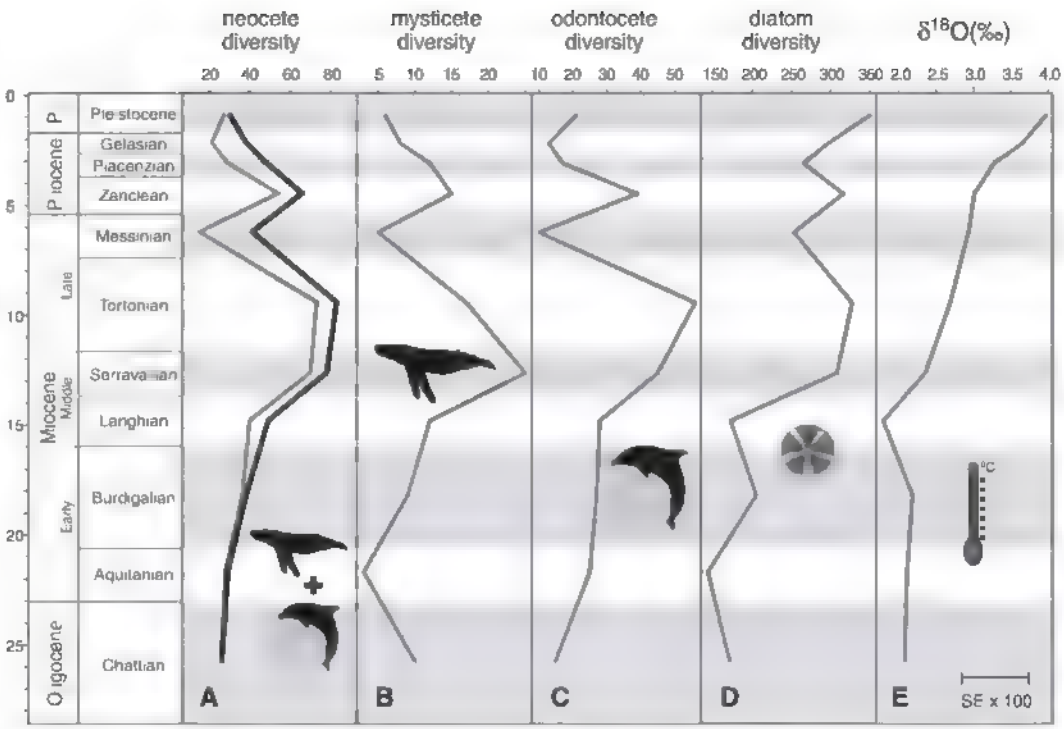

Fig. 1. Comparison of neocete (**A**), mysticete (**B**), and odontocete (**C**) paleodiversity with diatom paleodiversity (**D**) and global $\delta^{18}O$ values (**E**). Cetacean diversity is shown as sampled-in-bin data as downloaded from the Paleobiology Database (gray) and as a ranged-through estimate (black). Error for the $\delta^{18}O$ curve is shown as mean standard error (SE) multiplied by 100. The picture of a diatom is after Haeckel (*28*).

ering the relatively lower trophic levels (copepods, krill, and small fish) that many mysticetes feed on (*11*). Because these results depend on our choice of environmental and biological variables used as predictors here, they could substantially change if other or additional variables were used. Nonetheless, our study offers an entirely biological explanation of cetacean diversity, which, if correct, would seem to imply that the abundance of fossiliferous rock, previously proposed to affect or even overwhelm any biological signal in paleodiversity data sets (*10*, *12*–*14*), does not exert a major bias on cetacean paleodiversity.

One peculiar observation is the curious increase in explanatory power of rock abundance in combination with diatom diversity and $\delta^{18}O$ when the ranged-through data were used. Aside from the possibility of this being a coincidence, such an increase in fit in the face of a crude (fig. S1) but inherently biologically motivated correction of paleodiversity seems counterintuitive. One potential explanation might be found in the way the effects of rock abundance are commonly interpreted. Although often treated as a simple bias (*10*, *12*), it has also been proposed that both rock abundance and diversity may be influenced by a common third factor, such as sea-level change (*15*), thus potentially making rock abundance a covariate, rather than a determinant of observed cetacean diversity. Assuming that enough rock has been preserved per stage to overcome an initial and inevitable small-scale link between rock abundance and the number of fossil cetacean taxa preserved, it might thus be expected that in the presence of presumably genuine drivers of diversity, such as plankton abundance or climate change, rock abundance should explain none or hardly any of the diversity patterns observed. However, the amount of preserved sedimentary rock may be influenced by a complex interplay of factors, such as changes in sea-level or climate, influencing both deposition and erosion, all of which may also have an effect on cetacean diversity to various degrees. Assuming the ranged-through estimate to be a better reflection of actual cetacean paleodiversity than the data as sampled per bin, it might thus be possible that the increase in the explanatory power of rock abundance might reflect the effects of one or more genuine common-cause drivers of both cetacean evolution and rock abundance not represented in our models. This view may be supported by the negative coefficient for rock abundance in our ranged-through model (Table 2), which implies that an increase in rock abundance is linked with a decrease in neocete diversity—an observation clearly inconsistent with the interpretation of the latter as a simple bias, at least in the case of cetacean paleodiversity.

Table 2. Estimated best-fit model parameters for the neocete, mysticete, and odontocete data sets. $\delta^{18}O$, oxygen isotope records used as proxy for climate change (*8*); diatom, diatom species diversity (Neptune database) (*7*); rock, total number of fossiliferous marine formations as downloaded from the Paleobiology Database (*4*); st. dur., geologic stage duration; the latter was included as a nonoptional predictor in all models to account for the potentially biasing effects of unequal Cenozoic stage durations.

	Neoceti sampled-in-bin		Neoceti ranged-through		Mysticeti sampled-in-bin		Odontoceti sampled-in-bin	
	Estimate	SE	Estimate	SE	Estimate	SE	Estimate	SE
Intercept	6.694	1.465	6.649	1.111	2.214	0.179	5.566	1.179
St. dur.	−0.047	0.189	−0.068	0.167	0 096	0.023	0.049	0.166
Diatom	0.029	0.005	0.028	0.003	0 015	<0 001	0.020	0.003
$\delta^{18}O$	−2.881	0.577	−2.253	0.422	−1 077	0.081	−2.147	0.351
Rock	–	–	−0.013	0.006	–	–	–	–

One prominent hypothesis regarding the evolution of neocetes is that the onset of the Antarctic Circumpolar Current (ACC) may have triggered the radiation of modern whales by greatly increasing the availability of nutrients in the upper layers of the sea through deep mixing in the Southern Ocean (*1*, *16*–*19*). Indeed, the effects of the ACC provide the Southern Ocean with one of the highest surface concentrations of silica, the major component of diatom frustules, anywhere in the world (*20*, *21*). Although most of this silica is used up by local diatom growth, the water leaving the area in the form of Subantarctic Mode Water still supplies high concentrations of other nutrients, such as nitrate, to the world's oceans, supporting as much as 75% of global export production north of 30°S in the process (*20*). Together with local sources of silica, particularly in the North Pacific (*20*), the ACC thus seems to offer a credible mechanism supporting the high rates of biological production needed to sustain large apex predators such as cetaceans. Although paleontological evidence suggests that neocetes appeared and possibly started to radiate in the latest Eocene

close to the Eocene-Oligocene boundary (*22*, *23*), the time of the actual establishment of the ACC is still a matter of debate (*24*, *25*), and thus no firm conclusion can be drawn. However, our results imply that, if the onset of the ACC indeed triggered the evolution and diversification of neocetes, it likely must have done so through a great increase in diatom-based productivity, possibly by increasing the bioavailability of silica and other nutrients in the Southern Ocean and coastal upwelling zones around the world through deep-mixing occurring around Antarctica (*1*).

References and Notes

1. W. H. Berger, *Deep Sea Res. Part II Top. Stud. Oceanogr.* **54**, 2399 (2007).
2. J. H. Ryther, *Science* **166**, 72 (1969).
3. C. Le Quéré *et al.*, *Glob. Change Biol.* **11**, 2016 (2005).
4. Materials and methods are available as supporting material on *Science* Online.
5. N. Sugiura, *Comm. Statist. Theory Methods* **7**, 13 (1978).
6. K. P. Burnham, D. R. Anderson, *Model Selection and Multimodel Inference: A Practical Information-Theoretic Approach* (Springer, New York, 2001).
7. C. Spencer-Cervato, *Palaeontol. Electronica* **2**, 1 (1999).
8. J. C. Zachos, G. R. Dickens, R. E. Zeebe, *Nature* **451**, 279 (2008).
9. H. Whitehead, B. McGill, B. Worm, *Ecol. Lett.* **11**, 1198 (2008).
10. A. B. Smith, A. J. McGowan, *Paleontology* **50**, 765 (2007).
11. J. L. Bannister, in *Encyclopedia of Marine Mammals* 2nd ed., W. F. Perrin, B. Würsig, J. G. M. Thewissen, Eds. (Academic Press, Burlington, MA, 2008) pp. 80–89.
12. P. M. Barrett, A. J. McGowan, V. Page, *P. R. Soc. B* **276**, 2667 (2009).
13. S. E. Peters, M. Foote, *Paleobiology* **27**, 583 (2001).
14. J. S. Crampton *et al.*, *Science* **301**, 358 (2003).
15. S. E. Peters, *Proc. Natl. Acad. Sci. U.S.A.* **102**, 12326 (2005).
16. J. H. Lipps, E. D. Mitchell, *Paleobiology* **2**, 147 (1976).
17. R. E. Fordyce, *Palaeogeogr. Palaeocl.* **21**, 265 (1977).
18. R. E. Fordyce, *Palaeogeogr. Palaeocl.* **31**, 319 (1980).
19. R. E. Fordyce, in *From Greenhouse to Icehouse: The Marine Eocene-Oligocene Transition*, D. R. Prothero, L. C. Ivany, E. A. Nesbitt, Eds. (Columbia Univ. Press, New York, 2003), 154–170.
20. J. L. Sarmiento, N. Gruber, M. A. Brzezinski, J. P. Dunne, *Nature* **427**, 56 (2004).
21. P. Pondaven, D. Ruiz-Pino, J. N. Druon, C. Fravalo, P. Treguer, *Deep Sea Res. Part I Oceanogr. Res. Pap.* **46**, 1923 (1999).
22. E. D. Mitchell, *Can. J. Fish. Aquat. Sci.* **46**, 2219 (1989).
23. R. E. Fordyce, *J. Vertebr. Paleontol.* **23** (Suppl. 3), 50A (2003).
24. P. F. Barker, E. Thomas, *Earth Sci. Rev.* **66**, 143 (2004).
25. P. F. Barker, G. M. Filippelli, F. Florindo, E. E. Martin, H. D. Scher, *Deep Sea Res. Part II Top. Stud. Oceanogr.* **54**, 2388 (2007).
26. G. S. Maddala, *Limited-Dependent and Qualitative Variables in Econometrics*, (Cambridge Univ. Press, 1983).
27. N. J. D. Nagelkerke, *Biometrika* **78**, 691 (1991).
28. E. Haeckel, *Kunstformen der Natur* (Bibliographisches Institut, Leipzig, 1899–1904).

29. We thank three referees for their comments, as well as G. Hunt for advice and help with R programming and M. Katz for the provision of data. L. Kavalieris, I. Jolliffe, M. Carrano, D. Thomas, M. Benton, and the participants of the August 2009 Encyclopedia of Life synthesis meeting on marine tetrapod evolution at the Field Museum, Chicago, provided advice and helpful discussions about earlier versions of this work and related topics. F.M. was supported by a University of Otago Postgraduate Scholarship. This is Paleobiology Database publication 108.

Supporting Online Material

www.sciencemag.org/cgi/content/full/327/5968/993/DC1
Materials and Methods
Fig. S1
Tables S1 to S3
References

7 December 2009; accepted 25 January 2010
10.1126/science.1185581

Regulation of Alternative Splicing by Histone Modifications

Reini F. Luco,[1] Qun Pan,[2] Kaoru Tominaga,[3] Benjamin J. Blencowe,[2] Olivia M. Pereira-Smith,[3] Tom Misteli[1]*

Alternative splicing of pre-mRNA is a prominent mechanism to generate protein diversity, yet its regulation is poorly understood. We demonstrated a direct role for histone modifications in alternative splicing. We found distinctive histone modification signatures that correlate with the splicing outcome in a set of human genes, and modulation of histone modifications causes splice site switching. Histone marks affect splicing outcome by influencing the recruitment of splicing regulators via a chromatin-binding protein. These results outline an adaptor system for the reading of histone marks by the pre-mRNA splicing machinery

Most human genes are alternatively spliced in a cell type– and tissue-specific manner, and defects in alternative splicing (AS) contribute to disease (*1*–*4*). Pre-mRNA splicing occurs largely cotranscriptionally, and alternative splice site choice is influenced by RNA polymerase II elongation rate, chromatin remodelers, and histone deacetylase inhibitors (*5*–*14*). Genome-wide mapping of histone modifications has revealed nonrandom distributions of nucleosomes and several histone modifications across exons (*15*–*19*). Given these observations, we probed the role of histone modifications in AS.

[1]National Cancer Institute, National Institutes of Health, Bethesda, MD 20892, USA. [2]Banting and Best Department of Medical Research, Terrence Donnelly Centre for Cellular and Biomolecular Research, University of Toronto, Toronto, Ontario M5S 3E1, Canada. [3]The Barshop Institute for Longevity and Aging Studies, Department of Cellular and Structural Biology, University of Texas Health Science Center, San Antonio, TX 78245-3207, USA.

*To whom correspondence should be addressed. E-mail: mistelit@mail.nih.gov

The human fibroblast growth factor receptor 2 (*FGFR2*) gene is an established AS model, in which exons IIIb and IIIc undergo mutually exclusive and tissue-specific AS (Fig. 1A) (*20*, *21*). In human prostate normal epithelium cells (PNT2s), exon IIIb is predominantly included, whereas in human mesenchymal stem cells (hMSCs), it is repressed and exon IIIc is exclusively used (Fig. 1, A and B). The differential inclusion of these two exons is regulated by the polypyrimidine tract–binding protein (PTB) which binds to silencing elements around exon IIIb, resulting in its repression (*20*, *22*). We comparatively mapped by quantitative chromatin immunoprecipitation a set of histone modifications across the alternatively spliced region in PNT2 cells and hMSCs (Fig. 1, C to H, and fig. S1, A to F). No differences in the levels of H3-K4me2, H3-K9ac, H3-K27ac, and pan-H4ac histone modifications were detected (Fig. 1H and fig. S1, D to F). In contrast, H3-K36me3 and H3-K4me1 were enriched over the *FGFR2* gene in hMSCs, where exon IIIb is repressed, whereas H3-K27me3, H3-K4me3, and H3-K9me1 were reduced as compared to PNT2 cells, where the exon is included (Fig. 1, C to G, and fig. S1, A to C). Histone mark enrichments were not limited to the alternatively spliced exons but extended along the locus with the highest differences around the alternatively spliced region (Fig. 1 and fig. S1).

Several other PTB-dependent alternatively spliced exons (*23*), including tropomyosin 2 (TPM2) exon 7 and TPM1 exon 3 in hMSCs and pyruvate kinase type M2 (PKM2) exon 9 in PNT2 cells, exhibited similar splicing-specific histone modification patterns (fig. S2), whereas PTB-independent alternative exons or constitutively spliced genes did not (figs. S3 and S4). Chromatin signatures correlated with the inclusion pattern of the PTB-dependent exon regardless of cell type or steady-state transcription levels of the alternatively spliced genes (Fig. 1 and figs. S2 and S3). These observations reveal a correlation between histone mark signatures and PTB-dependent repression of alternatively spliced exons.

To investigate whether histone modifications have a causal role in alternative splice site selection, we modulated the levels of H3-K36me3, which is the most prominently enriched modification on *FGFR2*. Overexpression of the H3-K36 methyltransferase SET2 led to a significant increase in H3-K36me3 globally and along *FGFR2* in both PNT2 and hMSC cells (Fig. 2A and fig. S5, A and B) and, consistent with a role of H3-K36me3 in alternative splice site selection, reduced the inclusion of PTB-dependent exons in *FGFR2*, *TPM2*, *TPM1*, and *PKM2* mRNA (Fig. 2B and figs. S6, A to D, and S7, A to C). Usage of PTB-independent alternatively spliced exons and constitutive splicing were unaffected (Fig. 2, C and D, and fig. S8, A and B). Overexpression of SET2 also significantly reduced the inclusion of FGFR2 IIIb in HEK 293 cells, where both isoforms are included to a similar extent, demonstrating that H3-K36me3–mediated modulation of

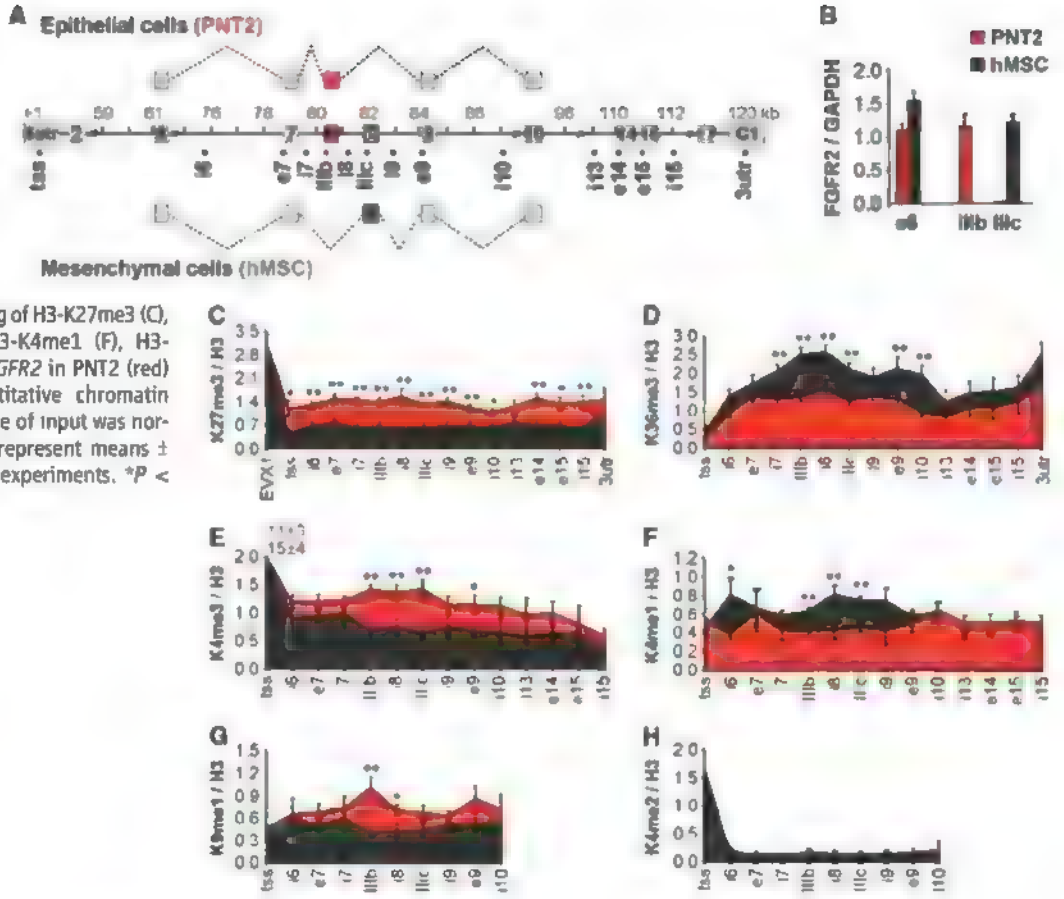

Fig. 1. Splicing-specific histone modifications. (**A**) Schematic representation of the human *FGFR2* gene. Exon IIIb (red) is included in PNT2 epithelial cells, exon IIIc (black) is included in hMSCs. Square dots indicate oligonucleotide pairs used in analysis. (**B**) Levels of FGFR2 exon inclusion relative to GAPDH in PNT2 (red) or hMSCs (black) determined by quantitative polymerase chain reaction (PCR). (**C** to **H**) Mapping of H3-K27me3 (C), H3-K36me3 (D), H3-K4me3 (E), H3-K4me1 (F), H3-K9me1 (G), and H3-K4me2 (H) in *FGFR2* in PNT2 (red) and hMSC (black) cells by quantitative chromatin immunoprecipitation. The percentage of input was normalized to unmodified H3. Values represent means ± SEM from four to six independent experiments. $^{*}P < 0.05$, $^{**}P < 0.01$, Student's *t* test.

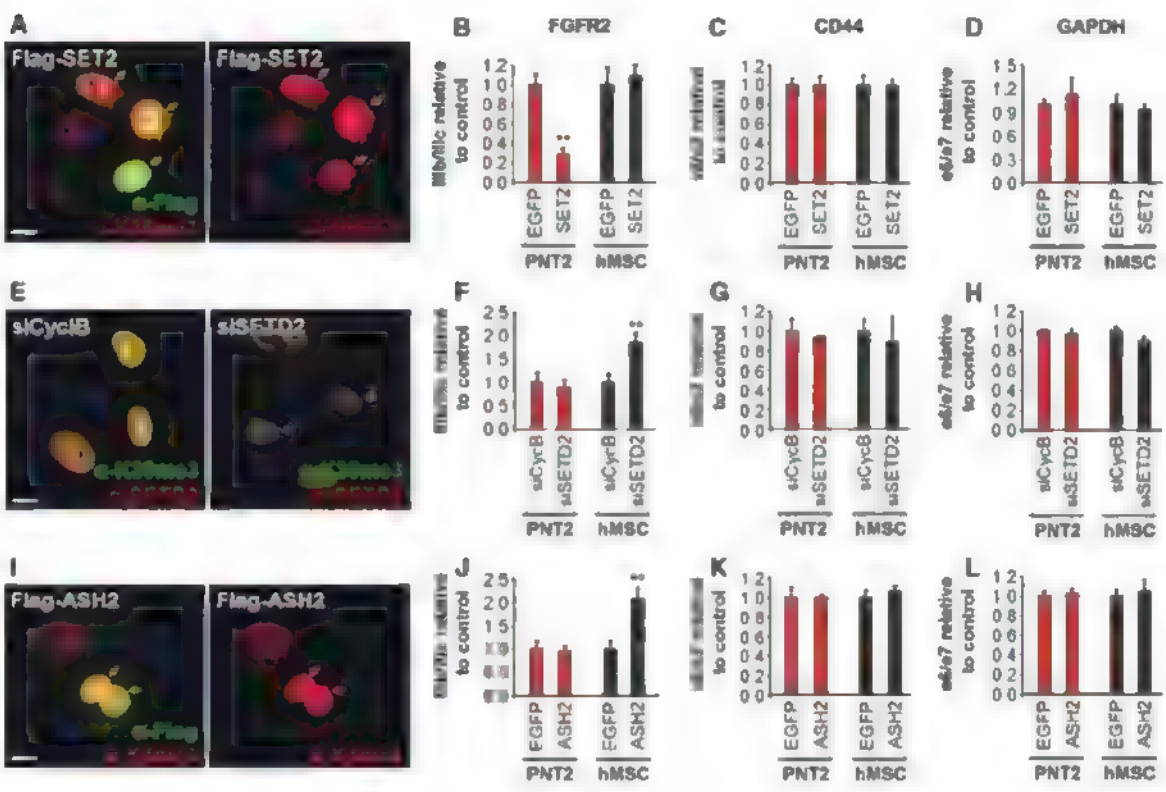

Fig. 2. Modulation of alternative splicing by histone modifications. (**A**, **E**, and **I**) H3-K36me3 levels after SET2/SETD2 modulation [(A) and (E)] and H3-K4me3 after ASH2 overexpression (I). Arrows indicate transfected cells. Scale bar, 10 μm. (**B** to **D**, **F** to **H**, and **J** to **L**) Quantitative reverse transcription PCR (RT-PCR) analysis of exon ratios after overexpression of Flag-SET2 [(B) to (D), SET2], down-regulation of SETD2 [(F) to (H), siSETD2], or overexpression of Flag-ASH2 [(J) to (L), ASH2] in PNT2 (red) or hMSC cells (black). Ratios are as follows: exon IIIb/IIIc for FGFR2, exon v6/e2 for CD44, and exon e6/e7 for GAPDH. Values represent means ± SEM of percentages relative to EGFP or siCyclophilin B used as controls from four to six independent experiments. $^{**}P < 0.01$, Student's *t* test compared to control.

Fig. 3. MRG15 modulates alternative splicing. (**A** and **B**) Chromatin immunoprecipitation of MRG15 along FGFR2 (A) and CD44 (B) in PNT2 (red) and hMSC (black) cells. Input was normalized to unmodified H3. The RPL13a promoter was a positive control. Values represent means ± SEM from three to six independent experiments. (**C** to **F**) Quantitative RT-PCR analysis of exon ratios after overexpression of EGFP-MRG15 [(C) and (D), MRG15] or down-regulation of both MRG15 and MRGX [(E) and (F), siMRG] in PNT2 (red) or hMSC (black) cells. Ratios are as follows: exon IIIb/IIIc for FGFR2 and exon v6/e2 for CD44. Values represent means ± SEM of percentages relative to EGFP or siCyclophilin B used as controls from five independent experiments. *P<0.05, **P<0.01, Student's t test compared to control.

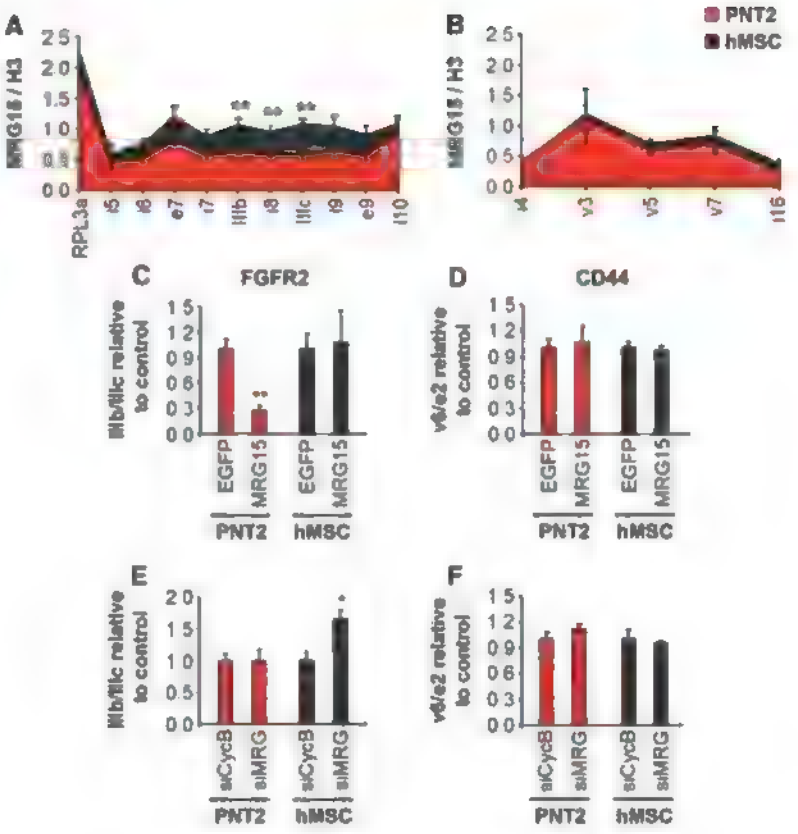

Fig. 4. H3-K36me3 recruits PTB to exon IIIb via MRG15. (**A**) Immunoblot detection of PTB and MRG15 after immunoprecipitation of PTB. (**B**) Reciprocal coimmunoprecipitation of overexpressed MRG15-V5/His and PTB-HA in Hela cells. (**C** to **E**) RNA immunoprecipitation of PTB, MRG15, or Sm proteins in FGFR2 exons IIIb and IIIc in PNT2 (red) or hMSC (black) cells. Values represent means ± SEM from three independent experiments. (**F** and **G**) Overexpression of MRG15 (F) or SET2 (G) in PNT2 (red) or hMSC (black) cells for 48 hours before RNA immunoprecipitation of PTB. Values represent means ± SEM from three independent experiments. (**H** and **I**) Quantitative RT-PCR analysis of exon ratios in PNT2 cells depleted of MRG15 and MRGX (siMRG, yellow) or cyclophilin B (siCycB, red) after overexpression of SET2 or EGFP. Ratios are as follows: exon IIIb/IIIc for FGFR2 (H) and exon v6/e2 for CD44 (I). Values represent means ± SEM from five independent experiments. *P < 0.05, **P < 0.01, Student's t test compared to control.

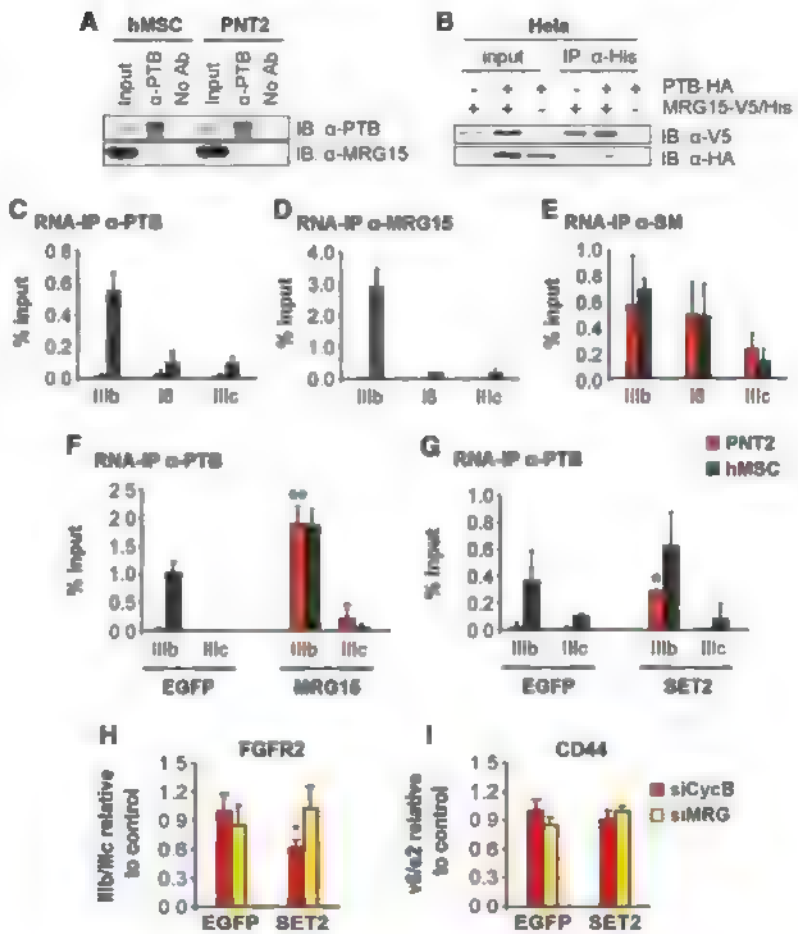

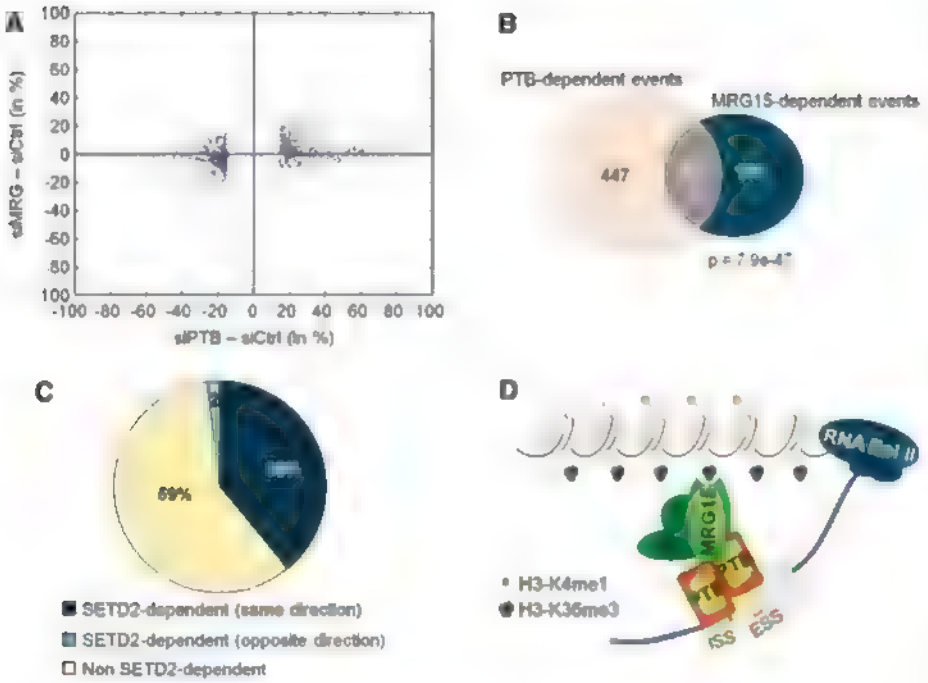

Fig. 5. Genome-wide identification of SETD2, MRG15, and PTB alternative splicing events in hMSC cells. **(A)** Scatterplot of AS events in MRG15- (siMRG) or PTB-depleted cells (siPTB) as compared to small interfering RNA control (siCtrl) transfected cells. The cutoff is ≥15% change in exon usage. Red indicates codependent splicing events. **(B)** Venn diagram of PTB- and MRG15-dependent events with >15% change in exon usage. **(C)** Percentage of MRG15/PTB codependent events that are also sensitive to SETD2 down-regulation. **(D)** An adaptor system for reading histone marks by the splicing machinery, consisting of a histone mark signature, a chromatin-binding protein (MRG15), and a splicing regulator (PTB).

PTB-dependent splicing is not cell type–specific (fig. S9, A to E). Conversely, down-regulation of the H3-K36 methyltransferase SETD2 by RNA interference (RNAi) promoted inclusion of the normally repressed PTB-dependent exons (Fig. 2F and figs. S6, M to P, and S7, D to F) but did not affect the PTB-independent exons and constitutively spliced exons (Fig. 2, G and H, and fig. S8, E and F). The changes in splicing patterns were not an effect of changes in total FGFR2 or PTB transcription levels (fig. S8, C and D and G and H), nor were they due to epithelial-to-mesenchymal transition forced by overexpression or knockdown of SET2 (fig. S10). We similarly tested the effect of H3-K4 methylation, because H3-K4me3 is enriched over the FGFR2 gene in PNT2 cells as compared to hMSCs. Overexpression of the H3-K4 methyltransferase ASH2 led to increased usage of the normally repressed PTB-dependent exons (Fig. 2J and fig. S7, G to I) but not of PTB-independent alternatively spliced exons or a constitutively spliced exon (Fig. 2, K and L). These results demonstrate that histone modifications can modulate AS outcome.

To define the molecular mechanism by which histone marks influence splice site choice, we focused on the histone tail–binding protein MORF-related gene 15 (MRG15), a component of the retinoblastoma binding protein 2 (RBP2)/H3-K4 demethylase complex (*24*). MRG15 specifically binds to H3-K36me3 and recruits RBP2, which depletes H3-K4me3 (*24*, *25*), reminiscent of the chromatin signature found in the PTB-repressed alternatively spliced regions of FGFR2. MRG15 distribution along the PTB-dependent alternatively spliced genes *FGFR2*, *TPM2*, *TPM1*, and *PKM2*, but not along the control gene *CD44*, mimicked H3-K36me3 distribution (Fig. 3, A and B, and fig. S11, A to C). Overexpression of MRG15 was sufficient to force exclusion of the PTB-dependent exons but did not significantly alter the inclusion levels of *CD44* exon v6 (Fig. 3, C and D, and S11D-F). Conversely, knockdown of MRG15, and its functionally redundant paralog MRGX, led to increased use of the PTB-dependent exons but did not affect *CD44* AS (Fig. 3, E and F, and fig. S11, G to I). We conclude that the chromatin-binding protein MRG15 is a modulator of PTB-dependent alternative splice site selection.

To delineate the mechanism of the chromatin-associated protein MRG15 in PTB-dependent AS, we tested the possibility that MRG15 may act by recruiting PTB to its target exons via physical interaction. Endogenous PTB coimmunoprecipitated endogenous MRG15 in both PNT2 and hMSC cells, and reciprocally overexpressed tagged MRG15 interacted with PTB (Fig. 4, A and B). Consistent with a role for MRG15 in the recruitment of PTB, MRG15 associated with FGFR2 pre-mRNA, and its distribution mirrored that of PTB on the repressed exon IIIb in hMSCs, suggesting simultaneous association of the two proteins with *FGFR2* pre-mRNA (Fig. 4, C and D). As a control, the general splicing small nuclear ribonucleoprotein Sm proteins associated uniformly with the *FGFR2* exon IIIb/IIIc region (Fig. 4E).

To directly test whether MRG15 is responsible for the accumulation of PTB on *FGFR2* pre-mRNA, MRG15 was overexpressed in PNT2 cells. MRG15 expression forced the recruitment of PTB to its target *FGFR2* exon IIIb, inducing its repression (Figs. 4F and 3C). Consistent with a role for H3-K36me3 in PTB-mediated splice site selection, SET2 overexpression also induced PTB binding to *FGFR2* exon IIIb pre-mRNA in PNT2 cells (Fig. 4G), concomitant with increased binding of MRG15 to *FGFR2* chromatin (fig. S12) and exon IIIb repression (Fig. 2B). The effect of SET2 on *FGFR2* AS was MRG15-dependent, because down-regulation of MRG15 by RNAi blocked the SET2-dependent splice site shift in PNT2 cells (Fig. 4, H and I), demonstrating that the SET2 effect on AS is mediated via MRG15.

To obtain an estimate of how many PTB-dependent AS events are regulated by H3-K36me3/MRG15–mediated recruitment of PTB, we carried out a genome-wide comparative analysis of AS using high-throughput cDNA sequencing in hMSCs depleted of either SETD2, MRG15, or PTB (*26*, *27*). Depletion of PTB, together with its functional paralog neuronal PTB (nPTB), by RNAi led to changes (≥15% exon usage) in 447 AS events among 12,235 detected alternative exons (Fig. 5, A and B). Knockdown of MRG15, together with its paralog MRGX, resulted in changes in 186 AS events, and down-regulation of the H3-K36 methyltransferase SETD2 affected 186 AS events. Sixty-five AS events were sensitive to both PTB and MRG15 depletion, representing ~15% of PTB-dependent and 35% of MRG15-dependent events (Fig. 5, A and B). The majority (61 out of 65) of codependent splicing events changed in the same direction, further supporting a functional relationship between these two factors. In line with a role for H3-K36me3 in the regulation of AS, 41% of MRG15- and PTB-dependent splicing events were also sensitive to SETD2 down-regulation, with 96% of these codependent events changing in the same direction (Fig. 5C). The overlap between SETD2-dependent and MRG15/PTB codependent exons was statistically significant ($P < 1.0 \times 10^{-32}$, hypergeometric test), and exons codependent on these factors were independently validated by RT-PCR assays (fig. S13, B to I). MRG15/PTB codependence was more pronounced for exons that display relatively moderate changes upon PTB depletion as compared to strongly PTB-dependent exons (Fig. 5A and fig. S13A). Furthermore, MRG15/PTB codependent exons contained, on average, weaker PTB-binding sites than did strongly PTB-dependent exons (fig. S13A) (*28*). These results suggest that histone modifications preferentially modulate the splicing of alternative exons that are weakly regulated by PTB.

Our results demonstrate a role for histone modifications in AS control. We propose the existence of adaptor systems consisting of histone modifications, a chromatin-binding protein that reads the

histone marks, and an interacting splicing regulator (Fig. 5D). Such complexes are a means for epigenetic information to be transmitted to the pre-mRNA processing machinery and probably act by favoring the recruitment of specific splicing regulators to the pre-mRNA, thus defining splicing outcome. We show here that for a subset of PTB-dependent genes, this adaptor system consists of H3-K36me3, its binding protein MRG15, and the splicing regulator PTB. It is tempting to speculate that other combinations of adaptor systems exist that act on other types of alternatively spliced exons. Physical interaction between several chromatin-associated proteins and splicing components has been reported (*9*, *14*). Our results are in line with recent indirect evidence based on genome-wide mapping of histone modifications for a role for chromatin structure and histone modifications in exon definition and alternative splice site selection (*5*, *13*, *15*–*19*).

Although our observations argue for a direct link between histone modifications and the splicing machinery, histone marks may also affect splice site choice indirectly. Extensive evidence demonstrates a role for RNA polymerase II elongation rate or higher-order chromatin structure in splicing outcome, and it is likely that histone modifications act in concert with these mechanisms (*6*–*8*, *10*–*12*). Based on our findings, we propose that the epigenetic memory contained in histone modification patterns is not only used to determine the level of activity of a gene but also transmits information to establish, propagate, and regulate AS patterns during physiological processes such as development and differentiation.

References and Notes

1. B. J. Blencowe, *Cell* **126**, 37 (2006).
2. A. J. Matlin, F. Clark, C. W. J. Smith, *Nat. Rev. Mol. Cell Biol.* **6**, 386 (2005).
3. E. T. Wang *et al.*, *Nature* **27**, 456 (2008).
4. G. S. Wang, T. A. Cooper, *Nat. Rev. Genet.* **8**, 749 (2007).
5. M. Allo *et al.*, *Nat. Struct. Mol. Biol.* **16**, 717 (2009).
6. E. Batsche, M. Yaniv, C. Muchardt, *Nat. Struct. Mol. Biol.* **13**, 22 (2006).
7. M. de la Mata *et al.*, *Mol. Cell* **12**, 525 (2003).
8. A. R. Kornblihtt, M. de la Mata, J. P. Fededa, M. J. Munoz, G. Nogues, *RNA* **10**, 1489 (2004).
9. R. J. Loomis *et al.*, *Mol. Cell* **33**, 450 (2009).
10. M. J. Muñoz *et al.*, *Cell* **137**, 708 (2009).
11. G. Nogues, S. Kadener, P. Cramer, D. Bentley, A. R. Kornblihtt, *J. Biol. Chem.* **277**, 43110 (2002).
12. N. D. Robson-Dixon, M. A. Garcia-Blanco, *J. Biol. Chem.* **279**, 29075 (2004).
13. I. E. Schor, N. Rascovan, F. Pelisch, M. Allo, A. R. Kornblihtt, *Proc. Natl. Acad. Sci. U.S.A.* **106**, 4325 (2009).
14. R. J. Sims 3rd *et al.*, *Mol. Cell* **28**, 665 (2007).
15. R. Andersson, S. Enroth, A. Rada-Iglesias, C. Wadelius, J. Komorowski, *Genome Res.* **19**, 1732 (2009).
16. P. Kolasinska-Zwierz *et al.*, *Nat. Genet.* **41**, 376 (2009).
17. S. Schwartz, E. Meshorer, G. Ast, *Nat. Struct. Mol. Biol.* **16**, 990 (2009).
18. N. Spies, C. B. Nielsen, R. A. Padgett, C. B. Burge, *Mol. Cell* **36**, 245 (2009).
19. H. Tilgner *et al.*, *Nat. Struct. Mol. Biol.* **16**, 996 (2009).
20. R. P. Carstens, E. J. Wagner, M. A. Garcia-Blanco, *Mol. Cell. Biol.* **20**, 7388 (2000).
21. C. C. Warzecha, T. K. Sato, B. Nabet, J. B. Hogenesch, R. P. Carstens, *Mol. Cell* **33**, 591 (2009).
22. E. J. Wagner, M. A. Garcia-Blanco, *Mol. Cell* **10**, 943 (2002).
23. R. Spellman, M. Llorian, C. W. J. Smith, *Mol. Cell* **27**, 420 (2007).
24. T. Hayakawa *et al.*, *Genes Cells* **12**, 811 (2007).
25. P. Zhang *et al.*, *Nucleic Acids Res.* **34**, 6621 (2006).
26. Q. Pan *et al.*, *Mol. Cell* **16**, 929 (2004).
27. Q. Pan, O. Shai, L. J. Lee, B. J. Frey, B. J. Blencowe, *Nat. Genet.* **40**, 1413 (2008).
28. D. Ray *et al.*, *Nat. Biotechnol.* **27**, 667 (2009).

29. We thank J. Patton, D. Skalnik, B. Strahl, J. Stentz, D. Black, M. Garcia-Blanco, and H. Kimura for reagents; P. Scaffidi for discussions; J. Calarco for validations; C. Misquitta for technical assistance; H. Kosucu and Q. Morris for advice on statistical analysis; and E. Tominaga for cell culture. This research was supported by the Intramural Research Program of NIH, the National Cancer Institute, the Center for Cancer Research (T.M.), grants from the National Cancer Institute of Canada, Canadian Institutes of Health Research (grant MOP-67011) and Genome Canada (administered through the Ontario Genomics Institute) to B.B., NIA/NIH grant RO1 AG032134 (OMPS) to O.P.S., and American Heart Association grant 0765084Y to K.T. Complete RNA deep-sequencing data are available at the Gene Expression Omnibus (accession no. GSE19373).

Supporting Online Material

www.sciencemag.org/cgi/content/full/science.1184208/DC1
Materials and Methods
Figs. S1 to S13
Tables S1 and S2
References

4 November 2009; accepted 17 December 2009
Published online 4 February 2010
10.1126/science.1184208
Include this information when citing this paper

Regulation of Cellular Metabolism by Protein Lysine Acetylation

Shimin Zhao,[1,2] Wei Xu,[1,2]* Wenqing Jiang,[1,2]* Wei Yu,[1,2] Yan Lin,[2] Tengfei Zhang,[1,2] Jun Yao,[3] Li Zhou,[4] Yaxue Zeng,[4] Hong Li,[5] Yixue Li,[6] Jiong Shi,[6] Wenlin An,[7] Susan M. Hancock,[7] Fuchu He,[3] Lunxiu Qin,[5] Jason Chin,[7] Pengyuan Yang,[3] Xian Chen,[3,4] Qunying Lei,[1,2,8] Yue Xiong,[1,2,4]† Kun-Liang Guan[1,2,8,9]†

Protein lysine acetylation has emerged as a key posttranslational modification in cellular regulation, in particular through the modification of histones and nuclear transcription regulators. We show that lysine acetylation is a prevalent modification in enzymes that catalyze intermediate metabolism. Virtually every enzyme in glycolysis, gluconeogenesis, the tricarboxylic acid (TCA) cycle, the urea cycle, fatty acid metabolism, and glycogen metabolism was found to be acetylated in human liver tissue. The concentration of metabolic fuels, such as glucose, amino acids, and fatty acids, influenced the acetylation status of metabolic enzymes. Acetylation activated enoyl–coenzyme A hydratase/3-hydroxyacyl–coenzyme A dehydrogenase in fatty acid oxidation and malate dehydrogenase in the TCA cycle, inhibited argininosuccinate lyase in the urea cycle, and destabilized phosphoenolpyruvate carboxykinase in gluconeogenesis. Our study reveals that acetylation plays a major role in metabolic regulation.

Protein acetylation has a key role in the regulation of transcription in the nucleus (*1*), but much less is known about non-nuclear protein acetylation and its role in cellular regulation. To investigate non-nuclear protein acetylation, we separated human liver tissues into nuclear, mitochondrial, and cytosolic fractions. Proteins in cytosolic and mitochondrial fractions were digested with trypsin and acetylated peptides were purified with an antibody to acetyllysine (fig. S1). The purified peptides were analyzed by tandem liquid chromatography–tandem mass spectrometry (LC/LC-MS/MS). From three independent experiments, we identified more than 1300 acetylated peptides, which matched to 1047 distinct human proteins (table S1), including 703 proteins not previously reported to be acetylated. A previous report identified 195 acetylated proteins from mouse liver (*2*), and 135 (70%) of these were also present in our data set (Fig. 1A), indicating that our proteomic analysis reached a high degree of coverage. Choudhary *et al.* very recently reported the identification of 1750 acetylated proteins from a human leukemia cell line (*3*), but only 240 of these were present in our data set (Fig. 1A). Comparison of these three acetylome data sets indicates that the spectrum of acetylated proteins is highly conserved in the liver between mouse and human, but is very different between liver and leukemia cells.

We compared the acetylated proteins with the total liver proteome and discovered that enzymes that participate in intermediate metabolism were preferentially acetylated (Fig. 1B). Indeed, almost

[1]School of Life Sciences, Fudan University, Shanghai 20032, China. [2]Molecular and Cell Biology Lab, Fudan University Shanghai 20032, China. [3]Center of Proteomics, Institute of Biomedical Sciences, Fudan University, Shanghai 20032, China. [4]Department of Biochemistry and Biophysics, Lineberger Comprehensive Cancer Center, University of North Carolina, Chapel Hill, NC 27599, USA. [5]Affiliated Zhongshan Hospital, Fudan University, Shanghai 20032, China. [6]Bioinformatics Center, Key Lab of Systems Biology, Shanghai Institutes for Biological Sciences, Chinese Academy of Sciences, Shanghai 200031, China. [7]Medical Research Council Laboratory of Molecular Biology, Hills Road, Cambridge CB2 0QH, UK. [8]Department of Biological Chemistry, Fudan University, Shanghai 20032, China. [9]Department of Pharmacology and Moores Cancer Center, University of California, San Diego, La Jolla, CA 92093, USA.

*These authors contributed equally to this work.
†To whom correspondence should be addressed. E-mail: yxiong@email.unc.edu (Y.X.); kuguan@ucsd.edu (K.L.G.)

every enzyme in glycolysis, gluconeogenesis, the TCA cycle, the urea cycle, fatty acid metabolism, and glycogen metabolism was acetylated (Fig. 1, C to G). The high occurrence of metabolic enzymes identified in our MS analysis is apparently not due to the abundance of these proteins, because only a few ribosomal proteins (7 of approximately 80 cytosolic ribosomal proteins) were acetylated (table S1). These results indicate a previously unrecognized and potentially extensive role of acetylation in regulation of cellular metabolism. Therefore, we investigated the effect of acetylation on representative enzymes from four metabolic pathways.

Enoyl–coenzyme A hydratase/3-hydroxyacyl coenzyme A (EHHADH; EC code 1.1.1.35) catalyzes two steps in fatty acid oxidation (Fig. 1E) (*4*, *5*), and its deficiency causes abnormal fatty acid metabolism (*6*). We identified four acetylated lysine residues (Lys^{165}, Lys^{171}, Lys^{346}, and Lys^{584}) in EHHADH (table S2). Immunoprecipitation of ectopically expressed FLAG-tagged EHHADH and Western blotting with antibody to acetyllysine confirmed that EHHADH was indeed acetylated. Its acetylation was enhanced by 80% after treatment of cells with trichostatin A [TSA, an inhibitor of histone deacetylase (HDAC) I and II] and nicotinamide (NAM, an inhibitor of the SIRT family deacetylases) (Fig. 2A and fig. S2A). To quantify the acetylation of EHHADH, we used isobaric tags for relative and absolute quantitation (iTRAQ) MS of immunoprecipitated EHHADH. TSA and NAM treatment increased Lys^{171} acetylation from 43.5% to 62% and Lys^{346} acetylation from 46.8% to 77.8% (Fig. 2B), respectively. Consistently, the corresponding unacetylated peptides were decreased by TSA and NAM treatment. These results show that a substantial portion of EHHADH is acetylated and that EHHADH acetylation can be dynamically regulated in vivo.

To determine the effect of acetylation on enzymatic activity, we treated cultured Chang human liver cells with TSA and NAM and detected a doubling of endogenous EHHADH activity (Fig. 2C). Similar observations were also made with ectopically expressed EHHADH in HEK293T cells (Fig. 2C, right panel). Acetylation of an $EHHADH^{4KQ}$ mutant, which had the four putative acetylation lysine residues replaced by glutamine, was decreased (fig. S2C) and its activity was no longer regulated by TSA and NAM (Fig. 2C). Addition of fatty acids to the culture medium increased acetylation and activity of EHHADH by factors of 1.7 and 1.3, respectively (Fig. 2D and fig. S2D). Thus, acetylation of EHHADH can be regulated by extracellular fuels; this finding supports a physiological role of acetylation in the regulation of EHHADH and fatty acid metabolism.

All seven enzymes in the TCA cycle were acetylated (Fig. 1C and table S1), including malate dehydrogenase (MDH, EC code 1.1.1.37), in which four acetylated lysines were identified (Lys^{185}, Lys^{301}, Lys^{307}, and Lys^{314}; tables S2 and S3). Ectopically expressed MDH was acetylated and its acetylation was increased by a factor of 2.4 in cells treated with TSA and NAM (Fig. 2E and fig. S2E). To quantify MDH acetylation, we performed Fourier transform ion cyclotron resonance (FTICR) MS. This approach identified the unmodified full-length MDH and two additional peaks, each with a mass increment of 42.01 daltons, corresponding to mono- and diacetylation

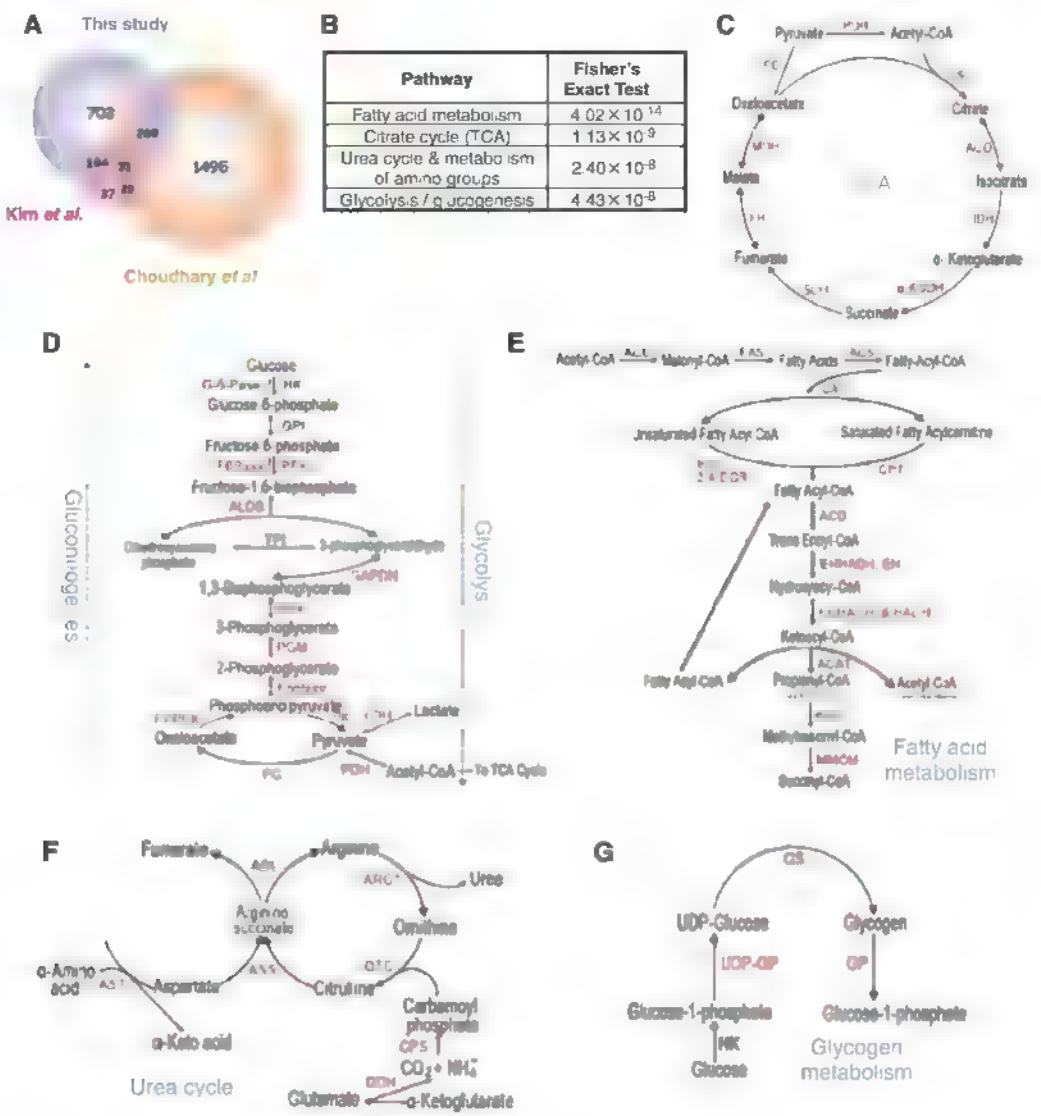

Fig. 1. Acetylation of liver metabolic enzymes. (**A**) Comparison of three acetylation proteomic studies: this study and (*2*, *3*). (**B**) Preferential acetylation of enzymes in intermediary metabolism. Fisher's exact test of comparing acetylated proteins to total liver proteins shows that acetylation is much more prevalent in intermediary metabolic enzymes. (**C** to **G**) Acetylated metabolic enzymes identified by proteomic survey are marked in red. See supporting online material for key to abbreviations.

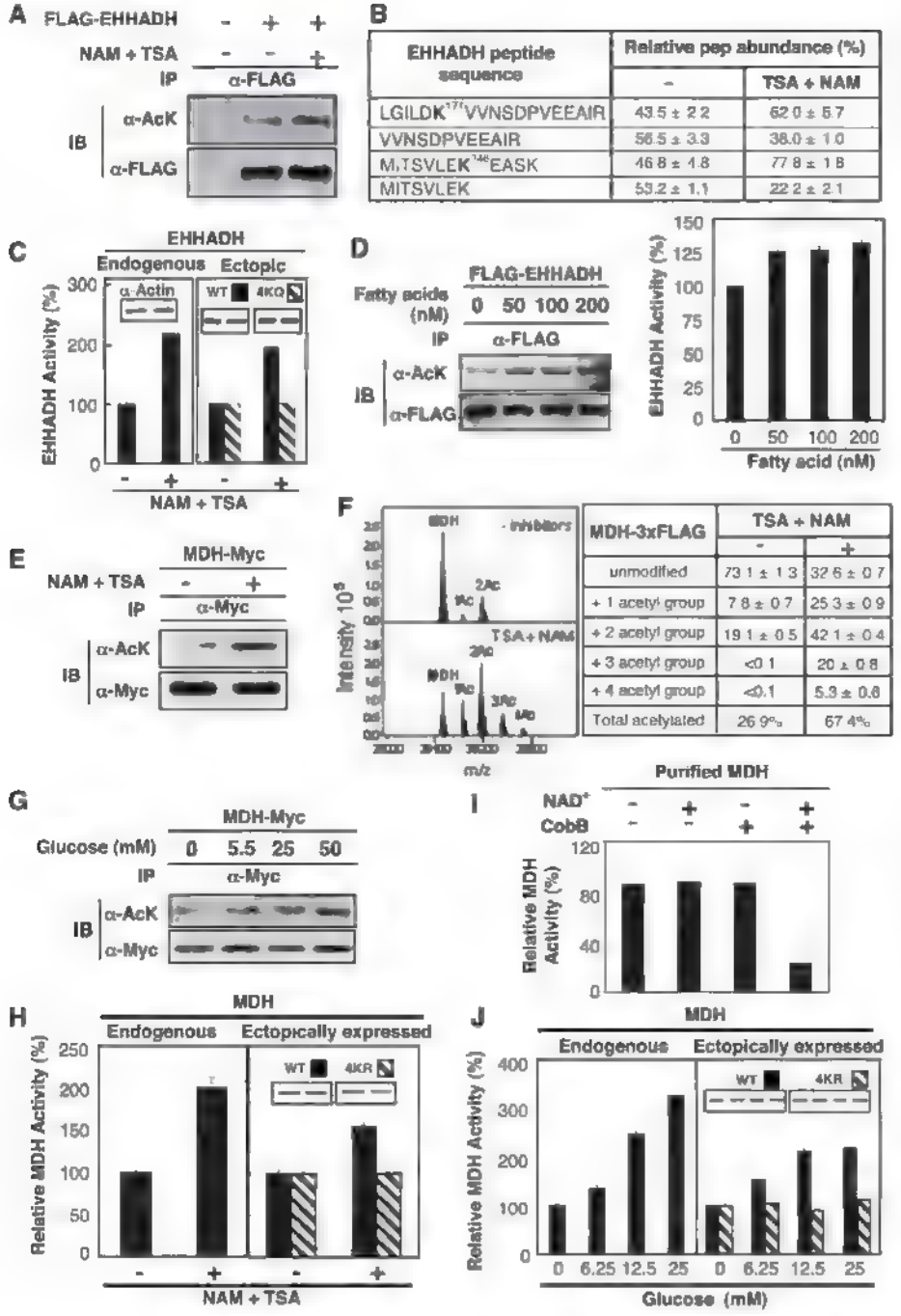

Fig. 2. Activation of EHHADH and MDH by acetylation. **(A)** Acetylation of EHHADH was increased by deacetylase inhibitors. Ectopically expressed and immunoprecipitated (IP) EHHADH was examined by immunoblotting (IB) with antibody to acetyllysine (α-AcK). **(B)** Quantification of EHHADH acetylation by iTRAQ MS. Quantification of peptides was calculated on the basis of relative intensity of the iTRAQ tags. **(C)** Activation of EHHADH in cells expose to deacetylase inhibitors. Data in this panel and subsequent figures are from triplicate experiments. **(D)** Fatty acid induced EHHADH acetylation and activity. Acetylation and activity of EHHDH ectopically expressed in HEK293T cells were monitored. **(E)** MDH acetylation. MDH-Myc was expressed in HEK293T cells and acetylation was determined by immunoblotting. **(F)** Quantitative MS analysis of MDH FLAG tagged MDH was overexpressed in HEK293T cells and purified by immunoprecipitation. Eluted intact MDH proteins were analyzed by FTICR MS. **(G)** Glucose enhances MDH acetylation. **(H)** Activation of MDH by acetylation The activity of endogenous and ectopically expressed MDH from Chang and HEK293T cells, respectively, were assayed and normalized against actin. **(I)** Inactivation of MDH by in vitro deacetylation. Immunoprecipitated MDH was incubated with or without CobB deacetylase and activity was assayed. NAD, an essential cofactor for CobB, was omitted as a negative control. **(J)** Activation of MDH by glucose. Experiments were similar to (H) except cells were treated with glucose.

(Fig. 2F). When cells were treated with TSA and NAM, MDH acetylation was increased from 26.9% to 67.4% with the appearance of tri- and tetraacetylated forms. Subsequent MS/MS analysis confirmed three of four previously identified acetylation sites (fig. S2F and table S1). These data indicate that acetylation is the predominant form of modification and that a substantial fraction of MDH can be acetylated in the cell.

Exposure of cells to high concentrations of glucose enhanced MDH acetylation by 60% (Fig. 2G and fig. S2G). Inhibition of deacetylase doubled endogenous MDH activity in Chang liver cells (Fig. 2H). Consistently, treatment with TSA and NAM activated the wild-type MDH but not the MDH^{4KR} mutant, in which the four acetylation lysine residues were replaced with arginine, in transfected HEK293T cells (Fig. 2H). Furthermore, in vitro deacetylation of immunopurified MDH by CobB deacetylase decreased MDH1 activity (Fig. 2I), indicating that acetylation directly activates MDH. Moreover, high glucose concentrations stimulated enzyme activity of both endogenous and ectopically expressed MDH but had little effect on the MDH^{4KR} mutant (Fig. 2J). These observations indicate that glucose-induced activation of MDH is mediated at least in part through acetylation

The urea cycle is indispensable for detoxification of ammonium, a product of amino acid catabolism. Mutations in argininosuccinate lyase (ASL, EC code 4.3.2.1) cause argininosuccinic aciduria, the second most common neonatal disorder due to urea cycle malfunction in humans (*7*). We identified two acetylated peptides in ASL—Lys^{69} and Lys^{288} (Fig. 1F and table S2)—and confirmed the acetylation of ectopically expressed ASL (Fig. 3A and fig. S3A). Western blotting with an antibody to acetylated Lys^{288} showed a factor of 2.8 increase of ASL Lys^{288} acetylation in cells treated with TSA and NAM (Fig. 3B and fig. S3B). Addition of extra amino acids decreased both total and Lys^{288} acetylation (Fig. 3C and fig. S3C). An enzymatic assay showed that ASL activity decreased in cells treated with TSA and NAM treatment but increased in cells exposed to amino acids, supporting an inhibitory effect of acetylation on ASL activity (Fig. 3, D and E). The activity of the Lys^{288} → Arg mutant ASL^{K288R} was refractory to inhibition by TSA and NAM (Fig. 3D) or activation by amino acids (Fig. 3E). The ASL^{K288R} mutation did not alter global protein structure, as determined by limited proteolysis and circular dichroism analyses (fig. S3, D and E). Therefore, extra amino acids appear to activate ASL by decreasing acetylation of Lys^{288}.

The urea cycle is coupled with the TCA cycle because fumarate generated from the urea cycle can be fed into the TCA cycle for energy production or gluconeogenesis (*8*). We therefore determined the effect of glucose on ASL activity and acetylation. Glucose increased acetylation of ASL by a factor of 2.7 (Fig. 3F and fig. S3F) and decreased activity of ASL by 50% (Fig. 3G). In vitro incubation of ASL immunopurified from

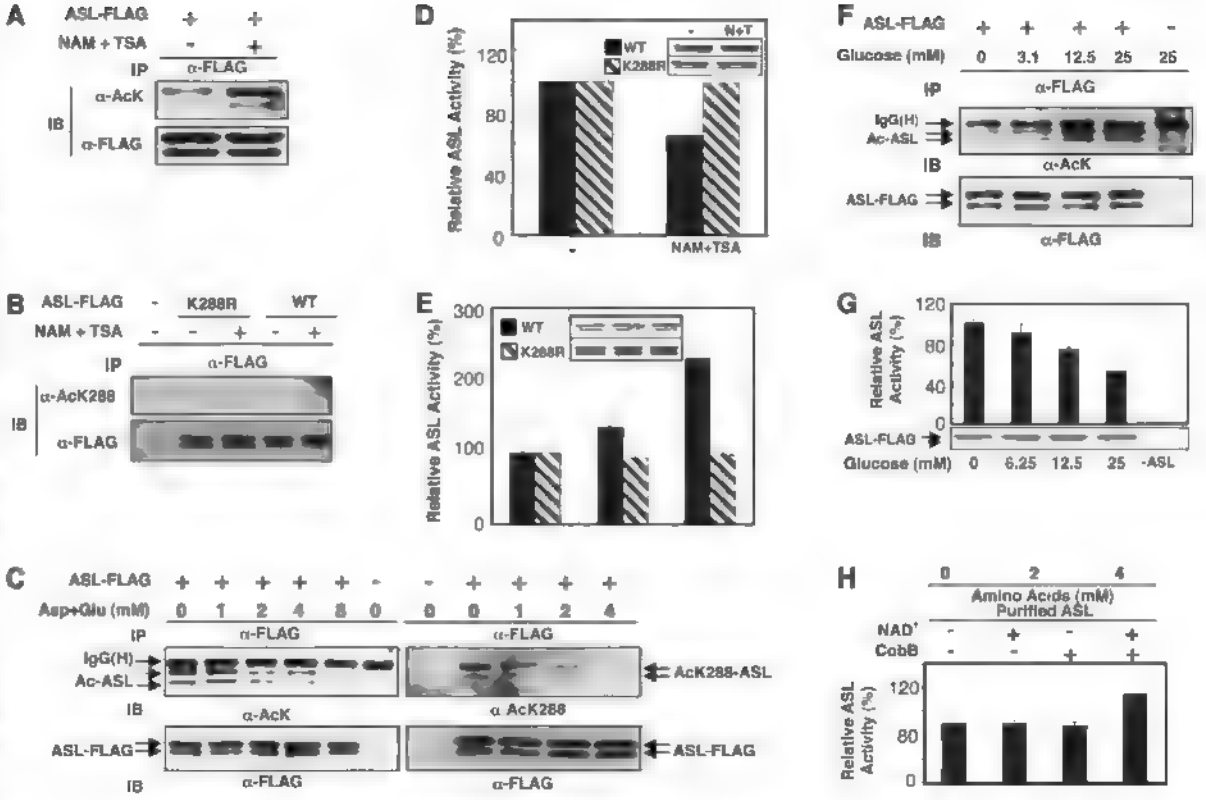

Fig. 3. Inactivation of ASL by acetylation. (**A** and **B**) ASL acetylation. FLAG-tagged ASL or ASL^{K288R} was overexpressed in HEK293T cells, immunoprecipitated, and probed with antibody to acetyllysine (**A**) or to acetyl-Lys^{288} (**B**). (**C**) Inhibition of ASL acetylation by extra amino acids. ASL was immunoprecipitated from transfected HEK293T cells, which were treated with various amino acid concentrations. (**D**) Inhibition of ASL in response to NAM and TSA. Wild-type and mutant ASL-K288R (132% of wild-type activity) proteins were expressed in HEK293T cells that were treated with NAM and TSA as indicated. Activity of immunoprecipitated ASL was normalized to total protein. (**E**) Requirement of Lys^{288} acetylation for ASL activation by amino acids. Wild-type and mutant ASL proteins were overexpressed in HEK293T cells incubated in medium containing various amino acid concentrations. (**F** and **G**) Effects of glucose on acetylation and activity of ASL. ASL was overexpressed in HEK293T cells that were treated with various concentrations of glucose. Acetylation and activity of immunoprecipitated ASL were determined. (**H**) Activation of ASL by in vitro deacetylation. In vitro deacetylation was similar to Fig. 2I.

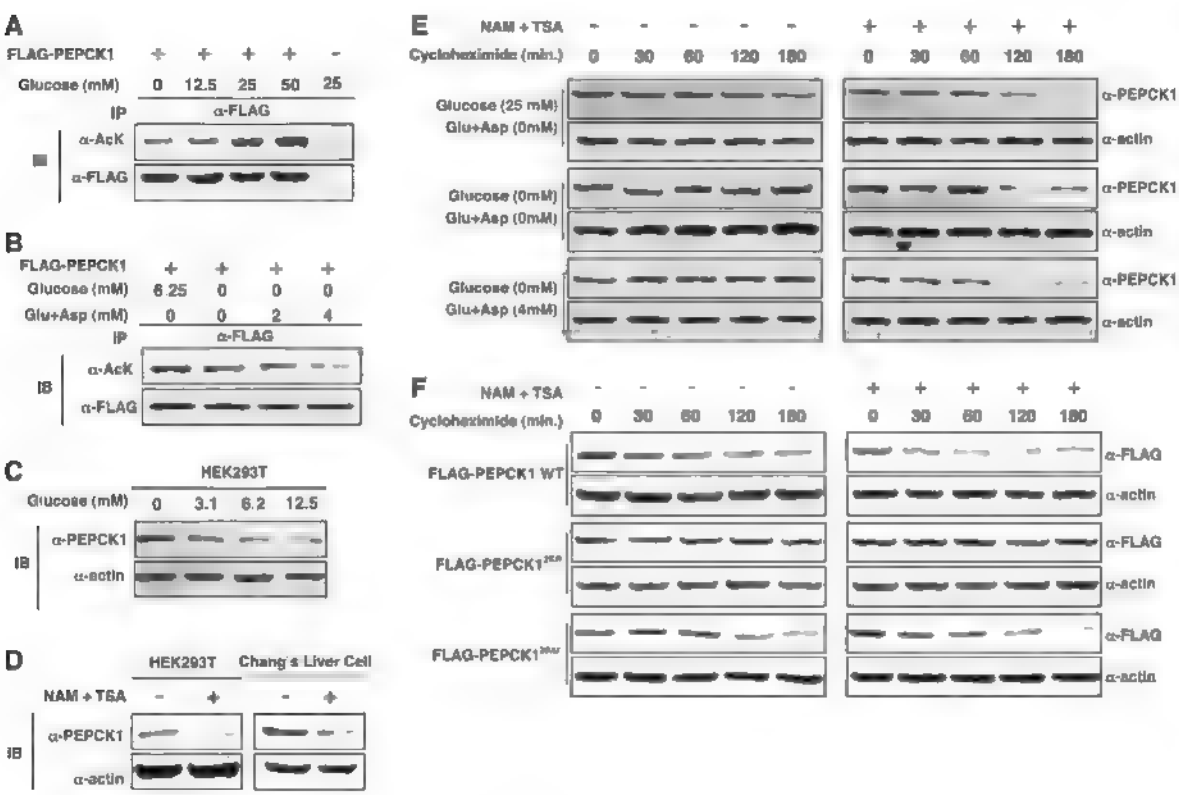

Fig. 4. Destabilization of PEPCK1 by acetylation. (**A**) Glucose induces PEPCK1 acetylation. (**B**) Amino acids decrease PEPCK1 acetylation. (**C**) Glucose induces depletion in of PEPCK1 protein. Endogenous PEPCK levels were detected with a PEPCK1 antibody. (**D**) TSA and NAM reduce PEPCK1 protein abundance. (**E**) Glucose destabilizes PEPCK1. Cycloheximide was added at time zero to block translation in HEK293 cells. PEPCK1 protein abundance was determined by Western blotting. (**F**) Inhibition of deacetylases destabilizes the wild type but not the acetylation-defective mutant PEPCK1.

mammalian cells with CobB deacetylase increased ASL activity (Fig. 3H), supporting a direct role of acetylation in ASL inactivation. The dual regulation of ASL by both amino acids and glucose indicates that acetylation may have an important role in the coordination of metabolic pathways. In the presence of sufficient glucose, amino acid catabolism for energy production and gluconeogenesis would be inhibited. In the presence of abundant amino acids and low glucose, cells would switch to using amino acids for energy production with enhanced urea cycle activity. Cells may use acetylation to coordinate multiple pathways in order to achieve these metabolic adaptations

Phosphoenolpyruvate carboxykinase 1 (PEPCK1, EC code 4.1.1.32) is a key regulatory enzyme in gluconeogenesis (Fig. 1D) (*9*, *10*). Three acetylated lysine residues were identified in PEPCK1 by MS analysis (Lys^{70}, Lys^{71}, and Lys^{594}; table S2). Acetylation of PEPCK1 was enhanced in cells treated with high concentrations of glucose (Fig. 4A) but was decreased by addition of amino acids in glucose-free medium (Fig. 4B). These results suggest a potential mechanism by which cells could regulate gluconeogenesis through regulating acetylation of PEPCK1 in response to the availability of extracellular fuels.

In searching for an effect of acetylation on the regulation of PEPCK1, we noticed that levels of endogenous PEPCK1 protein were decreased by high glucose (Fig. 4C). Furthermore, treatment with TSA and NAM caused a 70% reduction in the amount of PEPCK1 protein in both HEK293T and Chang liver cells (Fig. 4D). PEPCK1 was stable in cells in glucose-free medium but unstable in high-glucose medium (Fig. 4E). When cells were treated with TSA and NAM, PEPCK1 was unstable even in glucose-free medium or in the presence of amino acids. These results indicate that acetylation may regulate the stability of PEPCK1. We replaced the three putative acetylation lysine residues by arginine ($PEPCK1^{3KR}$) or glutamine ($PEPCK1^{3KQ}$) to abolish or mimic acetylation, respectively. The $PEPCK1^{3KR}$ mutant was more stable than the wild type, whereas the $PEPCK1^{3KQ}$ mutant remained unstable (Fig. 4F). Moreover, treatment of cells with TSA and NAM failed to destabilize the $PEPCK1^{3KR}$ mutant.

The importance of lysine acetylation in the regulation of chromatin dynamics and gene expression is well appreciated. Our study and others extend the scope of cell regulation by lysine acetylation to an extent comparable to that of other major posttranslational modifications such as phosphorylation and ubiquitination. We show that most intermediate metabolic enzymes are acetylated and that acetylation can directly affect the enzyme activity or stability. We found that acetylation of metabolic enzymes changed in response to the alterations of extracellular nutrient availability, providing evidence for a physiological role of dynamic acetylation in metabolic regulation. The mechanism of acetylation in regulating metabolism may be conserved during evolution. Many metabolic enzymes in *Escherichia coli* are acetylated, although the functional importance of these acetylations has not been investigated (*11*). We propose that lysine acetylation is an evolutionarily conserved mechanism involved in regulation of metabolism in response to nutrient availability and cellular metabolic status. Acetylation may play a key role in the coordination of different metabolic pathways in response to extracellular conditions.

References and Notes

1. X. J. Yang, E. Seto, *Mol. Cell* **31**, 449 (2008)
2. S. C. Kim *et al.*, *Mol. Cell* **23**, 607 (2006)
3. C. Choudhary *et al.*, *Science* **325**, 834 (2009)
4. K. Alvares *et al.*, *Cancer Res.* **54**, 2303 (1994)
5. C. S. Yeh *et al.*, *Cancer Lett.* **233**, 297 (2006)
6. P. A. Watkins *et al.*, *J. Clin. Invest.* **83**, 771 (1989)
7. E. Trevisson *et al.*, *Hum. Mutat.* **28**, 694 (2007)
8. R. L. Jungas, M. L. Halperin, J. T. Brosnan, *Physiol. Rev.* **72**, 419 (1992)
9. H. Lardy, P. E. Hughes, *Curr. Top. Cell. Regul.* **24**, 171 (1984)
10. P. She *et al.*, *Mol. Cell. Biol.* **20**, 6508 (2000)
11. J. Zhang *et al.*, *Mol. Cell. Proteomics* **8**, 215 (2009)

12. We thank members of Fudan MCB laboratory for their valuable inputs throughout this study and S. Jackson for reading the manuscript. Supported by the 985 program from the Chinese Ministry of Education, state key development programs of basic research of China (grants 2009CB918401 and 2006CB806700), the national high technology research and development program of China (grant 2006AA02A308), Chinese National Science Foundation grants 30600112 and 30871255, Shanghai key basic research projects (grants 06JC14086, 07PJ14011, 08JC1400900), and NIH grants R01GM51586, R01CA108941, and R01CA65572 (K.L.G., X.C., and Y.X.)

Supporting Online Material

www.sciencemag.org/cgi/content/full/327/5968/1000/DC1
Materials and Methods
Figs. S1 to S3
Tables S1 to S3
References

27 July 2009; accepted 7 January 2010
10.1126/science.1179689

Acetylation of Metabolic Enzymes Coordinates Carbon Source Utilization and Metabolic Flux

Qijun Wang,[1] Yakun Zhang,[2] Chen Yang,[3] Hui Xiong,[1,2] Yan Lin,[4] Jun Yao,[4] Hong Li,[3] Lu Xie,[3] Wei Zhao,[3] Yufeng Yao,[5] Zhi-Bin Ning,[3] Rong Zeng,[3] Yue Xiong,[4,6] Kun-Liang Guan,[4,7] Shimin Zhao,[1,4]* Guo-Ping Zhao[1,2,3,8]*

Lysine acetylation regulates many eukaryotic cellular processes, but its function in prokaryotes is largely unknown. We demonstrated that central metabolism enzymes in *Salmonella* were acetylated extensively and differentially in response to different carbon sources, concomitantly with changes in cell growth and metabolic flux. The relative activities of key enzymes controlling the direction of glycolysis versus gluconeogenesis and the branching between citrate cycle and glyoxylate bypass were all regulated by acetylation. This modulation is mainly controlled by a pair of lysine acetyltransferase and deacetylase, whose expressions are coordinated with growth status. Reversible acetylation of metabolic enzymes ensure that cells respond environmental changes via promptly sensing cellular energy status and flexibly altering reaction rates or directions. It represents a metabolic regulatory mechanism conserved from bacteria to mammals.

Protein lysine acetylation regulates wide range of cellular functions in eukaryotes, especially transcriptional control in the nucleus (*1*, *2*). It also plays an extensive role in regulation of metabolic enzymes through various mechanisms in human liver (*3*). In prokaryotes such as *Salmonella enterica*, reversible lysine acetylation is known to regulate the activity of acetyl coenzyme A (CoA) synthetase (*4*). To determine how lysine acetylation globally regulates the metabolism in prokaryotes, we determined the overall acetylation status of *S. enterica* proteins under either fermentable glucose-based glycolysis or under oxidative citrate-based gluconeogenesis. By immunopurification of acetylated peptides with antibody to acetyllysine and peptide identification

[1]State Key Laboratory of Genetic Engineering, Department of Microbiology, School of Life Sciences and Institute of Biomedical Sciences, Fudan University, Shanghai 200032, China. [2]MOST-Shanghai Laboratory of Disease and Health Genomics, Chinese National Human Genome Center at Shanghai, Shanghai 201203, China. [3]Key Laboratory of Synthetic Biology, Bioinformatics Center and Laboratory of Systems Biology, Institute of Plant Physiology and Ecology, Shanghai Institutes for Biological Sciences, Chinese Academy of Sciences, Shanghai 200032, China. [4]Molecular Cell Biology Laboratory, Institute of Biomedical Sciences, Fudan University, Shanghai 200032, China. [5]Laboratory of Human Bacteria Pathogenesis, Department of Medical Microbiology and Parasitology, Institute of Medical Sciences, Shanghai Jiao Tong University School of Medicine, Shanghai 200025, China. [6]Department of Biochemistry and Biophysics and Lineberger Comprehensive Cancer Center, University of North Carolina at Chapel Hill, Chapel Hill, NC 27599, USA. [7]Department of Pharmacology and Moores Cancer Center, University of California San Diego, La Jolla, CA 92093, USA. [8]Department of Microbiology and L. Ka Shing Institute of Health Sciences, The Chinese University of Hong Kong, Prince of Wales Hospital, Shatin, New Territories, Hong Kong SAR, China.

*To whom correspondence should be addressed. E-mail: zhaosm@fudan.edu.cn (S.Z.); gpzhao@sibs.ac.cn (G.-P.Z.)

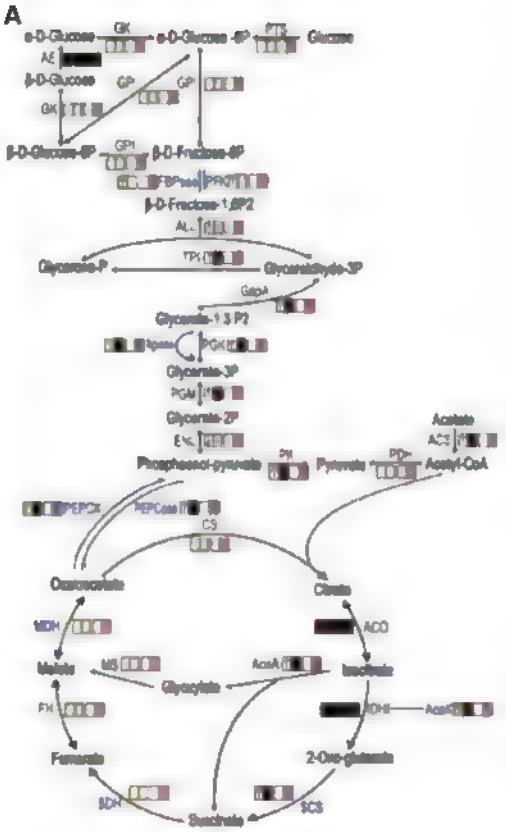

B

	Enzyme Name	WT $_{glu}$/ WT $_{cit}$	WT $_{glu}$/ *pat* $_{glu}$	WT $_{glu}$/ *cobB* $_{glu}$	WT $_{glu}$/ *cobB* $_{cit}$
Metabolic Enzymes	PTS	1/0.68 ± 0.12	1/0.10 ± 0.06	1/1.34 ± 0.17	1/0.05 ± 0.02
	PFK	1/0.56 ± 0.22	1/0.02 ± 0.01	1/1.68 ± 0.43	1/0.46 ± 0.21
	FBPase	1/0.28 ± 0.26	1/ ND	1/1.94 ± 0.11	ND/ ND
	ALD	1/0.12 ± 0.10	1/ ND	1/2.03 ±0.54	1/0.52 ± 0.22
	GapA	1/0.36 ± 0.27	1/ ND	1/3.25 ± 0.22	1/0.56 ± 0.42
	PGM	1/0.54 ± 0.19	1/ ND	1/1.23 ± 0.56	1/0.56 ± 0.22
	ENO	1/0.43 ± 0.20	1/ ND	1/3.12 ± 0.34	1/0.86 ± 0.26
	PEPCK	1/0.16 ± 0.11	1/ ND	1/ 4.22 ± 0.27	1/ 1.03 ± 0.53
	PK	1/0.62 ± 0.23	1/ ND	1/ 2.06 ± 0.66	1/ 0.98 ± 0.11
	PGK	1/0.29 ± 0.13	1/0.01 ± 0.01	1/ 6.22 ± 1.36	1/ 0.77 ± 0.21
	AceA	1/0.24 ± 0.13	1/0.03 ± 0.01	1/ 3.29 ± 0.55	1/1.11 ± 0.27
	AceK	1/0.06 ± 0.04	1/ ND	1/ 4.23 ± 1.42	1/0.63 ± 0.25
	FH	1/0.88 ± 0.26	1/0.2 ± 0.04	1/ 3.11 ± 0.69	1/0.89 ± 0.37
	SCS	1/0.33 ± 0.12	1/ ND	1/ 2.27 ± 0.44	1/0.65 ± 0.36
	MDH	1/0.18 ± 0.06	1/ ND	1/ 2.86 ± 0.78	1/0.88 ± 0.39
Ribosomal Proteins	50SL4	1/0.88 ± 0.21	1/0.76 ± 0.25	1/0.91 ± 0.32	1/1.18 ± 0.37
	50SL11	1/1.02 ± 0.11	1/0.85 ± 0.34	1/0.96 ± 0.19	1/0.86 ± .019
	50SL14	1/0.96 ± 0.23	1/0.96 ± 0.19	1/1.08 ± 0.22	1/0.88 ± 0.34
	50SL35	1/1.15 ± 0.16	1/1.21 ± 0.33	1/1.05 ± 0.42	1/0.87 ± 0.22

by SILAC. Relative acetylation is presented with the top mean value (n = 3) of each pair set as 1 arbitrarily. ND indicates not detectable. Full names of abbreviations used in this figure are available in supporting online material (SOM) text.

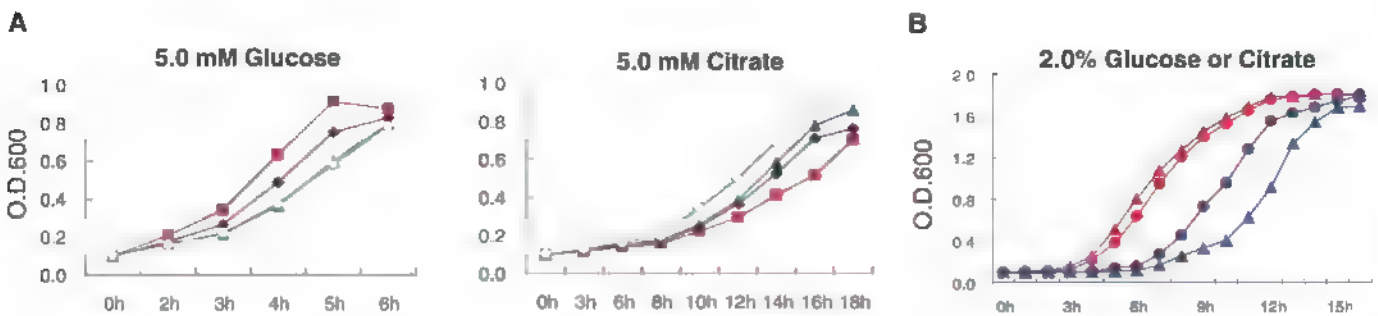

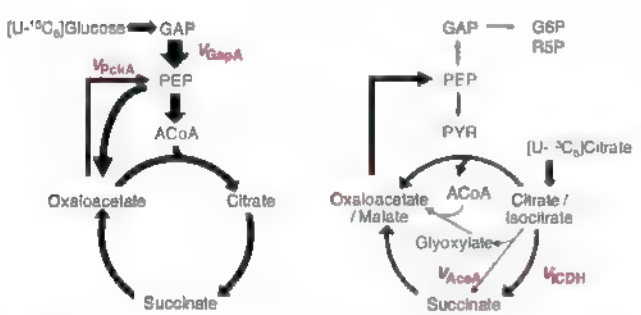

D

Flux ratio	C-source	wt	Δ*cobB*	Δ*pat*
v_{GapA} / v_{PckA}	glucose	3.77 ± 0.21	5.55 ± 0.26	2.68 ± 0.10
v_{AceA} / v_{ICDH}	citrate	0.20 ± 0.02	0.14 ± 0.03	0.31 ± 0.06

Fig. 2. Growth phenotypes of Δ*pat* and Δ*cobB*. **(A)** WT (black), Δ*pat* (blue), Δ*cobB* (red), or Δ*pat*/Δ*cobB* (green) strains were grown in minimal medium with indicated concentrations of glucose (left) or citrate (right). O.D. indicates optical density. **(B)** Growth curves of WT *S. enterica* in minimal medium containing glucose (red) or citrate (blue) with (▲) or without (●) NAD^+. **(C)** In vivo metabolic flux profiles in *S. enterica* during growth on glucose or citrate. Intracellular flux distribution was determined by ^{13}C labeling and GC-MS analysis. Arrows indicate the direction of net fluxes, and their widths are scaled to the flux values. **(D)** Altered metabolic flux ratio of Δ*pat* and Δ*cobB*. Flux profiles through glycolysis (represented by v_{GapA}), gluconeogenesis (v_{PckA}), glyoxylate bypass (v_{AceA}), and TCA flux (v_{ICDH}) were quantitated and used for calculating v_{GapA}/v_{PckA} and v_{AceA}/v_{ICDH} flux ratio. Data shown are mean values of three independent measurements with SD.

by mass spectrometry analyses, we identified a total of 235 acetylated peptides that matched to 191 proteins in *S. enterica*. About 50% of the acetylated proteins participated in multiple metabolic pathways (tables S1 and S2), and about 90% of the enzymes of central metabolism were acetylated (Fig. 1A). Stable isotope labeling with amino acids in cell culture (SILAC) quantitative analysis showed that, among 15 enzymes that had altered acetylation in response to different carbon sources, all showed greater acetylation in cells grown in glucose than in cells grown in citrate (Fig. 1B), consistent with our estimations based on numbers of repetitive detection of acetylated fragments (Fig. 1A).

The abundant acetylation of metabolic enzymes and the concerted changes in acetylation dependent on carbon source indicate that acetylation may mediate adaptation to various carbon sources in *S. enterica*, which has only one major bacterial protein acetyltransferase, Pat, and one nicotinamide adenine dinucleotide (NAD^+)–dependent deacetylase, CobB (*4*, *5*) (fig. S1). Acetylation of central metabolic enzymes in a *pat* null mutant (*Δpat*) was reduced, whereas acetylation of these enzymes was elevated in a *cobB* null mutant (*ΔcobB*) compared with that of the wild-type strain when grown in glucose (Fig. 1B). When grown in citrate, the acetylation of metabolic enzymes in *ΔcobB* cells was also increased over the wild-type cells (Fig. 1B). On the other hand, there was no change in acetylation of ribosomal proteins in either *ΔcobB* or *Δpat* cells (Fig. 1B), supporting the notion that Pat and CobB are the major enzymes responsible for the reversible acetylation of central metabolic enzymes in *S. enterica*.

A physiological role of enzyme acetylation in mediating cellular adaptation to different metabolic fuels was suggested by the different growth properties of wild-type, *Δpat*, or *ΔcobB* strains grown on different carbon sources (Fig. 2). The *ΔcobB* cells (with increased acetylation) grew faster than wild-type cells in minimal glucose medium but grew slower than wild-type cells in minimal citrate medium (Fig. 2A), whereas the *Δpat* cells (with decreased acetylation) had the opposite growth properties (Fig. 2A). The *Δpat/ΔcobB* double mutant behaved similarly to the *Δpat* strain, consistent with the notion that the CobB deacetylase would have no effect on target proteins if they were not acetylated by Pat (Fig. 2A). Treatment of wild-type cells with nicotinamide (NAM), an inhibitor for CobB (*6*), like *cobB* mutation, suppressed cell growth in the citrate-containing minimal medium but had little effect on cell growth in minimal medium containing glucose (Fig. 2B), consistent with the fact that metabolic enzyme acetylation is higher in *S. enterica* when cells grow on glucose (Fig. 1).

We tested the regulatory role of Pat and CobB in coordinating carbon source adaptation by mea-

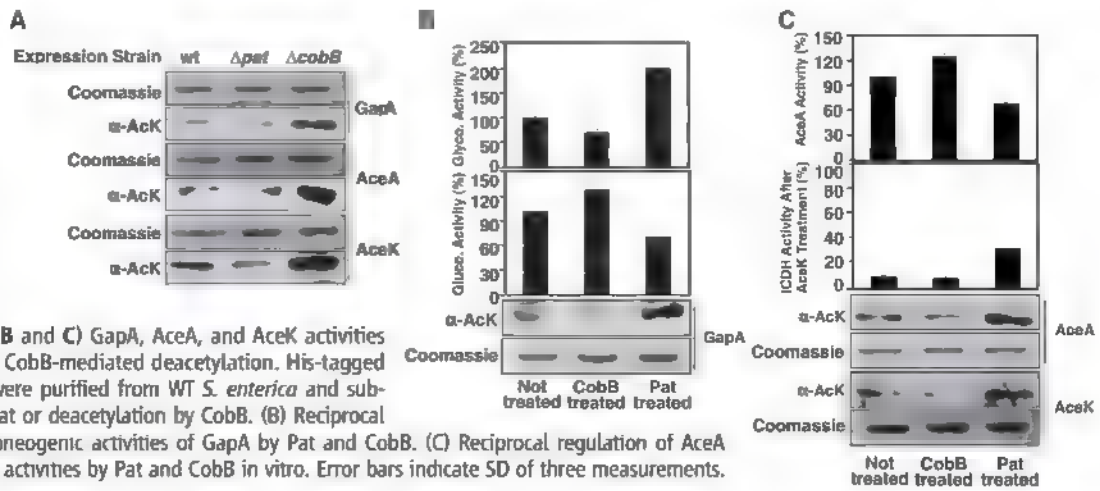

Fig. 3. Regulation of central metabolic enzymes by acetylation. (**A**) Acetylation of metabolic enzymes expressed in *ΔcobB* and *Δpat* strains. His-tagged GapA, AceA, or AceK proteins were overexpressed in the WT, *ΔcobB*, and *Δpat* strains and purified to homogeneity. Equal amounts of each protein were used and acetylation was determined. SDS PAGE indicates SDS polyacrylamide gel electrophoresis. (**B** and **C**) GapA, AceA, and AceK activities by Pat-mediated acetylation and CobB-mediated deacetylation. His-tagged GapA, AceA, and AceK proteins were purified from WT *S. enterica* and subjected to in vitro acetylation by Pat or deacetylation by CobB. (**B**) Reciprocal regulation of glycolytic and gluconeogenic activities of GapA by Pat and CobB. (**C**) Reciprocal regulation of AceA activity and AceK-controlled ICDH activities by Pat and CobB in vitro. Error bars indicate SD of three measurements.

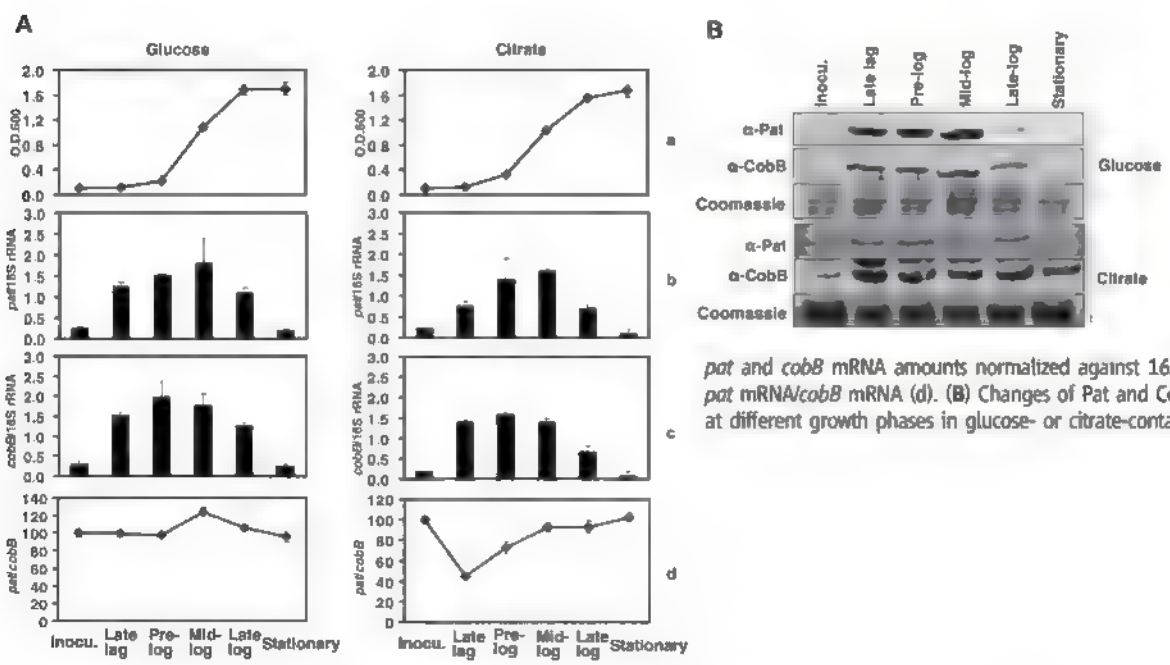

Fig. 4. Differential transcription of *pat* and *cobB* in response to metabolic status and various carbon sources. *S. enterica* cells were incubated in LB and then washed and transferred into minimal medium containing 50 mM glucose or citrate. Cells were sampled at indicated growth phases. (**A**) Growth curve (a); *pat* and *cobB* mRNA amounts normalized against 16*S* rRNA (b and c); ratio of *pat* mRNA/*cobB* mRNA (d). (**B**) Changes of Pat and CobB protein concentrations at different growth phases in glucose- or citrate-containing medium.

suring in vivo metabolic flux profiles with ^{13}C-labeled glucose or citrate as the tracer followed by gas chromatography–mass spectrometry (GC-MS) analysis (*7*, *8*). The overall metabolic flux profiles in *S. enterica* showed distinct patterns during growth on glucose or citrate (Fig. 2C). The glyoxylate bypass was activated, and the carbon flow favored gluconeogenesis when cells were grown on citrate. We also quantitatively compared the flux profiles through glycolysis (v_{GapA}), gluconeogenesis (v_{PckA}), tricarboxylic acid (TCA) cycle (v_{ICDH}), and glyoxylate bypass (v_{AceA}) of the wild-type, Δ*pat*, and Δ*cobB* strains to assess the relation between metabolic flux profiles and acetylation status. When cells were grown in the presence of glucose, the Δ*cobB* strain had 2.07-fold greater glycolysis/gluconeogenesis flux ratio than the Δ*pat* strain had (Fig. 2D), whereas the glycolysis/gluconeogenesis flux ratio of the wild-type strain was 47% lower than that of the Δ*cobB* strain but 40.7% higher than that of the Δ*pat* strain (Fig. 2D). When cells were grown in the presence of citrate, the Δ*pat* strain had 2.21-fold greater glyoxylate bypass/TCA flux ratio than that of the Δ*cobB* strain (Fig. 2D), whereas the glyoxylate/TCA flux ratio of the wild-type strain was 55% lower than that of the Δ*pat* strain but 43% higher than that of the Δ*cobB* strain (Fig. 2D). These results and the effect of glucose on acetylation of metabolic enzymes (Fig. 1) indicate that carbon source–associated acetylation may affect the relative activities of metabolic enzymes and thus modulate metabolic flux profiles.

Direct evidence of acetylation-mediated regulation for central metabolic enzymes was derived from biochemical studies with three enzymes (table S1): the glyceraldehyde phosphate dehydrogenase (GapA), which channels glycolysis or gluconeogenesis flux bidirectionally, as well as the isocitrate lyase (AceA) and the isocitrate dehydrogenase (ICDH) kinase/phosphatase (AceK), both of which control the flux distribution of isocitrate between the energy-generating TCA cycle and the gluconeogenesis-requiring glyoxylate pathway when only an oxidative carbon source (such as citrate) is available (*9*). Anti-acetylysine immunoblot showed that all three enzymes had increased acetylation in the Δ*cobB* strain (Fig. 3A). Acetylation of these three enzymes decreased to various degrees in the Δ*pat* strain. The remaining acetylation detected in the Δ*pat* strain may reflect the presence of other acetyltransferases (fig. S1). All these enzymes were more heavily acetylated in cells grown in minimal media with glucose than those grown with citrate (fig. S4). These observations confirmed that GapA, AceA, and AceK are under regulation of Pat and CobB.

To demonstrate a direct effect of acetylation on enzyme activity, we purified recombinant Pat and CobB protein and treated GapA, AceK, and AceA enzymes in vitro (fig. S2). Increasing GapA acetylation by Pat acetylase treatment increased its glycolysis activity by 100%, whereas its activity in promoting gluconeogenesis was inhibited by more than 30% (Fig. 3B), supporting the notion that acetylation stimulates glycolysis but inhibits gluconeogenesis. Consistently, in vitro deacetylation of GapA by CobB caused a 30% increase in gluconeogenic activity but a 27% decrease in glycolytic activity (Fig. 3B). The increase of AceA acetylation by in vitro treatment with Pat (Fig. 3C) or acetylation-mimicked mutation (fig. S3) led to 30% and 20% loss in AceA-specific activity, respectively. In vitro deacetylation of AceA by CobB, on the other hand, led to a 24% increase in AceA-specific activity (Fig. 3C). The activity of AceK was measured by its ability to inactivate its native substrate, ICDH, which catalyzes the conversion of isocitrate to α-ketoglutarate. In vitro acetylation of AceK by Pat led to a 60% reduction of its ability to inactivate ICDH (by phosphorylating ICDH), whereas in vitro deacetylation of AceK by CobB increased AceK's ability to inactivate ICDH (Fig. 3C), suggesting that acetylation may activate the phosphatase activity of AceK toward ICDH, consistent with the fact that both acetylation and the acetylation mimetic mutation of AceK activated the phosphorylated ICDH (figs. S4 and S5). Together, these results demonstrate that activities of GapA, AceA, and AceK enzymes are regulated through acetylation, which in turn may direct the flux direction toward glycolysis or gluconeogenesis or the distribution of isocitrate between the TCA cycle and glyoxylate bypass.

We also investigated the expression of *pat* and *cobB* genes in cells grown on different carbon sources. Real-time reverse transcription polymerase chain reaction (PCR) analysis, using 16*S* ribosomal RNA (rRNA) as the internal control, revealed that both *pat* and *cobB* genes were more actively transcribed during log phase growth than other growth phases when cells were grown in the presence of either glucose or citrate (Fig. 4A). Accordingly, the concentrations of Pat and CobB proteins were increased (fig. S6 and Fig. 4B). During the stationary phase, cells that grew in the presence of either glucose or citrate had similar ratios of *pat* mRNA/*cobB* mRNA. However, when rich medium–incubated cells were transferred to minimal medium containing glucose, acetylation peaked at mid-log phase (Fig. 4A), whereas if they were transferred to minimal medium containing citrate, acetylation decreased in both prelog and early log phases before it returned to basal level in late log and stationary phases (Fig. 4A). The lower amount of cellular acetylation was apparently needed for efficient utilization of citrate. These results indicate that the expression (and probably total cellular activities) of Pat and CobB are regulated differentially in response to different carbon sources, although its underlying mechanism is yet to be revealed.

The central metabolic pathways constitute the backbone of cell metabolism. Such pathways use various carbon sources to provide building blocks, cofactors, and energy for cell growth. For cells to respond flexibly and promptly to availability of environmental carbon sources, the directions and/or rates of the metabolic reactions need to be modulated concomitantly and globally. Transcription regulations merely adjust the amount of metabolic enzymes in a unidirectional manner, whereas allosteric effects only modulate the catalytic activities of individual enzymes responsible for specific reactions of metabolic pathways (*10*). We have found a potential regulatory circuit coordinating the carbon flow of *S. enterica* central metabolism by reversible acetylation. Acetylation uses acetyl-CoA and NAD^+, two molecules that directly involved both in metabolism and energy sensing, as substrates, provides unparallel advantages in sensing cellular energy status, and thus could fit the role for global metabolic modulation. The identification of extensively acetylated metabolic enzymes in both human and prokaryotes and reports of broad metabolic regulatory roles of this modification (*11*–*16*) indicate that reversible lysine acetylation may represent an evolutionarily conserved mechanism of metabolic regulation in both eukaryotes and prokaryotes.

References and Notes

1. M. Grunstein, *Nature* **389**, 349 (1997).
2. X. J. Yang, E. Seto, *Oncogene* **26**, 5310 (2007).
3. S. Zhao *et al.*, *Science* **327**, 1000 (2010).
4. V. J. Starai, I. Celic, R. N. Cole, J. D. Boeke, J. C. Escalante-Semerena, *Science* **298**, 2390 (2002).
5. V. J. Starai, J. C. Escalante-Semerena, *J. Mol. Biol.* **340**, 1005 (2004).
6. K. J. Bitterman, R. M. Anderson, H. Y. Cohen, M. Latorre-Esteves, D. A. Sinclair, *J. Biol. Chem.* **277**, 45099 (2002).
7. Q. Hua, C. Yang, T. Baba, H. Mori, K. Shimizu, *J. Bacteriol.* **185**, 7053 (2003).
8. N. Zamboni, E. Fischer, U. Sauer, *BMC Bioinformatics* **6**, 209 (2005).
9. A. J. Cozzone, *Annu. Rev. Microbiol.* **52**, 127 (1998).
10. F. C. Neidhardt, Escherichia coli *and* Salmonella (ASM Press, Washington, DC, ed. 2, 1996).
11. J. Zhang *et al.*, *Mol. Cell. Proteomics* **8**, 215 (2009).
12. C. Choudhary *et al.*, *Science* **325**, 834 (2009); published online 16 July 2009 (10.1126/science.1175371).
13. Y. Y. Lin *et al.*, *Cell* **136**, 1073 (2009).
14. O. R. Bereshchenko, W. Gu, R. Dalla-Favera, *Nat. Genet.* **32**, 606 (2002).
15. J. Landry *et al.*, *Proc. Natl. Acad. Sci. U.S.A.* **97**, 5807 (2000).
16. W. C. Hallows, S. Lee, J. M. Denu, *Proc. Natl. Acad. Sci. U.S.A.* **103**, 10230 (2006).

17. We thank members of Fudan Molecular Cell Biology laboratory for their inputs throughout this work. L. Wang of Nankai University, China, provided the *S. Enterica* G2466 for this study. This work is supported by state key development programs of basic research of China (2009CB918401 and 2006CB806700), national high technology research and development program of China (2006AA02A308), National Natural Science Foundation of China (30830002), and Shanghai key basic research project, China (08JC1400900).

Supporting Online Material

www.sciencemag.org/cgi/content/full/327/5968/1004/DC1
Materials and Methods
SOM Text
Figs. S1 to S6
Tables S1 and S2
References

27 July 2009; accepted 7 January 2010
10.1126/science.1179687

Significant Acidification in Major Chinese Croplands

J. H. Guo,[1*] X. J. Liu,[1*] Y. Zhang,[1] J. L. Shen,[1] W. X. Han,[1] W. F. Zhang,[1] P. Christie,[1,2] K. W. T. Goulding,[3] P. M. Vitousek,[4] F. S. Zhang[1]†

Soil acidification is a major problem in soils of intensive Chinese agricultural systems. We used two nationwide surveys, paired comparisons in numerous individual sites, and several long-term monitoring-field data sets to evaluate changes in soil acidity. Soil pH declined significantly ($P < 0.001$) from the 1980s to the 2000s in the major Chinese crop-production areas. Processes related to nitrogen cycling released 20 to 221 kilomoles of hydrogen ion (H^+) per hectare per year, and base cations uptake contributed a further 15 to 20 kilomoles of H^+ per hectare per year to soil acidification in four widespread cropping systems. In comparison, acid deposition (0.4 to 2.0 kilomoles of H^+ per hectare per year) made a small contribution to the acidification of agricultural soils across China.

Acidification can alter the biogeochemistry of ecosystems and adversely affect biota (*1*, *2*). Poorly buffered freshwater systems have been changed substantially by anthropogenic acidification (*3*), mostly by sulfuric and nitric acids, and the surface ocean has acidified measurably from increased carbon dioxide (CO_2) in the atmosphere, raising concerns about marine biodiversity and ecosystem function (*4*–*6*). Anthropogenic acidification of soils has received less attention. Soils are strongly buffered by ion exchange reactions, by the weathering of soil minerals, and (in the acidic range) by interactions with aluminum (Al) and iron (*7*). Soils acidify very slowly under natural conditions over hundreds to millions of years. Old soils and soils in high-rainfall regions tend toward greater acidity (*8*). Naturally acid soils occupy approximately 30% of the world's ice-free land and are commonly associated with phosphorus (P) deficiency, Al toxicity, and reduced biodiversity and productivity (*9*).

Chinese agriculture has intensified greatly since the early 1980s on a limited land area with large inputs of chemical fertilizers and other resources. Grain production and fertilizer nitrogen (N) consumption reached 502 million and 32.6 million tons nationally in 2007, respectively, increases of 54 and 191% as compared with 1981 (*10*). High levels of N fertilization can drive soil acidification both directly and indirectly (*11*–*13*), and the rates of N applied in some regions are extraordinarily high (*14*) as compared with those of North America and Europe (*15*). These have degraded soils and environmental quality in the North China Plain (*16*) and in the Taihu Lake region in south China (*14*). Here, we investigate whether they also cause significant soil acidification at a national scale.

A national soil survey was conducted during the early 1980s, and pH was determined in all topsoils that were sampled (*17*). For comparison, we collected all published data (*13*) on topsoil pH from 2000 to 2008 and compiled two (unpaired) data sets (1980s versus 2000s) on the basis of six soil groups according to geography and use, with two subgroups per soil group: cereal crops and cash crops (tables S1 and S2 and fig. S1) (*13*). In China, both systems receive very high nutrient inputs as compared with those of other agricultural systems worldwide (*18*), especially the cash crops (such as greenhouse vegetable systems), which have developed rapidly since the 1980s (*19*).

The results reveal significant acidification of all topsoils (average pH declines for the soil groups of 0.13 to 0.80) except in the highest-pH soils, which represent only a small percentage of Chinese cultivated soils (table S1). In all other soil groups, acidification has been greater in cash crop systems (pH decreased by 0.30 to 0.80) than under cereals (0.13 to 0.76) (Table 1). These are substantial changes. The pH scale is logarithmic and a pH decrease of 0.30 corresponds to a doubling in hydrogen ion (H^+) activity.

Soils in group I [for example, leached red soils (*Argi-Udic Ferrosols*) and yellow soils (*Ali-Perudic Argosols*)] are the most acidic in south China and have acidified further since the 1980s, with pH declines of 0.23 and 0.30 ($P < 0.001$) in cereal and cash crop systems, respectively (Table 1). Although net pH decreases for group I soils were small as compared with those of other groups, the impact may be more pronounced because these soils are approaching pH values at which potentially toxic metals such as Al and manganese (Mn) could be mobilized (*20*, *21*).

At the other extreme, soils in group V [mainly fluvo-aquic soils (*Ochri-Aquic Cambosols*), which are widely distributed in north China] are

[1]College of Resources and Environmental Sciences, China Agricultural University, Beijing 100193, China. [2]Agri-Environment Branch, Agri-Food and Biosciences Institute, Belfast BT9 5PX, UK. [3]Department of Soil Science, Rothamsted Research, Harpenden, Herts AL5 2JQ, UK. [4]Department of Biology, Stanford University, Stanford, CA 94305, USA.

*These authors contributed equally to this work.
†To whom correspondence should be addressed. E-mail zhangfs@cau.edu.cn

Table 1. Topsoil pH changes in major Chinese croplands between the 1980s and 2000s. The soil groups are defined in (*13*). NS, not significant; pH range is an average (5 to 95 percentile).

Soil group	1980s		2000s					
			Cereal crop systems*			Cash crop systems†		
	Sample number	pH value	Sample number	pH value	pH change	Sample number	pH value	pH change
I	301	5.37 (4.40–6.60)	505	5.14 (4.17–6.52)	−0.23‡	337	5.07 (3.93–6.44)	−0.30‡
II	1157	6.33 (5.00–8.04)	1101	6.20 (5.00–7.70)	−0.13‡	413	5.98 (4.58–7.49)	−0.35‡
III	297	6.42 (4.50–8.30)	211	5.66 (4.27–8.06)	−0.76‡	98	5.62 (4.27–7.73)	−0.80‡
IV	562	6.32 (5.10–7.89)	537	6.00 (4.84–7.60)	−0.32‡	238	5.60 (4.07–7.42)	−0.72‡
V	995	7.96 (6.39–8.80)	850	7.69 (5.37–8.70)	−0.27‡	520	7.38 (5.69–8.20)	−0.58‡
VI	493	8.16 (7.10–8.80)	250	8.16 (7.49–8.82)	−0.00 (ns)	10	8.17 (7.43–8.93)	0.01 (ns)

*Cereal/fiber crops (such as rice, wheat, maize, and cotton). †High-input cash crops (such as vegetables, fruit trees, and tea). ‡$P < 0.001$.

considered resistant to acidification because of their relatively high $CaCO_3$ content (5 to 10%). However, they have also acidified significantly ($P < 0.001$), with pH decreases averaging 0.27 and 0.58 under cereals and cash crops, respectively. The pH decline in group V is small compared with those of groups III and IV (Table 1) (*13*) but probably resulted in substantial loss of $CaCO_3$. Therefore, soil pH decline might be expected to accelerate in the future.

The broad-scale comparative results are supported by data from 154 agricultural fields, in which strictly paired data were available from the same sites in the 1980s and the 2000s (*13*). Paired *t* tests show that these topsoils were significantly ($P < 0.001$) acidified, with an average pH decline of 0.50 (Fig. 1). Topsoil pH in 53.2% of the sites decreased by over 0.50, 18.2% by 0.30 to 0.50, and 18.9% by 0 to 0.30; only 9.7% of the sites increased in pH. The paired national data strongly support widely occurring soil acidification in Chinese croplands.

We also summarized information from 10 long-term monitoring field (LTMF) sites in which soil pH was measured regularly over an 8- to 25-year period (*13*). Decreases in pH were substantial, from 0.45 to 2.20 (Fig. 2). We found significant soil acidification occurred only in NPK (conventional fertilization) plots ($P < 0.001$), whereas soil pH did not show obvious change in CK (no fertilization) and Fallow (no fertilization and no crop) plots (fig. S2) (*13*).

Further analysis shows that recent soil acidification in China has resulted mainly from high-N fertilizer inputs and the uptake and removal of base cations (BCs) by plants. In the three major Chinese double-cropping cereal systems (wheat-maize, rice-wheat, and rice-rice), annual N fertilizer rates are usually above 500 kg N ha^{-1} with N use efficiencies of only 30 to 50% (table S3). Calculations based on inputs and outputs of ammonium and nitrate N indicate that N loading contributes 20 to 33 kmol H^+ ha^{-1} $year^{-1}$ of proton generation in these systems (Fig. 3 and table S3). Greenhouse vegetable systems, the major cash crops, receive even higher N fertilizer inputs; in Shandong province, N fertilizer rates above 4000 kg N ha^{-1} $year^{-1}$ are common with N use efficiencies below 10% (*22*, *23*). Under this management, about 220 kmol H^+ ha^{-1} $year^{-1}$ of potential acidity accumulates in each hectare of soil (Fig. 3 and table S3). The proton generation related to N cycling (20 to 221 kmol H^+ ha^{-1} $year^{-1}$) in China is extremely high as compared with values (1.4 to 11.5 kmol H^+ ha^{-1} $year^{-1}$) at lower N fertilizer rates in other regions (*24*).

Plant uptake of BCs together with removal of economic yields and crop residues from fields is another driver of soil acidification because the net removal of excess cations over anions leaves behind equivalent H^+ released to the soil. At current fertilization levels, approximately 25 tons of dry biomass (grain and stalk) (table S4) is harvested annually in the three double-cropping systems, leading to an estimated H^+ production rate by BCs uptake of 15 to 20 kmol H^+ ha^{-1} $year^{-1}$ (Fig. 3 and table S3). In greenhouse vegetable systems, the importance of BCs uptake varies greatly with plant species and yield but overall appears similar to the cereal systems.

Increasing N fertilizer applications has been a major management technique driving high crop yields, which in turn increase the removal of BCs. These factors combined have produced potential acidity equivalent to 30 to 50 kmol H^+ ha^{-1} $year^{-1}$ in double-cropping cereal systems and ~230 kmol H^+ ha^{-1} $year^{-1}$ in greenhouse vegetable systems (Fig. 3). Although acid deposition is an important regional environmental problem in China, strongly affected areas with a precipitation pH of 4.00 to 5.60 (*25*) receive 0.4 to 2.0 kmol H^+ ha^{-1} $year^{-1}$, much of which is buffered by other depositional or soil processes. Overall, anthropogenic acidification driven by N fertilization is at least 10 to 100 times greater than that associated with acid rain (*13*, Fig. 3). In other regions, serious acidification was found in the long-term $(NH_4)_2SO_4$-treated Park Grass soils at Rothamsted in England when no lime was applied to buffer soil acidity (*26*), and Wallace (*27*) reported soil acidification from routine fertilization practices for crop production.

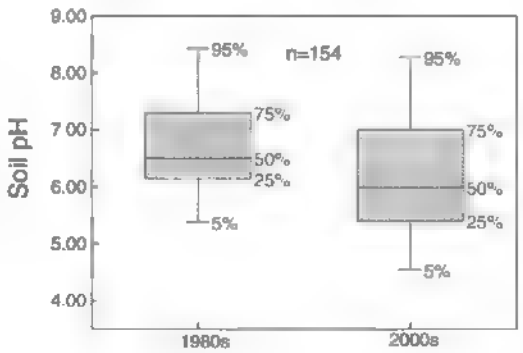

Fig. 1. Topsoil pH changes from 154 paired data over 35 sites in seven Chinese provinces between the 1980s and the 2000s. The line and square within the box represent the median and mean values of all data; the bottom and top edges of the box represent 25 and 75 percentiles of all data, respectively; and the bottom and top bars represent 5 and 95 percentiles, respectively.

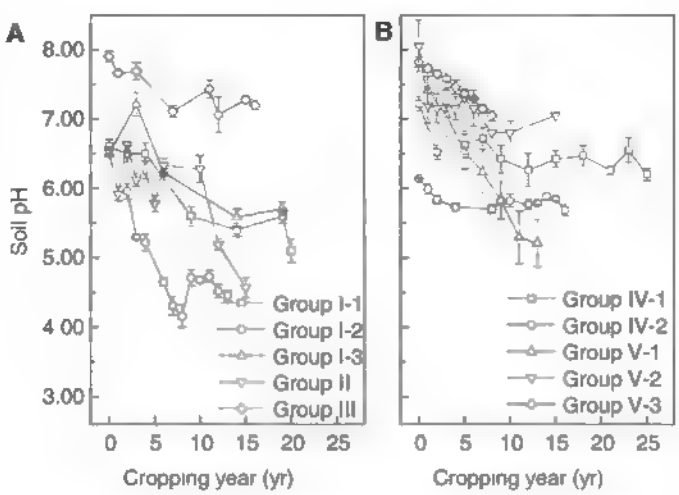

Fig. 2. Long-term changes in topsoil pH in some typical Chinese soils. (**A**) Groups I to III. (**B**) Groups IV and V received conventional rates of NPK fertilizers for 8 to 25 years. Soil groups are described in (*13*). Data are means ± SD.

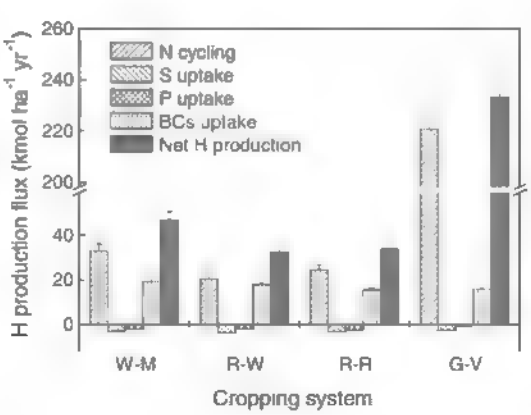

Fig. 3. H^+ production budget of main factors in four typical Chinese cropping systems. W-M, wheat-maize; R-W, rice-wheat; R-R, rice-rice; and G-V, greenhouse vegetables. N cycling, S uptake, and P uptake denote the H produced by N cycling and S and P uptake processes. BCs uptake indicates H released by BCs uptake. Net H production is the algebraic sum of H resulting from N cycling and P, S, and BCs uptake. Data are means ± SD.

Anthropogenic acidification of Chinese agricultural soils will be difficult to correct as long as excessive levels of N fertilization continue. Goulding and Annis (*28*) found that each 50 kg ha^{-1} of added ammonium-N generates ~4 kmol H^+ ha^{-1} $year^{-1}$ and requires ~500 kg $CaCO_3$ ha^{-1} $year^{-1}$ to neutralize in their field conditions. Similar theoretical calculations show that each kg of applied NH_4-N leached as NO_3-N demands 7.2 kg of $CaCO_3$ to neutralize the acidity generated (*29*, *30*). Adding appropriate amounts of lime in China would be arduous, intensive double-cropping systems that generate 30 to 50 kmol H^+ ha^{-1} $year^{-1}$ would theoretically require 1.5 to 2.5 tons $CaCO_3$ ha^{-1} $year^{-1}$ to counteract soil acidification—and greenhouse vegetable systems would require ten times this amount.

Overuse of N fertilizer contributes substantially to regional soil acidification in China. Since 1980, crop production has increased with rapidly increasing N fertilizer consumption (fig. S5). Decreasing N use efficiency (fig. S5) indicates that more fertilizer N is being lost to the environment (*31*), causing further negative environmental impacts. Optimal nutrient-management strategies can significantly reduce N fertilizer rates without decreasing crop yields (*14*, *32*, *33*), with multiple benefits to agriculture and the environment (*15*), including the slowing of dangerous rates of anthropogenic acidification. Fertilization based on comprehensive, knowledge-based N management practices has become one of the most urgent requirements for sustainable agriculture in China and in other rapidly developing regions worldwide.

References and Notes

1. E. Delhaize, P. R. Ryan, *Plant Physiol.* **107**, 315 (1995).
2. O. Hoegh-Guldberg *et al.*, *Science* **318**, 1737 (2007).
3. P. M. Vitousek *et al.*, *Ecol. Appl.* **7**, 737 (1997).
4. J. C. Orr *et al.*, *Nature* **437**, 681 (2005).
5. R. A. Feely *et al.*, *Science* **305**, 362 (2008).
6. J. M. Hall-Spencer *et al.*, *Nature* **454**, 96 (2008).
7. O. A. Chadwick, J. Chorover, *Geoderma* **100**, 321 (2001).
8. H. R. von Uexküll, E. Mutert, *Plant Soil* **171**, 1 (1995).
9. L. Blake, A. E. Johnston, K. W. T. Goulding, *Soil Use Manage.* **10**, 51 (1994).
10. *China Agriculture Yearbook* (China Agricultural Press, Beijing, 1982–2008).
11. A. S. R. Juo, A. Dabiri, K. Franzluebbers, *Plant Soil* **171**, 245 (1995).
12. N. Matsuyama *et al.*, *Soil Sci. Plant Nutr.* **51**, 117 (2005).
13. Materials and methods are available as supporting material on *Science* Online.
14. X. T. Ju *et al.*, *Proc. Natl. Acad. Sci. U.S.A.* **106**, 3041 (2009).
15. R. Howarth *et al.*, in *Ecosystems and Human Well-being: Policy Responses*, K. Chopra, R. Leemans, P. Kumar, H. Simons, Eds. (Island Press, Washington, DC, 2005), pp. 295–311.
16. X. J. Liu, X. T. Ju, F. S. Zhang, J. R. Pan, P. Christie, *Field Crops Res.* **83**, 111 (2003).
17. Soil Survey Office of China, *China Soil Species*, vols. 1 to 6 (China Agriculture Press, Beijing, 1994).
18. P. M. Vitousek *et al.*, *Science* **324**, 1519 (2009).
19. www.luna.com.cn/showScfx.aspx?ID=37 (2009).
20. Q. G. Zhao *et al.*, *Mechanism, Temporal-Spatial Changes and Controlling Countermeasures of Soil Degradation in Hilly Red Soil Region of Southeastern China* (Science Press, Beijing, 2002), pp. 202–204.
21. J. H. Guo *et al.*, *Environ. Monit. Assess.* **129**, 321 (2007).
22. J. H. Zhu, X. L. Li, P. Christie, J. L. Li, *Agric. Ecosyst. Environ.* **111**, 70 (2005).
23. X. T. Ju, C. L. Kou, P. Christie, Z. X. Dou, F. S. Zhang, *Environ. Pollut.* **145**, 497 (2007).
24. K. Fujii, S. Funakawa, C. Hayakawa, T. Sakartoningsih, *Plant Soil* **316**, 241 (2009).
25. www.mep.gov.cn/plan/zkgb/2008zkgb/200906/t20090609_152566.htm (2009).
26. L. Blake, K. W. T. Goulding, C. J. B. Mott, A. E. Johnston, *Eur. J. Soil Sci.* **50**, 401 (1999).
27. A. Wallace, *Commun. Soil Sci. Plant Anal.* **25**, 87 (1994).
28. K. W. T. Goulding, B. Annis, *Proc. Int. Fertil. Soc.* **410**, 36 (1998).
29. B. Upjohn, G. Fenton, M. Conyers, www.dpi.nsw.gov.au/__data/assets/pdf_file/0007/167209/soil-acidity-liming.pdf (2005).
30. W. M. Porter, www.regional.org.au/au/roc/1981/roc198131.htm (1998).
31. G. X. Xing, Z. L. Zhu, *Biogeochemistry* **57/58**, 405 (2002).
32. X. P. Chen *et al.*, *Nutr. Cycl. Agroecosyst.* **74**, 91 (2006).
33. G. H. Wang, Q. C. Zhang, C. Witt, R. J. Buresh, *Agric. Syst.* **94**, 801 (2007).

34. We thank X. J. Xiang for data collection, J. Wang for reference correction, and X. Shi and J. Ren for providing soil pH dynamics at two LTMF sites. Financial support for this work was provided by the Chinese National Basic Research Program (2009CB118600 and 2005CB422206), the Innovative Group Grant from NSFC (30821003), and the Special Fund for Agricultural Profession (200803030).

Supporting Online Material

www.sciencemag.org/cgi/content/full/science.1182570/DC1
Materials and Methods
SOM Text
Figs. S1 to S5
Tables S1 to S4
References and Notes

28 September 2009; accepted 14 January 2010
Published online 11 February 2010;
10.1126/science.1182570
Include this information when citing this paper.

Peptidomimetic Antibiotics Target Outer-Membrane Biogenesis in *Pseudomonas aeruginosa*

Nityakalyani Srinivas,[1] Peter Jetter,[1] Bernhard J. Ueberbacher,[1] Martina Werneburg,[1] Katja Zerbe,[1] Jessica Steinmann,[1] Benjamin Van der Meijden,[1] Francesca Bernardini,[2] Alexander Lederer,[2] Ricardo L. A. Dias,[2] Pauline E. Misson,[2] Heiko Henze,[2] Jürg Zumbrunn,[2] Frank O. Gombert,[2] Daniel Obrecht,[2] Peter Hunziker,[3] Stefan Schauer,[3] Urs Ziegler,[4] Andres Käch,[4] Leo Eberl,[5] Kathrin Riedel,[5] Steven J. DeMarco,[2]* John A. Robinson[1]*

Antibiotics with new mechanisms of action are urgently required to combat the growing health threat posed by resistant pathogenic microorganisms. We synthesized a family of peptidomimetic antibiotics based on the antimicrobial peptide protegrin I. Several rounds of optimization gave a lead compound that was active in the nanomolar range against Gram-negative *Pseudomonas* spp., but was largely inactive against other Gram-negative and Gram-positive bacteria. Biochemical and genetic studies showed that the peptidomimetics had a non–membrane-lytic mechanism of action and identified a homolog of the β-barrel protein LptD (Imp/OstA), which functions in outer-membrane biogenesis, as a cellular target. The peptidomimetic showed potent antimicrobial activity in a mouse septicemia infection model. Drug-resistant strains of *Pseudomonas* are a serious health problem, so this family of antibiotics may have important therapeutic applications.

Naturally occurring peptides and proteins make interesting starting points for the design and synthesis of biologically active peptidomimetics. We previously synthesized libraries of β-hairpin–shaped peptidomimetics (*1*, *2*) based on the membranolytic host-defense peptide protegrin I (PG-I) (*3*). These mimetics contain loop sequences related to that in PG-I, but linked to a D-proline–L-proline template, which helps to stabilize β-hairpin conformations within the macrocycle (*4*, *5*) (Fig. 1A). One sequence variant, L8-1, had broad-spectrum antimicrobial activity like that of PG-I, but with a reduced hemolytic activity on human red blood cells (*2*). To optimize this lead, we performed iterative cycles of peptidomimetic library synthesis and screening for improved antimicrobial activity. The optimal hit from each library was used as a starting point for the synthesis and testing of variations in a subsequent library. This structure-activity trail led sequentially to mimetics L19-45, L26-19, and L27-11 (Fig. 1). L27-11

[1]Chemistry Department, University of Zurich, Winterthurerstrasse 190, 8057 Zurich, Switzerland. [2]Polyphor AG, Hegenheimermattweg 125, 4123 Allschwil, Switzerland. [3]Functional Genomics Center Zürich, Winterthurerstrasse 190, 8057 Zurich, Switzerland. [4]Center for Microscopy and Image Analysis, University of Zurich, Winterthurerstrasse 190, 8057 Zurich, Switzerland. [5]Department of Microbiology, University of Zurich, Winterthurerstrasse 190, 8057 Zurich.

*To whom correspondence should be addressed. E-mail: robinson@oci.uzh.ch (J.A.R.); steve.demarco@polyphor.com (S.J.D.)

possessed an interesting spectrum of antimicrobial activity, including minimal inhibitory concentrations (MIC's) in the nanomolar range against many *Pseudomonas aeruginosa* (*PA*) strains and other *Pseudomonas* spp.; the mimetic is only weakly active or inactive against other Gram-positive and Gram-negative bacteria [Table 1 (*6*)]. In contrast, PG-I displays broad-spectrum antimicrobial activity against Gram-positive and Gram-negative bacteria in the low micromolar range (*7*). The enantiomeric (mirror image) form of L27-11 is essentially inactive (MIC ≥ 32 μg/ml) against *PA*, unlike the two enantiomers of PG-I (*8*), suggesting that the antibacterial target of the mimetic is chiral and not the achiral lipid chains of the cell membrane targeted by PG-I (*9*–*12*). Further efforts focused on optimizing plasma stability and drug-like properties. The compounds POL7001 and POL7080 displayed much improved plasma half-lives while retaining a potent and selective action against *PA*; the MIC's covering 90% of more than 100 *PA* clinical isolates tested (MIC_{90}) were 0.13 and 0.25 μg/ml, respectively, for these two mimetics. These isolates were of European and North American origin and most were resistant to one or more classes of clinically used antibiotics (*6*).

We next focused on identifying the mechanism of action of this family of peptidomimetics. Their mode of action against *PA* at concentrations close to the MIC was clearly different from the rapid membranolytic actions of both PG-I (*7*) and polymyxin B, a cationic macrocyclic peptide antibiotic of bacterial origin (*13*). Whereas PG-I or polymyxin at 4× MIC caused rapid cell lysis, the killing caused by the peptidomimetics was much slower (Fig. 1B). The ability of the peptidomimetics to permeabilize the *PA* cell membrane was also tested with the fluorescent nucleic acid stain SYTOX (*14*). No fluorescence increase was apparent over 120 min when *PA* cells were exposed to SYTOX and L26-19, L27-11, or POL7001, compared with a rapid fluorescence increase upon exposure to PG-I or polymyxin B [Fig. 1C (*6*)]. A direct interaction between the peptidomimetic antibiotics and lipopolysaccharide (LPS) was examined with a dansyl-polymyxin displacement binding assay (*15*). This revealed an interaction between LPS and L27-11 in the low micromolar range [median inhibitory concentration (IC_{50}) 0.8 μM], which was not enantioselective (IC_{50} 1.1 μM for the enantiomer of L27-11), suggesting that LPS is not the primary site of antimicrobial action. Also, L26-19, L27-11, and POL7001 caused no notable lysis of human red blood cells at concentrations up to 100 μg/ml

We tested whether the peptidomimetics have any effect on protein or nucleic acid biosynthesis in *PA* by examining the kinetics of incorporation of radiolabeled precursors into macromolecules. No notable influence was detected (*6*), suggesting that inhibition of protein, DNA, or RNA biosynthesis are not the primary modes of action. Similar attempts to monitor effects on cell wall biosynthesis by radiolabeled *N*-acetylglucosamine were frustrated by low levels of incorporation of this precursor into cell wall biopolymers.

As an alternative approach to investigate the mechanism of action, a forward genetic screen was established to characterize the genetic basis for resistance to the antibiotics. Spontaneous resistant mutants of *PA* PAO1 could be selected on the antibiotic POL7080 at 5× MIC, at an estimated frequency of $\leq 1 \times 10^{-10}$. Three mutants ($PAO1^{RES1-3}$) showed MICs toward POL7080 and L26-19 of >32 μg ml, but were more sensitive toward POL7001 (MIC 8 μg ml, versus 0 06 μg/ml for wild-type *PA* PAO1). No other changes in growth rate were observed. Compared to wild-type *PA* PAO1, the mutants showed only minor changes in sensitivity toward several other antibiotics (Table 2). To identify the causative mutation(s), we constructed three plasmid libraries from restriction-digested fragments of *PA* $PAO1^{RES1}$ genomic DNA and transformed wild-type *PA* PAO1 with selection for growth on agar

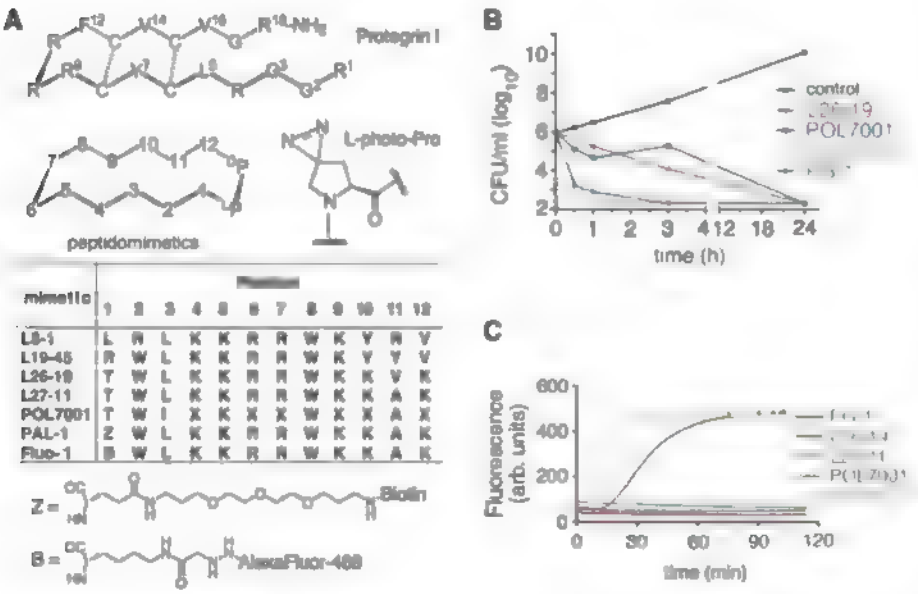

Fig. 1. (**A**) Structures of PG-1 and peptidomimetics. Dashed lines indicate disulfide bridges in PG-1. The single-letter code is used for amino acids (*30*), except as shown, and X is L-2,4-diaminobutyric acid, ^{D}P= D-proline, and ^{L}P is L-proline. PAL-1 contains L-photo-Pro in place of ^{L}P. (**B**) The kinetics of bacterial cell death at 37°C is shown for *PA* PAO1 in MH broth after treatment with the indicated antibiotics at 4× MIC, or for the control (no drug). The remaining colony-forming units (CFU) are shown as a function of time after exposure to the antibiotic. (**C**) *PA* membrane integrity was measured by fluorescence spectroscopy. *PA* PAO1 cells in MH broth were treated with SYTOX and each of the antibiotics (added at time $t = 0$) at a concentration of 5 μg/ml. The fluorescence change is shown versus time.

Table 1. Antimicrobial activities of the peptidomimetics. The MIC values were determined by the microdilution method in MH broth in the presence of 0.02% bovine serum albumin (BSA). The MIC values are typically four to eight times as high when the assays are performed in cation-adjusted MH (MH-II) broth in the presence of BSA. ND, not determined. Strains: *Pseudomonas aeruginosa*, *Acinetobacter baumannii*, *Klebsiella pneumoniae*, *Stenotrophomonas maltophilia*, *Escherichia coli*, *Enterococcus faecalis*, *Staphylococcus aureus*. ATCC, American Type Culture Collection; DSM, Deutsche Sammlung von Mikroorganismen.

Strain		MIC (μg/ml)					
		L8-1	L19-45	L26-19	L27-11	POL7001	POL7080
P. aeruginosa	ATCC 27853	8	1	0.02	0.01	0.008	0.008
P. aeruginosa	PAO1	8	2	0.03	0.004	0.008	0.004
A. baumannii	DSM3008	ND	ND	>64	>64	>64	>64
K. pneumoniae	ATCC 13883	ND	ND	>64	>64	>64	>64
S. maltophilia	ATCC 13637	ND	ND	>64	>64	>64	>64
E. coli	ATCC 25922	8	8	32	64	>64	>64
E. faecalis	DSM 12956	ND	ND	>64	>64	>64	>64
S. aureus	ATCC 29213	8	64	64	>64	>64	>64

containing carbenicillin and POL7080. Resistant clones were isolated from all three libraries. Plasmid DNA isolated from 12 clones contained a common 5.4-kb overlapping DNA fragment [nucleotides (nt) 652,070 to 657,452 in the genome sequence (*16*) of *PA* PAO1] containing two contiguous open reading frames identified as homologs of *surA* and *ostA* [also called *imp* and more recently *lptD* (used below)] (*17*). The 5.4-kb DNA fragment conferred the resistant phenotype on *PA* PAO1, whereas a smaller fragment containing only *surA* had no effect on resistance. The *surA* gene possessed the expected wild-type nucleotide sequence, whereas the *lptD* homolog from *PA* PAO1^{RES1} (here called *lptD1*) contained a mutation, consisting of a single 18 base pair tandem duplication of nt 628 to 645, corresponding to a tandem duplication of residues 210 to 215 with the sequence LRDKGM (*6*), with no other changes in the coding or upstream promoter sequences. The *lptD1* gene appears to act as a dominant resistance marker in the wild-type *PA* PAO1 background. This does not appear to be a gene dosage effect, because introduction of the wild-type allele on plasmid pVLT31 (*18*) does not influence antibiotic sensitivity for *PA* PAO1 or PAO1^{RES1}. Moreover, neither wild-type *PA* PAO1, containing plasmid-borne copies of *lptD1*, nor PAO1^{RES1}, containing copies of *lptD*, has altered sensitivity to most of the other antibiotics tested (Table 2). This argues against a general change in the permeability of the outer membrane caused by this mutation.

LptD is an outer-membrane protein widely distributed in Gram-negative bacteria that functions in the assembly of LPS in the outer leaflet of the outer membrane (*17*, *19*–*21*). LptD is an essential low-abundance outer-membrane protein in *Escherichia coli* (*19*), depletion of which causes stress in outer-membrane biogenesis (*21*, *22*). LptD in *PA* PAO1 is predicted to contain a C-terminal β-barrel domain (approximately residues 300 to 924) embedded in the outer membrane and an N-terminal domain (approximately residues 34 to 300) (*19*), which may reside in the periplasm and/or partly plug the β barrel (Fig. 2A). The β-barrel sequence is highly conserved in LptD homologs in Gram-negative bacteria (*17*), although the N-terminal domain is more variable in length, comprising about 300 residues in *PA* but only about 180 residues in *E. coli* K12 (*6*). The size difference in the periplasmic domains of LptD in *E. coli* and *PA*, the location within this domain of the *lptD1* mutation, and the key function of LptD in outer-membrane biogenesis suggest that LptD may be a primary target of the peptidomimetic antibiotics.

Photoaffinity labeling experiments (*23*) were performed to determine whether the antibiotics bind to LptD in intact cells. For this task, an analog (PAL-1) was produced that contains a L-4,4-diazarinylproline (L-photo-proline) in place of L-proline, as well as a biotin tag at position 1 (MIC of PAL-1 against *PA* PAO1 = 0.05 μg/ml) (Fig. 1A) (*6*). Photoaffinity labeling with PAL-1 consistently revealed a major photolabeled protein with an apparent mass by SDS polyacrylamide gel electrophoresis of ≈100 kD, close to that expected for *PA* LptD (calculated molecular weight = 100,751) (Fig. 2B). When the photoaffinity labeling was repeated in the presence of a 100× excess of L27-11, the labeled band disappeared from the blot, demonstrating a competition between L27-11 and PAL-1 for binding to LptD. The identity of the photolabeled protein was proven to be LptD (PA0595) by two-dimensional (2D) gels and in-gel protease digestion/LC-ESI-MS-MS (liquid chromatography–electrospray ionization–tandem mass spectrometry) analysis and by immunoblotting with polyclonal antibodies raised against a synthetic C-terminal peptide fragment of LptD (*6*). When the photolabeling experiment was repeated with the resistant PAO1^{RES1} mutant, photolabeling of LptD was not detected, indicating that the protein was no longer able to bind the antibiotic with comparable affinity.

If the function of LptD is impaired upon binding to the peptidomimetic, then some effect on outer-membrane structure and biogenesis should become apparent (*19*, *24*). When grown in Mueller-Hinton (MH) broth for several hours in the presence of growth-inhibitory amounts of L27-11, *PA* cells became more sensitive to detergents (Triton X-100 and SDS) and to various antibiotics, including tetracycline and rifampicin (*6*). *PA* PAO1 cells grown in MH broth with L27-11 or POL7001 were also examined in thin sections by transmission electron microscopy (TEM). This revealed internal accumulation of membrane-like material in many apparently intact cells (Fig. 2C), by two different fixation methods, an effect not seen in cells grown without the antibiotic. Similar accumulations have been observed in *E. coli* cells depleted of *lptD* (*21*, *22*) and in other bacteria exposed to antimicrobial peptides (*25*). Some cells (≈10%) grown in this way formed filaments comprising multiple concatenated cells (Fig. 2D), suggesting an impairment in cell division, which was not observed with untreated *PA* PAO1 cells or with L27-11 treated PAO1^{RES1} cells. Cells grown in the presence of growth-inhibitory amounts of L27-11 could be uniformly stained with the membrane dye 3,5-dipropylthiacarbocyanine [diSC$_3$(5)] (Fig. 2E), whereas untreated *PA* PAO1 or L27-11 treated PAO1^{RES1} cells exposed to this dye did not fluoresce. Thus, the action of L27-11 during growth impairs the outer-membrane permeability barrier.

Table 2. Antibacterial activities (MICs in MH-II broth) of various antibiotics toward wild-type *PA* PAO1 (PAO^{WT}) and resistant mutant (PAO1^{RES1}), as well as toward bacterial cells containing plasmid-borne copies of wild-type *lptD* or the resistance gene (*lptD1*) isolated from PAO1^{RES1}. The plasmid vector used for these experiments (pVLT31) has no effect on resistance to the antibiotics shown, when introduced into *PA* PAO1^{WT} or PAO1^{RES1}.

Antibiotic	MIC (μg/ml)				
	PAO1^{WT}	PAO1^{RES1}	PAO1^{WT} +*lptD1*	PAO1^{RES1} +*lptD*	PAO1^{RES1} +*lptD1*
POL7080	0.06	64	4	64	64
L26-19	0.1	>64	16	>64	>64
Gentamicin	0.5	1	0.5	1	1
Tobramycin	0.25	0.25	0.12	0.25	0.25
Ciprofloxacin	0.5	0.06	1	0.12	0.12
Colistin	1	0.5	0.5	0.5	0.25

Interference with the function of LptD may also allow entry of phospholipids into the outer leaflet of the outer membrane. In *E. coli* and *Salmonella* spp., this is known to activate the outer-membrane enzyme PagP, which modifies LPS by converting the hexa-acyl form of lipid A into the hepta-acyl form by transferring a palmitate group from outer-leaflet phospholipids to lipid A (*26*, *27*). The same effect has been observed in *lptD*-depleted *E. coli* (*21*). *PA* can also modify its lipid A by addition of a C16 fatty acid, to generate from the normal penta-acylated form (molecular weight 1447) a hexa-acylated derivative (molecular weight 1686) (*28*). This palmitate-containing hexa-acylated form has been observed in lipid A from *PA* clinical isolates from patients with cystic fibrosis (*29*), although it is normally absent from laboratory-adapted strains (such as PAO1) (*28*).

We first confirmed that the lipid A prepared from LPS isolated from *PA* PAO1 grown normally in MH broth was indeed the expected penta-acylated form {negative-mode matrix-assisted laser desorption/ionization (MALDI)–MS mass/charge ratio (*m/z*) 1446 [M-H]$^-$}. However, when cells were grown in MH broth with L27-11, after 5 hours the only lipid A detectable by MALDI-MS was the hexa-acylated form (observed mass *m/z* 1684 [M-H]$^-$) containing a palmitoyl residue (*6*). A further indication of a perturbed membrane structure came from fractionation of membrane extracts from cells by sucrose density ultracentrifugation. Fractions containing LPS and LptD appeared at higher density in the gradient when they came from L27-11–cultivated cells as compared to untreated cells (*6*), a result similar to that reported for *lptD*-depleted *E. coli* cells (*19*, *21*).

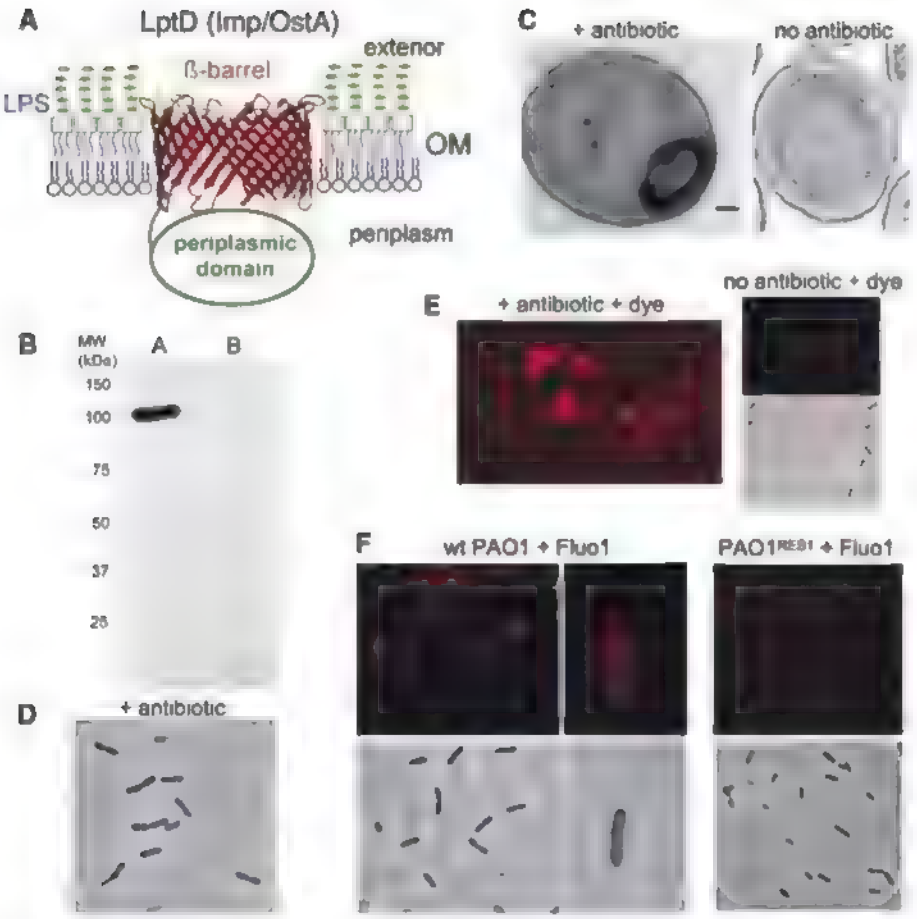

Fig. 2. **(A)** The predicted β-barrel domain of LptD (924 residues) is shown integrated in the outer membrane. **(B)** Photoaffinity labeling of membrane proteins in *PA* PAO1. PAL-1 (1 μg/ml) was incubated with *PA* cells at 37°C and irradiated with ultraviolet light. Membrane proteins were extracted, separated from cytoplasmic proteins by ultracentrifugation, and subjected to gel electrophoresis. Biotinylated proteins were detected by a streptavidin-based chemiluminescence detection system after blotting to a polyvinylidene difluoride membrane, with (100× excess, lane B) and without (lane A) competing L27-11 during photolysis (*6*). **(C** to **E)** Effects on *PA* cells after growth for 1 to 3 hours at 37°C in MH broth either with L27-11 (+ antibiotic) or without antibiotic (no antibiotic); (C) TEM showing accumulation of extra membrane-like material within cryo-fixed *PA* PAO1 cells (bar, 0.1 μm); (D) formation of filaments comprising multiple concatenated *PA* PAO1 cells; (E) staining *PA* PAO1 with the membrane-sensitive dye $diSC_3(5)$ and washing. **(F)** Staining and light microscope images of wild-type (wt) *PA* PAO1 (left) and resistant mutant $PAO1^{RES1}$ (right), after growth in the presence of Fluo-1 and washing.

A fluorescently labeled derivative Fluo-1 (Fig. 1A) of L27-11 showed an MIC against *PA* PAO1 of 0.1 μg/ml, suggesting that it might label potential antibiotic binding sites. *PA* PAO1 cells in MH broth were incubated with Fluo-1 (5 μg/ml) for 1 hour at 37°C, washed, and examined by fluorescence microscopy. The resulting fluorescence staining was not uniform over the cell surface, but rather appeared to be concentrated in spots (Fig. 2F), suggesting a localized binding site. A similar labeling was not observed when the *PA* $PAO1^{RES1}$ mutant was stained in this way.

The ability of the antibiotics to provide protection against a lethal *PA* infection in a whole animal was also tested. For this, the in vivo efficacy of POL7001 and POL7080 was evaluated in a mouse septicemia model at doses of 10, 3, 1, 0.3, and 0.1 mg per kilogram of body weight given subcutaneously at 1 and 5 hours after bacterial inoculation with either *PA* ATCC 9027 or ATCC 27853. Both antibiotics demonstrated substantial activity against both strains with calculated median effective doses (ED_{50} values) in the range 0.25 to 0.55 mg/kg, as compared to gentamicin (used as a positive control), which showed an ED_{50} of 3.1 and 2.9 mg/kg, respectively, against these strains.

The mechanism of action of the peptidomimetic antibiotics reported here likely includes perturbation of the critical LPS transport function of LptD. The in vivo activity reported here raises the prospect that this family of antibiotics may be useful in a clinical setting to combat nosocomial infections and lung infections in patients with cystic fibrosis, where multiple drug-resistant *PA* strains are a serious health problem.

References and Notes

1. J. A. Robinson *et al.*, *Bioorg. Med. Chem.* **13**, 2055 (2005)
2. S. C. Shankaramma *et al.*, *ChemBioChem* **3**, 1126 (2002)
3. V. N. Kokryakov *et al.*, *FEBS Lett.* **327**, 231 (1993)
4. L. Jiang, K. Moehle, B. Dhanapa., D. Obrecht, J. A. Robinson, *Helv. Chim. Acta* **83**, 3097 (2000)
5. J. A. Robinson, S. Demarco, F. Gombert, K. Moehle, D. Obrecht, *Drug Discov. Today* **13**, 944 (2008)
6. Supporting material is available on *Science* Online.
7. D. A. Steinberg *et al.*, *Antimicrob. Agents Chemother.* **41**, 1738 (1997)
8. Y. Cho, J. S. Turner, N.-N. Dinh, R. I. Lehrer, *Infect. Immun.* **66**, 2486 (1998)
9. J. J. Buffy *et al.*, *Biophys. J.* **85**, 2363 (2003)
10. D. Gidalevitz *et al.*, *Proc. Natl. Acad. Sci. U.S.A.* **100**, 6302 (2003)
11. R. Mani *et al.*, *Proc. Natl. Acad. Sci. U.S.A.* **103**, 16242 (2006)
12. R. Mani *et al.*, *Biochemistry* **45**, 8341 (2006)
13. M. Vaara, *Microbiol. Rev.* **56**, 395 (1992)
14. B. L. Roth, M. Poot, S. T. Yue, P. J. Millard, *Appl. Environ. Microbiol.* **63**, 2421 (1997)
15. R. A. Moore, R. E. Hancock, *Antimicrob. Agents Chemother.* **30**, 923 (1986)
16. C. K. Stover *et al.*, *Nature* **406**, 959 (2000)
17. M. P. Bos, V. Robert, J. Tommassen, *Annu. Rev. Microbiol.* **61**, 191 (2007)
18. V. de Lorenzo, L. Eltis, B. Kessler, K. N. Timmis, *Gene* **123**, 17 (1993)
19. M. Braun, T. J. Silhavy, *Mol. Microbiol.* **45**, 1289 (2002)
20. T. Wu *et al.*, *Cell* **121**, 235 (2005)
21. T. Wu *et al.*, *Proc. Natl. Acad. Sci. U.S.A.* **103**, 11754 (2006)
22. P. Sperandeo *et al.*, *J. Bacteriol.* **190**, 4460 (2008)
23. G. Dornán, G. D. Prestwich, *Trends Biotechnol.* **18**, 64 (2000)
24. B. A. Sampson, R. Misra, S. A. Benson, *Genetics* **122**, 491 (1989)
25. C. L. Friedrich, D. Moyles, T. J. Beveridge, R. E. Hancock, *Antimicrob. Agents Chemother.* **44**, 2086 (2000)
26. L. Guo *et al.*, *Cell* **95**, 189 (1998)
27. W. Jia *et al.*, *J. Biol. Chem.* **279**, 44966 (2004)
28. R. K. Ernst *et al.*, *J. Bacteriol.* **188**, 191 (2006)
29. R. K. Ernst *et al.*, *Science* **286**, 1561 (1999)
30. Single-letter abbreviations for the amino acid residues are as follows: A, Ala; C, Cys; F, Phe; G, Gly; I, Ile; K, Lys; L, Leu; R, Arg; T, Thr; V, Val; W, Trp; and Y, Tyr

31. We thank A. Meier for technical support. This study was supported by grants from the Swiss National Science Foundation, the Swiss Commission for Technology and Innovation, and the European Union 7th Framework Programme (project NABATIVI). Relevant patents are WO 2007/079605, WO 2007/079597, and WO/2004/018503. J.R. is a consultant for Polyphor AG. Patents that cover the structure, synthesis, and activity of the antibiotics (AGWO/2007/079605, WO/2007/079597, WO/2004/018503) are owned jointly by University of Zurich and Polyphor AG.

Supporting Online Material

www.sciencemag.org/cgi/content/full/327/5968/1010/DC1
Materials and Methods
Figs. S1 to S11
Tables S1 to S7
References

1 October 2009; accepted 19 January 2010
10.1126/science.1182749

NMR Structure Determination for Larger Proteins Using Backbone-Only Data

Srivatsan Raman,[1*†] Oliver F. Lange,[1*] Paolo Rossi,[2] Michael Tyka,[1] Xu Wang,[3] James Aramini,[2] Gaohua Liu,[2] Theresa A. Ramelot,[4] Alexander Eletsky,[5] Thomas Szyperski,[5] Michael A. Kennedy,[4] James Prestegard,[3] Gaetano T. Montelione,[2] David Baker[1,6‡]

Conventional protein structure determination from nuclear magnetic resonance data relies heavily on side-chain proton-to-proton distances. The necessary side-chain resonance assignment, however, is labor intensive and prone to error. Here we show that structures can be accurately determined without nuclear magnetic resonance (NMR) information on the side chains for proteins up to 25 kilodaltons by incorporating backbone chemical shifts, residual dipolar couplings, and amide proton distances into the Rosetta protein structure modeling methodology. These data, which are too sparse for conventional methods, serve only to guide conformational search toward the lowest-energy conformations in the folding landscape; the details of the computed models are determined by the physical chemistry implicit in the Rosetta all-atom energy function. The new method is not hindered by the deuteration required to suppress nuclear relaxation processes for proteins greater than 15 kilodaltons and should enable routine NMR structure determination for larger proteins.

The first step in protein structure determination by nuclear magnetic resonance (NMR) is chemical-shift assignment for the backbone atoms. In contrast to the subsequent assignment of the side chains, this process is now rapid, reliable, and largely automated (*1*–*5*). Global backbone structural information complementing the local structure information provided by backbone chemical-shift assignments (*6*, *7*) can be obtained from H^N-H^N nuclear Overhauser effect spectroscopy (NOESY), residual dipolar coupling (RDC) (*8*), and other (*9*, *10*) experiments. For larger proteins, deuteration becomes necessary to circumvent the efficient spin relaxation properties resulting from their higher rotational correlation times (*11*, *12*), but removing protons also eliminates long-range NOESY information from side chains, except for selectively protonated side-chain moieties (*13*). The difficulty in determining accurate structures with no or limited side-chain information is a major bottleneck that currently prevents routine application of NMR to larger (>15 kD) systems (*14*).

Here we show that structures of proteins up to 200 residues (23 kD) can be determined with the use of information from backbone (H^N, N, C^α, C^β, C′) NMR data by taking advantage of the conformational sampling and all-atom energy function in the Rosetta structure prediction methodology (*15*), which, for small proteins in favorable cases, can produce atomic accuracy models starting from sequence information alone (*16*, *17*). Structure prediction in Rosetta proceeds in two steps: (i) a low-resolution exploration phase using Monte Carlo fragment assembly and a coarse-grained energy function, and (ii) a computationally expensive refinement phase that cycles between combinatorial side-chain optimization and gradient-based minimization of all torsional degrees of freedom in a physically realistic all-atom forcefield (*16*). The primary obstacle to Rosetta structure prediction from amino acid sequence information alone is conformational sampling; native structures almost always have lower energies than non-native conformations, but they are very seldom sampled in unbiased trajectories. Incorporating NMR chemical-shift information in the selection of the fragments used in the exploration phase [chemical shift (CS)–Rosetta] (*18*, *19*) provides a robust approach to determining accurate structures of small (<100-residue) proteins using only backbone and $^{13}C^\beta$ chemical-shift data. For larger (>12-kD) proteins, the performance of CS-Rosetta is very target-dependent: Structures sufficiently close to the native structure for the energy to drop substantially may be generated rarely or not at all.

We investigated whether RDC data, which provide long-range information on the orientations between bond vectors, can guide the low-resolution search closer to the native structure and overcome the sampling problem for larger (100 to 200 residue) proteins. For every attempted Monte Carlo move, the alignment tensor is calculated by singular value decomposition (*20*), and the decision to accept or reject the conformation is biased by the change in the agreement between the back-calculated and experimental couplings (*21*). Incorporation of RDCs dramatically improved convergence on the correct structure in a benchmark of 11 α, β, and α/β proteins ranging in size from 62 to 166 residues (Fig. 1, Table 1, and fig. S1). As indicated in Table 1, CS-RDC-Rosetta consistently generates accurate models for proteins up to 120 residues and, in favorable cases, for larger proteins.

For proteins with more than 120 residues, conformational sampling becomes limiting, even for the CS-RDC-Rosetta protocol, and the low-

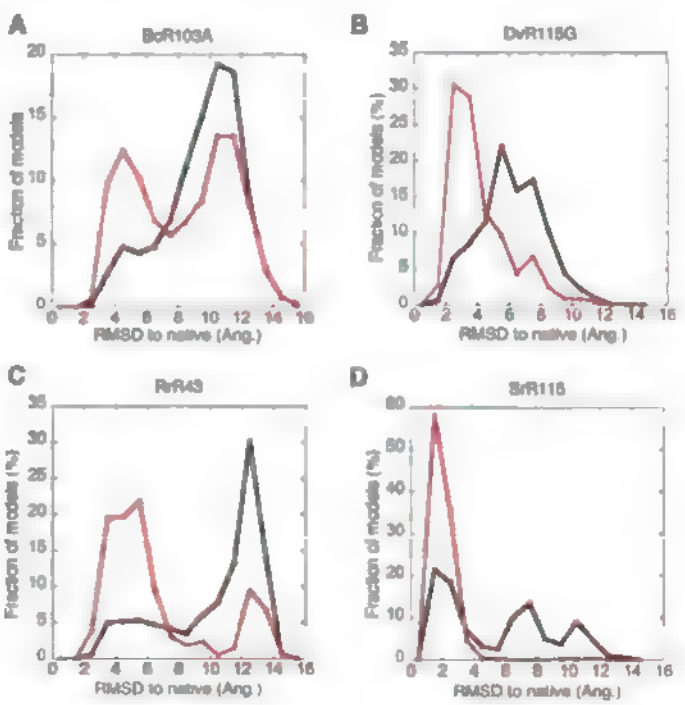

Fig. 1. Impact of RDC data on conformational search. Lines depict RMSD histograms of structures selected in the lowest 10th percentile of coarse-grained energy for ensembles generated with the use of CS-Rosetta (black) or CS-RDC-Rosetta (red). (**A**) BcR103A, (**B**) DvR115G, (**C**) RrR43, and (**D**) SrR115C. Ang., angstrom.

[1]Department of Biochemistry, University of Washington, Seattle, WA 98195, USA. [2]Department of Molecular Biology and Biochemistry, Center for Advanced Biotechnology and Medicine, and Northeast Structural Genomics Consortium, Rutgers University, Piscataway, NJ 08854, USA. [3]Complex Carbohydrate Research Center, University of Georgia, Athens, GA 30602, USA. [4]Department of Chemistry and Biochemistry and Northeast Structural Genomics Consortium, Miami University, Oxford, OH 45056, USA. [5]Department of Chemistry, State University of New York at Buffalo, Buffalo, NY 14260, USA. [6]Howard Hughes Medical Institute (HHMI), Seattle, WA 98195, USA.

*These authors contributed equally to this work.
†Present address: Department of Genetics, Harvard Medical School, Boston, MA 02115, USA.
‡To whom correspondence should be addressed. E-mail: dabaker@u.washington.edu.

energy ensemble is not always close to the native structure. To further focus sampling, we developed an iterative refinement protocol that incorporates assigned backbone H^N-H^N nuclear Overhauser effects (NOEs) in addition to backbone RDCs. As in the previously described "rebuild and refine" protocol, a pool of diverse low-energy conformations is maintained, and the highest-energy structures in the pool are periodically replaced with offspring (*22*). The new protocol, a genetic algorithm, generates hybrid conformations by recombining first β-sheet pairings and, subsequently, fragments of the low-energy structures (*17*). To further enhance sampling, trajectories are seeded with conformations harvested from previous trajectories that led to low-energy conformations (*23*).

The improvement in the model population with increasing generations in the iterative protocol is illustrated in Fig. 2 for the 200-residue ALG13 protein using experimentally determined chemical shift, RDC, and assigned backbone amide H^N-H^N NOE data (*24*). The C^α root mean square deviation (RMSD) to the native structure and the energy improve from generation to generation, and after several rounds, discrimination toward lower RMSD structures is apparent (Fig. 2A, light blue to yellow). After high-resolution refinement (Fig. 2A, orange to red), the lowest-energy structures are close to the native structure. The final low-energy structural ensemble (Fig. 2B) recapitulates the unusual topology in the previously determined NMR structure (*24*) (Fig. 2D) to within 3.4 Å RMSD (Table 1). The Rosetta ensemble fits independent RDC data, as well as the NMR structure, and the backbone variation in the ensemble is correlated with backbone dynamics as probed by the R1 relaxation rate (Fig. 2C). The iterative CS-RDC-NOE-Rosetta models of ALG13 thus appear to be comparable in quality to the previously published structure that required substantial effort, including preparation of selectively methyl- and aromatic-protonated samples (*24*).

The iterative CS-RDC-NOE protocol was tested further on 12 proteins ranging in size from 120 to 266 residues (Table 1 and fig. S3). For all proteins except 1g68, a considerable part of the structure converges (Table 1). Backbone H^N-H^N NOE data were required for convergence of 2z2i, 1i1b, arf1, 2m2, and 1sua but not for 5pnt, 1s0p, 1f21, and cr553. The RMSDs to the native structures over the converged regions range from 1.7 to 4.3 Å, with the exceptions of 1sua and 1f21. For 1f21, high accuracy (1.6 Å) was reached for a 92-residue subset (fig. S3). Side-chain accuracy was generally quite high in the converged regions (fig. S5).

Table 1. Accuracy of models generated with backbone-only NMR data.

Protein name*	Native PDB ID	Topology	Number of residues/ number of residues converged in computed structure	Median RMSD to native over converged region† (Å)	Median GDT-TS among lowest-energy models‡	Depth of converged ensemble energy minimum§	Median energy change resulting from inclusion of experimental data‖
			Noniterative				
GmR137	2k5p	a/b	62/47	2.6	95.4	−32.5¶	−1.8
TR80	2jxt	a/b	78/73	1.5	84.9	−16.7¶	−0.3
DvR115G#	2kct	B	86/66	1.4	80.0	−24.3	−0.7
LkR15	2k3d	a/b	92/74	2.0	85.4	−18.0¶	−1.2
BcR103A	2kd1	B	100/65	3.4	61.3	−22.7	−1.3
SrR115C#	2kcl	A	100/95	1.4	86.1	−25.1¶	0.7§§
MaR214A#	2kbn	B	102/96	2.1	82.1	−43.9	−0.6
RrR43	2k0m	a/b	104/82	2.1	66.8	−12.9	2.9§§
BcR268F#	2k5w	A	118/115	1.4	78.4	−45.7¶	−1.6
ER553	2k1s	a/b	143/115	5.2	46.1§§	−5.1	−2.5
ARF1	2k5u	a/b	166/141	2.6	73.3	−21.6	−9.5
			Iterative				
AtT7#	2ki8	a/b	122/98	3.0	70.0	−37.5	−12.5
ER541**	2jyx	a/b	124/115	2.5	76.7	−31.6	−9.9
X-ray**	1f21	a/b	142/122	9.4	76.6	−28.5	3.5§§
ER553	2k1s	a/b	143/136	1.9	85.2	−38.5	−15.4
BtR324B**	2kd7	B	150/148	2.4	79.3	−51.6	−29.1
X-ray**	1i1b	B	151/111‡‡	2.5	71.1	−53.3	−25.5
X-ray**	1i1b_2††	B	151/133‡‡	1.7	84.8	−100.9	−30.5
X-ray**	2rn2	a/b	155/76	3.1	72.9	−67.5	−24.0
X-ray**	5pnt	a/b	157/134	3.0	71.6	−34.4	−3.0
X-ray**	1s0p	A	160/116	4.3	70.8	−19.9	−10.4
ARF1	2k5u	a/b	166/122	2.5	77.2	−28.6	−8.7
X-ray**	2z2i	a/b	179/143	1.8	77.7	−46.5	−21.6
ALG13	2jzc	a/b	201/155‡‡	3.4	63.7	−77.8	−12.8
X-ray**	1sua	a/b	263/173	6.2	57.0	−43.5	−26.5
X-ray**	1g68	a/b	266/119	3.2	41.4§§	−36.3	−25.1

*NESG codes are used for protein structures obtained with conventional NMR methods in the NESG, and PDB codes for the remaining proteins. The results shown in the top 11 rows were generated with the CS-RDC-Rosetta protocol and the remaining with the iterative CS-RDC-Rosetta protocol. †For the iterative protocol, residues were considered converged if they are members of the largest set of residues that is superimposable within 4 Å. For the noniterative protocol, the residues were selected with the FindCore algorithm (*26*, *27*) based on the conventional NMR ensemble. ‡The global distance test–total score (GDT-TS) is the average number of C_α superimposable within 1, 2, 3, 4, and 7 Å, respectively (*28*). Shown is the median of GDT-TS scores computed for each pair of structures out of the 10 lowest-energy models. §Energy difference between the median energy of the 10 lowest-energy models and the 10 lowest-energy models that differ by at least 7 Å RMSD from the lowest-energy model. Rosetta energy units). ‖Difference between the median energy of the 10 lowest-energy models obtained with RDC and/or NOE data and the median energy of the 10 lowest-energy CS-Rosetta models (Rosetta energy units). ¶Energy gap computed with 4 Å cutoff radius (instead of 7 Å). #Blind test case. **Partially or fully synthetic data were used (see table S2). ††All pairs of H^N protons within 5 Å generated an H^N-H^N NOE distance constraint of 6 Å (*17*). ‡‡Results are shown with a reduced convergence cutoff of 3 Å (with cutoff 4 Å, 151, 151, and 176 residues converge and yield a median RMSD of 3.5, 2.3, and 4.9 Å for 1i1b, 1i1b_2, and 2jzc, respectively). §§Violation of validation criterion.

We carried out a blind test of the new methods on five data sets generated in the Northeast Structural Genomics (NESG) Center before conventional NMR structures were determined. For four of the proteins, the CS-RDC protocol converged (Fig. 3, A to D), whereas for a fifth, convergence was not observed, and blind structure determination was instead carried out with the iterative CS-RDC-NOE protocol (Fig. 3E). In

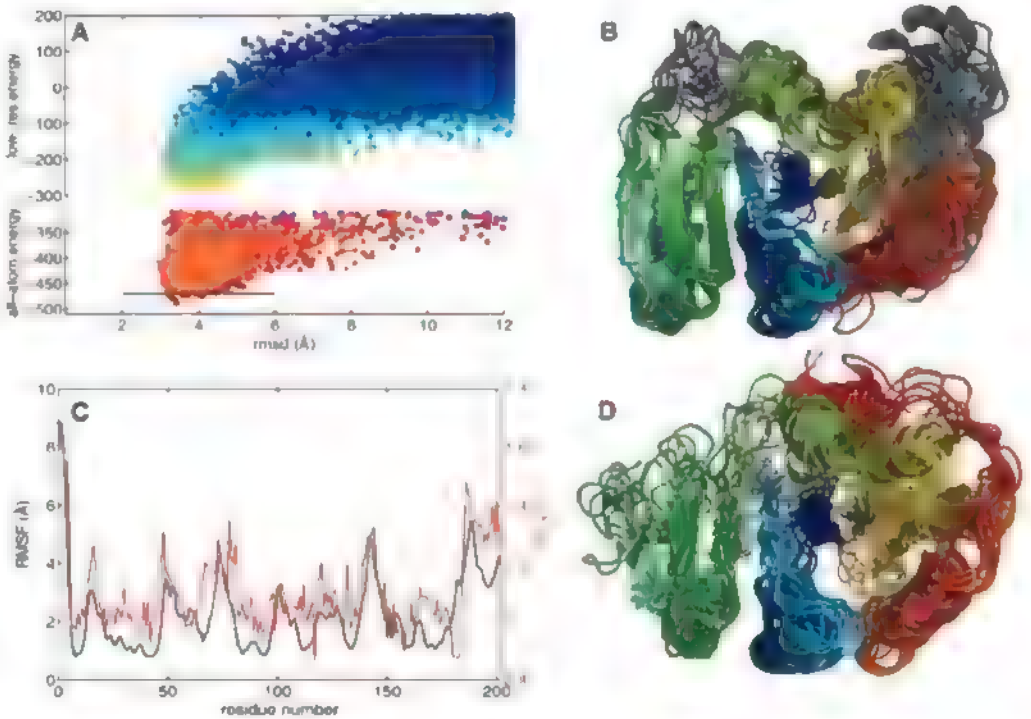

Fig. 2. Determination of ALG13 structure from backbone NMR data with Rosetta. **(A)** RMSDs and energies of structures generated in batches of 2000 during the iterative protocol. Each generation of structures (color code: blue to red, corresponds to number of generation) is based on information from previous runs (*17*). Strong convergence is reached already in the computational less expensive, low-resolution mode. The last generations (orange to red) increase both the precision and accuracy of the ensemble by refining the structures within the Rosetta all-atom energy. The RMSD is computed over the residues for which convergence within 3 Å root mean square fluctuations (RMSF) was reached in the 50 lowest-energy Rosetta models (residues 5 to 70, 81 to 139, 151 to 180). **(B)** Ensemble of 10 lowest-energy Rosetta structures [below line in (A)]. Regions with more than 3 Å RMSF are depicted in gray. **(C)** Comparison of the RMSF at each residue in the low-energy Rosetta ensemble to NMR R1 relaxation rate (red, relaxation rates; black, RMSF in Rosetta ensemble). The relaxation data were not used in the structure calculation. Regions variable in the low-energy structures exhibit increased dynamics in solution, these data were not used in the structure calculation. **(D)** NMR solution ensemble based on side-chain NOEs (PDB ID: 2jzc).

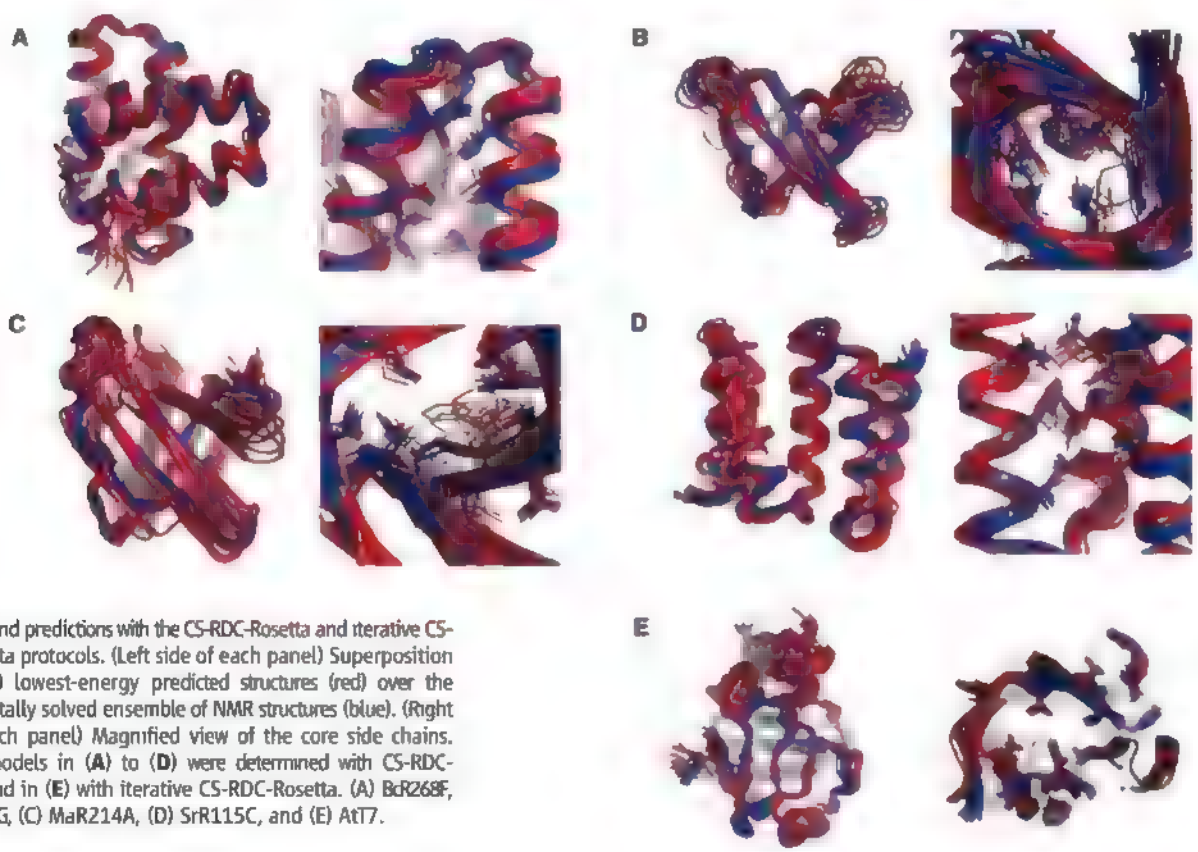

Fig. 3. Blind predictions with the CS-RDC-Rosetta and iterative CS-RDC-Rosetta protocols. (Left side of each panel) Superposition of the 10 lowest-energy predicted structures (red) over the experimentally solved ensemble of NMR structures (blue). (Right side of each panel) Magnified view of the core side chains. Rosetta models in **(A)** to **(D)** were determined with CS-RDC-Rosetta, and in **(E)** with iterative CS-RDC-Rosetta. (A) BcR268F, (B) DvR115G, (C) MaR214A, (D) SrR115C, and (E) AtT7.

all five cases (Table 1), the resulting Rosetta-determined structure is very similar to the conventionally determined NMR solution structure over both the backbone (Fig. 3, left side of each panel) and the core side chains (Fig. 3, right side of each panel), which is notable because no experimental side-chain information is used in the Rosetta protocol; the details of core packing are determined by the Rosetta all-atom energy function (magnified views of core side chains are shown for all of the remaining targets in fig. S6).

Thus, our methodology is able to generate accurate structures of proteins up to ~25 kD from sparse NMR data without side-chain assignments. To be useful in practice, it is important that there be a means of assessing the reliability of the computed models. Cross-validation with independently collected data are an excellent way to do this, but truly independent data may not always be available, and if the available data are already sparse, it may not be possible to remove a subset for independent validation.

Our approach to structure validation is based on the interplay between the two contributing sources of structural information: (i) the detailed physical chemistry implicit in the Rosetta all-atom energy function and (ii) the experimental NMR data. As illustrated in Fig. 4A, the all-atom energy landscape (black) is rugged with many local minima, making optimization difficult. The experimental bias based on backbone NMR data (red), though smoother, is degenerate and lacks resolution. Because the constrained minimization of a function will almost always result in higher function values than unconstrained minimization, NMR data–constrained optimization, in general, should result in higher-energy structures than bias-free optimization (arrow 1 in Fig. 4A). This scenario may hold for traditional structure determination in which the search is almost completely driven by the experimental data. However, if the two sources of information are in concordance, the bias from the experimental data can have two favorable effects (Fig. 4B). First, optimization far from the native minimum is impeded, resulting in an upward shift of the energy of non-native structures (arrow 1), and second, optimization near the native minimum is improved as the data guide the search toward the global minimum (Fig. 4, A and B, arrow 2).

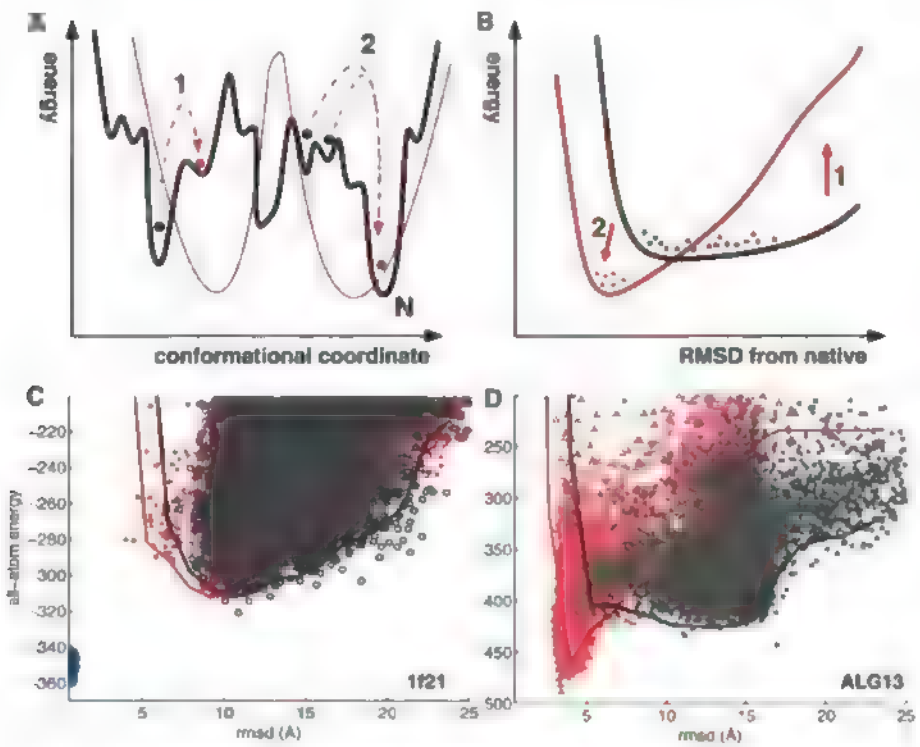

Fig. 4. Effect of incorporation of experimental data on energy minimization. **(A)** The Rosetta all-atom energy (black line) has many local minima, making minimization difficult, but the global minimum is generally close to the native structure (N). The experimental bias (red line), though smoother, has degeneracies and lacks resolution because the data are sparse. Local minima of the all-atom energy and the experimental bias are uncorrelated far away from the native structure but coincide close to the native structure. Accordingly, far from the global minimum, including the experimental data during optimization usually results in higher energies (arrow 1), whereas close to the native structure (N), including the data results in lower energies (arrow 2). **(B)** Lines represent the lowest energies sampled by structures at various RMSDs after optimization in the absence (black line) or presence (red line) of experimental data. Generally, the all-atom energy and experimental data are in concordance for conformations close to the native protein structure but not for conformations far from the native structure. If this concordance condition is met, the experimental data can guide sampling toward the global minimum close to the native structure (arrow 2), and thus, constrained optimization can result in lower-energy conformations than unconstrained optimization, whereas biased optimization is less effective than unconstrained optimization distant from the native structure leading to higher energies (arrow 1). **(C** and **D)** In contrast, all-atom energy and RMSD of final Rosetta ensemble from iterative refinement, with and without experimental data, are shown. Lines represent the median of the 10 lowest-energy models per RMSD bin. (C) 1f21, an unsuccessful calculation. Biased optimization with RDC data (red) yields similar energies as unbiased optimization (black); there is a large remaining energy gap to the native structure (blue dots). (D) Alg13, a successful calculation. Biased optimization with the experimental data (red) results in lower energies than unbiased optimization (black).

Better optimization in the presence of experimental data (Fig. 4B) is unlikely to occur if there is no sampling near the correct structure, as data and the energy function will almost never independently favor the same incorrect structure. Hence, we propose the following three criteria for evaluating the reliability of a calculated structure (Table 1, columns 6 to 8). First, the calculation should converge: The lowest-energy conformations should be very similar to each other over a large fraction of the structure. For both the CS-RDC-Rosetta and the iterative protocol, whenever the calculation converged for more than 60% of the structure, the RMSD to native over this region was less than 4 Å (Table 1, column 6). Second, the converged structures should clearly be lower in energy than all significantly different (RMSD > 7 Å) structures; this was true for nearly all of our test cases (Table 1, column 7). Third, the structures generated with experimental data should be at least as low in energy as those generated without experimental data, for none of the successful calculations does the energy increase significantly when the experimental data are included in the optimization (Table 1, column 8). For larger proteins (>120 residues), the data in fact guide the trajectories to lower-energy structures than those obtained by unconstrained optimization (Fig. 4D and Table 1, column 8). As argued above, this is a strong indicator that the correct structure has been found.

When all three criteria were satisfied for the 20 proteins in our test set, the low-energy ensemble resembles the independently determined structures. Importantly, the clear structure calculation failure, 1f21, which converged to a wrong conformation with an RMSD of 9.4 Å to the native, fails the third criterion: The energy is higher rather than lower when the experimental data are included in the optimization (Fig. 4C and Table 1, column 8). Because we had only one such failure, we simulated additional failures by deleting all near-native structures from the model populations and computed the three metrics described above for these "fake" minima, (table S1) (*17*). For almost all of the proteins, these constructed pathological cases again fail the third

criterion: They have higher energies in the experimentally biased optimization.

For the proteins in our set in the ~30-kD molecular-weight range, the computed structures are not completely converged and have large disordered regions. This is clearly a sampling problem because the native structure has lower energy (Fig. 4C and fig. S3); even with the NMR data as a guide, Rosetta trajectories fail to sample very close to the native state. Increased convergence on the low-energy native state can be achieved either by collecting and using additional experimental data (1ilb_2 in fig. S3) or by improved sampling. Though at present the former is the more reliable solution, the latter will probably become increasingly competitive as the cost of computing decreases and conformational search algorithms improve.

We have shown that accurate structures can be computed for a wide range of proteins using backbone-only NMR data. These results suggest a change in the traditional NOE-constraint based approach to NMR structure determination (fig. S4). In the new approach, the bottlenecks of side-chain chemical-shift assignment and NOESY assignment are eliminated, and instead, more backbone information is collected: RDC's in one or more media and a small number of unambiguous H^N-H^N constraints from three- or four-dimensional experiments, which restrict possible β-strand registers. Advantages of the approach are that ^1H,^{15}N-based NOE and RDC data quality is relatively unaffected in slower tumbling, larger proteins and that the analysis of resonance and NOESY peak assignments can be done in a largely automated fashion with fewer opportunities for error. The approach is compatible with deuteration necessary for proteins greater than 15 kD and, for larger proteins, can be extended to include methyl NOEs on selectively protonated samples. The method should also enable a more complete structural characterization of transiently populated states (*25*) for which the available data are generally quite sparse.

References and Notes

1. D. E. Zimmerman *et al.*, *J. Mol. Biol.* **269**, 592 (1997).
2. C. Bartels, P. Güntert, M. Billeter, K. Wüthrich, *J. Comput. Chem.* **18**, 139 (1998).
3. M. C. Baran, Y. J. Huang, H. N. Moseley, G. T. Montelione, *Chem. Rev.* **104**, 3541 (2004).
4. Y. S. Jung, M. Zweckstetter, *J. Biomol. NMR* **30**, 11 (2004).
5. W. Lee, W. M. Westler, A. Bahrami, H. R. Eghbalnia, J. L. Markley, *Bioinformatics* **25**, 2085 (2009).
6. M. Berjanskii *et al.*, *Nucleic Acids Res.* **37** (Web Server issue), W670 (2009).
7. Y. Shen, F. Delaglio, G. Cornilescu, A. Bax, *J. Biomol. NMR* **44**, 213 (2009).
8. G. Kontaxis, F. Delaglio, A. Bax, *Methods Enzymol.* **394**, 42 (2005).
9. I. Bertini, C. Luchinat, G. Parigi, R. Pierattelli, *Dalton Trans.* **29**, 3782 (2008).
10. J. H. Prestegard, C. M. Bougault, A. I. Kishore, *Chem. Rev.* **104**, 3519 (2004).
11. S. Grzesiek, A. Bax, *J. Biomol. NMR* **3**, 627 (1993).
12. D. M. LeMaster, F. M. Richards, *Biochemistry* **27**, 142 (1988).
13. K. H. Gardner, M. K. Rosen, L. E. Kay, *Biochemistry* **36**, 1389 (1997).
14. G. Wagner, *J. Biomol. NMR* **3**, 375 (1993).
15. R. Das, D. Baker, *Ann. Rev. Biochem.* **77**, 363 (2008).
16. P. Bradley, K. M. S. Misura, D. Baker, *Science* **309**, 1868 (2005).
17. Materials and methods are available as supporting material on *Science* Online.
18. A. Cavalli, X. Salvatella, C. M. Dobson, M. Vendruscolo, *Proc. Natl. Acad. Sci. U.S.A.* **104**, 9615 (2007).
19. Y. Shen *et al.*, *Proc. Natl. Acad. Sci. U.S.A.* **105**, 4685 (2008).
20. J. A. Losonczi, M. Andrec, M. W. Fischer, J. H. Prestegard, *J. Magn. Reson.* **138**, 334 (1999).
21. C. A. Rohl, D. Baker, *J. Am. Chem. Soc.* **124**, 2723 (2002).
22. B. Qian *et al.*, *Nature* **450**, 259 (2007).
23. T. J. Brunette, O. Brock, *Proteins* **73**, 958 (2008).
24. X. Wang, T. Weldeghiorghis, G. Zhang, B. Imperiali, J. H. Prestegard, *Structure* **16**, 965 (2008).
25. H. van Ingen, D. M. Korzhnev, L. E. Kay, *J. Phys. Chem. B* **113**, 9968 (2009).
26. D. A. Snyder, G. T. Montelione, *Proteins* **59**, 673 (2005).
27. The FindCore algorithm is available at http://fips.nesg.org.
28. A. Zemla, *Nucleic Acids Res.* **31**, 3370 (2003).

29. We are thankful to the U.S. Department of Energy Innovative and Novel Computational Impact on Theory and Experiment Award for providing access to the Blue Gene/P supercomputer at the Argonne Leadership Computing Facility and to Rosetta@home participants for their generous contributions of computing power. We thank Y. Shen and A. Bax for fruitful discussions, Y. J. Huang and Y. Tang for their contribution during preliminary studies using sparse NOE constraints with CS-Rosetta, S. Bansal, H.-w. Lee, and Y. Liu for collection of RDC data, A. Lemak for providing the Crystallography and NMR System RDC refinement protocol, and the NESG consortium for access to other unpublished NMR data that has facilitated methods development. S.R., O.F.L., P.R., G.T.M., and D.B. designed research. S.R. designed and tested the CS-RDC-Rosetta protocol. O.F.L. designed and tested the iterative CS-RDC-NOE-Rosetta protocol. M.T. developed the all-atom refinement protocol; S.R., O.F.L. and D.B. designed and performed research for energy based structure validation; X.W. and J.P. analyzed the ALG13 ensemble; J.A, G.L, T.R, A.E, M.K, and T.S provided blind NMR data sets, and S.R., O.F.L., P.R., G.T.M., and D.B. wrote the manuscript. This work was supported by the Human Frontiers of Science Program (O.F.L.), NIH grant GM76222 (D.B.), the HHMI, the National Institutes of General Medical Science Protein Structure Initiative program grant U54 GM074958 (G.T.M.), and the Research Resource grant RR005351 (J.P.). M.T. holds a Sir Henry Wellcome Postdoctoral Fellowship. RDC and Paramagnetic Relaxation Enhancement data as deposited in the Protein Data Bank (PDB) with accession code 2jzc.

Supporting Online Material

www.sciencemag.org/cgi/content/full/science.1183649/DC1
Materials and Methods
SOM Text
Figs. S1 to S5
Tables S1 to S3
References

21 October 2009; accepted 14 January 2010
Published online 4 February 2010;
10.1126/science.1183649
Include this information when citing this paper

Limits of Predictability in Human Mobility

Chaoming Song,[1,2] Zehui Qu,[1,2,3] Nicholas Blumm,[1,2] Albert-László Barabási[1,2]*

A range of applications, from predicting the spread of human and electronic viruses to city planning and resource management in mobile communications, depend on our ability to foresee the whereabouts and mobility of individuals, raising a fundamental question: To what degree is human behavior predictable? Here we explore the limits of predictability in human dynamics by studying the mobility patterns of anonymized mobile phone users. By measuring the entropy of each individual's trajectory, we find a 93% potential predictability in user mobility across the whole user base. Despite the significant differences in the travel patterns, we find a remarkable lack of variability in predictability, which is largely independent of the distance users cover on a regular basis.

When it comes to the emerging field of human dynamics, there is a fundamental gap between our intuition and the current modeling paradigms. Indeed, although we rarely perceive any of our actions to be random, from the perspective of an outside observer who is unaware of our motivations and schedule, our activity pattern can easily appear random and unpredictable. Therefore, current models of human activity are fundamentally stochastic (*1*) from Erlang's formula (*2*) used in telephony to Lévy-walk models describing human mobility (*3*–*7*) and their applications in viral dynamics (*8*–*10*), queuing models capturing human communication patterns (*11*–*13*), and models capturing body balancing (*14*) or panic (*15*). Yet the probabilistic nature of the existing modeling framework raises fundamental questions: What is the role of randomness in human behavior and to what degree are individual human actions predictable? Our goal here is to quantify

[1]Center for Complex Network Research, Departments of Physics, Biology, and Computer Science, Northeastern University, Boston, MA 02115, USA. [2]Department of Medicine, Harvard Medical School, and Center for Cancer Systems Biology, Dana-Farber Cancer Institute, Boston, MA 02115, USA. [3]School of Computer Science and Engineering, University of Electric Science and Technology of China, Chengdu 610054, China.
*To whom correspondence should be addressed. E-mail: alb@neu.edu

the interplay between the regular and thus predictable and the random and thus unforeseeable, probing through human mobility the fundamental limits that characterize the predictability of human dynamics.

At present, the most detailed information on human mobility across a large segment of the population is collected by mobile phone carriers (*4*, *16*–*21*). Mobile carriers record the closest mobile tower each time the user uses his or her phone. Here we use a 3-month-long record, collected for billing purposes and anonymized by the data source, capturing the mobility patterns of 50,000 individuals chosen from ~10 million anonymous mobile phone users with the criteria that they visit more than two locations (tower vicinity) during the observational period and that their average call frequency f is ≥ 0.5 hour^{-1} [(*22*) sections S1 and S2].

The trajectories of two users with widely different mobility patterns are shown in Fig. 1A: The first user moves in the vicinity of $N = 22$ towers in a 30-km region, whereas the second visits as many as $N = 76$ towers spanning approximately a 90-km neighborhood. To understand the recurrent nature of individual mobility, we assigned to each user a mobility network (*23*) (Fig. 1B), in which nodes are the locations visited by the user (each location corresponding to a mobile phone tower, with about a 3-km^2 reception area on average, representing the uncertainty in our ability to determine the user's whereabouts), and links represent the observed movements between these. The uneven node sizes, corresponding to the percentage of time the user spent in the vicinity of the particular tower, indicate that individuals tend to spend most of their time in a few selected locations. Finally, each mobility network has an associated dynamical pattern (Fig. 1C), capturing the temporal sequence of towers visited by the user.

Entropy is probably the most fundamental quantity capturing the degree of predictability characterizing a time series (*24*). We assign three entropy measures to each individual's mobility pattern: (i) The random entropy $S_i^{\mathrm{rand}} \equiv \log_2 N_i$, where N_i is the number of distinct locations visited by user i, capturing the degree of predictability of the user's whereabouts if each location is visited with equal probability; (ii) the temporal-uncorrelated entropy $S_i^{\mathrm{unc}} \equiv -\sum_{j=1}^{N_i} p_i(j) \log_2 p_i(j)$, where $p_i(j)$ is the historical probability that location j was visited by the user i, characterizing the heterogeneity of visitation patterns; (iii) the actual entropy, S_i, which depends not only on the frequency of visitation, but also the order in which the nodes were visited and the time spent at each location, thus capturing the full spatiotemporal order present in a person's mobility pattern. To be specific, if $T_i = \{X_1, X_2, \cdots, X_I\}$ denotes the sequence of towers at which user i was observed at each consecutive hourly interval, the entropy S_i is given by $-\sum_{T_i' \subset T_i} P(T_i') \log_2[P(T_i')]$, where $P(T_i')$ is the probability of finding a particular time-ordered subsequence T_i' in the trajectory T_i [(*22*) section *S4*]. Naturally, for each user, $S_i \leq S_i^{\mathrm{unc}} \leq S_i^{\mathrm{rand}}$.

To calculate the real entropy S_i, we need a continuous (e.g., hourly) record of a user's momentary location. Mobile phone records provide location information only when a person uses his or her phone. The users tend to place most of their calls in short bursts (*11*–*13*, *25*) (Fig. 1D), followed by long periods with no call activity, during which we have no information about the user's location (Fig. 1C). This incompleteness of the collected data is captured by the parameter q, representing the fraction of hour-long intervals when the user's location is unknown to us. As Fig. 1E shows, $P(q)$ across our user base peaked around $q = 0.7$, which indicated that, for a typical user, we have no location update for about 70% of the hourly intervals, which masks the user's real entropy S_i. We therefore studied the dependence of the entropy $S(q)$ on the incompleteness q, which

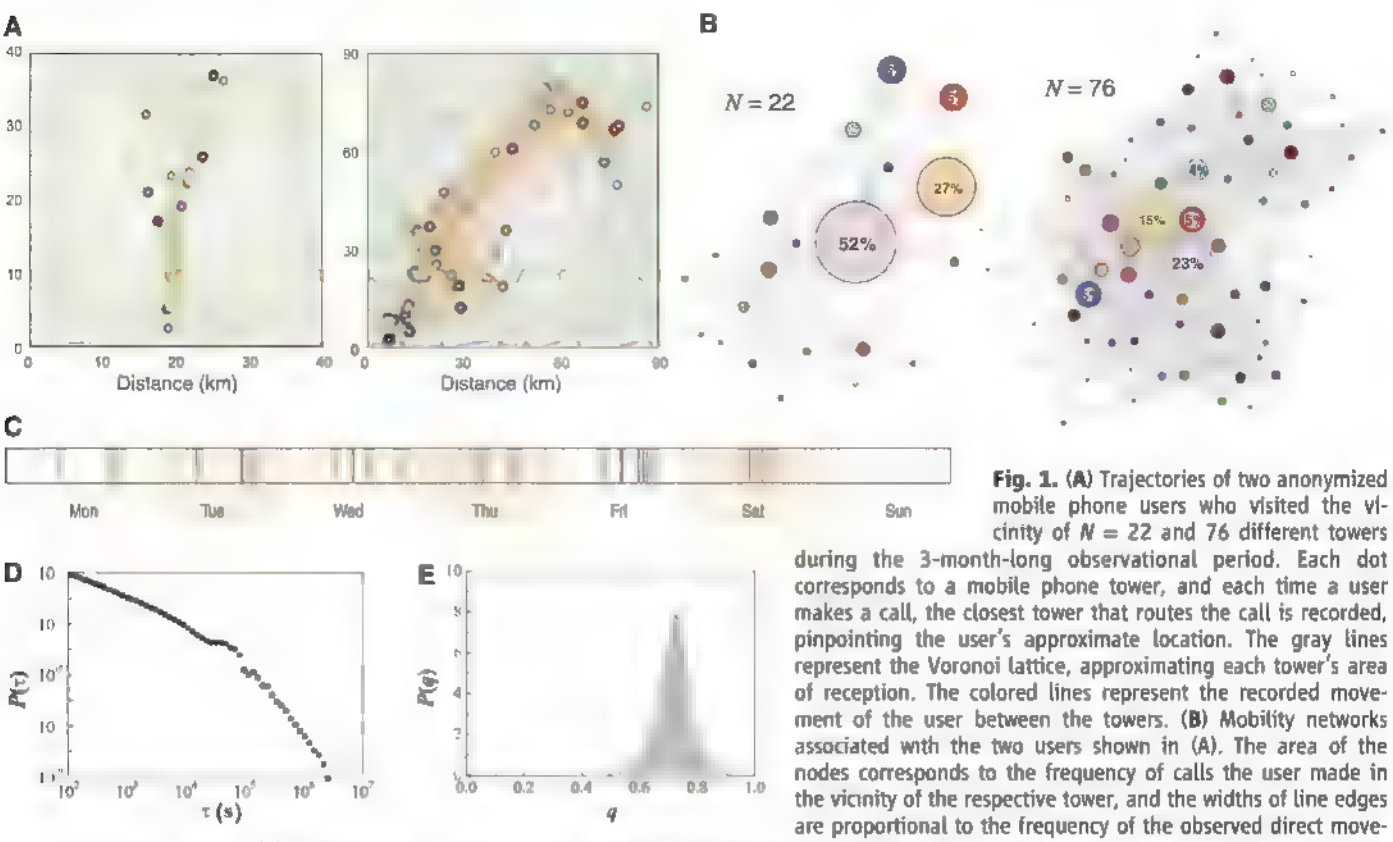

Fig. 1. (**A**) Trajectories of two anonymized mobile phone users who visited the vicinity of $N = 22$ and 76 different towers during the 3-month-long observational period. Each dot corresponds to a mobile phone tower, and each time a user makes a call, the closest tower that routes the call is recorded, pinpointing the user's approximate location. The gray lines represent the Voronoi lattice, approximating each tower's area of reception. The colored lines represent the recorded movement of the user between the towers. (**B**) Mobility networks associated with the two users shown in (**A**). The area of the nodes corresponds to the frequency of calls the user made in the vicinity of the respective tower, and the widths of line edges are proportional to the frequency of the observed direct movement between two towers. (**C**) A week-long call pattern that captures the time-dependent location of the user with $N = 22$. Each vertical line corresponds to a call, and its color matches the tower from where the call was placed. This sequence of locations serves as the basis of our mobility prediction. (**D**) The distribution of the time intervals between consecutive calls, τ, across the whole user population, documenting the nature of the call pattern as coming in bursts (*11*). (**E**) The distribution of the fraction of unknown locations, q, representing the hourly intervals when the user did not make a call, and thus his or her location remains unknown to us.

allowed us to extrapolate the entropy to $q = 0$. We tested the method's accuracy on the trajectory of 100 users whose whereabouts were recorded every hour [(*22*) section *S4*] and found that it performed well for $q < 0.8$, which represented 92% of the users in our data set. We therefore removed 5000 users with the highest q from our data set, which ensured that all remaining 45,000 users satisfied $q < 0.8$.

To characterize the inherent predictability across the user population, we determined S_i, S_i^{unc}, and S_i^{rand} for each user i; the obtained $P(S)$, $P(S^{unc})$, and $P(S^{rand})$ distributions are shown in Fig. 2A. The most striking result is the prominent shift of $P(S)$ compared with $P(S^{rand})$. Indeed, $P(S^{rand})$ peaks at $S^{rand} \approx 6$, which indicates that, on average, each update of the user's location represents six bits per hour of new information; that is, a user who chooses randomly his or her next location could be found on average in any of $2^{S^{rand}} \approx 64$ locations. In contrast, the fact that $P(S)$ peaks at $S = 0.8$ indicates that the real uncertainty in a typical user's whereabouts is not 64 but $2^{0.8} = 1.74$, i.e., fewer than two locations.

The typical distances covered by individuals during their daily mobility pattern, as captured by each user's radius of gyration, r_g, follows a fat-tailed distribution (*4*), which indicates that, although most individuals' daily activity is confined to a limited neighborhood of 1 to 10 km, a few users regularly cover hundreds of kilometers (fig. S2). These differences suggest that predictability should also follow a fat-tailed distribution. In other words, we expect that individuals who travel less should be easy to predict (small entropy), whereas those with large r_g should be much less predictable (high entropy).

An important measure of predictability is the probability Π that an appropriate predictive algorithm can predict correctly the user's future whereabouts. This quantity is subject to Fano's inequality (*24*, *26*). That is, if a user with entropy S moves between N locations, then her or his predictability $\Pi \leq \Pi^{max}(S,N)$, where Π^{max} is given by $S = H(\Pi^{max}) + (1 - \Pi^{max}) \log_2(N - 1)$ with the binary entropy function $H(\Pi^{max}) = -\Pi^{max} \log_2(\Pi^{max}) - (1 - \Pi^{max}) \log_2(1 - \Pi^{max})$. For a user with $\Pi^{max} = 0.2$, this means that at least 80% of the time the individual chooses his location in a manner that appears to be random, and only in the remaining 20% of the time can we hope to predict his or her whereabouts. In other terms, no matter how good our predictive algorithm, we cannot predict with better than 20% accuracy the future whereabouts of a user with $\Pi^{max} = 0.2$. Therefore, Π^{max} represents the fundamental limit for each individual's predictability.

We determined Π^{max} separately for each user in the database. To our surprise, we found that $P(\Pi^{max})$ does not follow the fat-tailed distribution suggested by the travel distances, but it is narrowly peaked near $\Pi^{max} \approx 0.93$ (Fig. 2B). This highly bounded distribution indicates that, despite the apparent randomness of the individuals' trajectories, a historical record of the daily mobility pattern of the users hides an unexpectedly high degree of potential predictability. We have also determined the maximal predictability Π^{unc} and the random predictability Π^{rand} extracted from S^{unc} and S^{rand}. As Fig. 2B shows, the result is strikingly different: $P(\Pi^{unc})$ is extremely widely distributed and peaked at $\Pi^{unc} \sim 0.3$, which indicates that, if we rely only on the heterogeneous spatial distribution, the predictability across the whole population is insignificant and varies widely from person to person. Similarly, $P(\Pi^{rand})$ has a peak at $\Pi^{rand} = 0$, which suggests not only that Π^{rand} and Π^{unc} are ineffective as predictive tools, but also that a significant share of predictability is encoded in the temporal order of the visitation pattern.

How can we reconcile the wide variability in the observed travel distances, as captured by the fat-tailed $P(r_g)$, with the highly bounded predictability observed across the user population? To answer this, we measured the dependency of Π^{max} on r_g, and found that, for $r_g \geq 10$ km, predictability becomes largely independent of r_g, saturating at $\Pi^{max} \approx 0.93$ (Fig. 2C). Therefore, Fig. 2C explains the failure of our earlier hypothesis: Individuals with $r_g \geq 100$ km, covering hundreds of kilometers on a regular basis, are just as predictable as those whose life is constrained to a $r_g \approx 10$-km neighborhood, a saturation that lies behind the high predictability observed across the whole user base.

To determine how much of our predictability is really rooted in the visitation patterns of the top locations, we calculated the probability $\tilde{\Pi}$ that, in a given moment, the user is in one of the top n most visited locations, where $n = 2$ typically captures home and work. Thus, $\tilde{\Pi}$ represents an upper bound for Π^{max}, as, even if our predictive algorithm is 100% accurate, it can foresee the future location only when the user is found in one of the top n locations monitored by the algorithm. As Fig. 2D shows, the top two locations ($n = 2$)

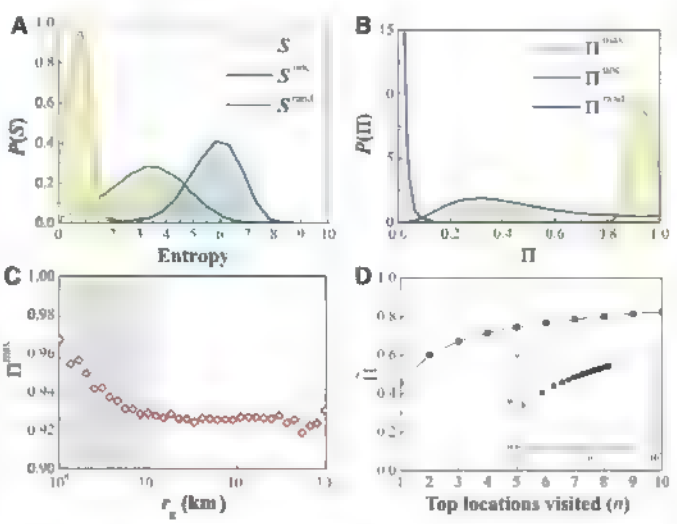

Fig. 2. **(A)** The distribution of the entropy S, the random entropy S^{rand}, and the uncorrelated entropy S^{unc} across 45,000 users. **(B)** The distribution of the Π^{max}, Π^{rand}, and Π^{unc} across all users. **(C)** The dependence of predictability Π^{max} on the user's radius of gyration r_g, capturing the distances regularly covered by each user. Note that, for $r_g > 10$ km, Π^{max} is largely independent of r_g, saturating at $\Pi^{max} \approx 0.93$. **(D)** The fraction of time a user spends in the top n most visited locations, the resulting measure $\tilde{\Pi}$ representing an upper bound of predictability Π^{max}. Thus for $n = 1$ we can predict correctly the user's location when he or she is found at the most likely location ("home"), whereas for $n = 2$, we can predict correctly the user's whereabouts when he is in one of his top two locations ("home" or "office"). (Inset) $\tilde{\Pi}$ appears to grow approximately logarithmically with n.

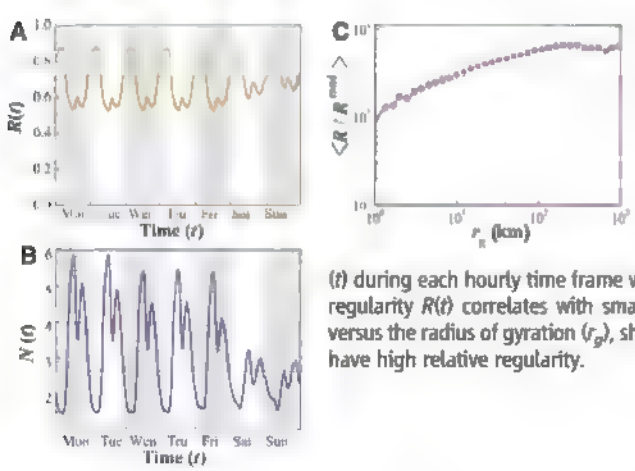

Fig. 3. **(A)** The hourly regularity $R(t)$ over a week-long time period, measuring the fraction of instances when the user is found in his or her most visited location during the corresponding hour-long period. **(B)** The average number of visited locations $N(t)$ during each hourly time frame within a week, revealing that high regularity $R(t)$ correlates with small $N(t)$. **(C)** The averaged R/R^{rand} versus the radius of gyration (r_g), showing that the users with large r_g have high relative regularity.

offer only a 60% overall predictability. Gradually adding more locations increases $\tilde{\Pi}(n)$, but we need several dozen distinct locations to converge to $\tilde{\Pi} = 1$ (Fig. 2D, inset).

To understand the origin of the observed high potential predictability, we segmented each week into $24 \times 7 = 168$ hourly intervals, and within each hour, we identified for each user the most visited location (Fig. 3, A and B). For example, if, between 8 and 9 a.m. on Monday, a user was found 10 times at tower 1, twice at tower 2, and once at tower 3, we assumed that her most likely location during this hour will be tower 1. Next, we measured each user's regularity, R, defined as the probability of finding the user in his most visited location during that hour. R represents a lower bound for predictability Π, as it ignores the temporal correlations in user mobility. We found that across the whole user base, $R \approx 0.7$, which meant that, on average, 70% of the time the most visited location coincides with the user's actual location. The pattern is time dependent: During the night, when most people tend to be reliably at home, R peaks at ≈ 0.9, but between noon and 1 p.m. and between 6 and 7 p.m., R has clear minima, corresponding to transition periods (travel to lunch or home). Indeed, if we measure the total number of distinct locations $N(t)$ a user visited each hour (Fig. 3B), we find that moments of low regularity R correspond to significant increase in $N(t)$, a signature of high mobility, and when R peaks there is a drop in $N(t)$.

If the users were to move randomly between their N locations, then $R^{\text{rand}} \quad 1/N$, which is $1/2^{S^{\text{rand}}} \approx 0.016$, an order of magnitude smaller than the observed $R \approx 0.7$. This gap once again indicates that the high regularity characterizing each user's mobility represents a significant departure from the expectation that they will be random. In Fig. 3C, we plot the relative regularity R/R^{rand} as a function of r_g, observing a clearly increasing tendency. That is, counterintuitively, the relative regularity of users who travel the most (i.e., have high r_g) is higher than the relative regularity of the more homebound individuals.

To explore whether demographic factors influence the users' regularity and predictability, we measured R and $\Pi^{\max}$ for different age and gender groups (fig. S10). It was surprising that we did not observe gender- or age-based differences in $\Pi^{\max}$, but only a systematic, but statistically insignificant, gender-based difference emerged in regularity. We also explored the impact of home, language groups, population density, and rural versus urban environment on predictability and found only insignificant variations (figs. S8, S12, and S13). Finally, we did not find significant changes in user regularity over the weekends compared with their weekday mobility (fig. S8), which suggested that regularity is not imposed by the work schedule, but potentially is intrinsic to human activities.

In summary, the combination of the empirically determined user entropy and Fano's inequality indicates that there is a potential 93% average predictability in user mobility, an exceptionally high value rooted in the inherent regularity of human behavior. Yet it is not the 93% predictability that we find the most surprising. Rather, it is the lack of variability in predictability across the population. Indeed, given the fat-tailed distribution of the distances over which users travel on a regular basis (see fig. S2), most individuals are well localized in a finite neighborhood, but a few travel widely. Furthermore, a number of demographic and external parameters, from age to population density and the number of towers visited, vary widely from user to user. It is not unreasonable to expect, therefore, that predictability should also vary widely. For people who travel little, it should be easier to foresee their location, whereas those who regularly cover hundreds of kilometers should have a low predictability. Despite this inherent population heterogeneity, the maximal predictability varies very little—indeed $P(\Pi^{\max})$ is narrowly peaked at 93%, and we see no users whose predictability would be under 80%.

Although making explicit predictions on user whereabouts is beyond our goals here, appropriate data-mining algorithms (*19*, *20*, *27*) could turn the predictability identified in our study into actual mobility predictions. Most important, our results indicate that when it comes to processes driven by human mobility, from epidemic modeling to urban planning and traffic engineering, the development of accurate predictive models is a scientifically grounded possibility, with potential impact on our well-being and public health. At a more fundamental level, they also indicate that, despite our deep-rooted desire for change and spontaneity, our daily mobility is, in fact, characterized by a deep-rooted regularity.

References and Notes

1. C. Castellano, S. Fortunato, V. Loreto, *Rev. Mod. Phys.* **81**, 591 (2009)
2. A. K. Erlang, *Nyt Tidsskrift for Matematik B* **20**, 33 (1909)
3. D. Brockmann, L. Hufnagel, T. Geisel, *Nature* **439**, 462 (2006)
4. M. C. González, C. A. Hidalgo, A.-L. Barabasi, *Nature* **453**, 779 (2008)
5. S. Havlin, D. Ben-Avraham, *Adv. Phys.* **51**, 187 (2002)
6. R. N. Mantegna, H. E. Stanley, *Phys. Rev. Lett.* **73**, 2946 (1994)
7. R. Metzler, A. V. Chechkin, V. Y. Gonchar, J. Klafter *Chaos Solitons Fractals* **34**, 129 (2007)
8. V. Colizza, A. Barrat, M. Barthelemy, A.-J. Valleron, A. Vespignani, *PLoS Med.* **4**, e13 (2007)
9. L. Hufnagel, D. Brockmann, T. Geisel, *Proc. Natl. Acad. Sci. U.S.A.* **101**, 15124 (2004)
10. P. Wang, M. C. González, C. A. Hidalgo, A.-L. Barabási, *Science* **324**, 1071 (2009)
11. A.-L. Barabasi, *Nature* **435**, 207 (2005)
12. G. Grinstein, R. Linsker, *Phys. Rev. E Stat. Nonlin. Soft Matter Phys.* **77**, 012101 (2008)
13. A. Gabrielli, G. Caldarelli, *Phys. Rev. Lett.* **98**, 208701 (2007)
14. J. D. Harry, J. B. Niemi, A. A. Pripata, J. J. Collins, *IEEE Spectr.* **42**, 36 (2005)
15. D. Helbing, I. Farkas, T. Vicsek, *Nature* **407**, 487 (2000)
16. W.-S. Sho, H. S. Kim, *IEEE Commun. Mag.* **41**, 86 (2002)
17. C. A. Hidalgo, C. Rodriguez-Sickert, *Physica A* **387**, 3017 (2008)
18. M. C. Gonzalez, P. G. Lind, H. J. Herrmann, *Phys. Rev. Lett.* **96**, 088702 (2006)
19. N. Eagle, A. Pentland, *Pers. Ubiquitous Comput.* **10**, 255 (2006)
20. N. Eagle, A. Pentland, *Behav. Ecol. Sociobiol.* **63**, 1057 (2009).
21. R. Lambiotte *et al.*, *Physica A* **387**, 5317 (2008)
22. Materials and methods are available as supporting material on *Science* Online.
23. J. R. Banavar, A. Maritan, A. Rinaldo, *Nature* **399**, 130 (1999)
24. N. Navet, S.-H. Chen, *Natural Computing in Computational Finance* (Springer, Berlin, 2008)
25. A. Vázquez *et al.*, *Phys. Rev. E Stat. Nonlin. Soft Matter Phys.* **73**, 036127 (2006)
26. R. M. Fano, *Transmission of Information* (the MIT Press and Wiley, New York and London, 1961)
27. L. Song, D. Kotz, R. Jain, X. He, *Proc. 23rd Annual Joint Conference of the IEEE Computer and Communications Societies (INFOCOM)* **2**, 1414 (2004)

28. We thank M. Gonzales, P. Wang, J. Bagrow, and J. A. Aslam for discussions and comments on the manuscript. This work was supported by the James S. McDonnell Foundation 21st Century Initiative in Studying Complex Systems, NSF within the Information Technology Research (DMR-0426737) and IIS-0513650 programs, the Defense Threat Reduction Agency award HDTRA1-08-1-0027, and the Network Science Collaborative Technology Alliance sponsored by the U.S. Army Research Laboratory under agreement number W911NF-09-2-0053. Z.D. was supported by a fellowship from the China Scholarship Council

Supporting Online Material

www.sciencemag.org/cgi/content/full/327/5968/1018/DC1
Materials and Methods
SOM Text
Figs. S1 to S13
References

2 June 2009; accepted 28 December 2009
10.1126/science.1177170

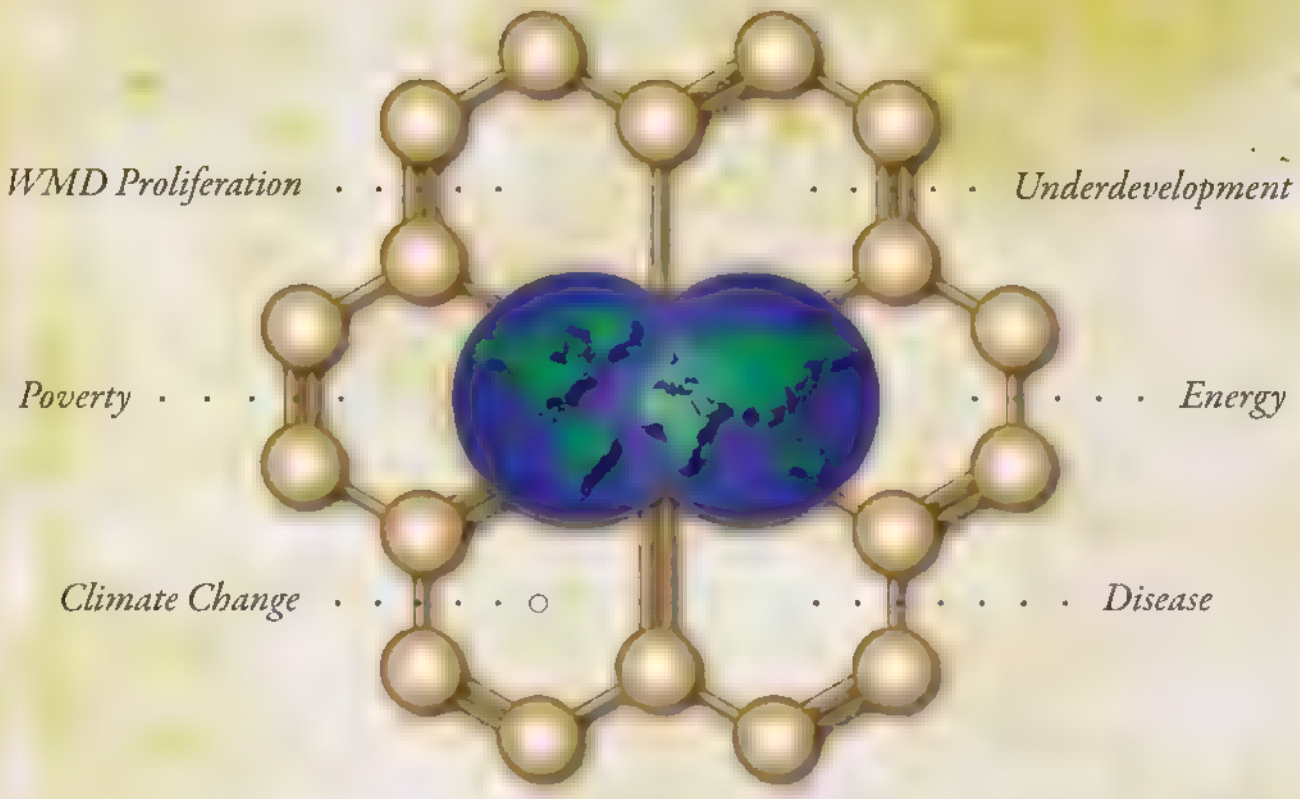

Science Diplomacy *is crucial to* U.S. Foreign Policy

Now is the time to draw upon every tool of U.S. power to promote our interests in the world. We should make maximum use of a core strength of our country — leadership in science and technology. We, the undersigned Democrats and Republicans, believe the Administration and Congress should elevate the role of Science Diplomacy in U.S. national security and foreign policy, and work to:

- Strengthen links between U.S. and foreign scientific communities as a key part of U.S. diplomacy;
- Offer scientific cooperation and technological assistance as a bridge to opening broader dialogue with former adversaries and as an incentive to prevent conflict;
- Bring the world's top scientists and engineers together to tackle pressing global challenges like energy security, climate change, poverty, disease, and WMD proliferation; and
- Provide funding for exchange programs, collaborative research, technical assistance and capacity building to fully qualified U.S. governmental and non-governmental organizations.

Peter Agre Nobel Prize, Chemistry, 2003; President, AAAS 2009-10
Howard Baker U.S. Senator (R-TN) 1967-85
David Baltimore Nobel Prize, Physiology or Medicine, 1975
Samuel Berger National Security Advisor 1997-2001
Vinton G. Cerf Vice President & Chief Internet Evangelist, Google
Rita Colwell Director, National Science Foundation 1998-2004
Paula J. Dobriansky Under Secretary of State 2001-09
Slade Gorton U.S. Senator (R-WA) 1981-87, 1989-2001
Lee Hamilton U.S. Congressman (D-IN) 1965-99; PSA Co-Chair
Gary Hart U.S. Senator (D-CO) 1975-87
Siegfried S. Hecker Director, Los Alamos National Laboratory 1986-97
Carla Hills U.S. Trade Representative 1989-93
Roald Hoffmann Nobel Prize, Chemistry, 1981
Alice Huang President, AAAS 2010-11
Nancy Kassebaum-Baker U.S. Senator (R-KS) 1978-97
Thomas Kean Governor, New Jersey 1982-90, 9/11 Commission Chair
Neal Lane Science Advisor to the President 1998-2001
David Lee Nobel Prize, Physics, 1996
John Lehman Secretary of the Navy 1981-87
John H. Marburger III Science Advisor to the President 2001-09
William Perry Secretary of Defense 1994-97
Thomas Pickering Under Secretary of State 1997-2000; Chair, CRDF Advisory Council
Peter Raven Director, Missouri Botanical Garden
John Whitehead Deputy Secretary of State 1985-88
Frank Wisner Under Secretary of State 1992-93
William Wulf President, National Academy of Engineering 1996-2007 Vice-Chair, CRDF Board of Directors

PARTNERSHIP FOR A SECURE AMERICA

AAAS

CRDF

Please read the complete statement at **www.psaonline.org/science** • Partnership for a Secure America: Chip Andreae and Jamie Metz, Co-Chairs

HIGH CONTENT SCREENING GOES LIVE

Faster, more powerful, and cheaper, platforms are expanding the use of high content screening. Researchers are increasingly using stem cells and primary cells to better understand real-life cell signaling, while the use of live cells is also on the rise. Key areas of development are likely to lie in biology, chemistry, and software, rather than hardware. **By Anne Harding**

"I believe that after a decade of developing high content screening techniques they've been validated as a superior discovery tool."

When high content screening (HCS) was introduced a decade ago, pharma companies were quick to see the technique's usefulness for compound toxicity screening and mode-of-action studies using fixed cells. HCS applications have expanded rapidly as the technology becomes increasingly sophisticated and powerful, and costs come down. Researchers in pharma and academia now use HCS to study cell signaling and RNA interference, increasingly with live cells.

And now that Bush-era restrictions have been lifted, investigators are shaping stem cells into models of tissue types and disease states; multiparametric data analysis of drug effects on these cells could, some say, edge out animal experimentation.

"I believe that after a decade of developing high content screening techniques they've been validated as a superior discovery tool," says Michael Sjaastad, marketing director of cellular imaging products for **MDS Analytical Technologies,** now the parent company of **Molecular Devices.** The next step, Sjaastad and many of his colleagues agree, will be industrial-scale HCS capable of, for example, screening "a million compounds in a couple of weeks."

Meanwhile, companies that make HCS systems are coming out with more powerful, less expensive, and ever-more-flexible machines, like **GE Healthcare's** IN Cell 2000, **Thermo Fisher Cellomics'** ArrayScan, **PerkinElmer's** Operetta, Molecular Devices' ImageXPress Micro and IsoCyte, **TTP Labtech's** Acumen eX3, and **Compucyte's** iCyte.

"What we're seeing is a lot of more affordable platforms that are extremely powerful," says Randall K. Wetzel, who manages clinical applications and cytometry at Danvers, Massachusetts–based **Cell Signaling Technology.** "And that's good for the industry. More competition means better machines."

Seeing with Automated Eyes

High content analysis (HCA) involves extracting data from images, while HCS is essentially the same process, taken to the next level: data from images becomes high throughput, and analysis is automated.

In HCS, a microscope or laser scanner records multiple fluorescent readouts within thousands of individual cells. The investigator will "tell" the system what to look at—for example, the shape of cells or structures within them, the fluorescence intensity of nuclei, or one of many other parameters illustrating temporal and spatial changes within the cell. Then the numbers get crunched.

There are also confocal cytometers, including GE's IN Cell 3000, PerkinElmer's Opera, and Molecular Devices' ImageXPress Ultra, that produce ultrahigh resolution images. GE's new IN Cell 2000 is not confocal, but produces comparably high resolution images, quickly, thanks to image restoration, according to Cathy Howat, marketing director for cell technologies at GE Healthcare.

A key advantage of HCS is that, unlike the human eye, it's unbiased. "It's a robot that's taking the images," explains Marc Bickle, who directs the High-Throughput Technology Development Studio at the **Max Planck Society's** Institute of Molecular Cell Biology and Genetics in Dresden, Germany. "A human being will look for the nice cells to take pictures of, introducing a bias." A human eye is still needed to check the robot's work, Bickle adds, but "the primary analysis is done purely by extracting numbers."

And images mean unprecedented quantities of digital information, he notes, such that garden-variety software just can't handle it. A single screen, for example, can yield 23 terabytes of data.

This means HCS users are having to come up with entirely new ways of making sense of the data it produces, says continued »

UPCOMING FEATURES

Genomics 1: Preparative Technologies for Next Gen Sequencing—April 9

Flourescent Labels—April 16

Proteomics 1: Mass Spectrometry—May 14

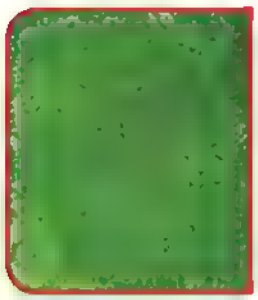

"You sometimes see surprises when you look at the images, something that you were not thinking of to measure"

Steven Finkbeiner, who directs the Taube-Koret Center for Huntington's Disease Research at the **University of California, San Francisco.** "It turns out that you have to actually invent new statistics for a lot of this stuff, because it just hasn't been handled before," says Finkbeiner, who uses HCS to study molecular mechanisms of neurodegeneration and plasticity

Cells As 'Little Patients'

Using HCS to study live cells is a lot like making a movie of that cell's life, according to Finkbeiner But instead of just one subject, that "movie" meshes together the biographies of thousands or even millions of cells. This makes it possible for researchers to observe processes like neurodegeneration with unprecedented sensitivity

Finkbeiner and his team are using the technique to predict whether a cell exhibiting a particular change lives longer, or dies sooner. They've developed a way to ensure that images taken of cell cultures from one day to the next will track the exact same individual cells every time. "The big leap for us has been that we can now follow them for as long as we need to, up to months if we have to We can essentially treat them like little patients," he explains. The technique is indeed a bit like conducting a clinical trial, with microscopic subjects in the millions Survival statistics normally used for patient studies can be employed in high content screening, because of the massive number of cells included in these analyses

And while HCS eliminates the human element of bias, it doesn't eliminate serendipity. "You sometimes see surprises when you look at the images, something that you were not thinking of to measure," says Mario Goette, who is head of the high content screening lab at **Novartis Pharma** in Basel, Switzerland

"Imaging is an approach that allows you to, on the one hand, go in and ask a specific question, but you also get a lot of information for free," Finkbeiner concurs

Making Sense of Terabytes of Data

Software is a major focus of development in HCS technology, from applications that allow less experienced users to do "out of the box" assays, to programs for analyzing, retrieving, and storing massive amounts of data There are third-party companies that make back-end software for HCS, and most companies that make HCS imaging equipment write their own software, too

Cellomics, now part of Thermo Fisher Scientific, released a new data visualization and mining tool, HCSDiscover, in April 2009. The software, developed in collaboration with **Genedata,** is built for dealing with large volumes of multiparameter high content data, particularly for scientists working on "compound or RNA screening, toxicity profiling, or systems biology research," according to the company's website GE Healthcare launched its own data mining system, the IN Cell Miner High-Content Manager, in 2008

Molecular Devices' Sjaastad says great flexibility in software is a shared advantage of its three HCS systems, the ImageXpress Micro Wide-field, CCD-based imaging system; the ImageXpress Ultra Confocal Imaging System; and the IsoCyte High-Speed Scanning Cytometer. MetaXpress software for high-content acquisition and analysis is built upon the backbone of MetaMorph software, "the industry standard tool for cell biology and imaging research for well over 20 years," according to Sjaastad.

MetaXpress offers a suite of validated application modules, database communication, and other user-friendly bells and whistles for high content research. Given that it is based on a widely accepted imaging package, "MetaXpress doesn't give up any of the capability of the original research-grade software," he adds

Additional offerings from the company include software to accelerate image analysis and to link directly to MDS's imaging database to retrieve and mine multiparametric data AcuityXpress, for example, allows users to click on plotted data points and "drill right down" to original images of single cells, Sjaastad explains

In addition to finding the desired results and "hits," tools for data mining allow users to spot outliers or unexpected results and investigate them further, notes Sjaastad. For example, data mining in AcuityXpress can reveal trends for quality control. One example was the ability to track down a malfunction in a liquid handling device; a subpopulation of the analysis showed no cells in a particular set of wells on several plates in a screen This turned out to be due to a plugged pipette tip. "That fell out of basic QC analysis tools applied by an experienced user," Sjaastad says

For companies that are scaling up and want to avoid image analysis bottlenecks, Molecular Devices offers its MetaExpress Powercore software, which uses highly parallel image analysis to increase capacity by orders of magnitude, as needed. "Your image analysis can be conducted in at least the same time frame as image acquisition, and in many cases can allow multiple instruments to be used simultaneously," says Sjaastad

Integrating images taken in different formats or using equipment from different vendors—which is something that most major centers doing HCS need, because each system has its advantages for particular applications—remains a major challenge, says Novartis's Goette. "There are some applications being developed, but they are not yet really mature."

Checking in with Reality

Gerardo Turcatti, who runs the Biomolecular Screening Facility at the School of Life Sciences of the **École Polytechnique Fédérale de Lausanne** (EFPL) in Switzerland, started using HCS two years ago "We are learning a lot, and we are seeing the limitations," Turcatti said

He's currently running two whole-genome screens in parallel using genomewide siRNA collections. One project is investigating

CREDIT ISTOCKPHOTO COM/DRA SCHWARTZ

the genes regulating the translocation of cholesterol and other lipids from the cell membrane to internal compartments of cells. He and his colleagues are looking at three siRNAs per gene, in duplicate, for a total of about 160,000 data points, including controls.

"Our projects have been a bit of a reality check," Turcatti says, after the initial enthusiasm and excitement about the potential of HCS. "Users of screening by imaging are starting to understand that these are not trivial projects; assay validation is time-consuming and expensive, in particular for the academic community."

In Turcatti's opinion, the big advances in HCS technology are likely to be made in biology and chemistry: handling live cells, multiplexing dyes, and identifying more relevant biomarkers applicable to both RNA and chemical screens. Right now, he notes, researchers do have biomarkers for particular cellular processes or properties, such as apoptosis and probes of viability in general. "I think there is a lot of progress to be made there," he said.

Some companies that produce HCS instrumentation have gotten into the business of selling reagent kits, but these are costly, according to Turcatti. While these kits might be useful and affordable for assays in a research lab, he argues, it can make more sense for investigators to develop their own approaches and strategies for generating labeled species for major projects, such as some large screening campaigns. Building the necessary capacity and expertise in bioorganic chemistry to do this could offer major competitive advantages, says Turcatti, because "you may have more flexibility with your own invented or customized tools," at a lower cost.

Lending a Hand with Antibodies

Unsurprisingly, Wetzel of Cell Signaling Technology (CST) sees things differently. His company makes validated and optimized antibodies for use in HCS, and now has nearly 700 on offer for use in cell-based assays.

These types of products are worthwhile, according to Wetzel, because they eliminate down time spent developing antibodies and assays. Rather than have customers in pharma, biotech, and academia take highly skilled screening teams offline to work on developing antibodies and assays, Wetzel explains, CST gives them a "validable toolbox to monitor signaling from just about any pathway in a cell with the specific mutations and cellular signaling that best matches the disease they're targeting—not in an engineered cell with artificially expressed proteins."

CST can also align antibodies in panels and do multiplex staining to answer key questions more quickly, like whether a compound is getting into a cell and whether it acts on its intended target. "We can combine endpoints to monitor downstream signaling, off-target effects, proliferation, apopotosis, autophagy, DNA damage, and/or toxicity—in one plate or even in one well, through multiplexing," he explains.

Invitrogen, now a part of Life Technologies, also offers an array of ready-made assays for use in HCS, reagents for image segmentation, fluorescent protein and expression tags, and more, and will also develop custom HCS assays.

GE Healthcare makes several reagents for use in HCS, and Thermo Fisher offers a wide range of Cellomics HCS Reagent Kits.

FEATURED PARTICIPANTS

Cellomics (Thermo Fisher)
www.cellomics.com

Cell Signaling Technology
www.cellsignal.com

Compucyte
www.compucyte.com

École Polytechnique Fédérale de Lausanne
www.epfl.ch/index.en.html

GE Healthcare
www.gehealthcare.com

Genedata
www.genedata.com

Geron
www.geron.com

Invitrogen (Life Technologies)
www.invitrogen.com

Max Planck Society
www.mpg.de/english

MDS Analytical Technologies (Molecular Devices)
www.moleculardevices.com

Novartis Pharma
www.novartis.com

PerkinElmer
www.perkinelmer.com

Thermo Fisher Scientific
www.thermofisher.com

TTP Labtech
www.ttplabtech.com

University of California, San Francisco
www.ucsf.edu

MDS Analytical Technologies, Molecular Devices' parent company, offers cell-based reagent kits and also licenses its Transfluor assay, which is used to screen for GPCR ligands and other potentially GPCR-regulating compounds.

Getting into the Cell Business

More and more investigators working in HCS are moving from using mouse, hamster, HeLa, and other generic cell lines in their research to studying primary cells and stem cells, while analysis of live cells is also becoming an increasingly important feature of this research. "The trend is that people are trying to develop more physiological assays," says Novartis's Goette.

Nobody has gotten into the business of making and commercializing these cells, until now. GE Healthcare has hired Stephen Minger, who directed the first group in the UK that banked an embryonic stem cell in the UK cell bank, as head of research and development for the cell technology business. In collaboration with **Geron,** Minger's team will develop cardiomyocytes and hepatocytes, and possibly neural cells later on, that will make "a more predictive model" for toxicity to specific tissue types, says Cathy Howat. "Not only will we have the hardware and the software for sophisticated cell analysis; we will also have the cells themselves." Howat said GE Healthcare expects to begin marketing the cells this year.

Anne Harding is a freelance science writer based near New York City.

DOI: 10.1126/science.opms.p1000041

NEW PRODUCTS: HIGH CONTENT SCREENING

FLUIDIC HEATING CONTROL

The Mitos Hotplate Adapter enables exact temperature control of microfluidic chips in conjunction with a range of hotplates. It is compatible with the Mitos Micromixer chip, the Mitos T-junction chip, the Mitos Thin-layer chip, and the Mitos Droplet Generator chip. With a compact footprint of 39 mm by 43 mm, the Hotplate Adapter provides precise control over reaction temperatures. Its excellent chemical compatibility, along with quick-chip connection and release, makes it easy to use in heat-controlled microfluidic applications. The Mitos Hotplate provides a temperature range of room temperature to 300°C, facilitating a wide range of processes. This hotplate is digitally controlled with an external thermocouple temperature probe, which can be attached to the Hotplate Adapter for optimal temperature control.

Dolomite **For info: +44-1763-242491 | www.dolomite-microfluidics.com**

HIGH-VOLUME MICROPLATE

The Krystal 24 microplate's 3.1-ml well volume makes it suitable for screening applications that require high sensitivity combined with photometrics accuracy and repeatability. The large surface area of the wells makes the tissue-culture-treated version of the plate suitable for cell-growth applications. The Krystal 24 microplates are constructed of ultrapure-grade polystyrene and available in opaque white and solid black formats. The black plate provides the all-absorbing background needed to minimize background interference for sensitive fluorescence measurements. The opaque white plate maximizes reflectivity, enabling even weakly emitting luminescence assays to be routinely undertaken. In addition to optimized luminescence and fluorescence measurements, the unique design offers improved cell-binding efficiency and provides the convenience of direct measurement on bottom-reading spectrophotometers and inverted microscopes.

Porvair Sciences

For info: +44-1372-824290 | www.porvair-sciences.com

MICROFLUIDIC GLASS CHIP

The glass Mitos Capillary Electrophoresis Chip A is designed to separate small quantities of biological molecules by capillary electrophoresis. Measuring only 15 mm by 45 mm by 2 mm, this electrophoresis chip combines a cross-channel design with a 20-µm channel depth and a 30-mm long channel for accurate analysis of the separation. Offering excellent chemical compatibility, the chip separates species in the interior of the microchannel based on their size-to-charge ratio. The high surface-to-volume ratio of the microchannels enables the application of high voltages without overheating the samples. An extremely smooth channel surface, in combination with a wide pressure and temperature range, makes it suitable for a broad range of applications.

Dolomite

For info: +44-1763-242491 | www.dolomite-microfluidics.com

ASSAY PANELS

The Milliplex MAP EpiQuant assay panels are a new family of phosphotyrosine multiplex assays designed to advance cell signaling research. Compared with existing techniques, these assays give researchers a more complete view of how cells send molecular signals. The Milliplex MAP EpiQuant platform can quantify numerous signals coming from either a single protein, multiple proteins in a pathway, or multiple pathways. The assays allow the simultaneous measurement of more than 40 analytes in one well, so whole pathways can be analyzed in a single 96-well plate. Researchers can also use the panels to detect cross-talk between pathways. The assays provide absolute quantitation of total and phosphorylated proteins, enabling direct comparison of signaling events in different pathways.

Millipore

For info: 800 548 7853 | www.millipore.com/4multiplexing

CELL MIGRATION ASSAY

The Oris Pro Cell Migration Assay makes use of a nontoxic biocompatible gel to form a cell-free zone on cell culture surfaces. After cells are seeded into the 96-well plate, the gel dissolves, permitting cells to migrate into the well centers. The kit enables researchers to save time and money by using automated liquid-handling equipment for fast setup of high throughput assays. Researchers can capture and quantify real-time cell migration data using microscopes and high content screening, and high content imaging instruments. The new Oris Pro Assay complements the Oris line of cell migration assay products that feature patent-pending, cell-seeding stoppers to create cell-free detection zones in the center of each well.

Platypus Technologies

For info: 608-237-1270 | www.platypustech.com

Electronically submit your new product description or product literature information! Go to **www.sciencemag.org/products/newproducts.dtl** for more information. Newly offered instrumentation, apparatus, and laboratory materials of interest to researchers in all disciplines in academic, industrial, and governmental organizations are featured in this space. Emphasis is given to purpose, chief characteristics, and availability of products and materials. Endorsement by *Science* or AAAS of any products or materials mentioned is not implied. Additional information may be obtained from the manufacturer or supplier.

Scientist positions at Novo Nordisk China R&D center

Zhongguancun Life Science Park, Beijing, China

novo nordisk

Novo Nordisk China R&D center is an integrated part of Novo Nordisk's R&D organization. Currently, the R&D center has four research departments: Molecular Biology, Protein Chemistry, Cell Biology, and the newly formed Diabetes Research. The center is expanding its Protein Engineering & Antibody Development capabilities to leverage its core competencies to support ongoing projects and contribute to the identification of new molecular targets for the treatment of diabetes, autoimmune and inflammatory diseases. We are seeking innovative and energetic scientists who plan to advance their career in China to fill in the open positions described below:

1. Scientist/Senior Scientist, Antibody Phage Display (Job Code: MB1)

Responsibility

Lead effort on antibody discovery generation via phage display selection process. Strategic and scientific activities related to the discovery and design of recombinant antibody.

Requirements

- Ph.D. in Molecular Biology, Biochemistry or Immunology, and > 3 years of relevant post-doc experience
- A proven track record with phage display or other display platforms
- Solid knowledge and hands-on in-depth experience in various molecular biology techniques, in particular in antibody library construction, engineering, expression, purification and characterization

2. Scientist in Molecular biology/Protein Expression (2 positions)

Responsibility

Play a direct role in developing and optimizing recombinant protein expression systems for multiple proteins to support therapeutic protein production, protein engineering and assay development.

Requirements

- Ph.D. in Molecular Biology, Biochemistry or relevant biological science, 2-5 years experience in protein expression and engineering
- Proven hands-on experience in transient transfections and in stable cell line development or through-put cell culture
- Expert knowledge of applicable state-of-art cell scale-up or through-put technologies and methods in molecular biology

In addition, specific requirements for the individual positions

Job Code MB2: Experience in immunology or inflammatory research

Job Code MB3: A proven track record in diabetes research, some bio-informatics experience is preferred

3. Scientist/Senior Scientist/Principal Scientist in Protein Chemistry (2 positions)

Responsibility

Purify and characterize various proteins at laboratory to pilot scale to support therapeutic protein drug R&D, and actively participate in discovery of new and improved therapeutic proteins or antibodies against diabetes and/or inflammatory diseases.

Requirements

- Ph.D. in biochemistry, protein chemistry, proteomics or other life sciences with a minimum of two years post doctorate research experience
- A thorough understanding and solid hands-on experience on protein engineering, refolding, purification, characterization and assay development
- Solid hands-on experience with some of the following equipments: AKTA, HPLC, LC-MS, HT ELISA, HT AlphaScreen, and other HT biophysical screening experience would be a plus

In addition, specific requirements for the individual positions

Job Code PC1: A good track record of research in immunology or inflammation is preferred

Job Code PC2: A proven track record in diabetes research would be an advantage; experience in protein stability and initial formulation would be an advantage

For all positions, excellent communication skills in English, flexibility and the desire to work within a multidisciplinary team are required. Industry and patent experience is strongly preferred. Title and compensation will be commensurate with the individual candidate's qualifications. For detailed information, please browse **www.ebiotrade.com** for positions from our center, or visit our website **www.novonordisk.com.cn** (science and research section). For application, please send your application and a cover letter in e-mail to **InfoNNST@novonordisk.com**, and indicate Job Code in your mail subject.

POSITIONS OPEN

UNIVERSITY of CALIFORNIA, SAN DIEGO
SCHOOL OF MEDICINE

DIRECTOR

The Department of Pediatrics at the University of California, San Diego and Rady Children's Hospital of San Diego are recruiting a senior physician scientist to be the Director of the newly created Pediatric Diabetes Research Center (PDRC). The academic series will be determined based on the background and qualifications of the successful candidate, and will include the tenured series. The faculty currently includes seven scientists and/or physician-scientists, with a variety of interests in basic research in type 1 diabetes, all of whom are receiving extramural funding. This is complemented with a strong clinical component provided by the Division of Pediatric Endocrinology which includes nine faculty members and an Accreditation Council for Graduate Medical Education–approved fellowship program with three fellows. This program operates a busy diabetic service at the Rady Children's Hospital of San Diego, a 220 bed facility that serves as a major regional tertiary care hospital for children and is the major teaching facility for the Department of Pediatrics of the UCSD School of Medicine.

The ideal candidate will have expertise in fostering scientific excellence while developing an integrated program that will bridge the gap between basic science and clinical medicine. Although responsibility for clinical care is not mandatory, an appreciation of the impact of type 1 diabetes on an individual is essential.

The position carries with it an Endowed Chair. Please electronically send curriculum vitae to **Kenneth Lyons Jones, M.D., Chair of the Search Committee, e-mail: klyons@ucsd.edu,** or by surface mail to: **9500 Gilman Drive, La Jolla, CA 92093-0828.** Applications will be considered until April 30, 2010, or until a final applicant has been selected. *UCSD is an Affirmative Action/Equal Opportunity Employer with a strong institutional commitment of excellence through diversity.*

POSTDOCTORAL FELLOWSHIP
Molecular Biology
Research and Teaching

The Department of Biology at Villanova University invites applications for a Postdoctoral Fellowship (50 percent teaching, 50 percent research) in molecular biology, starting August 2010. One-year position, renewable for up to two years. Positions are ideal for establishing credentials in research and teaching, critical in applications to many undergraduate tenure-track positions. Teaching assignments include a methods course in molecular techniques/research and a molecular biology course in area of specialization or a team-taught assignment in molecular biology. Specific research area is open, and several opportunities for collaboration with faculty in the Department exist (see **website: http://www.biology.villanova.edu**). A Ph.D. is required. Applicants must apply online at **website: https://jobs.villanova.edu**. The online application should include a letter of application, curriculum vitae, and statements of teaching and research philosophy. Please mail undergraduate and graduate transcripts and have three letters of recommendation sent to: **Postdoctoral Search Committee, Department of Biology, Villanova University, 800 Lancaster Avenue, Villanova, PA 19085-1699.** Review of applications begins March 15, 2010, and will continue until the position is filled. *Villanova is a Roman Catholic university and an Affirmative Action/Equal Employment Opportunity Employer.*

CLIMATE ANALYSIS/PREDICTION SCIENTIST. Experience required to work in Greenbelt, Maryland. For immediate consideration, submit your resume at **website: http://www.saic.com/career, reference job code 164687.** At SAIC, the Fortune 500 scientific, engineering, and technology applications company that is working to solve problems of vital importance to the nation and the world. Consider joining the ranks of SAIC's 45,000 employees who are committed to success and innovation.

POSITIONS OPEN

RICE

Applications are invited for a tenure-track **ASSISTANT PROFESSOR** faculty position in the Biochemistry and Cell Biology Department of Rice University. We seek an outstanding scientist with expertise in broad areas of experimental and/or theoretical biological research, with particular emphasis in cell, developmental, and/or cancer biology. Candidates using interdisciplinary approaches and/or model organisms are especially encouraged to apply. Candidates must have a Ph.D., postdoctoral training, and outstanding research potential. Successful candidates are expected to develop and maintain a vigorous research program supported by extramural funding and to participate in graduate and undergraduate education. Review of applications will commence March 1, 2010, and continue until the position is filled.

Please compile a PDF containing a cover letter, curriculum vitae, summary of past research, and statement of future research plans. Please send electronically to **e-mail: bcbsearch@rice.edu.** Also, please arrange for four letters of reference to be sent to the same e-mail address.

Rice University is an Equal Opportunity/Affirmative Action Employer; women and minority candidates are especially encouraged to apply.

ASSISTANT/ASSOCIATE PROFESSOR of TOXICOLOGY
University of Connecticut, Storrs, CT

The Department of Pharmaceutical Sciences at the University of Connecticut, School of Pharmacy, invites applications for a tenure-track faculty position in neurotoxicology at the Assistant or Associate Professor level, starting August 23, 2010. We are seeking a toxicologist with a strong background in research and teaching with a focus on the toxic effects of xenobiotics on the central and/or peripheral nervous system and/or developmental neurotoxicology. This will complement the interests of the faculty in the Department of Pharmaceutical Sciences, which includes integrative approaches to elucidate mechanisms of drug or toxicant action, drug discovery and design, and pharmaceutical technology. The Department is housed in a new 200,000 square foot state-of-the-art building in the science quad of the University of Connecticut and encourages faculty interdisciplinary interactions with other programs of the University such as Physiology/Neurobiology and the Molecular and Cell Biology Program. The successful candidate is expected to develop a strong, extramurally funded research program and to effectively participate in teaching at the graduate and professional levels. A competitive salary along with startup funds will be provided. Qualifications: Applicants must possess a Ph.D. degree or equivalent, strong oral and written communication skills, and a strong background in research and teaching with a focus on the toxic effects of xenobiotics on the central and/or peripheral nervous system and/or developmental neurotoxicology.

Applicants should submit curriculum vitae, a brief statement of research and teaching interests, and names and full addresses of three references. We would prefer to receive your application electronically at **e-mail: leslie.lebel@uconn.edu** or by surface mail sent to: **Leslie LeBel, University of Connecticut, School of Pharmacy, Department of Pharmaceutical Sciences, 69 North Eagleville Road, Unit 3092, Storrs, CT 06269-3092.** Review of applications will start on April 16, 2010, and continue until the position is filled. *In keeping with our commitment to build a culturally diverse community, the University of Connecticut invites applications from women, people with disabilities, and members of minority groups.*

ulm university universität

uulm

The **Medical Faculty of Ulm University** invites applications for the position of a

Professorship in Immunology W3 (Head of the Institute)

We are seeking a candidate with an outstanding international research record in the field of molecular immunology. Teaching experience as well as excellent third party funding are also required. The successful candidate should cooperate with research centres of the Medical Faculty and University (among others DFG-funded Collaborative Research Centres, Clinical Research Units, Max-Planck-Research Group) and should interact with institutions of the University Hospital. In addition, we expect the candidate to actively participate in the development of novel interdisciplinary research centres/units.

Candidates must have a MD and/or PhD, or equivalent doctoral degree. Teaching obligations require the candidate to have a postdoctoral lecture qualification (Habilitation in German or comparable qualification like Junior Professor). The major teaching language is German.

Ulm University and its University Hospital are certified in a family program and offer a dual career service program.

Ulm University aims to increase the number of women among the faculty staff and therefore explicitly encourages the application of female scientists.

Applications including the application form, a full CV, a complete list of grants and publications and a summary of current research activities and objectives should be sent to (and received **not later than March 15, 2010**): Ulm University, Professor Dr. K.-M. Debatin, Dean of the Medical Faculty, D-89069 Ulm.

The University is an equal opportunity employer and handicapped applicants with equivalent qualifications will be given preference.

Zertifikat seit 2008 audit familiengerechte hochschule

PRESIDENT AND CHIEF EXECUTIVE OFFICER
THE METHODIST HOSPITAL RESEARCH INSTITUTE

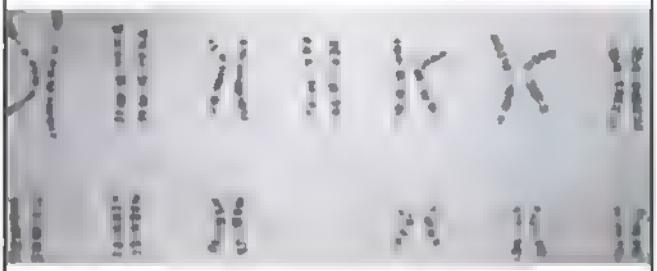

The Methodist Hospital Research Institute (TMHRI) is a cornerstone in The Methodist Hospital's strategy for continued development as an academic medical center. Since its inception in 2004, the Research Institute has received more than $21 million in funding from the National Institutes of Health, and its peer-reviewed funding is increasing exponentially each year. TMHRI oversees all clinical trials at The Methodist Hospital, with 700 clinical trials currently under way and 1,700 credentialed research team members, including more than 400 principal investigators. The Research Institute is affiliated with Weill Cornell Medical College and the University of Houston.

With the planned retirement of the founding director of the Institute, Methodist is in need of a collaborative leader to guide TMHRI to its next level of accomplishment. The Methodist Hospital Research Institute Clinical and Translational Research Building, a new 440,000 square foot facility, will open this year and will add substantially to the Research Institute's space portfolio. The building includes open laboratory space designed to house 90 principal investigators, large and small animal vivarium, core facilities to enhance interdisciplinary research, a Good Manufacturing Practice facility, state-of-the-art imaging equipment including cyclotron for both preclinical and clinical studies, and a BSL-3 laboratory for infectious disease research.

Candidates must have an earned doctoral degree and a record of personal research achievement commensurate with a Weill Cornell Medical College appointment at the rank of full Professor. Additional relevant education or experience will be advantageous. Previous experience in research administration is preferred

The Methodist Hospital is the flagship of The Methodist Hospital System and located in the heart of The Texas Medical Center. The Methodist Hospital is the only hospital in Texas named to *U.S.News & World Report*'s 2009 "America's Best Hospitals" Honor Roll.

Join us as we celebrate our 90th year as a leading health care provider in our community and the world! The successful candidate will receive a generous salary, fringe benefits, and relocation package. To apply or nominate a candidate in confidence, e-mail CV to **Michelle Baehl, Executive Recruitment for The Methodist Hospital Research Institute, mabaehl@tmhs.org.**

FORTUNE 100 BEST COMPANIES TO WORK FOR 2010

Methodist The Methodist Hospital Research Institute

Houston, Texas

LEADING MEDICINE®

An Equal Opportunity Employer

The Methodist Hospital System is the official health care provider of the Houston Texans, Houston Astros, Houston Dynamo, Rice Athletics, Houston Ballet, Houston Grand Opera and Houston Symphony.

Texans Dynamo Rice HOUSTON BALLET Houston Grand Opera Houston Symphony

MJA

Whitacre Chair in Energy Science and Engineering

The Department of Chemical Engineering at Texas Tech University is actively seeking to fill the newly endowed Whitacre Chair in Sustainable Energy. Candidates for the position will be exceptional individuals whose research areas are aligned with the university goals of creating a strong multi-departmental research base in Sustainable Energy at Texas Tech University. The selected individual will be an internationally recognized leader in his or her field as demonstrated by such metrics as the peer reviewed publication and citation records, national recognitions such as major awards or fellowships in technical societies, and a strong track record of competitive research funding. The Department of Chemical Engineering at Texas Tech University has embarked on building a nationally recognized research-intensive department with strengths in Polymers and Materials, Bioengineering and Biotechnology, Computational Chemical Engineering, and Process Systems and Engineering. The successful candidate is expected to expand the research portfolio of the department into Sustainable Energy. The position is an Endowed Chair at the level of Full Professor and incumbents will be expected to participate in research, service, and teaching at this level. It is anticipated that successful candidates will have very strong records of scholarship supported by extramural funding and that externally sponsored research will be brought to Texas Tech University.

Interested candidates should apply online at **https://jobs.texastech.edu/**. Please use requisition number **80764**. Interested candidates should include a detailed CV, a research statement, and a list of five referees. For further information, please contact the search committee chair, **Dr. Raghu Rengasamy** at **raghu.rengasamy@ttu.edu**.

Texas Tech is an Equal Opportunity Employer

UMKC
University of Missouri-Kansas City
School of Biological Sciences

Professor and Head, Division of Cell Biology and Biophysics

Applications are invited for Professor and Head of the Division of Cell Biology and Biophysics at the School of Biological Sciences, University of Missouri-Kansas City. The successful candidate should have a record of excellence in research with sustained extramural funding. The candidate will be expected to play a leadership role in graduate and undergraduate education, faculty mentorship, determining future research directions, and in the overall development and growth of the School. The School of Biological Sciences is positioning itself to become a regional leader in the areas of structural, molecular, and cellular biology, and microbiology, and welcomes applications from qualified candidates in those areas. However, outstanding scientists from all areas of basic life sciences are encouraged to apply. The successful candidate will receive an endowed professorship accompanied by a generous annual research stipend, a competitive 12-month salary, renovated research space, a start-up package commensurate with rank, and the availability of excellent research support facilities within the School of Biological Sciences. Candidates should have a Ph.D. and currently hold a tenured academic position at the rank of Professor.

To apply, please submit electronically (MS Word or pdf) a CV, a statement of present and future research interests, and the names and addresses of 3 references to **Ms. Micaela Escareno (escarenom@umkc.edu)**. All materials will be handled with strict confidentiality. The position will remain open until filled.

UMKC is an Equal Access, Equal Opportunity Affirmative Action Employer that is fully committed to achieving a diverse faculty and staff. Women, minorities, veterans, and individuals with disabilities are encouraged to apply.

ASSISTANT, ASSOCIATE, FULL PROFESSOR (Bioinformatics)

Hunter College of The City University of New York invites applications for a tenure-track faculty position in bioinformatics and high performance computing with expertise in the development, adaptation and implementation of HPC algorithms applied to such data-intensive biological areas as (but not limited to) next-generation sequencing, biomedical ontologies, and systems biology.

The successful candidate will be appointed to the doctoral faculty at the CUNY Graduate Center and will participate actively in Hunter's NIH-funded Quantitative Biology (QuBi) Project.

The anticipated start date is Fall 2010. The appointment will be made in the Department of Computer Science or Biological Sciences depending on qualifications. Preference will be given to candidates with well-established strong records of peer-reviewed publications and external funding, but exceptional junior candidates will also be considered. Evaluation is ongoing and will continue until the position is filled.

Hunter's computing and biomedical research community is supported by extensive funding from NIH and NSF. Hunter College is strategically located in Manhattan near other major biomedical research centers and universities and attracts an engaging and diverse student body.

For information on how to apply, visit
http://www.hunter.cuny.edu/qubi/
Questions may be emailed to
bioinformatics@hunter.cuny.edu

The City University of New York
An Equal Employment Opportunity/Affirmative Action/Immigration Reform and Control Act/ Americans with Disabilities Act Employer

HUNTER IS CUNY

CLINICAL ASSISTANT PROFESSOR OF BIOINFORMATICS
Department of Biology
Arts and Science

The Department of Biology at New York University invites applications for a Clinical Assistant Professor appointment to start September 1, 2010, pending budgetary and administrative approval. Responsibilities include developing and teaching a curriculum in bioinformatics, as well as coordinating the Department's Academic Affairs portfolio. Teaching duties will include four course offerings annually (2 per semester) in addition to the above academic administrative responsibilities. Previous research, teaching and administrative experience is preferred. Successful candidates will have a PhD in Biology and/or Informatics as well as prior teaching experience. The Department of Biology (http://biology.as.nyu.edu) offers an outstanding and collegial research environment.

Candidates should submit a single PDF file containing a Cover Letter, CV, and Statement that outlines previous teaching experience to **biology.informaticssearch@nyu.edu**. The following address can be used for the cover letter: **Dr. Gloria Coruzzi, Department of Biology, New York University, 1009 Silver Center, 100 Washington Square East, New York, NY 10003.** Three PDF letters of reference should also be submitted separately to **biology.informaticssearch@nyu.edu**. *Closing date for all materials is **March 31, 2010**.*

NEW YORK UNIVERSITY

NYU is an Equal Opportunity/Affirmative Action Employer

www.uva.nl/vacancies

The Faculty of Science of the University of Amsterdam attaches great importance to the contribution of female scientists in research and education. For this reason we are offering:

5 MacGillavry fellowships for women (tenure track) 0.8 – 1.0 FTE

in a concerted recruitment programme named after the ground breaking crystallographer Carolina MacGillavry, an UvA alumnus. We are looking for women who excel in one of the faculty's disciplines and who aspire to a career as full professor at the University of Amsterdam.
The fellowship comprises a tenure track, whereby the fellow starts as *assistant professor* (UD) in a temporary position, with the prospect of a permanent appointment as associate professor (UHD) as well as a subsequent career path leading to a full professorship. Depending on the fellow's qualifications, entrance at a higher level is also possible.

We offer among other things a suitable start-up package, and assistance in finding a job for your partner, child care and accommodation. Fellows can also count on excellent guidance.

The scientific disciplines of the Faculty are:
- Biological Science and Biomedical Science
- Earth Sciences (Physical Geography)
- Informatics and Logic
- Physics
- Chemistry
- Astronomy
- Mathematics and Statistics

More information:
At the website www.science.uva.nl/mgf
At the website www.uva.nl/vacancies
(subject: MacGillavry fellowship)

UNIVERSITY OF AMSTERDAM

Acquisition will not be appreciated

John Innes Centre

INDEPENDENT RESEARCH FELLOWSHIPS

The John Innes Centre (JIC), Norwich, UK is a world leading centre of excellence in plant and microbial sciences based on the Norwich Research Park. We are inviting applications from outstanding researchers who either hold, or wish to apply for Independent Research Fellowships to attend a Conference at the JIC on 7th June 2010. At the meeting you will have an opportunity to present your proposed area of research and to discuss your proposal, the development of your group and your future career plans in depth with senior JIC Scientists.

After the Conference we will select and mentor outstanding candidates in writing Fellowship applications and/or offer the opportunity to move existing Fellowships to the JIC.

Further details and particulars can be found at http://www.jic.ac.uk/corporate/opportunities/vacancies/fellows.htm

Please e-mail a 2-page summary of your research plan, a copy of your CV and arrange for three letters of recommendation to be emailed to dawn.barrett@bbsrc.ac.uk by Friday 23rd April 2010.

The John Innes Centre is a registered charity (No223852)grant-aided by the Biotechnology and Biological Sciences Research Council and is an Equal Opportunities Employer.

FACULTY POSITION IN CANCER RESEARCH

The University of Texas M.D. Anderson Cancer Center, Science Park – Research Division is entering into a new recruitment phase. Applications are being accepted for a tenure-track position at the Assistant Professor level, from individuals with postdoctoral or independent research experience and strong publication records. Research at Science Park focuses on cellular and molecular mechanisms of carcinogenesis and cancer prevention. For this position, we seek applicants working in the general areas of molecular and genetic mechanisms of carcinogenesis, including genetic susceptibility, epigenetic reprogramming, genomic instability, inflammation/immune responses, signal transduction, transcriptional regulation and cancer stem cells. Applications are welcomed from individuals utilizing novel molecular, cellular or animal model systems focused on mechanism-based cancer research. Preference will be given to candidates interested in working in a highly collaborative, interdisciplinary environment. MD Anderson provides an outstanding research environment, and offers a highly competitive recruitment package. The successful candidate will be expected to develop and maintain a world-class externally funded research program and to participate in graduate training programs. Required qualifications include a PhD (or equivalent) and demonstrated scholarly research experience.

Interested candidates should submit a statement of research interests and their CV to the Email address below. Applicants should also request that 3 letters of recommendation be sent to **Mark T. Bedford, Chair of the Search Committee, at: mfendley@mdanderson.org. The application deadline: May 1st, 2010. Information about Science Park can be found at: http://sciencepark.mdanderson.org/**

THE UNIVERSITY OF TEXAS
MD ANDERSON
CANCER CENTER
Making Cancer History®

M.D. Anderson Cancer Center is an equal opportunity employer and does not discriminate on the basis of race, color, national origin, gender, sexual orientation, age, religion, disability or veteran status except where such distinction is required by law. All positions at The University of Texas M.D. Anderson Cancer Center are security sensitive and subject to examination of criminal history record information. Smoke-free and drug-free environment.

CECAD
COLOGNE

Sustainable research perspectives – CECAD offers highly qualified and motivated Ph.D. students training possibilities in its different areas of research complemented by a specific graduate school program. For more information please visit our website (http://www.excellenzcluster.uni-koeln.de/) or contact

Prof. Dr. Carien Niessen (carien.niessen@uni-koeln.de)
Dr. Christopher Schlüpens (c.schluepens@uni-koeln.de)

CECAD Cologne is being funded by the German Research Foundation (DFG) within the Excellence Initiative

Assistant/Associate Professor of Surgery (Research) Rhode Island Hospital

Rhode Island Hospital, Hasbro Children's Hospital, and the Division of Surgical Research are seeking a full-time faculty member with an interest in core areas of surgical research in the cellular-molecular mechanisms of inflammation, matrix biology and/or tissue injury to join the Department of Surgery at the Alpert Medical School of Brown University.

A PhD and/or MD and 2 years of postdoctoral experience are required. Successful candidates must have a background in cellular-molecular methods strong enough to allow them to achieve the goals of their independent research but also advance potential collaborations with nationally recognized faculty in the Department and at Brown. Candidates must qualify for appointment to the rank of Assistant or Associate Professor of Surgery (Research) at the Alpert Medical School of Brown University. For faculty seeking appointment at the rank of Associate Professor, evidence of sustained high quality research program with external funding and a national reputation are required.

Current areas of research interest in the Department cross all Divisions, including cellular-molecular mechanisms of inflammation after injury or surgery, wound healing, fibrosis and matrix metabolism; along with projects in development and cancer immunology. The search will also consider new areas of investigation from funded candidates that are seen as enhancing current programs. Candidates with strong backgrounds in translational programs are also encouraged to apply. For a complete listing of the Division of Surgical Research, Department of Surgery members and their research interests, please visit: **http://bms.brown.edu/surgery/research/**

Review of applicants is ongoing and will continue until a candidate is selected or the search is closed.

All applications received by **March 31, 2010** will be given full consideration. Interested applicants should send (preferably as PDFs) their curriculum vitae, a set of representative reprints, a concise description of their research interests and goals as well as arrange for three letters of reference to be submitted on your behalf, to: **Alfred Ayala, Ph.D., Professor of Surgery (Research) , C/O Ms. Courtney Coto (CCoto@lifespan.org), Division of Surgical Research/Department of Surgery, Rhode Island Hospital/the Warren Alpert Medical School at Brown University, Aldrich 230, 593 Eddy Street, Providence, RI 02903**

Rhode Island Hospital is an equal opportunity/ affirmative action employer and actively solicits applications from minorities, women and protected persons.

FACULTY POSITIONS

DEPARTMENT OF BIOCHEMISTRY AND MOLECULAR BIOLOGY SAINT LOUIS UNIVERSITY SCHOOL OF MEDICINE

Saint Louis University, a Catholic Jesuit institution dedicated to student learning, research, health care, and service, is seeking outstanding applicants for tenure-track faculty positions at the **ASSISTANT PROFESSOR** level in the Edward A. Doisy Department of Biochemistry and Molecular Biology **(http://medschool.slu.edu/biochem/).** The Department has an outstanding faculty and a long tradition of excellence in research. **Enrico Di Cera, M.D.,** was recently recruited as Chairman to lead this Department through an important expansion made possible by the state-of-the-art Doisy Research Center completed in 2007. We are interested in candidates with demonstrated ability to develop strong and independent research programs that would complement existing strengths in the Department. Research programs should involve biological systems relevant to health and disease, and the molecular basis of their structure, function and regulation. A Ph.D. or M.D. degree, evidence of competing successfully for external funding and enthusiasm for teaching and mentoring research trainees are important criteria for selection.

Interested candidates should submit a cover letter, current curriculum vitae, relevant publications, future research plans, a detailed 3-year budget and addresses of three references to **http://jobs.slu.edu.**

Saint Louis University is an Affirmative Action, Equal Opportunity Employer, and encourages nominations and applications of women and minorities

UNIVERSITY OF OXFORD

www.ox.ac.uk/jobs

Tasso Leventis Professorship of Biodiversity

in association with Merton College

The University of Oxford intends to make an appointment to the Tasso Leventis Professorship of Biodiversity in the Department of Zoology (part of the Mathematical, Physical and Life Sciences Division) with effect from 1 October 2010 or as soon as possible thereafter. The new Professor will set up and run an international ly recognised Institute of Biodiversity within the department, provide leadership in research and teaching in biodiversity and teach aspects of the subject at undergraduate and postgraduate level.

Biodiversity as a research field at Oxford has been strengthened by recent appointments in ecology and conservation biology, and by the development of the Department's Wildlife Conservation Research Unit at Tubney (see http://www.zoo.ox.ac.uk). In parallel, new and related positions have been created in the School of Geography and the Environment, while the recently formed Smith School for Enterprise and the Environment brings political and policy expertise to the area. This new Professorship is endowed by a generous benefaction from the Tasso Leventis Conservation Foundation. In addition, the research area will be further supported for five years by funds from the James Martin 21st Century School. This funding will allow the incoming Professor to appoint several five-year post-doctoral fellows and to establish a programme for meetings and visiting fellows in the new Institute.

Please see the further particulars at **www.admin.ox.ac.uk/fp/** for more details about the post and for full instructions before making an application. Further information may be obtained from paul.harvey@zoo.ox.ac.uk - Head of the Department of Zoology. All enquiries will be treated in strict confidence and will not form part of the selection decision. Applications, including a covering letter and full CV and naming three referees, should be received no later than 19 April 2010 by Dr Gwen Booth, Personnel Officer, Senior Appointments at professorships@admin.ox.ac.uk. If you have a query about how to apply, please contact Mrs Elaine Eastgate at professorships@admin.ox.ac.uk or telephone +44 (0)1865 280189.

Committed to equality and valuing diversity

UNITED NATIONS UNIVERSITY

INTERNATIONAL RECRUITMENT
(Tokyo, Japan)

ACADEMIC PROGRAMME OFFICER
(circa: USD128,532-USD137,699 p.a.)

United Nations University (UNU) is an international community of scholars engaged in research, postgraduate training and dissemination of knowledge in furtherance of the purposes and principles of the United Nations, its member states and peoples. For more information, please visit: **www.unu.edu.**

United Nations University-Institute for Sustainability & Peace (UNU-ISP), takes an innovative, integrated approach to sustainability — one that encompasses global change, development, peace and security and bridges these cross-cutting issues through research, educational, and collaborative initiatives with the aim of solving current problems and anticipating future challenges. For more information, visit **http://www.isp.unu.edu/.**

Under the authority and direct supervision of the Director of UNU-ISP, the key responsibilities of the successful incumbent includes project management in the area of environmental management and academic capacity building; develop and conduct research in the field of Sustainability Science; fundraising and teach graduate and other short academic courses hosted by UNU-ISP, including managing the Editorial Office for Sustainability Science.

The successful incumbent is required to have a Ph.D. in Environmental Sciences/Engineering or related field of science, minimum 5 years of post Ph.D. related work experience in sustainability, strong background and skills in applied research and international capacity development, proven track record of academic and policy publications, fluent in English; and sound project management skills in academic/research institution. Experience in teaching, research supervision, fund-raising and knowledge management is desirable. Full Job Description including salary and benefits entitlement is available at **www.unu.edu/employment/** .

Interested applicants should submit a signed UNU Personal History Form (P.11 form) (downloadable from UNU website), with a cover letter explaining why they believe they are qualified for the position and what contribution they intend to bring to UNU. Application is preferably to be emailed to **jsp2010apo@unu.edu** before **31 March 2010.**

SOUTH CAROLINA CoEE

Endowed Chairs in Childhood Neurosciences

South Carolina offers a tremendous opportunity through its Centers of Economic Excellence (CoEE) Program, through which the state recruits elite researchers. This visionary program is evidence of the commitment to innovation demonstrated by South Carolina's government, industry, and universities.

The Center for Childhood Neurotherapeutics will establish an integrated, state-wide team to understand and treat childhood neurological disorders. It will support research at the Greenville Hospital System in Greenville (GHS), at the University of South Carolina in Columbia (USC), at the USC School of Medicine in Columbia (USC-SOM), and at the Medical University of South Carolina in Charleston (MUSC). The center will be anchored by three endowed professors carrying out basic and/or clinical studies related to understanding and treating childhood diseases of the nervous system. Each endowed chair position will benefit from significant programmatic and departmental support, and will have the opportunity to work closely with researchers and clinicians at the nationally renowned Greenwood Genetics Center in the study of neurogenetic disorders.

(1) Endowed Chair in Translational Therapeutics: Based at GHS with academic appointment in USC-SOM. Applicant must have training in one or more of the following: developmental behavioral pediatrics; neurology; psychology, basic mechanisms of developmental genetic diseases, and have experience in design and management of clinical trials. Preference will be given to persons who have experience working in clinical settings, especially those involving the study of autism spectrum disorders and neurogenetic disorders. Inquiries and nominations should be sent electronically to **Dr. Desmond Kelly, dkelly@ghs.org.**

(2) Endowed Chair in Neurodevelopmental Disorders: Based at USC. Applicant should have training in neuroscience, psychology, biology, or related areas and should address questions related to brain development and neurogenetic disorders, particularly those linked to behavior or cognition. Preference for this position will be given to applicants that use functional brain imaging of animal models and/or neurogenetic approaches to address developmental alterations that affect cognition and behavior. Inquiries and nominations should be sent electronically to **Dr. Roger Sawyer, RHSawyer@mailbox.sc.edu.**

(3) Endowed Chair for Basic Research in Childhood Disorders: Based at MUSC. Applicant must have training and expertise in basic mechanisms of disease processes and therapeutic approaches for childhood diseases of the nervous system. Preference will be given to applicants working in a neuroscience group utilizing applications for neuroprotection and neurorepair using stem cells and other approaches in animals or humans. Inquiries and nominations should be sent electronically to **Dr. Inderjit Singh, singhi@musc.edu.**

All three positions require an M.D. or Ph.D. If applicable, board certification in a subspeciality is required. Applicants should have established records of grant funding, scholarly activities, and the ability to foster interdisciplinary research. References will not be contacted without candidate's permission. Applicants should submit a statement of research interests, CV, and contact information for at least three references to. Position **(1) Desmond Kelly, M.D.,** Medical Director, Developmental – Behavioral Pediatrics, Children's Hospital of Greenville Hospital System, 200 Patewood, A200, Greenville, SC 29615, Position **(2) Roger H. Sawyer, Ph.D.,** College of Arts & Sciences, University of South Carolina, Columbia, SC 29208, Position **(3) Inderjit Singh, Ph.D.,** Charles P. Darby Children's Research Institute, Medical University of South Carolina, 173 Ashley Avenue, CRI 516, Charleston, SC 29425.

For more information about the CoEE Program, please visit **www.sccoee.org.**

GHS, USC, and MUSC are equal opportunity employers committed to excellence through diversity. Minorities and women are especially encouraged to apply.


AAAS is here.
Evolution
AAAS + U = Δ

HBCU-UP National Research Conference

[illegible] (HBCUs) increase the number of underrepresented ethnic minorities qualified for education and research in science, technology, engineering, and mathematics (STEM). AAAS partners with NSF to host a national gathering that highlights undergraduate student research to enhance the quality of STEM education. And this is just one of the ways that AAAS is committed to advancing science to support a healthy and prosperous world. Join us. Together we can make a difference. **aaas.org/plusyou/hbcuup**

AAAS + U = Δ

Rwanda

A country devastated by genocide and a crippling AIDS epidemic. Together with the Rwandan Ministry of Education, AAAS, the world's largest multidisciplinary scientific society and publisher of *Science* magazine, is working to ensure that local children gain science, technology, math, and engineering. And this is just one of the ways that AAAS is committed to advancing science to support a healthy and prosperous world. Join us. Together we can make a difference. aaas.org/plusyou/rwanda

AAAS + U = Δ

PRIZE

KUWAIT PRIZE 2010
Invitation for Nominations

The **Kuwait Foundation for the Advancement of Sciences (KFAS)** institutionalized the **KUWAIT Prize** to recognize distinguished accomplishments in the arts, humanities and sciences. The Prizes are awarded annually in the following categories:

A. Basic Sciences
B. Applied Sciences
C. Economics and Social Sciences
D. Arts and Literature
E. Arabic and Islamic Scientific Heritage

The Prizes for 2010 will be awarded in the following fields:

1.	**Basic Sciences**	:	Chemistry
2.	**Applied Sciences**	:	Biomedical Technology
3.	**Economic and Social Sciences**	:	Role of Islamic Financial Institutions in the Arab World
4.	**Arts and Literature**	:	Studies in Al-Jahili Poetry
5.	**Arabic and Islamic Scientific Heritage**	:	Architecture

Foreground and **Conditions** of the Prize:

1. Two prizes are awarded in each category:
   * A Prize to recognize the distinguished scientific research of a Kuwaiti citizen,
   and,
   *A Prize to recognize the distinguished scientific research of an Arab citizen.
2. The candidate should not have been awarded a Prize for the submitted work by any other institution.
3. Nominations for these Prizes are accepted from individuals, academic and scientific centers, learned societies, past recipients of the Prize, and peers of the nominees. No nominations are accepted from political entities.
4. The scientific research submitted must have been published during the last ten years.
5. Each Prize consists of a cash sum of K.D. 30,000/- (approx. U.S.$100,000/-), a Gold medal, a KFAS Shield and a Certificate of Recognition.
6. Nominators must clearly indicate the distinguished work that qualifies their candidate for consideration.
7. The results of KFAS decision regarding selection of winners are final.
8. The documents submitted for nominations will not be returned regardless of the outcome of the decision.
9. Each winner is expected to deliver a lecture concerning the contribution for which he was awarded the Prize.

Inquiries concerning the KUWAIT PRIZE and nominations including complete curriculum vitae and updated lists of publications by the candidate with **four copies** of each of the published papers should be received before **31/10/2010** and addressed to:

The Director General
The Kuwait Foundation for the Advancement of Sciences - P.O. Box: 25263, Safat - 13113, Kuwait.
Tel: (+965) 22429780 / Fax: 22403891 / E-Mail: prize@kfas.org.kw

AWARDS

ROBERT J. AND CLAIRE PASAROW FOUNDATION

22nd ANNUAL MEDICAL RESEARCH AWARD RECIPIENTS
23rd ANNUAL MEDICAL RESEARCH AWARDS CALL FOR NOMINATIONS

Cancer, Cardiovascular Disease, Neuropsychiatry

THE PASAROW FOUNDATION PROUDLY ANNOUNCES THE RECIPIENTS OF THE 22ND ANNUAL MEDICAL AWARDS:

CANCER
Brian J. Druker, M.D. - Oregon Health & Science University, Howard Hughes
Inder M. Verma, Ph.D. - Salk Institute

CARDIOVASCULAR DISEASE
David Ginsburg, M.D. - University of Michigan Medical School, Howard Hughes

NEUROPSYCHIATRY
Jean-Pierre Changeux, Ph.D. - Institut Pasteur, Paris, France

The deadline for the submission of nominations for the **23rd Annual Medical Research Awards** has been extended to **Monday, March 22, 2010.** Please see the January 1, 2010 issue of ***Science*** for details regarding nomination submission or contact **Jack D. Barchas, M.D.** at **(212) 746–3770** or **jbarchas@med.cornell.edu.**

UNIVERSITY OF DELAWARE

Assistant/Associate Professor of Critical Zone Science

Appointment: This is a 9 month, tenure track position with responsibilities divided between research (80%) and teaching (20%).

Position Description: The Department of Plant and Soil Sciences (http://ag.udel.edu/plsc/) in coordination with the newly formed Delaware Environmental Institute (http://denin.udel.edu/) invites applications for a tenure track faculty position at the Assistant or Associate Professor level in the area of Critical Zone Science. Longstanding strengths in environmental sciences at the University of Delaware are expanding through interdisciplinary investigations of human and earth system processes that govern terrestrial ecosystems of the critical zone - the top of the plant canopy to the base of the weathering zone. Successful candidates will complement environmental research at the University through expertise in the role and importance of soils to large scale issues such as climate change and the biogeochemical cycling of nutrient elements. The successful applicant will develop or bring a nationally recognized research program supported by extramural funding and will teach one course per year at the undergraduate or graduate levels.

Qualifications: The candidate must have a Ph.D. and research interests focused on soil processes relevant to land use issues and emergent impacts on ecosystems. Desirable areas of expertise include geomorphology, geochemistry, biogeochemistry, pedology, eco-hydrology, and land-atmosphere exchange. Candidates with experience bridging laboratory and field-scale investigations as well as interdisciplinary studies are especially encouraged to apply. Interest and ability to contribute effectively to collaborative research efforts is essential.

Salary: Commensurate with experience and training. The University of Delaware provides an excellent employee benefits package including health and dental insurance, retirement contributions, pre-tax flexible spending accounts, and complete tuition remission for family members.

Facilities: Teaching and research facilities are located at the University of Delaware, Newark, DE. The University is a Land Grant, Sea Grant & Space Grant institution located midway between Philadelphia and Baltimore. Further information on the Environmental Sciences at the University of Delaware (http://www.environmentalportal.udel.edu), the Delaware Environmental Institute and the Christina River Basin Critical Zone Observatory (www.udel.edu/czo/) can be found on the web.

Date Position is Available: As early as Sept 1, 2010.

Application Process: By March 19th, interested persons should submit: (i) letter of application; (ii) resume; (iii) two page statement of research and teaching interests; (iv) names, e-mail and postal addresses, and telephone numbers of three references. Complete applications should be assembled into a single pdf document and sent by e-mail to: Dr. K. Eric Wommack, Search Committee Chair: PLSC-faculty-search@anr.udel.edu .

The UNIVERSITY OF DELAWARE is an Equal Opportunity Employer which encourages applications from Minority Group Members and Women.

POSITIONS OPEN

SENIOR LECTURER IN MATHEMATICAL BIOLOGY
The University of Chicago
Biological Sciences Collegiate Division

The Biological Sciences Collegiate Division at the University of Chicago invites applications for a Senior Lectureship in mathematical biology beginning in the fall 2010. The Senior Lecturer is expected to teach a three-quarter postcalculus course sequence in basic applied mathematics for advanced science majors who are interested in quantitative approaches to biology and to develop an integrated biocalculus curriculum for premeds. Applicants must have received a Ph.D. in mathematics or a related field with thesis research in an area of applied mathematics such as, but not restricted to, biophysics, biomechanics, computational neuroscience, genomics, or population biology and must document interest and proficiency in undergraduate teaching. The appointment will be for three years and is renewable.

To apply for this position visit our **website: http://academiccareers.uchicago.edu/ job posting 00252.** Please complete your application and submit supporting materials by April 2, 2010.

The University of Chicago is an Affirmative Action/Equal Opportunity Employer.

ASSISTANT RESEARCH INVESTIGATOR
Center for Regenerative Developmental Biology
The Forsyth Institute, a Harvard Medical and Dental School Affiliate

An Assistant Research Investigator position to focus on mouse developmental biology of the skin and wound healing is available immediately. A Ph.D., with two to three years of postdoctoral experience and at least two postdoctoral first-author papers are required. Background in molecular biology, gene targeting inactivation, and mouse skin developmental biology is required. Send curriculum vitae and names of three references to:

Dr. Marianna Bei
Assistant Professor, Harvard Medical School
Director, Center for Regenerative Developmental Biology
The Forsyth Institute
E-mail: mbei@forsyth.org or mbei@partners.org

The Forsyth Institute is an Equal Opportunity Employer, Minorities/Females/Veterans/Persons with Disabilities.

GROUP LEADER, BIOINFORMATICS/ SYSTEMS BIOLOGY
Uni Research, Norway

The Computational Biology Unit (CBU) at Uni BCCS (Bergen Center for Computational Science) is searching for an additional group leader in the field of computational biology/ bioinformatics. CBU is colocated and integrated with several departments at the University of Bergen. Please electronically send your curriculum vitae, your 10 most relevant publications, and a research plan to **Prof. Inge Jonassen, e-mail: inge.jonassen@ii.uib.no, Head of CBU.** The evaluation of applications will commence March 15, 2010, and continue until a suitable candidate is found. To read a full-text version of this ad, please visit **website: http://www.bccs.uni.no/positions.**

Position available for a highly motivated **POSTDOCTORAL FELLOW** with proven experience in cloning and expression of mammalian proteins to study eukaryotic DNA replication. Experience in baculovirus expression system is highly desirable. Excellent salary and benefits. Electronically send curriculum vitae to **e-mail: ebiswas@umdnj.edu.**

POSITIONS OPEN

THE NEUROSCIENCES INSTITUTE

Positions are currently open for **POSTDOCTORAL FELLOWS** in computational neuroscience to join a team of researchers in creating large-scale, spiking network models of sensorimotor control in the mammalian central nervous system. Building on two decades of experience at The Neurosciences Institute, these simulations will be incorporated into autonomous brain-based devices that perform various behavioral tasks.

A suitable candidate should have a background in neurobiology, neural modeling experience, and strong programming skills.

Located in La Jolla, California, The Neurosciences Institute focuses its theoretical and experimental research on the principles underlying how we perceive and act upon the world, how we learn and remember, and how consciousness arises.

Interested candidates should send curriculum vitae including the names of three references to: **Dr. W. Einar Gall, Research Director, The Neurosciences Institute, 10640 John Jay Hopkins Drive, San Diego, CA 92121. Or to e-mail: jobs7@nsi.edu.**

The Neurosciences Institute is an Equal Opportunity Employer.

MARKETPLACE

AAAS, publisher of *Science*,
thanks the sponsors and supporters of the

2010 Annual Meeting

Bridging Science and Society

18—22 February ▸ San Diego

Presenting Sponsor

SUBARU

OSA The Optical Society

Canada

HELMHOLTZ ASSOCIATION

EUROPEAN RESEARCH

Johnson & Johnson PHARMACEUTICAL RESEARCH & DEVELOPMENT, L.L.C.

UCSD

SOYCONNECTION.COM

THE ROYAL SOCIETY

PATHWAY GENOMICS

THE KAVLI FOUNDATION

In addition generous funding for AAAS Awards is provided by the ***Kavli Foundation*** and ***Affymetrix.***

AAAS
ADVANCING SCIENCE, SERVING SOCIETY

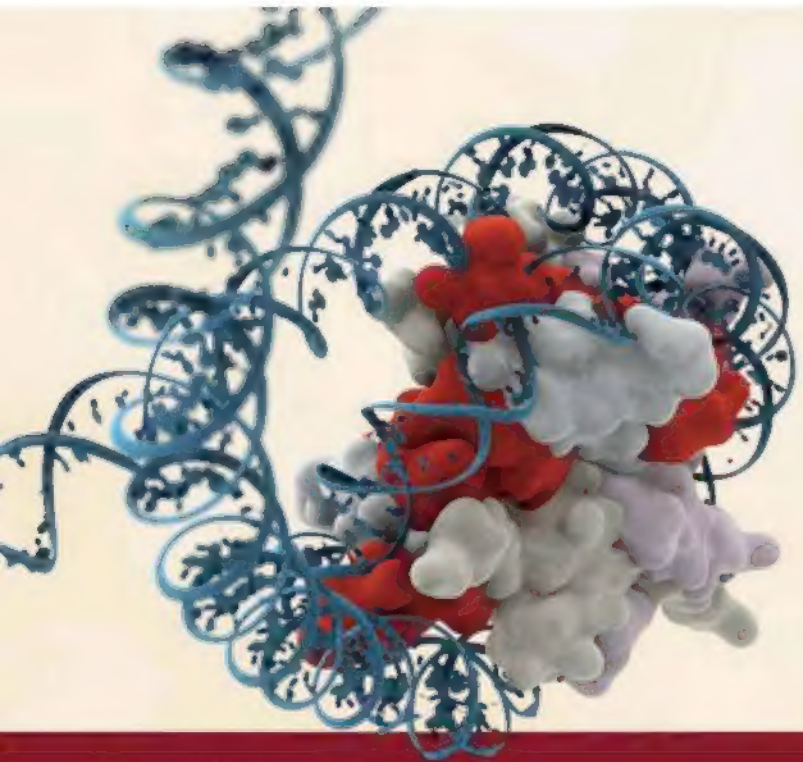

- Over 70 antibodies validated for ChIP by the same rigorous standards as all other recommended applications – optimization is not left up to you.
- SimpleChIP™ Enzymatic Chromatin IP Kits are used in-house for antibody validation and work optimally with our antibodies, facilitating your experimental success.
- Technical support is provided by the same scientists that produce and validate the products, allowing a fast, thorough and accurate response.

The highest quality

ChIP Antibodies & Kits

...from Cell Signaling Technology®

Unparalleled product quality, validation and technical support.

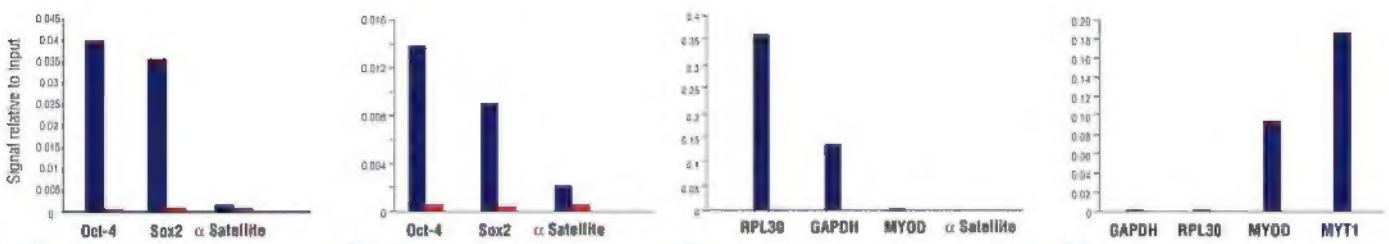

A ■ Oct-4A (C30A3C1) Rabbit mAb (ChIP Formulated) #5677
■ Normal Rabbit IgG #2729

B ■ Sox2 (D6D9) XP™ Rabbit mAb (ChIP Formulated) #5024
■ Normal Rabbit IgG #2729

C ■ Tri-Methyl-Histone H3 (Lys4) (C42D8) Rabbit mAb #9751
■ Normal Rabbit IgG #2729

D ■ Tri-Methyl-Histone H3 (Lys27) (C36B11) Rabbit mAb #9733
■ Normal Rabbit IgG #2729

*ChIP assays were performed with cross-linked chromatin from 4 x 10⁶ NCCIT (A,B) or HeLa cells (C,D) and either 10 µl of **Oct-4A (C30A3C1) Rabbit mAb (ChIP Formulated) #5677** (A), **Sox2 (D6D9) XP™ Rabbit mAb (ChIP Formulated) #5024** (B), **Tri-Methyl-Histone H3 (Lys4) (C42D8) Rabbit mAb #9751** (C) or **Tri-Methyl-Histone H3 (Lys27) (C36B11) Rabbit mAb #9733** (D), using **SimpleChIP™ Enzymatic Chromatin IP Kit (Magnetic Beads) #9003**. Normal Rabbit IgG #2729 (1 µl) was used as negative control. The enriched DNA was quantified by Real-Time PCR, using primers specific for the transcriptionally active Oct-4 and Sox2 (A,B) or RPL30 and GAPDH genes (C,D), and the transcriptionally inactive heterochromatic α satellite repeat element, MYOD or MYT1 genes. The amount of immunoprecipitated DNA in each sample is represented as signal relative to the total amount of input chromatin, which is equivalent to one.*

for quality products you can trust...

www.cellsignal.com

Cell Signaling TECHNOLOGY®

Orders (toll-free) 1-877-616-2355 | **Technical support** (toll-free) 1-877-678-8324 support@cellsignal.com | **Inquiries** info@cellsignal.com | **Environmental Commitment** eco.cellsignal.com